

Mechanisms of cell regulation by the immunosuppressive L-amino acid oxidase IL4i1

Leonie Kristin Zeitler

Vollständiger Abdruck der von der Fakultät für Medizin der Technischen Universität München
zur Erlangung einer
Doktorin der Naturwissenschaften (Dr. rer. nat.)
genehmigten Dissertation.

Vorsitz: Prof. Dr. Percy A. Knolle

Prüfer*innen der Dissertation:

1. Prof. Peter Murray, Ph.D.
2. Prof. Dr. Matthias Feige
3. Prof. Dr. Anne Krug

Die Dissertation wurde am 20.12.2022 bei der Technischen Universität München eingereicht
und durch die Fakultät für Medizin am 13.06.2023 angenommen.

Abstract

Regulated amino acid metabolism has evolved as a mechanism to control and limit immune responses. Immune cells can upregulate the expression of distinct amino acid-metabolizing enzymes to provoke a local depletion of amino acids and the simultaneous generation of metabolites, which can both contribute to immunoregulatory effects. One of these enzymes is IL4i1, a secreted L-amino acid oxidase (LAAO) catalyzing the oxidative deamination of aromatic amino acids generating the respective α -keto acids, hydrogen peroxide (H_2O_2) and ammonia. IL4i1 was found to impair T cell responses and promote the emergence of regulatory immune cell subsets. In the context of cancer, IL4i1 is often expressed in tumor-associated myeloid cells and linked to cancer progression and poor prognosis. However, the mechanisms by which IL4i1-dependent amino acid metabolism controls the biology of immune and cancer cells remain poorly understood. As LAAO homologues of IL4i1 are evolutionarily conserved and can for example be found in snake venoms, I used a comparative approach to better understand IL4i1 and LAAO biology. Generation and testing of recombinant mammalian IL4i1 and a cobra (*Naja naja*) venom LAAO suggested divergent functions of the related enzymes. While the snake venom LAAO killed cells by fast production of H_2O_2 , mammalian IL4i1 generated sub-lethal amounts of H_2O_2 and instead promoted cellular protection from redox stress. Specifically, IL4i1-mediated amino acid metabolism protected cells from ferroptosis, a form of oxidative cell death characterized by uncontrolled, iron-dependent membrane lipid peroxidation. Mechanistically, the α -keto acids generated by IL4i1 from tryptophan and tyrosine, indole-3-pyruvate (I3P) and 4-hydroxyphenylpyruvate (4HPP) respectively, conferred cellular protection by free radical scavenging and the stimulation of anti-oxidative gene expression involving the activation of the Nrf2 pathway. Additionally, I observed that I3P can activate immunoregulatory aryl hydrocarbon receptor (AhR) signaling; however, this was dispensable for the anti-ferroptotic effect of the metabolite. Overall, the results of my work suggest that IL4i1-mediated amino acid metabolism in the extracellular space can generate a ferroptosis-suppressive environment, which may contribute to the enzyme's pro-tumorigenic effect.

To study and mechanistically dissect the interplay between IL4i1 secreting immune cells and different cells in their microenvironment, more complex *in vitro* models containing cells endogenously expressing IL4i1 are required. Macrophages and dendritic cells (DCs) appear to be the main IL4i1 producing cells in the tumor microenvironment, but the knowledge about the expression and regulation of IL4i1 in these myeloid cell types, especially on protein level is limited. Therefore, I characterized IL4i1 expression in bone-marrow derived DCs (BMDCs) and macrophages (BMDMs). My results show that IL4i1 is expressed in distinct populations of BMDCs and highly inducible in BMDMs, which did not exhibit baseline IL4i1 expression (on

protein level). Specifically, the combination of IL4, signaling via STAT6, and NF- κ B-activating stimuli such as TNF or LPS synergized to activate IL4i1 expression and secretion. These findings can serve as basis for future research investigating the interplay of IL4i1-expressing myeloid cells and other cells in their environment.

Table of contents

Abstract.....	I
Table of contents.....	III
List of figures.....	VII
List of abbreviations	IX
1. Introduction	1
1.1. Balance between immunity and regulation of immune responses.....	1
1.2. Immune regulation by amino acid metabolism.....	2
1.2.1. Arginine metabolism in myeloid cells by inducible nitric oxide synthase and arginases	4
1.2.2. Tryptophan metabolism by indoleamine 2,3-dioxygenases	5
1.2.3. Sensing of amino acid depletion and its effects on immune regulation	7
1.2.4. Regulation of immune responses by kynurenines	9
1.2.4.1. The Kynurenine (Kyn) pathway	9
1.2.4.2. The aryl hydrocarbon receptor pathway	10
1.2.4.3. Immunoregulation via AhR signaling	11
1.2.4.4. AhR independent effects of kynurenines	12
1.2.5. Arginine and tryptophan metabolizing enzymes in cancer	13
1.2.6. The L-amino acid oxidase IL4i1.....	14
1.2.6.1. L-amino acid oxidases in snake venoms	15
1.2.6.2. Discovery of IL4i1 and its LAAO function.....	17
1.2.6.3. Expression and immunoregulatory properties of IL4i1	17
1.2.6.3.1. Expression and effects of IL4i1 in B cells	17
1.2.6.3.2. IL4i1 in myeloid cells.....	18
1.2.6.3.3. IL4i1 and T cells.....	20
1.2.6.4. Mechanisms of IL4i1-mediated immune regulation.....	21
1.2.6.5. IL4i1 in cancer.....	22
1.3. The oxidative cell death ferroptosis	24
1.3.1. Ferroptosis-suppressive mechanisms	25
1.3.1.1. The GPX4 – glutathione – cysteine axis.....	25
1.3.1.2. GPX4-independent ferroptosis suppression	27
1.3.1.3. The Keap1-Nrf2 pathway	28
1.3.2. Ferroptosis in cancer biology.....	30
1.3.2.1. Pro-ferroptotic effects of tumor suppressors.....	30
1.3.2.2. Dependence of tumor cells on ferroptosis-suppressive pathways	31
1.3.2.3. Ferroptosis and immunosurveillance of cancer.....	32
2. Rationale and aims of the thesis.....	34

3.	Materials and Methods	35
3.1.	Overview of materials	35
3.1.1.	Chemicals and reagents.....	35
3.1.2.	Antibodies	37
3.1.3.	Commercial Kits	38
3.1.4.	Plastics.....	38
3.1.5.	Buffers.....	39
3.2.	DNA-based methods	40
3.2.1.	Agarose gel electrophoresis and DNA purification from agarose gels	40
3.2.2.	Genomic DNA extraction from cells	40
3.2.3.	Basic PCR protocol for amplification DNA fragments	40
3.2.4.	Plasmid amplification in competent cells	41
3.2.4.1.	Heat shock transformation	41
3.2.4.2.	Plasmid isolation	41
3.2.5.	Molecular cloning	41
3.2.5.1.	Generation of PiggyBac PB-T-PAF plasmids for recombinant expression of <i>N. naja</i> LAAO, murine and human IL4i1	41
3.2.5.2.	Generation of pX458 plasmids for AhR and Nrf2 knockout.....	43
3.3.	Mice	43
3.4.	Cell culture	44
3.4.1.	Cell lines and cultivation	44
3.4.2.	Primary cell cultures	44
3.4.2.2.	Bone marrow-derived dendritic cells.....	45
3.4.2.2.1.	GM-CSF-differentiated dendritic cells.....	45
3.4.2.2.2.	FLT3L-differentiated dendritic cells	45
3.4.2.2.3.	CD103 dendritic cells	45
3.4.2.3.	Stimulation of macrophages and dendritic cells.....	45
3.4.2.4.	Infection of BMDMs with <i>Salmonella enterica</i> serovar Typhimurium.....	46
3.5.	Manipulation of gene expression in cell lines.....	46
3.5.1.	Transient transfection with Lipofectamine.....	46
3.5.2.	Generation of knockout cell lines using the CRISPR/Cas9 system.....	46
3.5.2.1.	Generation of knockout clones	46
3.5.2.2.	Verification of knockouts	46
3.5.3.	siRNA-mediated knockdown	47
3.5.4.	Generation of stable cell lines using the PiggyBac expression system	47
3.6.	Protein-based methods	48
3.6.1.	Generation and isolation of secreted recombinant proteins	48
3.6.2.	Deglycosylation of recombinant proteins by PNGaseF digest.....	48

3.6.3.	Cell lysis, protein extraction and determination of protein concentration.....	48
3.6.4.	SDS-PAGE and Immunoblotting	49
3.6.5.	Mass spectrometry-based secretomics	49
3.7.	Gene expression analysis	51
3.7.1.	RNA isolation, cDNA generation and quantitative real-time PCR.....	51
3.7.2.	mRNA-Seq based transcriptomics.....	53
3.8.	Fluorimetric and optical methods.....	54
3.8.1.	Fluorescence microscopy of fluorescence-tagged AhR	54
3.8.2.	Cell death analysis by live cell imaging	54
3.8.3.	Determination of I3P fluorescence spectrum	54
3.8.4.	Flow cytometry	55
3.8.4.1.	Staining, analysis and sorting of bone marrow-derived dendritic cells	55
3.8.4.2.	Monitoring of I3P uptake	55
3.8.4.3.	Analysis of lipid peroxidation	55
3.8.5.	Quantification of L-amino acid oxidase activity	56
3.8.6.	Free radical scavenging assay	56
3.8.7.	Determination of GSH/GSSG ratio	56
3.9.	Additional use of software	56
4.	Results	57
4.1.	Generation and characterization of recombinant <i>Naja naja</i> LAAO and mammalian IL4i1 proteins	57
4.1.1.	The PiggyBac expression system.....	57
4.1.2.	Construct design	58
4.1.3.	Generation of the recombinant proteins.....	59
4.1.4.	Enzymatic activity of the purified proteins.....	60
4.1.5.	Loss of enzymatic activity in mutant <i>N. naja</i> LAAO and murine IL4i1	63
4.1.6.	Comparison of <i>N. naja</i> LAAO, human and murine IL4i1 enzyme activity towards the proteinogenic amino acids	64
4.2.	Downstream cellular effects of L-amino acid oxidases	65
4.2.1.	Toxicity of LAAOs.....	65
4.2.1.1.	<i>Naja naja</i> LAAO mediates cytotoxicity via generation of H ₂ O ₂	65
4.2.1.2.	Mammalian IL4i1 exhibits low cytotoxicity	67
4.2.2.	Downstream effects of IL4i1-produced aromatic amino acid metabolites.....	69
4.2.2.1.	I3P induces stress-protective gene expression.....	69
4.2.2.2.	I3P uptake can be visualized by flow cytometry.....	71
4.2.2.3.	I3P is an activator of AhR signaling	72
4.2.3.	Anti-ferroptotic effects of IL4i1 and its amino acid metabolites	74
4.2.3.1.	I3P is a potent and 4HPP a weak ferroptosis suppressor	74

4.2.3.2.	Ferroptosis inhibition is mediated by free radical scavenging and anti-oxidative gene expression	78
4.2.3.2.2.	HO-1 induction is not required for I3P-mediated ferroptosis protection ...	82
4.2.3.2.1	Nrf2 contributes to I3P-mediated ferroptosis suppression	84
4.2.3.2.3.	I3P-mediated ferroptosis suppression is independent of AhR activation .	86
4.2.3.3.	IL4i1 generates a ferroptosis-suppressive milieu.....	88
4.3.	Expression and regulation of IL4i1 in bone marrow-derived myeloid cells	92
4.3.1.	Baseline expression of IL4i1 in BMDMs and BMDCs	92
4.3.2.	IL4i1 expression in GM-CSF differentiated dendritic cells.....	93
4.3.3.	IL4i1 expression in bone marrow-derived CD103 ⁺ dendritic cells	94
4.3.4.	IL4i1 induction in bone marrow-derived macrophages.....	95
4.3.4.1.	IL4i1 is highly inducible by the combination of IL4 and TNF	95
4.3.4.2.	IL4 enhances the induction of IL4i1 by TLR ligands	97
4.3.4.3.	High increase of IL4i1 secretion can be detected by MS-based secretome analysis	98
4.3.4.4.	LPS-mediated IL4i1 induction does not depend on TNF signaling.....	100
4.3.4.5.	NF- κ B is involved in TNF- and LPS-mediated IL4i1 induction.....	101
4.3.4.6.	IL4-mediated IL4i1 induction depends on STAT6.....	104
4.3.5.	IL4i1 induction in GM-DC and CD103 DC cultures	105
5.	Discussion and perspectives	107
5.1.	Divergent functions of IL4i1 and snake venom LAAOs	107
5.2.	Activation of AhR signaling by the aromatic α -keto acids I3P and 4HPP	108
5.3.	Ferroptosis suppression by IL4i1-mediated amino acid metabolism	109
5.4.	Implications of IL4i1-mediated amino acid metabolism in the TME	112
5.5.	IL4i1 expression in bone-marrow derived myeloid cells.....	114
5.5.1.	IL4i1 is expressed in distinct subsets of BMDCs	114
5.5.2.	Induction of IL4i1 in BMDMs.....	116
5.6.	Perspectives.....	117
6.	References.....	119
7.	Supplement.....	142
8.	Acknowledgements	152

List of figures

Figure 1: Balance of immune responses.....	2
Figure 2: Immunoregulatory amino acid-metabolizing enzymes expressed by immune cells	3
Figure 3: Overview of the kynurenine pathway	9
Figure 4: Scheme of the AhR signaling pathway	11
Figure 5: Feed forward loop of IDO maintenance and propagation of IDO expression via AhR activation	12
Figure 6: Enzymatic activity of L-amino acid oxidases	15
Figure 7: Alignment of snake venom LAAOs with murine and human IL4i1	16
Figure 8: Chemical basis of phospholipid peroxidation	25
Figure 9: Overview of cell intrinsic ferroptosis-suppressive pathways	28
Figure 10: Scheme of the Keap1-Nrf2 pathway	30
Figure 11: Plasmid map of PB-T-PAF_mIL4i1 encoding murine IL4i1	42
Figure 12: Validation of AhR and Nrf2 knockouts	47
Figure 13: Schematic overview of PiggyBac transposon system	58
Figure 14: Design of constructs for recombinant <i>N. naja</i> LAAO, murine and human IL4i1 expression.....	59
Figure 15: Expression of recombinant <i>N. naja</i> LAAO, murine IL4i1 and human IL4i1	60
Figure 16: Enzymatic activity of the purified proteins	61
Figure 17: Activity of human IL4i1.....	62
Figure 18: Catalytically inactive enzyme versions.....	63
Figure 19: Comparison <i>N. naja</i> LAAO, human and murine IL4i1 enzymatic activity.....	64
Figure 20: Cytotoxic effects of <i>N. naja</i> LAAO require enzymatic activity	66
Figure 21: <i>N. naja</i> LAAO induced cell death is H ₂ O ₂ -dependend and non-apoptotic.....	67
Figure 22: Mammalian IL4i1 is only toxic at high concentrations	68
Figure 23: I3P induces stress-protective gene expression.....	70
Figure 24: I3P uptake can be monitored by flow cytometry.....	72
Figure 25: I3P activates the aryl hydrocarbon receptor.....	73
Figure 26: I3P and 4HPP can protect cells from ferroptosis.....	75
Figure 27: Anti-ferroptotic activity of I3P and 4HPP	77
Figure 28: Free radical scavenging activity of I3P and 4HPP.....	78
Figure 29: Conceptual model used for testing mechanisms of I3P-mediated ferroptosis protection	79
Figure 30: Distinct modes of anti-ferroptotic effects mediated by I3P.....	81
Figure 31: HO-1 induction is not required for I3P-mediated ferroptosis protection	83
Figure 32: Nrf2 contributes to I3P-mediated ferroptosis suppression.....	85
Figure 33: AhR is not required for I3P-mediated ferroptosis suppression	87

Figure 34: Effects of IL4i1 on gene expression in HeLa cells.....	88
Figure 35: Anti-ferroptotic effects of IL4i1	90
Figure 36: IL4i1-mediated changes in culture medium are sufficient to block ferroptosis	91
Figure 37: Baseline IL4i1 expression in bone marrow-derived macrophages and dendritic cells	93
Figure 38: IL4i1 expression in GM-CSF differentiated culture.....	94
Figure 39: IL4i1 expression in CD103 DCs.....	95
Figure 40: IL4i1 is highly inducible by the combination of IL4 and TNF.....	96
Figure 41: IL4 enhances the induction of IL4i1 by TLR ligands.....	98
Figure 42: Secretome analysis of BMDMs treated with IL4 and LPS	99
Figure 43: LPS-mediated IL4i1 induction does not depend on TNF signaling	101
Figure 44: NF-κB is involved in TNF- and LPS-mediated IL4i1 induction.....	103
Figure 45: IL4-mediated IL4i1 induction depends on STAT6	105
Figure 46: IL4i1 induction in GM-DC and CD103 DC cultures	106
Figure 47: Model of IL4i1-dependent amino acid metabolism in the TME	114
Figure 48: Model of synergistic IL4i1 induction by the combination of IL4 with TNF/LPS ...	117

List of abbreviations

3FTx	three-finger toxin
3HAA	3-hydroxyanthranilic acid
3HK	3-hydroxykynurenine
4HPP	4-hydroxyphenylpyruvate
AhR	aryl hydrocarbon receptor
AhRR	AhR repressor
AIP	AhR-interacting protein
AKR1C	aldo-keto reductase 1C
ARE	antioxidant response element
Arg	arginine
Arg1	arginase-1
Arg2	arginase-2
ARNT	AhR nuclear translocator
AUR	Amplex UltraRed
BCR	B cell receptor
BH2	dihydrobiopterin
BH4	tetrahydrobiopterin
BMDCs	bone marrow-derived dendritic cells
BMDMs	bone marrow-derived macrophages
BSO	buthionine sulfoximine
bZIP	basic leucine zipper
CD103 DCs	CD103 ⁺ BMDCs differentiated with GM-CSF and FLT3L
cDCs	conventional DCs
CLL	chronic lymphocytic leukemia
CoQ	ubiquinone
CoQH ₂	ubiquinol
CTLA-4	Cytotoxic T-Lymphocyte-Associated Protein 4
CYP1	cytochrome P450 family-1
DAMPs	damage-associated molecular patterns
DCs	dendritic cells
DHFR	dihydrofolate reductase
dox	doxycycline
DPPH	diphenyl-2-picrylhydrazyl
DRE	dioxin-responsive element
EAE	experimental autoimmune encephalitis
EMT	epithelial-mesenchymal transition

FAD	flavin adenine dinucleotide
FDR	false recovery rate
FL-DCs	BMDCs differentiated with FLT3L
FSP1	ferroptosis suppressive protein 1
GCH1	GTP cyclohydrolase 1
GCL	glutamate cysteine ligase
GCN2	general control nonderepressible 2
GM-DCs	BMDCs differentiated with GM-CSF
GO	gene ontology
GPX4	glutathione peroxidase 4
gRNA	guideRNA
GSH	glutathione
GSR	glutathione-disulfide reductase
GSS	GSH synthase
GSSG	oxidized GSH
H ₂ O ₂	hydrogen peroxide
hIL4i1	human IL4i1
HO-1	heme oxygenase-1
HO-2	heme oxygenase-2
HSP90	90-kDa heat shock protein
I3P	indole-3-pyruvate
IDO1	indoleamine 2,3-dioxygenase 1
IDO2	indoleamine 2,3-dioxygenase 2
IFN	interferon
IκB	inhibitor of NF-κB
IL4i1	interleukin 4 induced 1
IL4Rα	IL4 receptor α
ILC2	type 2 innate lymphoid cells
iNOS	inducible nitric oxide synthase
KAT	Kyn aminotransferase
Kyn	kynurenine
KynA	kynurenic acid
LAAO	L-amino oxidase
Leu	leucine
LPS	lipopolysaccharide
MAIT cells	mucosal-associated invariant T cells
MDSCs	myeloid-derived suppressor cells

mIL4i1	murine IL4i1
mregDCs	mature DCs enriched in immunoregulatory molecules
MS	mass spectrometry
mTOR	mammalian target of rapamycin
mTORC1	mTOR complex 1
<i>Naja naja</i>	<i>N. naja</i>
NF-κB	Nuclear factor kappa B
NLR	NOD-like receptor
NO	nitric oxide
NQO	NAD(P)H-quinone oxidoreductase
PAMPs	pathogen-associated molecular patterns
PD-1	Programmed Cell Death Protein 1
Phe	phenylalanine
PL	phospholipid
PLOO•	peroxyl radical
PLOOH	PL peroxides
PP	phenylpyruvate
PPP	pentose phosphate pathway
PUFA	polyunsaturated fatty acid
QA	quinolinic acid
RBC	red blood cell
ROS	reactive oxygen species
Sesn2	Sestrin2
TAMs	tumor-associated macrophages
TCDD	2,3,7,8-tetrachlorodibenzo-p-dioxin
TCR	T cell receptor
TDO2	tryptophan dioxygenase
TLR	Toll-like receptor
TME	tumor microenvironment
TNFR	TNF receptor
TRE	tetracycline response element
Tregs	regulatory T cells
Trp	tryptophan
WT	wild type
XRE	xenobiotic-responsive element
ZnPP	Zinc protoporphyrin

1. Introduction

1.1. Balance between immunity and regulation of immune responses

The function of the immune system is to protect the organism from infection with bacteria, viruses, fungi and parasites. The immune system must recognize and eliminate these pathogens but also distinguish harmful pathogens from commensals. Cells of the innate immune system recognize molecular patterns that are broadly conserved between pathogens, termed pathogen-associated molecular patterns (PAMPs), via receptors including the family of toll-like receptors (TLRs) and NOD-like receptors (NLRs), which recognize bacterial lipopolysaccharide (LPS) components and many other molecules specific to bacteria, viruses, fungi and parasites [1,2]. By contrast, cells of the adaptive immune system, B lymphocytes (B cells) and T lymphocytes (T cells), possess highly specific receptors to recognize distinct antigens. The diversity of these receptors is constructed by genetic rearrangements during the development of B cells and T cells in the primary lymphoid organs, bone marrow and thymus respectively [3].

Stimulation of an immune response eventually leads to the activation of destructive mechanisms that aim to neutralize and kill the pathogen or pathogen-infected cells, including for example the generation of free radicals like nitric oxide and superoxide, or the induction of programmed cell death [4,5]. Therefore, if temporally or spatially dysregulated, the immune system can cause severe damage to the specific tissues or the entire organism. Thus, immune responses need to be tightly controlled to maintain the delicate balance of effective immunity versus the prevention of self-destruction (Figure 1). By extension, the immune system must also develop tolerance to self-antigens to avoid autoimmunity characterized by the attacking and destruction of the body's own structures [6]. The genetic rearrangements during B and T cell receptor development can not only generate receptors that recognize pathogens but also lead to the emergence of receptors that recognize self-antigens. While most self-reactive lymphocytes are eliminated during their development [7,8], residual self-reactive lymphocytes can egress from the primary lymphoid organs. These self-reactive lymphocytes must be controlled to prevent autoimmunity, a process known as peripheral tolerance, which involves specialized regulatory immune cells including regulatory T cells (Tregs) or tolerogenic dendritic cells (DCs), as well as regulatory cytokine mediators such as IL10 or TGF β [9,10]. Besides the prevention of autoimmunity, immunoregulatory processes are required for the termination of inflammatory processes to limit overshooting immune responses and to allow wound healing. Uncontrolled release of pro-inflammatory cytokines, a so-called cytokine storm, can lead to multiorgan failure and death [11]. Moreover, effective immunoregulatory mechanisms are essential for successful organ transplantation since the undesirable activation of immune responses against the graft tissue leads to transplant rejection [6]. However, while it is required

to limit immune responses to prevent self-damage, loss of the balance favoring immunoregulatory pathways can also be detrimental since the immune system's function to control infectious diseases and to eliminate pathogens can be corrupted leading to uncontrollable pathogen spread and chronic infections. Additionally, in cancer, tolerogenic processes in the tumor micro environment (TME) reduce immune responses towards malignant cells facilitating tumor progression [12].

Cells and pathways involved in the modulation of immune responses therefore represent a vast array of existing and promising new targets for the treatment of several diseases. While for organ transplantation and treatment of autoimmune diseases therapies aim to limit immunity and enforce immunoregulatory mechanisms, approaches targeting the immune system in cancer therapy aim to restore immune responses towards the tumor tissue by blocking regulatory pathways. Prominent examples for molecules currently targeted in cancer immunotherapy are Cytotoxic T-Lymphocyte-Associated Protein 4 (CTLA-4) and Programmed Cell Death Protein 1 (PD-1), two proteins expressed on the surface of T cells and associated with the activation of regulatory immune checkpoints [13]. Yet, inhibition of these immune checkpoints is only effective in a subset of cancer patients and the treatments can be associated with the occurrence of severe adverse events [14,15]. Nevertheless, further immunoregulatory pathways exist and may include additional targets that can be exploited for the treatment of cancer or further diseases.

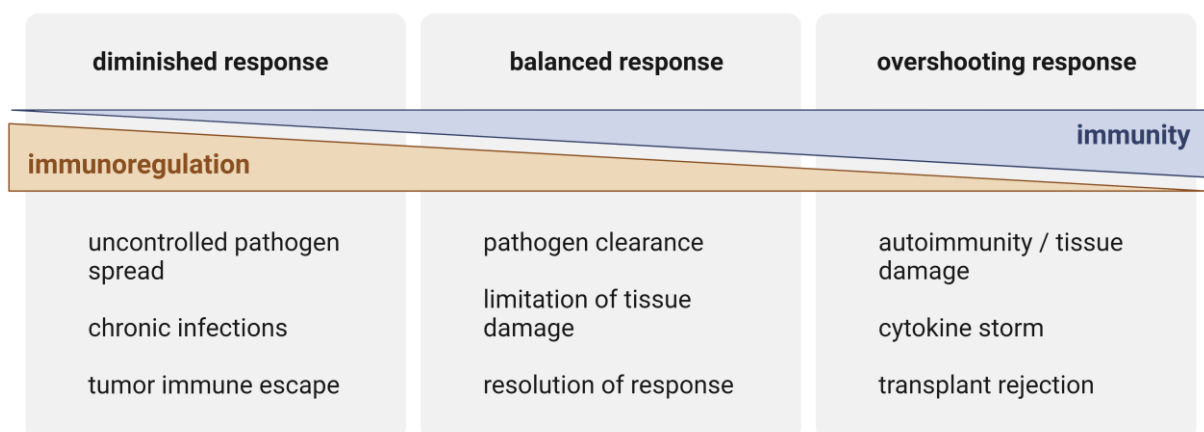


Figure 1 Balance of immune responses

1.2. Immune regulation by amino acid metabolism

Regulated amino acid metabolism in immune cells has evolved as one way of contributing to the control of immune responses. 9 of the 20 proteinogenic amino acids are essential, meaning that we cannot produce them and therefore require their uptake by nutrition. The requirement of nutrient uptake from an external supply is termed auxotrophy. Most cells of the immune system are also auxotrophs for many of the non-essential amino acids [16]. Amino acid availability can therefore represent an important factor controlling immune cell activity. In

immunoregulatory pathways, arginine (Arg) and tryptophan (Trp) represent key regulatory hubs as immune cells, mostly myeloid cells, can control the expression of enzymes metabolizing Arg and Trp (Figure 2). These enzymes are highly regulated and comprise the Arg metabolizing enzymes inducible nitric oxide synthase (iNOS), arginase-1 and arginase-2 (Arg1 and Arg2), and the Trp metabolizing enzymes indoleamine 2,3-dioxygenases IDO1 and IDO2 [16]. Another regulatory enzyme involved in amino acid metabolism is interleukin 4 induced 1 (IL4i1), which in contrast to the other enzymes is a secreted protein, suggesting that it acts in the extracellular space. IL4i1 is also an exception to the ‘Arg-Trp’ rule, since its main substrate was described to be phenylalanine (Phe) [17]. However, IL4i1 also metabolizes Trp and recent research by us and others suggests that Trp metabolism is central to key effects of IL4i1 [18,19].

To understand how amino acid metabolism by these enzymes regulates immune responses, we have to consider that two potentially regulatory processes happen at the same time: On one hand, the enzymes deplete their amino acid substrate(s) from the local environment and on the other hand they generate products that can serve as downstream mediators of immunomodulatory effects. While the depletion of amino acids can lead to the activation of common stress sensing pathways, the generated metabolites are specific for each enzyme and can activate distinct immunoregulatory downstream signals. These concepts are developed further in the following sections of my thesis.

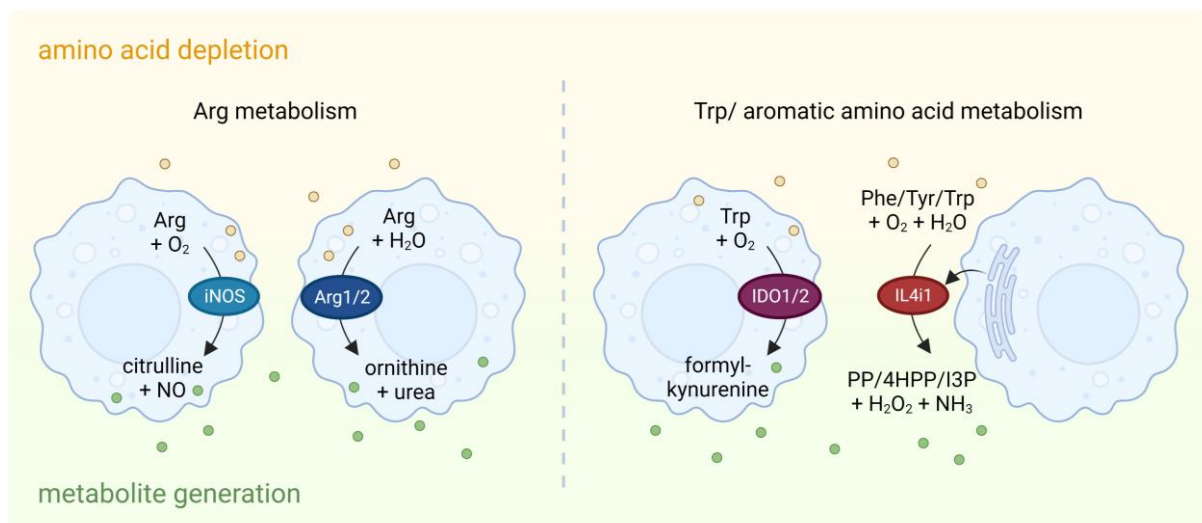


Figure 2 Immunoregulatory amino acid-metabolizing enzymes expressed by immune cells

Overview of amino acid-metabolizing enzymes expressed by immune cells and the catalyzed reactions leading to local amino acid depletion and enrichment of metabolites, which can both contribute to the immunoregulatory effects.

1.2.1. Arginine metabolism in myeloid cells by inducible nitric oxide synthase and arginases

Arg metabolism by inducible enzymes has most extensively been studied in macrophages over the last decades [16]. Expression of inducible nitric oxide synthase (iNOS; also NOS2) and the following generation of nitric oxide (NO) is an important marker of the pro-inflammatory M1 macrophage phenotype [20]. iNOS, as well as other NOS enzymes, catalyzes the degradation of Arg to produce NO and citrulline. However, while the other NOS isoforms NOS1 and NOS3 are constitutively expressed at low levels in different cell types, iNOS can be induced by different pro-inflammatory stimuli such as TLR agonists, IFN γ and TNF, and subsequently metabolizes Arg [21]. The production of NO in myeloid cells is important for the killing of microbes, especially intracellular bacteria, and additionally serves several signaling functions [22]. Although iNOS expression is strongly associated with the pro-inflammatory M1 macrophage phenotype, it also mediates immunoregulatory effects. NO generation can interfere with T cell activation at the level of the IL2 receptor signaling cascade [23,24] and is suggested to be involved in negatively regulating the emergence of further inflammatory M1-polarized macrophages [25]. High levels of NO however can also mediate toxic effects towards the producer cells e.g. by poisoning the respiratory chain which forces the cells to switch to glycolytic metabolism in order to survive [26-28]. iNOS activity can be regulated by upregulation of arginase expression in macrophages leading to competition for available Arg [27,29,30], which may be advantageous for iNOS-expressing cells but can also lead to insufficient host responses to pathogens as observed in *Mycobacterium tuberculosis* infections [29]. In terms of Arg metabolism in macrophages, the field often encounters a general misconception [16]: Arg metabolism in macrophages is often considered as a dualistic process, where pro-inflammatory M1 macrophages express iNOS to generate NO, whereas the 'alternatively activated' M2 macrophages associated with type-2 immunity (e.g. in parasite infections, allergy or tissue repair) express Arg1 to hydrolyze Arg [31,32]. However, as mentioned above, Arg1 is also expressed in M1-type macrophages, and its expression is often much higher than in M2 macrophages (which do not express iNOS) [27]. In M1 macrophages, Arg1 expression is mediated by combinations of IL6, G-CSF and IL10 via the transcription factor STAT3 [27,30]. Thus, Arg1 can limit iNOS activity by competing for the intracellular Arg. Nevertheless, in mice, Arg1 expression is strongly linked to the regulation of type-2 immune responses and also induced by the IL4/IL13 signaling pathway via STAT6 which is also promoting the emergence of M2 macrophages [20].

Arginases catalyze the hydrolysis of Arg while generating ornithine and urea. While Arg1 is a cytosolic enzyme, Arg2, the second arginase isoform, is localized in mitochondria [33]. Arg1 is essential for survival as it is required for ammonia detoxification via the urea cycle [34]. The generation of mice with a macrophage-specific deletion of Arg1 was used to investigate

functions of the enzyme in immune responses [29,35]. Arg1 expression in macrophages upon infections associated with Th2 responses and M2 polarized macrophages such as *Schistosoma mansoni* infection limits tissue damaging T cell responses by inhibiting T cell proliferation, promoting Treg emergence and suppressing Th17 cell differentiation [35,36]. T cell proliferation could be restored by increased levels of Arg, suggesting that Arg depletion is the main effector pathway mediating the regulatory effects [35]. Indeed, other studies report that Arg1-mediated regulation of immune responses, especially T cell responses, is due to Arg depletion [37-40]. Sensing and downstream effects of Arg deprivation will further be described in section 1.2.3. Compared to Arg1, the role of the mitochondrial Arg2 isoform in immunoregulation has not been studied as extensively. However, Arg2-deficient mice exhibit increased plasma levels of Arg arguing that the enzyme is also contributing to the regulation of Arg levels [41]. Yet, our current knowledge of the regulation of Arg2 in immune cells is limited. A recent study reported the upregulation of Arg2 by IL10 in macrophages encountering LPS, which was linked to anti-inflammatory metabolic reprogramming of the cells [42]. Moreover, during maturation of dendritic cells Arg2 levels are repressed by microRNA155 (miR155). Loss of miR155 causes increased Arg2 expression, which in turn limits T cell proliferation by Arg depletion [43], suggesting that both arginase isoenzymes mediate immunoregulatory effects via arginine depletion. The generation of ornithine by arginases may also be involved in tissue repair and wound healing processes [44], but the direct regulation of immune cells by arginases has mainly been linked to the deprivation of Arg. This can serve two important modulatory functions consisting of 1) the limitation of potentially toxic NO generation under conditions where iNOS is upregulated and 2) the regulation of T cell responses by activating pathways that sense the limitation of amino acids (described in 1.2.3).

1.2.2. Tryptophan metabolism by indoleamine 2,3-dioxygenases

Alongside with Arg metabolism, the degradation of Trp represents a main regulatory node in control of immune responses. The two heme-dependent enzymes IDO1 and IDO2 catalyze the oxidation and thereby the breakage of the Trp indole ring. This leads to the generation of N-formyl-kynurenine, which is rapidly deformed into kynurenine, serving as the basis for the generation of further downstream kynurenine metabolites, such as kynurenic acid, 3-hydroxykynurenine or 3-hydroxyanthranilic acid in the so-called kynurenine pathway (Figure 3). Moreover, kynurenines can be converted into quinolones which are required for *de novo* NAD⁺ biosynthesis [45]. A further enzyme that can catalyze the same reaction as IDOs is the tryptophan dioxygenase (TDO2), which is mainly expressed in the liver (in normal physiology) where it is responsible for ~90 % of nutritional Trp degradation [46]. However, TDO2 expression in various cancer tissues, is associated with tumor immune resistance [47]. The genes encoding IDO1 and IDO2 are located in a tandem arrangement on the same chromosome, suggesting they may have evolved from a common ancestral gene [48,49]. Yet,

compared to IDO1, IDO2 exhibits a much lower catalytic activity (K_m 500 – 1000 fold lower) [48]. IDO1 expression is inducible in a broad range of tissues and is frequently found in myeloid immune cells, including different subsets of DCs, myeloid-derived suppressor cells (MDSCs) and macrophages [50-55]. IDO2 expression was initially found in kidney, epididymis, testis and liver [56], but may also be expressed in activated B cells and DCs [49,57]. In the context of immune regulation, the role of IDO2 is not very well understood and controversially discussed since IDO2 expression was also found in the context of autoimmunity [58]. Moreover, it is possible that IDO2 mainly acts independent of its weak enzymatic activity [59,60]. In contrast, IDO1-dependent immunoregulatory mechanisms were well characterized over the last three decades. IDO1 is highly inducible in various tissues and the strongest regulation of IDO1 expression is mediated by interferons (IFNs), especially IFN γ , via the transcription factor STAT1 which can induce thousands of fold increases in IDO1 transcript amounts [45,61]. Furthermore, CTLA-4 binding to CD80/CD86 on DCs can upregulate IDO1, which can occur in an IFN γ -dependent and independent manner [62,63]. While IDO1-mediated Trp depletion was first described to interfere with intracellular pathogen growth in the 1980s [64-66], the immunoregulatory potential of IDO1 was discovered later in the 1990s. Based on the use of first generation IDO inhibitors, Munn et al. proposed that IDO1-dependent Trp metabolism was required for immune tolerance in pregnancy towards allogenic fetuses [67] and additionally linked the catalytic activity of IDO1 to the limitation of T cell proliferation [68]. Yet, these early discoveries on IDO1 need to be interpreted with caution as there are doubts about the efficacy and specificity of the IDO1 inhibitor 1-methyl-tryptophan [61,69] and mice lacking both, IDO1 and IDO2, do not show breeding defects [57,70]. Nevertheless, since the first studies by Munn and colleagues, many studies manifested the important role of IDO1 in regulating immune responses, which comprises for example reduced CD8 $^+$ T cell proliferation [71-73], promotion of Treg differentiation [63,73,74] and suppression of Th17 cells [75,76]. IDO1 does not only affect T cell biology but is also involved in immunologic tolerance in macrophages and DCs. IDO1 expression is required to mediate a tolerogenic macrophage phenotype in response to apoptotic cells [77] and a recent study by Gargaro et al. [53] suggests that IDO1-expressing DCs can also induce IDO1 in other DC subtypes to propagate immune tolerance. Mechanistically, IDO-dependent immune regulation is mediated by both, depletion of Trp (described in detail in the next section) and the generation of kynurenine metabolites, which can act via activation of the immunoregulatory aryl hydrocarbon receptor (AhR) pathway (described in section 1.2.4). Additionally, IDO1 contributes to immunoregulation by signaling functions that do not depend on its enzymatic activity (reviewed by Palotta et al. [78]). Although IDO1 is not the focus of this thesis, understanding the complex literature about this enzyme and Trp metabolism provided important conceptual clues about IL4i1 biology.

1.2.3. Sensing of amino acid depletion and its effects on immune regulation

Cells integrate information about the availability of amino acids for cell fate decisions such as proliferation. Two kinases, general control nonderepressible 2 (GCN2) and mammalian target of rapamycin (mTOR), are involved in the sensing of amino acids and also linked to immunoregulatory effects. Simplistically, while GCN2 gets activated by amino acid deprivation [79], mTOR signaling via the the mTOR complex 1 (mTORC1) is switched off when amino acids, especially leucine (Leu) and Arg, are depleted [80-82]. Although the exact mechanisms of GCN2 activation are not completely understood, the sensing of increased levels of free, uncharged tRNAs (not coupled to an amino acid) is one mechanism involved. Uncharged tRNAs can bind to the histidyl-tRNA-synthetase-like domain of GCN2 leading to conformational changes of the protein and activation of the kinase domain [83]. Once activated, GCN2 phosphorylates a serine residue (serine 51 in humans/ serine 52 in mice) of the eukaryotic translation initiation factor eIF2 α , which blocks the initiation of protein translation by preventing the assembly of a functional eIF2–GTP–methionyl-initiator tRNA ternary complex. However, while blocking most mRNA translation, reduced availability of ternary complexes paradoxically also increases the translation of distinct transcripts associated with stress responses such as the transcription factors ATF4 and CHOP [84]. Upregulation of CHOP is suggested to be a marker for GCN2 activation in T cells [72], which in turn is proposed to mediate several immunoregulatory effects. Early studies from Munn et al. [72] and Rodrigues et al. [37], suggested that GCN2-dependent sensing of Trp depletion by IDO1 or Arg starvation suppresses T cell proliferation. Notably, the proliferative arrest was not directly caused by the lack of the amino acids as missing ‘building blocks’ for protein synthesis as GCN2-deficient T cells could still proliferate under these Trp or Arg limiting conditions [37,72]. However, this is controversially discussed as other studies could not observe a rescue of T cell proliferation in GCN2-deficient T cells under conditions where amino acid availability was restricted [85,86], suggesting that further amino acid sensing mechanisms, such as mTORC1 deactivation may be involved. Another possibility is that additional signals are required to mediate GCN2-dependent control of T cell biology. As stated before, we need to consider that immunomodulatory, amino acid depleting enzymes simultaneously generate metabolites that could contribute to the immunosuppressive effects. This concept is promoted by a study from Fallarino and colleagues showing that GCN2-dependent down-regulation of the T cell receptor (TCR) ζ -chain induced by IDO1 in CD8⁺ T cells required a combination of low Trp levels and the presence of kynurenines (IDO-dependent Trp metabolites) [73]. In addition, the study reported a synergism of low Trp levels and kynurenines on the differentiation of CD25⁺ Foxp3⁺ regulatory T cells [73]. Moreover, we could recently show that kynurenine can indirectly promote GCN2 signaling by competing with cysteine uptake [61]. Thus, it is possible that in the context of IDO1, kynurenine generation may be required to support the Trp starvation

induced GCN2-activation. Besides direct effects on T cell biology, a study from Halaby et al. [87] proposes that GCN2 is driving immunosuppressive macrophage and MDSC function. In macrophages, an IDO1-dependent GCN2 activation can induce a tolerogenic phenotype characterized by the production of anti-inflammatory IL10 and suppression of IL12 [77]. GCN2 also promoted increased tumor infiltration by MDSCs upon Arg depletion with pegylated Arg1 [39]. Thus, GCN2 activation by regulated amino acid metabolism may also contribute to the suppression T cell responses by promoting immunosuppressive myeloid cells.

By contrast to GCN2, the mTORC1 kinase complex integrates information about sufficient nutrient availability, including amino acid sufficiency, and thereafter promotes translation and cell division. Activated mTORC1 phosphorylates the ribosomal protein p70 S6 kinase (S6K) and (hyper)phosphorylates the eukaryotic translation initiation factor eIF4E binding proteins (4EBPs), which leads to release of eIF4E for the initiation of cap-dependent mRNA translation [88]. Upon amino acid starvation mTORC1 signaling gets deactivated – the extent of the effect however depends on the specific amino acid that is depleted. In this regard, withdrawal of Arg or Leu most potently suppresses mTOR activity [80]. The importance of mTORC1 in immune regulation is highlighted by the fact that rapamycin was found to be an effective immunosuppressant even before its target mTOR (mammalian target of rapamycin) was discovered [89]. Rapamycin can block the G1- to S-phase transition in IL-2 stimulated T cells [90,91] and was found to promote T cell anergy [92]. In line with this, genetic manipulation of TORC1 signaling revealed its requirement for the exit of naïve T cells from quiescence and proliferation upon antigen stimulation [93]. Additionally, while loss of mTOR in CD4⁺ T cells does not prevent the development of T cells, it promotes the differentiation of Foxp3⁺ Tregs and interferes with the emergence of Th1, Th2 and Th17 effector T cells [94]. Inhibition of mTOR signaling via amino acid starvation has been linked to infectious tolerance by Cobbold et al. [85]: This study showed that Tregs induce the expression of amino acid-metabolizing enzymes, including Arg1, iNOS, IDO1 and IL4i1, in DCs to limit T cell proliferation. Moreover, the authors linked the inhibition of mTOR signaling by amino acid starvation (in synergy with TGF- β signaling) to Treg differentiation. This suggests that Treg-induced amino acid consumption by myeloid cells can propagate the emergence of further regulatory T cells. Therefore, the depletion of amino acids from the local environment by upregulation of amino acid-metabolizing enzymes represents a powerful way of regulating immune responses. Signals of limited amino acid availability can be integrated by the kinases GCN2 (activated by amino acid limitation) and mTOR (inhibited by amino acid limitation) which promote immunoregulatory mechanisms such as decreased effector T cell proliferation and modulation of T cell differentiation towards regulatory T cell subsets.

1.2.4. Regulation of immune responses by kynurenines

1.2.4.1. The Kynurenine (Kyn) pathway

Besides amino acid depletion, the metabolites generated by amino acid catabolizing enzymes can have immunoregulatory functions. In this regard, kynurenines generated by IDO1 (and TDO2) exhibit a potent immunomodulatory potential, which I will address in the following sections. The kynurenine pathway is the major Trp-catabolizing pathway in mammals (Figure 3) [46]: The rate limiting reaction, the oxidative conversion of Trp to N-formyl-kynurenine is catalyzed by the IDO or TDO enzymes. N-formyl-kynurenine is then deformylated by the arylformamidase, a constitutively-expressed enzyme, to generate kynurenine (Kyn). In the main arm of the Kyn pathway, Kyn is converted into 3-hydroxykynurenine (3HK) and further into 3-hydroxyanthranilic acid (3HAA). Subsequently, 3HAA is degraded to the instable metabolite 2-amino-3-carboxymuconic semialdehyde, which can undergo non-enzymatic cyclization to form quinolinic acid (QA), which is used for the biosynthesis of NAD⁺ or can be converted via further enzymatic reactions to picolinic acid. In another arm of the Kyn pathway, Kyn is metabolized to kynurenic acid (KynA) which is catalyzed by isoforms of Kyn aminotransferase (KAT) enzymes. The latter two metabolites, Kyn and KynA, are endogenous ligands of the aryl hydrocarbon receptor (AhR), a key ligand-activated transcription factor involved in a multitude of physiological functions including immune regulation [95].

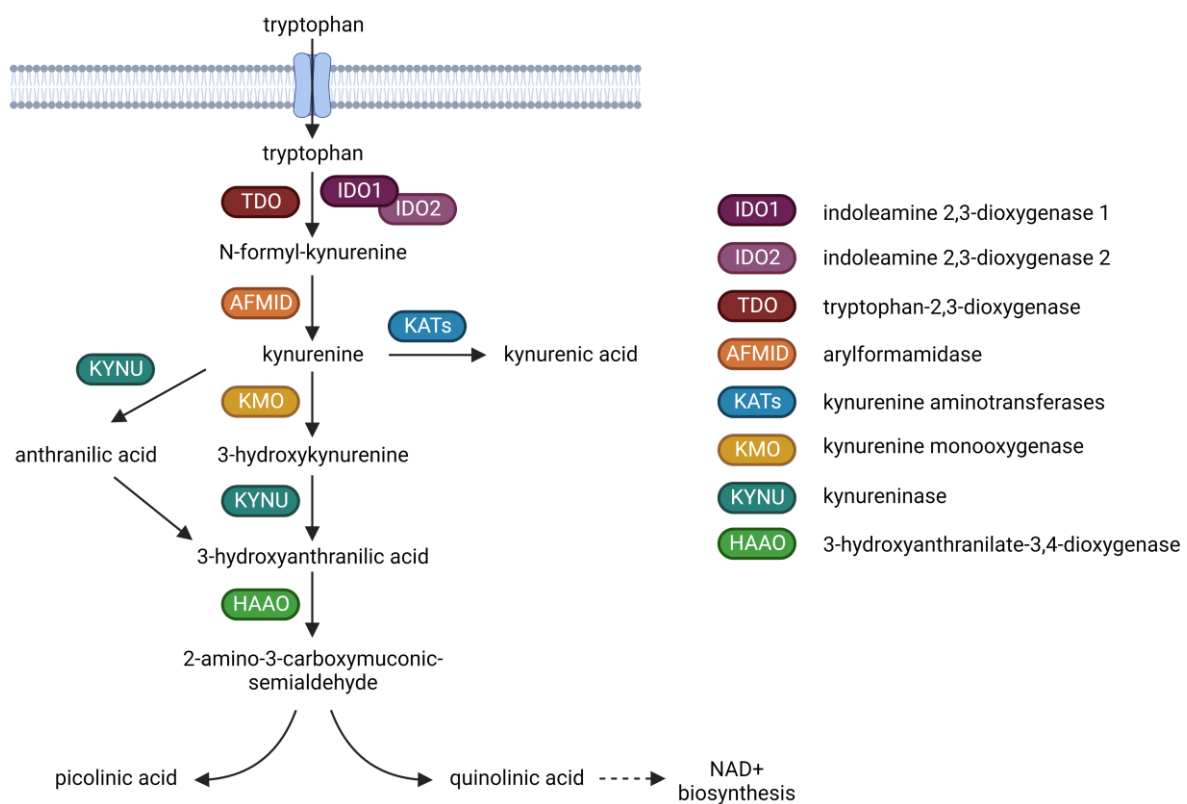


Figure 3 Overview of the kynurenine pathway adapted from Fiore & Murray [45]

1.2.4.2. The aryl hydrocarbon receptor pathway

The AhR is a ligand-activated transcription factor that is associated with the sensing of environmental signals including exogenous environmental toxins, but also endogenous stimuli [96]. The receptor was initially discovered to bind the toxin 2,3,7,8-tetrachlorodibenzo-p-dioxin (TCDD) [97] and is therefore also known as the dioxin receptor. Although AhR was first identified as a receptor involved in the sensing of xenobiotic agents, subsequent research revealed that AhR also has physiological ligands that derive from dietary uptake, microbiota, or can be generated endogenously [98]. Especially Trp and indole metabolites were found to activate the AhR pathway [99]. While most of these ligands seem to be generated by microbiota, the expression of IDO/TDO also generates AhR ligands via Trp catabolism. In the Kyn pathway, the metabolites Kyn and KynA were found to serve as endogenous AhR agonists [100-103].

When not activated by ligands, AhR is retained in the cytoplasm in a complex consisting of the 90-kDa heat shock protein (HSP90) [104], the co-chaperone p23 [105], the AhR-interacting protein (AIP, also XAP2) [106] and the protein kinase c-Src [107] (Figure 4). Herein, AIP binding plays an important role in the regulation of cellular AhR levels as it prevents proteasomal degradation of the receptor [108]. AhR ligand binding induces the dissociation of the complex, allowing the receptor to translocate into the nucleus. In the nucleus, AhR can bind to its co-factor AhR nuclear translocator (ARNT) to induce transcription of target genes by binding to the dioxin- or xenobiotic-responsive element (DRE or XRE) [109]. Finally, AhR is exported from the nucleus, ubiquitinated and degraded by the proteasome [110]. Target genes of AhR include e.g. enzymes that are involved in xenobiotic detoxification such as members of the cytochrome P450 family-1 (CYP1) CYP1A1, CYP1A2 and CYP1B1 or NAD(P)H-quinone oxidoreductases (NQOs). Thereby, AhR ligands can be detoxified/ degraded, which in turn deactivates AhR signaling [111]. A further feedback mechanism limiting AhR signaling is the induction of the AhR repressor (AhRR), which itself is an AhR target gene. By directly binding to ARNT, AhRR limits the formation of AhR/ARNT heterodimers and thereby interferes with the transcriptional activation of AhR target genes [112]. Besides the canonical signaling via ARNT, which likely accounts for the majority of AhR-mediated effects, AhR has also been found to interact with other transcription factors such as the retinoic acid receptor, retinoblastoma protein (Rb), c-Maf or nuclear factor kappa B (NF- κ B) [95]. Moreover, there is evidence for a non-transcriptional pathway mediated by AhR activation. Ligand binding induces the dissociation of the cytoplasmic AhR complex leading to activation and release of the c-Src kinase [107,113]. Activated c-Src has been found to phosphorylate IDO1 upon AhR activation, which was involved in the development of endotoxin tolerance [103].

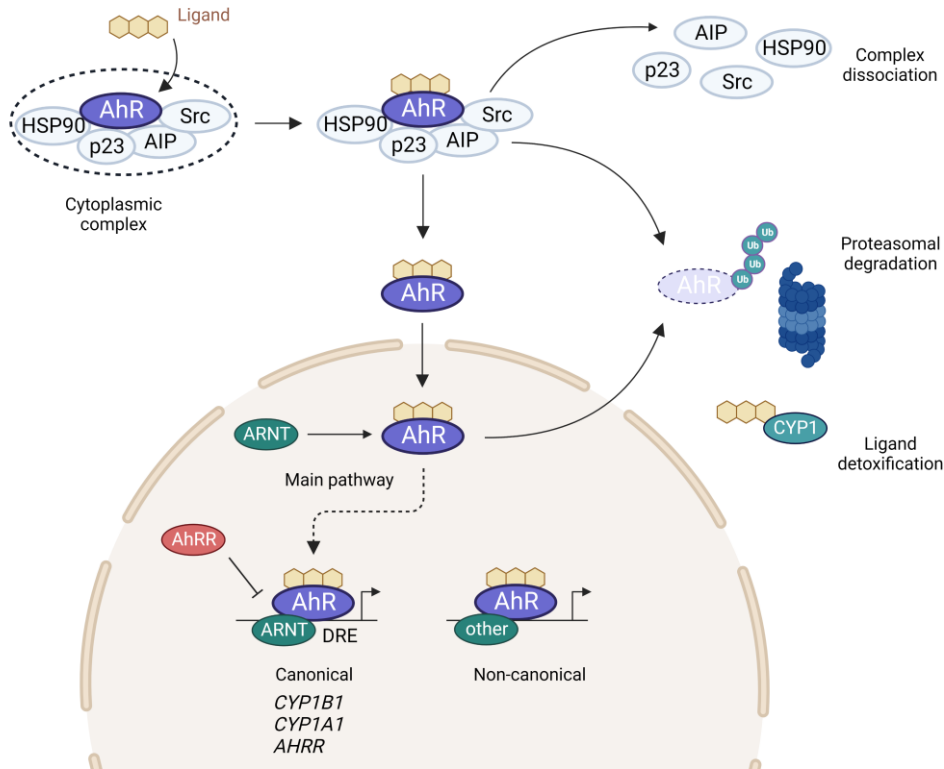


Figure 4 Scheme of the AhR signaling pathway

1.2.4.3. Immunoregulation via AhR signaling

AhR signaling is implicated in immune regulation and the control of T cell biology, which is mediated directly by signaling within T cells and indirectly by AhR activation in antigen presenting cells (reviewed by Gutiérrez-Vázquez [95]). Early research from Kerkvliet et al. [114,115] linked AhR activation by TCDD and further xenobiotic AhR ligands to the suppression of cytotoxic T cell responses. TCDD-mediated suppression of these cytotoxic T cell responses also required AhR expression in CD4⁺ T cells [116], which could subsequently be explained by the discovery that AhR signaling promotes the induction of regulatory T cells [117,118]. Regarding CD4⁺ T cell differentiation, AhR activation is associated with the emergence of regulatory Foxp3⁺ Tregs and Foxp3⁻ IL10⁺ type 1 regulatory T cells (Tr1) but also with the differentiation of the inflammatory Th17 cell subset [118-123]. However, a study from Gagliani et al. [124] reported AhR-dependent conversion of Th17 cells into IL10-producing Tr1 cells, suggesting that AhR signaling is involved in Th17 plasticity and may therefore have a role in the limitation of Th17-mediated inflammation. In line with these regulatory effects, AhR activation *in vivo* promoted transplant tolerance [125] and protective effects in mouse models of autoimmune diseases such as experimental autoimmune encephalitis (EAE) [126], colitis [127] and diabetes [128]. Yet, Th17-mediated autoimmunity has also been observed in association to AhR activation [123], suggesting that under certain conditions AhR signaling can accelerate inflammation. Nevertheless, in most of the studies,

AhR activation is associated with immunoregulatory effects (reviewed by Gutiérrez-Vázquez [95]). As IDO/TDO are the rate-limiting enzymes of the Kyn pathway (Figure 3), they therefore also have a pivotal role in the generation of the endogenous AhR agonists Kyn and KynA [100-103]. Thus, besides Trp depletion, the generation of endogenous AhR agonists is involved in the immunoregulatory effects mediated by the enzymes. Kyn-dependent AhR activation promotes the differentiation of Treg cells whereas it does not induce the emergence of Th17 cells [100]. Kyn is associated with reduced T cell proliferation [129] and decreased cytotoxic T cell infiltration in human gliomas in an AhR-dependent manner [101]. Moreover, AhR activation by Kyn is linked to tolerogenic DC functions. Bessede et al. [103] reported the requirement of IDO1 in conventional DCs (cDCs) which mediated AhR activation by Kyn to induce endotoxin tolerance. A further interesting aspect regarding the connection between IDO and AhR signaling is the fact that IDO1 and IDO2 expression themselves can be induced by AhR activation [53,129-131]. Thus, by generating Kyn and the following activation of AhR, IDO enzymes can induce their further expression. This feed forward loop is linked to the maintenance of IDO expression in tolerogenic DCs [131] and has recently been found to promote IDO expression and tolerogenic reprogramming of other dendritic cell subsets [53] (Figure 5).

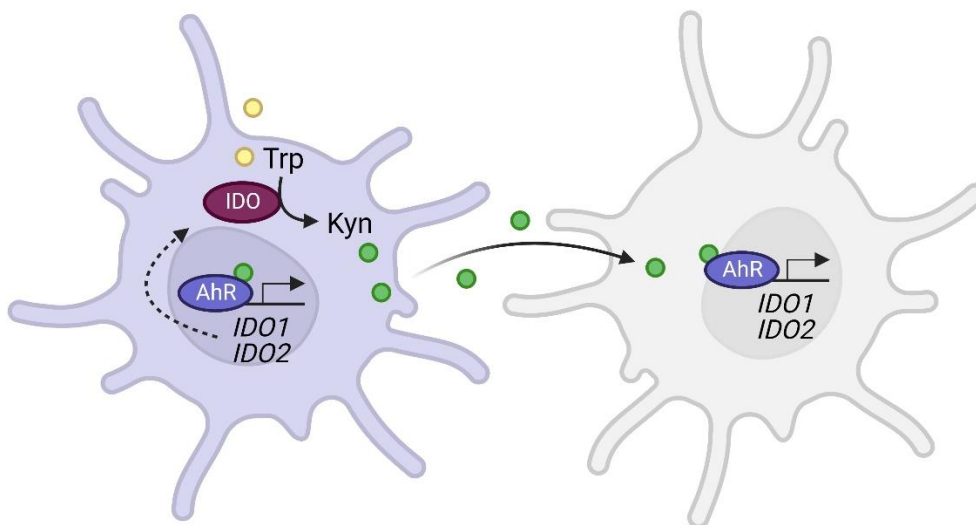


Figure 5 Feed forward loop of IDO maintenance and propagation of IDO expression via AhR activation

1.2.4.4. AhR independent effects of kynurenines

Besides the activation of the AhR pathway, Kyn metabolites may have additional effects on immune cell physiology; these processes are not very well understood. An important aspect seems to be the regulation of cell death and cell survival. The effect of Kyn metabolites has most extensively been studied in the context of the nervous system, as Kyn metabolites can mediate neurotoxicity but also protective effects, which is considered to partly depend on the modulation of the cellular redox balance (reviewed by Mor et al. [132] and Reyes Ocampo et

al. [133]). In regard to the immune system, the Kyn metabolites 3HAA and QA were found to induce apoptosis in thymocytes and Th1 cell clones at ~10 μ M, while on the other hand not killing Th2 cells, suggesting that the metabolites mediate a context specific toxicity [52]. However, the exact mechanisms underlying apoptosis induction by the metabolites remain unclear. As mentioned above, Kyn pathway metabolites may be involved in the regulation of the cellular redox state. Many of these Kyn metabolites were found to have anti-oxidative properties, including for example free radical scavenging activity, but in other studies the same metabolites promoted oxidative stress [132,133]. This suggests that the effects of the metabolites may be highly dependent on the cellular context and further research will be required to dissect the underlying mechanisms. Recently, we could show that IDO1-dependent Trp metabolism could protect tumor cells from ferroptosis (a form of oxidative cell death further described in section 1.3) by the generation of the Kyn pathway metabolites Kyn, 3HK and 3HAA, which activated anti-oxidative stress pathways and scavenged free radicals [61]. Yet, whether these findings are transferable to immune cells such as T cells or myeloid cells is currently under evaluation by our group. Nevertheless, as redox homeostasis is involved in the regulation of immune responses (reviewed by Gostner et al. [134]), Kyn metabolite-dependent redox modulation may be a further aspect of Trp metabolism in immunoregulation. Taken together, the findings of many studies reveal the potential of Trp metabolism in immune regulation, which is not only mediated by the depletion of Trp, but also by the generation of immunomodulatory Kyn metabolites. Most importantly, Kyn and KynA can act as ligands of the AhR, which for instance promotes regulatory T cell differentiation. Yet, Kyn metabolites may also serve further AhR-independent regulatory functions, involving for example the cellular redox balance, which however require further investigation.

1.2.5. Arginine and tryptophan metabolizing enzymes in cancer

Immunoregulatory mechanisms are essential to prevent autoimmunity and overshooting immune responses. However, a strong suppression of the immune response can also have detrimental effects. In the context of cancer, chronic inflammation is known to promote the development of tumors, while at later stages the evasion of immune responses is considered to be a hallmark of cancer [135]. Therefore, it is not surprising that elevated Trp and Arg catabolism, which is commonly associated with the TME [136], is linked to decreased immune responses towards the tumor by the mechanisms described above (reviewed by Lemos et al. [137]). Expression of amino acid-metabolizing enzymes such as Arg1 and IDO1 is found in myeloid cells infiltrating the tumor and in tumor-draining lymph nodes, but in tumor or stroma cells [137]. Additionally, TDO2 expression, which is usually not found in immune cells, is elevated in several tumors [138] and associated with reduced immune response, malignant progression and poor survival, especially in malignant brain tumors such as gliomas [101]. In

addition to the suppression of the immune response towards tumors, Trp catabolism can also directly affect tumor cell biology. IDO1/TDO2-mediated Trp catabolism can enhance tumor cell migration, invasiveness and metastasis formation [101,139,140]. Moreover, *de novo* NAD⁺ synthesis from Trp via the Kyn pathway was found to promote resistance of glioma cells towards oxidative stress induced by radiochemotherapy [141]. Taken together, these results suggest that immunomodulatory amino acid metabolism can be 'hijacked' by cancer cells to evade immune responses and drive tumor progression, for example by increasing the tumor cell invasiveness and resistance to stress. Therefore, arginases and the IDO/TDO enzymes are considered to be targets for cancer therapy [138,142]. Especially inhibition of IDO1 by several inhibitors including epacadostat and BMS986205 has been tested in multiple clinical trials. However, despite promising data from phase I/II clinical trials, a phase III trial combining epacadostat with a PD-1 blocking antibody in metastatic melanoma patients failed and led to the termination of other phase III trials that combined BMS986205 with immune checkpoint inhibitors [138]. Yet, there is much criticism of the overall study designs, including for example the fact that patients in the study have not been tested for IDO1 expression in the tumor or the tumor draining lymph nodes [143], suggesting that IDO1 may still represent a promising target in cancer therapy.

1.2.6. The L-amino acid oxidase IL4i1

Besides iNOS, arginases and IDO enzymes a further amino acid-metabolizing enzyme is found to be expressed in immune cells and associated with immune regulation. Thus far, the L-amino acid oxidase (LAAO) IL4i1 has not been as extensively studied as the aforementioned enzymes. Nevertheless, several studies suggest an involvement of IL4i1 in immunoregulatory processes. In contrast to iNOS, arginases and the IDO enzymes, IL4i1 is secreted [17], suggesting that the enzyme is active in the extracellular space. In general, LAAOs are dimeric enzymes that catalyze the oxidative deamination of L-amino acids generating the respective α -keto acids, hydrogen peroxide and ammonia (Figure 6A). Most LAAOs including IL4i1 are dependent on the cofactor flavin adenine dinucleotide (FAD) [144]. During the enzymatic reaction, the amino acid is first oxidized to form an imino acid intermediate while FAD is reduced to FADH₂. Subsequently, the imino acid undergoes non-enzymatic hydrolysis generating an α -keto acid and ammonia, and FAD is recovered by the generation of hydrogen peroxide (H₂O₂) from molecular oxygen [145] (Figure 6A). The main amino acid substrate metabolized by IL4i1 was reported to be Phe, which is converted into the α -keto acid phenylpyruvate (PP). However, the other two aromatic L-amino acids tyrosine (Tyr) and Trp can also be metabolized by IL4i1 to generate 4-hydroxyphenylpyruvate (4HPP) and indole-3-pyruvate (I3P) respectively (Figure 6B) [17,19,146]. Another study reports weak IL4i1 activity towards Arg [147], suggesting that although IL4i1 clearly exhibits the highest activity towards Phe, this amino acid is not the only IL4i1 substrate.

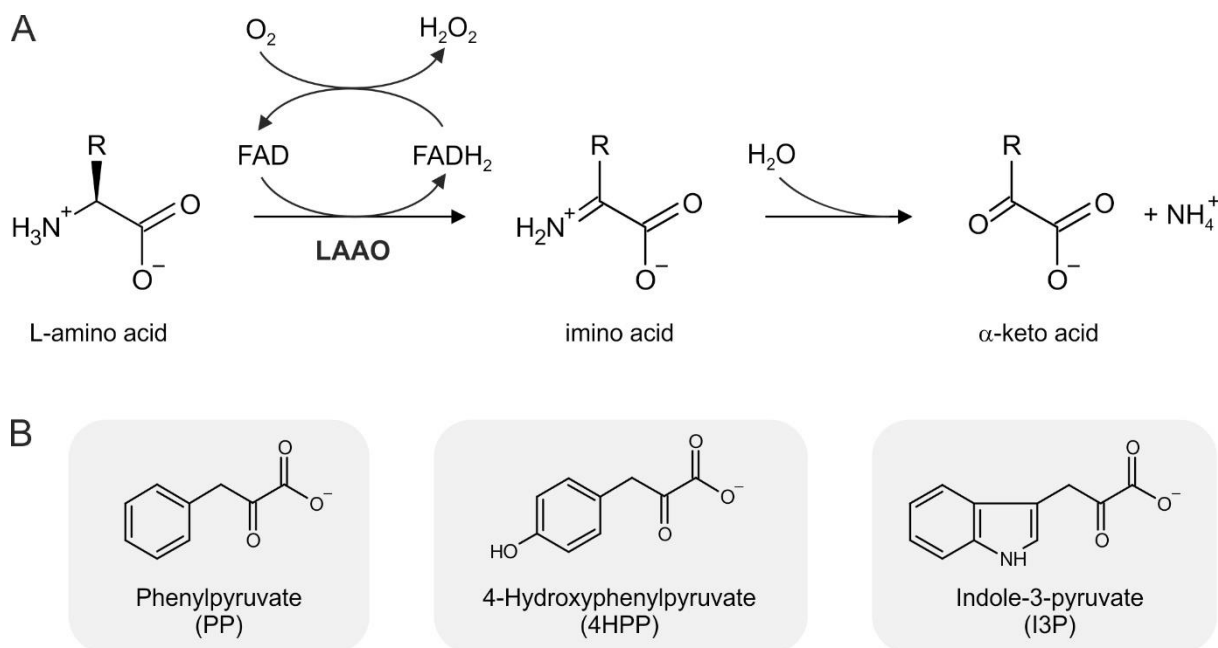


Figure 6 Enzymatic activity of L-amino acid oxidases

(A) Oxidative deamination reaction catalyzed by LAAOs (B) Aromatic α -keto acids generated by IL4i1

1.2.6.1. L-amino acid oxidases in snake venoms

LAAOs are found in many different organisms including not only vertebrates but also plants, bacteria and fungi, and probably gained most attention as a component of snake venoms [148]. Snake venoms consist of many different factors including e.g. phospholipases, metalloproteases, three-finger toxins (3FTxs) and LAAOs [149,150]. The percentage of LAAO in the total snake venom composition can largely vary within different species and lies between 1% in some venoms and 30% in the venom of the Malayan pit viper (*Calloselasma rhodostoma*) [151]. LAAOs from snake venoms generally exhibit preferential catalytic activity towards hydrophobic and aromatic L-amino acids, while showing low affinity for polar and basic amino acids [152]. Although phospholipases and 3FTxs, which can independently act as neurotoxins, are considered to mediate the major venom effects [150], it is intriguing that the occurrence of LAAOs is so conserved in the composition of snake venoms. This indicates that the presence of an LAAO is advantageous for venom function. In this regard, snake venom LAAOs are associated with hemorrhage, edema and platelet aggregation [152] and several studies described cytotoxic and apoptotic effects which are primarily linked to the LAAO-mediated generation of H_2O_2 [153-156]. Thus, even though LAAOs may not represent the most potent venom components, they likely mediate certain toxic effects.

Although separated by millions of years of evolution, the sequences of snake venom LAAOs and the mammalian LAAO IL4i1 share multiple conserved amino acid residues (Figure 7). The function of LAAOs in snake venom also raises questions about the potential toxicity of mammalian IL4i1, which can also generate H_2O_2 by catalyzing the same enzymatic reaction

as snake venom LAAOs. Indeed, one study reported that H₂O₂ production promotes antibacterial properties of mammalian IL4i1 [157], an effect that has previously been reported for several snake venom LAAOs [158-160]. Despite these observations, IL4i1-mediated cytotoxicity towards mammalian cells has not been a focus of research so far and may help to better understand the enzyme's function(s). Therefore, one aim of this thesis focused on the investigation of the potential toxicity of mammalian IL4i1 in comparison to an LAAO from snake venom.

<i>C. rhodostoma</i>	1	MNVFFMFSILFLA -----ALGSCADDRNPLAECFOENDYEEFLEIARNGLKATSNP
<i>N. naja</i>	1	-----DDRRSPLEECFOONDYEEFLEIARNGLKKTSNPK
<i>M. musculus</i>	1	MAGLALRI-VLAATLLGLAGSLDWKAASSLNPTKEKCMEDHDYEQLLKVVTLGLNRTSKPQ
<i>H. sapiens</i>	1	MAPLALHLLVLPILLSLVSODWKAERSQDPFEKCMODPDYEQLLKVVTVGLNRTLKPO
<i>C. rhodostoma</i>	53	HVVIIVGAGMAGLSAAYVLAGAGHQVTVLEASERPGRVRYRNEEAGWYANLGPMLPEK
<i>N. naja</i>	35	HVVVVGAGMAGLSAAYVLAGAGHKVTVLEASERVGGRVVTYHNDREGWYVNMGPMLPER
<i>M. musculus</i>	60	KVVVVGAGVAGLVAAKMLSDAGHKVTILEADNRIGGRIFTERDEKGTWIGELGAMRMPSS
<i>H. sapiens</i>	61	RVIVVAGVAGLVAAKVLSDAGHKVTILEADNRIGGRIFTYRDQNTGWIWIGELGAMRMPSS
<i>C. rhodostoma</i>	113	HRIVREYIRKFDLRLNEFSOENDNAWYFIKNIRKKVGEVKKDPLKYPVKPSEAGKSAG
<i>N. naja</i>	95	HRIVREYIRKFGKLNFEFFQENENAWYYINNRKRVWEVKKDPSLLKYVVKPSEEGKSAS
<i>M. musculus</i>	120	HRILHKL CRTI GLNLTOFTQYDENTWTEVHNVKLRNYVVEKMPKLGYNLNNRERGHSP
<i>H. sapiens</i>	121	HRILHKLCOGLGLNLTKFTQYDKNTWTEVHEVVKLRNYVVEKVPKLGVALRPOEKGHSP
<i>C. rhodostoma</i>	173	OLYEESLCKVVEELKRTNCSYILNKYDYTYSTKEYLIKEGDLSPGAVDMI GDLLNEDSGYY
<i>N. naja</i>	155	OLYQESLRKVI EELKRTNCSYILSKYDSYSTKEYLIKEGNLSRGAVDMI GDLLNEDSSYH
<i>M. musculus</i>	180	DIYQMALNKA FKDLKALGCKKAMNKENKHTLLEYLLEEGNLSRPAVQLLGDVMS EGGFFY
<i>H. sapiens</i>	181	DIYQMALNQALKDLKALGCRKAMKKEFERHTLLEYLLGEGNLSRPAVQLLGDVMS EDGFFY
<i>C. rhodostoma</i>	233	VSFIESLKHDDIFAYEKRFDEIVDGMCKLPTAMYRDIQDKVHFNAQVVKIQNDQKVTVV
<i>N. naja</i>	215	LSFIESLKSDFLFSYKRFDEIVGGEDQLPI SMYQAI AETVHLNARVVKIQYDAEKVRVT
<i>M. musculus</i>	240	LSFAEALRAHACLSDRLRYSRIVGGWDLPRALLSSLSGALLLNAPVVSITQGRNDVRVH
<i>H. sapiens</i>	241	LSFAEALRAHSCLSDRLOYSRIVGGWDLPRALLSSLSGLVLLNAPVAMTQGP HDVHVQ
<i>C. rhodostoma</i>	293	YE-T-LSKETPSVTADYVIVCTTSRAVRLKENPPLLPKKAHALRSVHYRSGTKIFLTCT
<i>N. naja</i>	275	YQ-T-PAKTF--VTADYVIVCSTSRARRIYFEPPLPPKKAHTLRSIHYRSATKIFLTCS
<i>M. musculus</i>	300	IATSLH--SEKTLTADVLLTASGPALQRITFSPPLTRKRQEA LRALHYVAASKVFLSFR
<i>H. sapiens</i>	301	IETSPPEARLNKVLKADVLLTASGPVAKRITFSPPLP RHMQEA LRRLHYVPATKVFLSFR
<i>C. rhodostoma</i>	351	TKFWEDDGIHGGKSTTDLPSRFIYYPNHNETNGVGVIIAYGIGDDANEFQALDFKDCADI
<i>N. naja</i>	331	KKFWEADGIHGGKSTTDLPSRFIHYPNHNETTGIGVIMAYVLADDSDFEQALDTKT CADI
<i>M. musculus</i>	358	RPFWEHEHIEGGHSNTDRPSRLIFYPARG--EGSLLLASYTWSDAAPFAGLSTDQTLRL
<i>H. sapiens</i>	361	RPFWREHEHIEGGHSNTDRPSRMIFYPFR--EGALLASYTWSDAAPFAGLSREEARLRL
<i>C. rhodostoma</i>	411	VFNDLSLIHQLPKKDIOFCYPSVIQKWSLDKYAMGGITFTFPYQFQHFSD-PLTASQGR
<i>N. naja</i>	391	VINDLSLIHDLPKREIQALCYP-SIKKWNLDKYTMGSITSFTFPYQFQDYFE-SAAAPVGR
<i>M. musculus</i>	416	VLQDVAALHGP-V-VFRLWDGRCVVKRWAEDPHSQGGFVVPPLYGREAEYDWSAPFGR
<i>H. sapiens</i>	419	ALDDVAALHGP-V-VRQLWDGTCVVKRWAEDQHSQGGFVVPPEALWQTEKD-DWTVPYGR
<i>C. rhodostoma</i>	470	IYFAGEYTAQAHGWIDSTIKSGLRAARDVNLA---SENPSGIHLSNDNE-----
<i>N. naja</i>	449	IHFAGEYTGREHGWIDSTIMTGLRAARDVNRA---SQKPSKIRLISDNQ-----
<i>M. musculus</i>	474	IYFAGEHTALPHGWVETAVKSGLRAAVRINNNYGYGEVDPQMMEHAYAEANYLDQYPEGE
<i>H. sapiens</i>	476	IYFAGEHTAYPHGWVETAVKSALRAAIKINSRKGPASDTASPEGHASDMEGQGHVHGVAS
<i>C. rhodostoma</i>	516	-----
<i>N. naja</i>	495	-----
<i>M. musculus</i>	534	RPEEQQAREEVS PDEQEP SHKHLVETSEEGQOHAFVEAIP ELQGHV FVETVPQEKGH AH
<i>H. sapiens</i>	536	----- SPSHDLAKEEGSHPPVQGLSLQ -----
<i>C. rhodostoma</i>	516	----- L
<i>N. naja</i>	495	----- L
<i>M. musculus</i>	594	QNIYPSEHVQVHGEV IPEWHGHGGSGTFQMHRVGDHS
<i>H. sapiens</i>	559	----- NTTHTRTS ----- H

Figure 7 Alignment of snake venom LAAOs with murine and human IL4i1

Alignment of murine and human IL4i1 (UniProt ID O09046 and Q96RQ9 respectively), Malayan pit viper (*Calloselasma rhodostoma*) LAAO (UniProt ID P81382) and Indian cobra (*Naja naja*) LAAO, which was investigated herein. The authentic *Naja naja* LAAO sequence was determined by a combination of genetic approaches and mass spectrometry, and provided by our collaborators [149].

1.2.6.2. Discovery of IL4i1 and its LAAO function

IL4i1 was discovered in 1997 by Charles Chu and William Paul [161] as a gene that could be induced by IL4 in murine B cells. This led to its name interleukin-four induced gene 1, which the authors first abbreviated to 'Fig1'. However, a few years later another study by the Chu group [146] introduced the abbreviation IL4i1 (in accordance with the recommendations from the Human Gene Nomenclature Committee), which has been used since then. Chu et al. already noted a signal sequence for translation into the endoplasmic reticulum and described homology to the LAAO-related monoamine oxidases, particularly in FAD binding domains, which led them to speculate that IL4i1 was a secreted FAD binding protein [161]. The connection to LAAOs manifested in 2002 with the discovery of the human IL4i1 homolog [162]. The authors found up to 43 % sequence identity with other LAAOs, yet at that point there was no functional evidence that IL4i1 could act as a LAAO. Chavan et al., also noted that human and murine IL4i1 proteins show high identity (79%) within the first 505 amino acids and mainly differ in their C-termini (Figure 7). By now we know that the C-terminus displays the most variable region between IL4i1 from different mammalian species [144], however its function is not yet understood. The study showing that IL4i1 indeed acts as an LAAO was published in 2004 [146] and revealed that murine IL4i1 preferentially metabolizes aromatic amino acids, exhibiting the highest substrate specificity towards Phe. In that study, IL4i1 was proposed to be localized in the lysosome. Yet, further research showed that human IL4i1 is secreted [17] and also murine IL4i1 was found to be secreted from myeloid cells (Section 4.3., [163,164]). Thus, IL4i1 is a secreted protein that can act as an LAAO in the extracellular space.

1.2.6.3. Expression and immunoregulatory properties of IL4i1

Two different protein isoforms of murine and human IL4i1 have been reported, which only vary in the signal peptide and should therefore lead to the identical secreted protein [144]. The first isoform is mainly restricted to lymphoid tissues [161,162], while the expression of isoform 2 (encoded by transcripts resulting from alternative promoter usage) is found in specific cells of testis and brain, such as Sertoli and Purkinje cells [165]. Within lymphoid tissues, IL4i1 expression is highly regulated in different immune cell subsets and involved in several aspects of immunoregulation, which will be described below. Yet, IL4i1-deficient mice, similar to IDO1, iNOS and macrophage-specific Arg1-deficient animals, do not spontaneously develop autoimmune diseases [16,166,167].

1.2.6.3.1. Expression and effects of IL4i1 in B cells

Although IL4i1 was discovered as an IL4-inducible gene in murine and human B cells [161,162], B cells are likely not the main producers of IL4i1 [168] and the knowledge of the enzyme's function in this cell type is limited. The expression of IL4i1 in B cells is controlled by IL4-receptor signaling via the transcription factor STAT6 [168,169]. Moreover, stimulation with

CD40 ligand (CD40L) can further enhance IL4i1 expression in IL4-stimulated B cells, which was suggested to depend on NF- κ B activation [168]. IL4i1 has been detected in germinal center B cells [170], but also in the phagocytic tingible body macrophages residing in germinal centers [17,171]. This indicates that IL4i1 in germinal centers could derive from both, B cells and macrophages. So far, IL4i1 effects on B cells were mainly investigated in one study from Bod et al. [166] comparing WT and IL4i1-deficient mice: The study showed that *in vitro*, IL4i1 limited B cell receptor (BCR) stimulation-induced B cell proliferation, by decreasing BCR downstream signaling. *In vivo*, IL4i1-deficient mice showed increased egress of immature B cells from the bone marrow. The effects on early B cell development however did not depend on IL4i1 expression in these cells as shown by the generation of mixed bone marrow chimeras. The IL4i1-producing cells involved in this process have not been identified and remain to be uncovered. Furthermore, B cell intrinsic IL4i1 expression resulted in decreased numbers of germinal center B cells and reduced plasma cell differentiation, suggesting that IL4i1 can act as a negative regulator of B cell responses.

1.2.6.3.2. IL4i1 in myeloid cells

Myeloid cells, especially macrophages and DCs, are probably the main IL4i1-producing cell types. Accordingly, stimulation of macrophages and DCs yielded in higher levels of IL4i1 (measured by enzymatic activity) than the stimulation of B cells [168]. IL4i1 is expressed in monocyte-derived dendritic cells [17], macrophages residing in granulomas [168], tumor-associated macrophages (TAMs) [171-173] and microglia [174]. Furthermore, single-cell RNA sequencing enabled the detection of distinct macrophage and DC populations exhibiting increased IL4i1 expression which are summarized in Table 1. Interestingly, many of the DC populations expressing IL4i1 resemble DCs associated with a gene expression program linked to maturation/migration (e.g. CCR7, CD40, FSCN1 and RELB) and immunoregulation (e.g. CD274 (encoding PD-L1), CD200 and SOCS2), which have been termed 'mature DCs enriched in immunoregulatory molecules' (mregDCs) [175,176]. mregDCs are proposed to develop from both main subsets of conventional DCs (cDCs), cDC1 and cDC2, upon capture of cell-associated antigens which is followed by migration into the draining lymph nodes to modulate tissue and tumor-specific immunity [175]. These results hint at a potential link between antigen uptake and IL4i1 expression. Consistently, IL4i1⁺ macrophage populations identified by single-cell RNA sequencing may be involved in phagocytic processes as recently reported by Matusiak et al. [177]. Furthermore, Mulder et al. [55] described a IL4i1⁺ macrophage population (IL4i1_Mac) in TME, which in their study represented the only macrophage population expressing genes involved in phagosome maturation. On protein level, this may be reflected by the finding that the highly phagocytic tingible body macrophages from germinal centers, which control the removal of apoptotic B cells, also stain positive for IL4i1 [17,171,177]. Whether phagocytosis is driving IL4i1 expression and if IL4i1 detection in distinct

macrophage and DC populations by single-cell RNA sequencing is also reflected on protein level remains to be investigated.

IL4i1 ⁺ population	species	context	selection of co-expressed genes	publication
mregDC	mouse/ human	non-small-cell lung cancer; tumor and non-involved lung tissue	Aldh1a2, Ccl22, Ccr7, Cd40, Cd83, Cd200, Cd274, Fas, Fscn1, IL4i1 , Il4ra, Pdcc1lg2, Relb, Socs2	Maier et al. [175]
DC3	mouse/ human	non-small-cell lung cancer; tumor infiltrating myeloid cells	Ccl22, Ccr7, Cd274, Fscn1, IL4i1 , Il12b, Marcksl1	Zilionis et al. [178]
LAMP3⁺ DCs	human	nasopharyngeal carcinoma	CCL17, CCL19, CCL22, CCR7, CD40, CD80, CD83, CD200, CD274, FSCN1, IDO1, IL4i1 , LAMP3, MARCKSL1, PDCD1LG2, SOCS2	Liu et al. [179]
migratory DC	mouse/ human	glioblastoma	Ccr7, Cd200, Cd274, Fscn1, IL4i1 , Marcksl1, Relb, Traf1	Pombo Antunes et al. [180]
migratory DC	mouse	dura mater	Ccl22, Ccr7, Fscn1, IL4i1 , Il12b, Nudt17, Socs2, Tnfrsf4	Van Hove et al. [181]
migratory cDC2	mouse	lung; infection with pneumonia virus of mice	Ccr7, Cdc42ep3, Fabp5, IL4i1 , Relb, Spint2, Tmem176a	Bosteels et al. [182]
IL4i1⁺ cDC2	mouse	splenic DCs	Ccr7, Cd40, Cd274, Fabp5, Fas, IL4i1 , Relb, Spint2, Tcf7	Lukowski et al. [183]
IL4i1_Mac	human	normal and tumor tissue 41 datasets from 13 tissues	CCL8, CD38, CD40, CD274, CXCL9, CXCL10, CXCL11, IDO1, IL4i1 , LAMP3, STAT1	Mulder et al. [55]
phagocytosing macrophages	human	colon, lymph node, tumor microenvironment	detected in different subpopulations associated with phagocytosis in benign tissue and malignancy	Matusiak et al. [177]

Table 1 IL4i1 expressing DC and macrophage populations detected by single-cell RNA sequencing

IL4i1 expression in macrophages and DCs is probably regulated by different signaling pathways, whose effects are far from being understood. IL4 induces IL4i1 expression in murine bone marrow-derived macrophages (BMDMs) [164] and mouse primary microglia [174] and may promote the IL4-driven M2 macrophage phenotype by increasing the levels of M2-associated gene expression [164]. In contrast, Marquet et al. did not find increased H₂O₂ generation in human monocyte-derived macrophages and DCs upon IL4 stimulation [168]. Furthermore, the authors detected IL4i1 expression only in macrophages from sections of granulomas associated with IFN γ -dominated Th1 immune responses, but not in granulomas from schistosomiasis linked to IL4-dominated Th2 responses. This led Marquet et al. to speculate that IL4 is not an inducer of IL4i1 in human myeloid cells [168]. However, IL4 is a driver of the mregDC state which is conserved between human and mouse DCs and associated with IL4i1 expression [175] (Table 1), suggesting that IL4 may have a context dependent effect and contribute to IL4i1 regulation in these DCs. More research will be required to elucidate the role of IL4 in the induction of IL4i1 in macrophages and dendritic cells. Another IL4i1-inducing mechanism in myeloid cells is IFN γ -signaling via the transcription factor

STAT1 [164,168] . This may also be reflected by the IL4i1⁺ macrophage population detected by Mulder et al. [55] in the TME which exhibited clear expression of IFN γ -regulated genes such as IDO1 (Table 1). Finally, TLR and TNF signaling, likely via NF- κ B, can lead to increased IL4i1 expression in myeloid cells [164,168]. Taken together, IL4i1 expression in macrophages and DCs may be controlled by several signaling pathways. Yet, whether these pathways intersect to drive the expression of the LAAO remains to be investigated. A further unknown factor of IL4i1 biology is the timing and regulation of IL4i1 secretion from myeloid cells, which could be relevant for IL4i1-mediated downstream effects.

1.2.6.3.3. IL4i1 and T cells

Overall, IL4i1 expression is not a general feature of T cells but seems to be strictly limited to distinct populations. Nevertheless, IL4i1 secreted by myeloid antigen presenting cells has profound effects on T cell biology. It has been suggested that IL4i1 can be secreted into the immune synapse that forms between an antigen presenting cell and a T cell [184,185], which may lead to high local IL4i1 concentrations. When describing IL4i1 as a secreted LAAO expressed by dendritic cells, Boulland et al. [17] noted that IL4i1 decreases CD4⁺ and CD8⁺ T cell proliferation and leads to downregulation of the TCR ζ chain, an effect that was also found to be mediated by IDO1- and Arg1-expressing DCs and macrophages [38,73]. Additionally, limitation of T cell proliferation by IL4i1 may be indirectly regulated by an IL4i1-mediated increase of IL10 secretion from myeloid cells [164]. IL4i1 is associated with decreased TCR downstream signaling [184] and influences the differentiation of CD4⁺ T cells as IL4i1 promotes the differentiation of Foxp3⁺ Tregs while limiting the emergence of Th1 and Th2 cells [186]. Besides limiting CD8⁺ T cell proliferation *in vitro* [17], IL4i1 modulates CD8⁺ T cell responses by favoring the activation of high-affinity TCR CD8⁺ T cells over lower affinity CD8⁺ T cells [187]. Furthermore, IL4i1 is linked to decreased CD8⁺ T cell responses towards tumors [188], suggesting a role of IL4i1 in cancer biology which is further described in section 1.2.6.5.

A subtype of T cells that is known to express IL4i1 are Th17 cells [189,190]. Within these cells IL4i1 expression is dependent on the Th17 master transcription factor ROR γ t and seems to be required for a negative feedback mechanism ensuring the limitation of Th17 emergence [189]. This is suggested to be mediated by IL4i1-dependent expression of Tob1, which inhibits T cell proliferation and IL2 expression [190]. Thus, by expressing IL4i1 Th17 cells limit their own expansion, suggesting that IL4i1 either secreted from myeloid cells or endogenously expressed can limit inflammatory T cell responses. This is supported by an *in vivo* mouse model of focal demyelination of the spinal cord, in which IL4i1 promoted remyelination [174]. This was suggested to result from decreased T cell activity and correlated to strongly reduced IFN γ and IL17 levels [174]. A second T cell subtype that exhibits endogenous expression of IL4i1 are the mucosal-associated invariant T (MAIT) cells [185,191,192], which are linked to

rapid, innate-like effector responses, including for example killing of cells infected with bacteria or viruses [193,194]. As many MAIT cells express ROR γ t [193], the transcription factor was speculated to also drive IL4i1 expression in MAIT cells [185], which however has not been experimentally confirmed so far. The function of IL4i1 in MAIT cells is not entirely clear. Bulitta et al. [185] observed IL4i1 secretion into the immune synapse between MAIT cells and cells that phagocytosed dead bacteria, leading them to speculate that IL4i1 may contribute to MAIT cell cytotoxicity by H₂O₂ production, which has not been experimentally validated. Further information about the function of MAIT cell-derived IL4i1 derives from an *in vivo* study of allergic airway inflammation in mice which was limited by MAIT cells [192]. In the animal model, IL4i1-expressing MAIT cells suppressed inflammatory IL5 and IL13 secretion from type 2 innate lymphoid cells (ILC2), which could also be achieved by injecting the mice with recombinant IL4i1. Finally, IL4i1 expression was also detected in some regulatory T cells [173,195], but its function within these populations remains unclear. Considering the immunoregulatory effects of the enzyme, IL4i1 expression may further contribute to the maintenance of an immunosuppressive environment. Overall, although not expressed by many T cell subtypes IL4i1 is regulating T cell biology by promoting the emergence of regulatory T cells while limiting pro-inflammatory T cell differentiation and proliferation. It is possible that IL4i1 mainly derives from antigen presenting cells that secrete the enzyme into the immune synapse when interacting with T cells.

1.2.6.4. Mechanisms of IL4i1-mediated immune regulation

Comparable to other immunoregulatory amino acid-metabolizing enzymes, IL4i1 may regulate immune responses by local amino acid depletion and the generation of regulatory products (Figure 2). However, the mechanisms underlying the immunoregulatory processes associated with IL4i1 are not entirely understood. It needs to be considered that IL4i1 can metabolize several amino acids. Besides Phe, the other two aromatic L-amino acids, Tyr and Trp, and possibly also Arg can serve as IL4i1 substrates [17,19,146,147]. Thereby, IL4i1 may reduce the availability of several amino acids, while simultaneously generating a mixture of different α -keto acids, H₂O₂ and ammonia. Some immunoregulatory effects downstream of IL4i1 may depend on the generation of H₂O₂: For instance, inhibition of T cell proliferation in presence of purified IL4i1 could be reversed by addition of catalase, an H₂O₂ decomposing enzyme [17]. Limited B cell proliferation was also observed in presence of H₂O₂ [166]. Yet, this has not directly been linked to IL4i1-mediated B cell inhibition as H₂O₂ was not depleted under conditions where cells were incubated with IL4i1. Nevertheless, the generation of H₂O₂ likely represents one arm of IL4i1-dependent immunoregulation. However, H₂O₂ production could not account for other IL4i1-mediated effects: Decreased TCR signaling [184] and the modulation of T cell differentiation [186] were found to be independent of H₂O₂ generation. Instead, increased Treg differentiation might partly depend on Phe depletion, as essential

amino acid starvation sensed by mTOR was reported to promote the development of Tregs [85]. Indeed, a slight reduction of mTOR signaling was observed when inducing Treg differentiation in the presence of IL4i1 [186]. However, it is not clear whether increased levels of Phe could reverse IL4i1-mediated effects on T cell differentiation or if GCN2-dependent sensing of amino acid deprivation may additionally be involved. A limitation of the studies aiming to determine mechanistic basics of IL4i1-mediated effects is that experiments were exclusively focusing on Phe catabolism [17,172,184,186]. Although Phe undoubtedly represents a substrate of IL4i1, the metabolism of other amino acids may be involved in IL4i1-mediated effects by further enhancing the sensing of amino acid limitation or via the generation of potentially regulatory α -keto acids. When starting my PhD project, PP generated from Phe, which so far could not be linked to any IL4i1-dependent immunoregulatory property, was the only α -keto acid that had been investigated in studies concerning the mechanistic basis of IL4i1-mediated effects [17,172,184,186]. Thus, one objective of my work was a better characterization of the downstream cellular effects of α -keto acids generated by IL4i1 including not only PP, but also the other aromatic α -keto acids 4HPP and I3P derived from Tyr and Trp respectively. Recent studies showed that I3P generated by IL4i1 is another Trp metabolite that can activate the AhR [19,196], which is a potent modulator of immunoregulation (1.2.4.3). Generation of I3P may therefore additionally contribute to the regulation of immune responses by IL4i1. However, it is also suggested that IL4i1 may act independent of its enzymatic activity. Aubatin et al. detected interactions between T cells and IL4i1 secreted by myeloid cells [184]. As Phe catabolism could not account for the observed reduction of TCR signaling, the authors proposed a mechanism independent of IL4i1 catalytic activity involving direct binding of the protein to a receptor, which had not been identified. A study from the same group recently suggested that a transmembrane serine protease (TMPRSS13) can interact with IL4i1 [197]. However, so far there is no evidence that this interaction affects T cell biology. Catalytically inactive IL4i1 mutants may represent helpful tools to distinguish between IL4i1 downstream effects that require the catalytic activity versus those effects that may potentially be caused by direct protein interaction.

1.2.6.5. IL4i1 in cancer

Considering 1) the expression of IL4i1 in tumor-associated myeloid cells [171-173] (Table 1), 2) the immunoregulatory effects of IL4i1 described above and 3) the involvement of other amino acid-metabolizing enzymes in the suppression of tumor immunosurveillance, it is not surprising that IL4i1 is associated with reduced immune responses towards malignancies [19,172,173,188] and poor survival in several cancer types including melanoma, glioma and ovarian cancer [19,173,198]. The only known exception of a cancer type in which IL4i1 expression appears to be favorable are follicular B cell lymphomas, where IL4i1 expression was initially detected in TAMs, but also in the neoplastic cells [171]. Yet, as IL4i1 expression

also occurs in non-malignant germinal center B cells [170], this may directly depend on the physiologic effect of IL4i1 limiting B cell expansion [166], which could outweigh reduced immune responses towards the neoplastic cells. Decreased CD8⁺ T cell control of tumors was first described in a melanoma model with ectopic expression of IL4i1, which resulted in diminished numbers of cytotoxic CD8⁺ T cells and reduced IFN γ secretion [188]. Subsequently, endogenous IL4i1 expression was found to be detrimental in the context of melanoma [172]. Bod et al. showed that genetic IL4i1 deficiency resulted in delayed primary tumor formation and reduced metastasis formation in a mouse melanoma model. In this study, absence of IL4i1 provoked major changes in the composition of the tumor infiltrating immune cells, increasing the fractions of infiltrating T and B lymphocytes while limiting the ratio of myeloid-derived suppressor cells and TAMs [172]. Additionally, in melanoma patients' samples high IL4i1 expression correlates with low CD8⁺ T cell infiltration and increased occurrence of FoxP3⁺ regulatory T cells [172,173]. Analyzing the Cancer Genome Atlas for tumors with high and low IL4i1 expression Sadik et al. [19] found that the enrichment of immunosuppressive cells such as myeloid-derived suppressor cells and regulatory T cells is a common feature of malignancies with high IL4i1 expression. Furthermore, in a mouse model of chronic lymphocytic leukemia (CLL) where IL4i1 deficiency correlated with reduced CLL tumor cell burden, Sadik et al. [19] observed that IL4i1 also caused increased CD8⁺ effector T cell exhaustion and PD1 expression in addition to increased levels of regulatory T cells. Taken together, these studies show that IL4i1 in cancer regulates the composition of tumor infiltrating immune cells, decreases the efficiency of effector T cells and is therefore associated with tumor immune escape. Thus, Sadik and colleagues [19] termed IL4i1 a 'metabolic immune checkpoint' which is capable of suppressing adaptive immune responses. Targeting IL4i1 in cancer immunotherapy may therefore represent a promising new strategy to restore cancer immune control. Besides immunoregulatory effects, IL4i1 may have direct influence on controlling cancer cell biology by modulating composition of the metabolic environment. *In vitro*, the IL4i1-generated Trp metabolite I3P enhances glioblastoma cell motility by activating AhR signaling [19] and also migration and invasion of ovarian cancer cell lines was promoted by IL4i1 [198]. Despite all this fragmentary information, our current knowledge of IL4i1 in the context of cancer cell biology is limited. Therefore, a main objective of my thesis was to investigate downstream effects of IL4i1 on cancer cells addressing the question how IL4i1-mediated amino acid metabolism mechanistically contributes to the pro-tumorigenic effects of the enzyme.

1.3. The oxidative cell death ferroptosis

A key component of this thesis concerns ferroptosis, an oxidative cell death pathway characterized by uncontrolled lipid peroxidation, described 10 years ago by Dixon et al. [199]. However, cell death induced by cysteine deprivation, glutathione (GSH) depletion or loss of the glutathione peroxidase 4 (GPX4), which can now be clustered under the term 'ferroptotic cell death', has been reported even earlier [200-202]. Nevertheless, the publication from Dixon and colleagues in 2012 marked the beginning of an exponentially growing research field over the last 10 years [203].

Ferroptosis is a consequence of uncontrolled, iron-dependent spreading of membrane lipid peroxidation which finally provokes the loss of cell membrane integrity, a late and probably essential step in ferroptotic cell death [199,203]. The chemical basis of lipid peroxidation occurring within the context of ferroptosis has been extensively reviewed by Conrad and Pratt in 2019 [204] (Figure 8): Reactive oxygen species (ROS) that are constantly produced during cellular metabolism can initiate the formation of free radicals from phospholipids (PLs) containing polyunsaturated fatty acids (PUFAs). These radicals can subsequently react with molecular oxygen to form peroxy radicals (PLOO•). In turn, PLOO• radicals propagate the emergence of further PUFA radicals, while iron promotes a Fenton-like reaction to generate reactive radicals from the emerging PL peroxides (PLOOH). This can trigger an 'avalanche-like' propagation of lipid peroxidation, which can disrupt the integrity of cell and/or organelle membranes, a process discussed to be essential in ferroptotic cell death [203,205]. This concept is supported by the observation that ACSL4 and LPCAT3, two enzymes involved in the incorporation of PUFAs into membrane phospholipids, sensitize cells to ferroptotic death [206,207]. Although the reaction of two PLOO• radicals can terminate their participation in further PL peroxidation [204], cells depend on additional ferroptosis-suppressive mechanisms, such as the constant detoxification of membrane PLOOHs and the highly reactive PLOO• radicals, which are described in the next section.

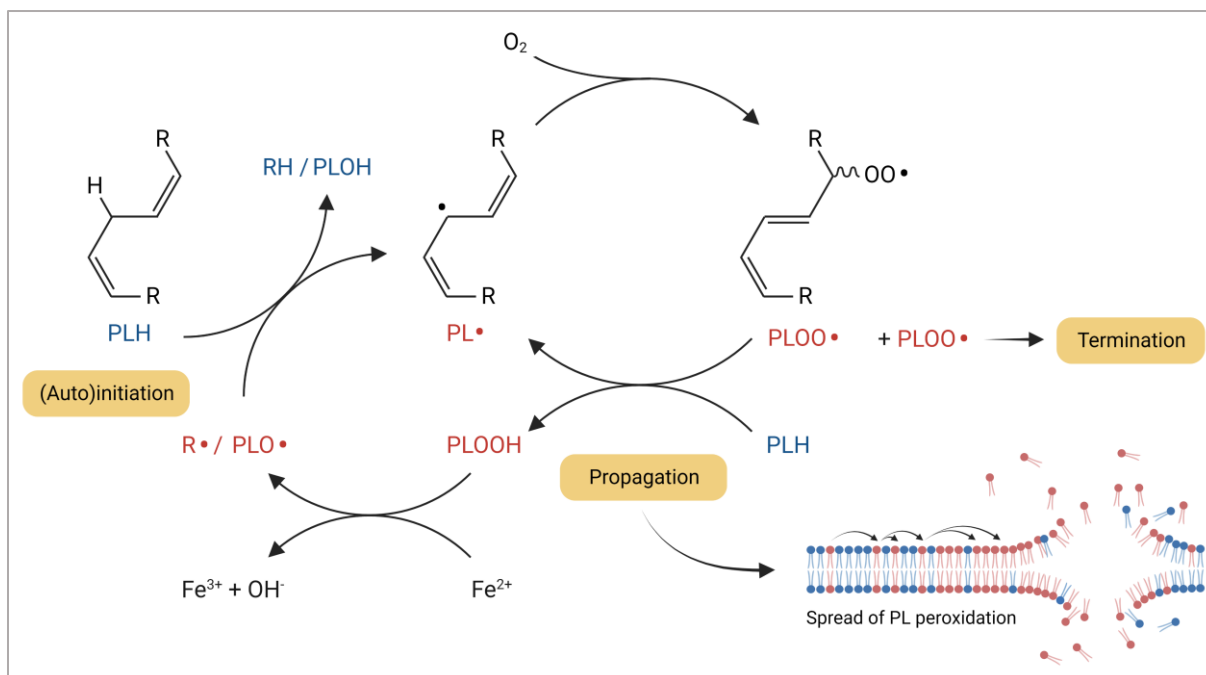


Figure 8 Chemical basis of phospholipid peroxidation adapted from Conrad & Pratt [204]

In an initiation step, free radicals can absorb a labile hydrogen atom (bound to a carbon atom flanked by C-C double bonds) in PLs containing PUFAs. The resulting carbon-centered PL radical (PL•) subsequently reacts with O₂ generating a peroxy radical (PLOO•). PLOO• radicals can propagate the peroxidation of further PLs containing PUFAs (PLOOH), which in a Fenton-like reaction aided by free iron form lipid alkoxy radicals (PLO•). These can in turn act as initiating radicals for the peroxidation of other PLs. While two PLOO• radicals can also react and terminate the peroxidation cycle, cells require additional mechanisms to prevent the propagation of PL peroxidation, which can ultimately cause a loss of membrane integrity.

1.3.1. Ferroptosis-suppressive mechanisms

1.3.1.1. The GPX4 – glutathione – cysteine axis

To prevent ferroptotic cell death, cells have developed protective mechanisms to interfere with the spread of PL peroxidation, which include enzymatic detoxification of PLOOHs and direct scavenging of reactive lipid peroxidation intermediates. The major enzyme involved in ferroptosis suppression in most cell types is glutathione peroxidase 4 (GPX4), which uses glutathione (GSH), the most abundant endogenous antioxidant [208], to enzymatically detoxify PLOOHs. GPX4 catalyzes the reduction of PLOOHs to the corresponding alcohols while oxidizing the thiol groups of two glutathione molecules resulting in the generation of oxidized GSH (GSSG) [209,210]. Notably, like several other related GPX enzymes that have differential and cell-type specific functions (e.g., GXP1), the active site of GPX4 contains a single selenocysteine residue, which is involved in the redox catalytic activity of the enzyme [211,212], indicating the importance of selenium in the control of ferroptosis (reviewed by Conrad and Proneth [213]). Decomposition of PLOOHs by GPX4 prevents the iron-dependent formation of radical intermediates propagating further PL peroxidation, while loss of GPX4 was

found to cause massive lipid peroxidation and cell death [202], which was discovered even before Dixon et al. coined the term ferroptosis [199].

A prerequisite for the detoxification of PLOOHs by GPX4 is the sufficient availability of intracellular GSH. GSH, which is considered to be the major intracellular antioxidant [208], is a tripeptide consisting of glutamate (linked via the γ -carboxyl group), cysteine and glycine. Of these amino acids, cysteine is the rate-limiting substrate for GSH synthesis [214]. Thus, cysteine availability is the upstream basis of the ferroptosis suppressive GPX4-GSH-cysteine axis (Figure 9). The intracellular pool of free cysteine can be maintained by uptake of cystine from the extracellular space or endogenous generation via the transsulfuration pathway from methionine and serine [215-217]. Many cells depend on the uptake of cystine, the oxidized form of cysteine, via the cystine/glutamate antiporter SLC7A11 (also termed xCT) which together with its co-factor SLC3A2 forms a transporter complex also known as system X_c⁻ [217,218]. Inside the cell, imported cystine is reduced to cysteine in an NADPH-dependent process [219,220] and can consequently serve as substrate for GSH synthesis consisting of two enzymatic reactions: First, the glutamate cysteine ligase (GCL) composed of a catalytic and a modifier subunit (GCLC and GCLM respectively) catalyzes the generation of γ -glutamylcysteine. Subsequently γ -glutamylcysteine is linked to glycine by the GSH synthase (GSS) terminating the GSH synthesis [221]. Besides *de novo* synthesis, GSH can be resolved from oxidized GSSG by the NADPH-dependent glutathione-disulfide reductase (GSR) [222]. As GPX4-mediated PLOOH detoxification requires the availability of GSH, cellular cysteine and GSH homeostasis are essential factors ensuring cell protection from ferroptosis. Accordingly, depletion of the intracellular cysteine and/or GSH pool can lead to massive lipid peroxidation and ferroptosis [201,223,224]. Importantly, several NADPH-dependent processes are involved in the maintenance of cysteine and GSH homeostasis, including the recovery of GSH from GSSG or the reduction of imported cystine to cysteine [219,220]. Thus, availability of NADPH, which can derive from glucose shunted to the pentose phosphate pathway (PPP) [219], appears to be an additional component of endogenous ferroptosis suppression. In agreement, NADPH levels have been suggested to represent a biomarker for ferroptosis susceptibility/resistance [225].

As many cells depend on GPX4-mediated PLOOH detoxification, small molecules targeting the different nodes of the GPX4-GSH-cysteine axis can be used to induce ferroptosis. While the alkylating small molecule RSL3 was found to induce ferroptosis by directly inhibiting GPX4 [223], the GCL inhibitor buthionine sulfoximine (BSO) promotes ferroptosis by interfering with GSH synthesis [223,224]. Furthermore, inhibition of SLC7A11 by Erastin and Sulfasalazine can induce ferroptosis by depleting the intracellular cysteine pool in several cell types/cell lines [224]. However, endogenous cysteine synthesis via the transsulfuration pathway [215] or high expression of other cysteine transporters [226] may interfere with the efficacy of SLC7A11

inhibitors. Although the GPX4-GSH-cysteine axis represents the major ferroptosis-suppressive pathway in most cells, there is evidence for the existence of further GPX4-independent mechanisms, which can act in parallel to the GPX4-dependent PLOOH detoxification.

1.3.1.2. GPX4-independent ferroptosis suppression

In 2019, the discovery of another protein directly involved in the suppression of ferroptotic cell death, 'ferroptosis suppressive protein 1' (FSP1, previously AIFM2), was reported by two independent groups: Using a synthetic lethal CRISPR-Cas9 screen towards sub-lethal concentrations of RSL3 or an overexpression screen compensating for loss of GPX4, Bersuker et al. and Doll et al. identified FSP1 as a protein that can suppress ferroptosis in a pathway acting in parallel to GPX4 [227,228]. Both studies showed that N-terminal myristoylation is required for FSP1 localization at phospholipid membranes where the enzyme interferes with lipid peroxidation. This is mediated by FSP1's NADH:ubiquinone oxidoreductase activity leading to the reduction of ubiquinone (CoQ; also known as coenzyme Q10) to ubiquinol (CoQH₂), which is a known scavenger of lipid radicals [229]. The oxidized CoQ generated in this process can be reduced again by FSP1 to recover the anti-oxidative CoQH₂ using NAD(P)H [227,228] (Figure 9). Overall, this suggests that FSP1 suppresses ferroptosis independently of GPX4 by maintaining the lipid radical scavenging function of CoQH₂. Recently, another enzyme was discovered to be involved in ferroptosis suppression via the CoQ/CoQH₂ system. The mitochondrial enzyme dihydroorotate dehydrogenase (DHODH) involved in pyrimidine synthesis was found to suppress mitochondrial PL peroxidation and ferroptosis in cancer cells expressing low levels of GPX4. While oxidizing dihydroorotate to generate orotate for pyrimidine synthesis, DHODH reduces CoQ to CoQH₂, which in turn interferes with lipid peroxidation in the mitochondrial membrane [230] (Figure 9). Thus, while FSP1 protects cells from PL peroxidation in the plasma membrane DHODH protects mitochondrial membranes via generation of CoQH₂.

Another GPX4-independent pathway involving the scavenging of lipid radicals acts via the enzyme GTP cyclohydrolase 1 (GCH1) and tetrahydrobiopterin (BH₄) (Figure 9). GCH1 is the rate-limiting enzyme of *de novo* BH₄ synthesis from GTP [231] and was found to mediate ferroptosis resistance in a CRISPR activation screen [232]. BH₄ suppresses ferroptosis by 1) direct scavenging of radicals in lipid membranes and 2) by increasing CoQ biosynthesis [232,233]. In addition, dihydrobiopterin (BH₂), partially oxidized BH₄, can also act as a radical scavenger [232]. Yet, recovery of BH₄ from BH₂ by recombinant dihydrofolate reductase (DHFR) strongly increased anti-oxidative effects of BH₂ in liposomes [233]. Therefore, DHFR, may represent another enzyme involved in the maintenance of GCH1-BH₄-mediated ferroptosis suppression.

Taken together, while GPX4 enzymatically detoxifies PLOOHs to interfere with the spread of lipid peroxidation, other anti-ferroptotic pathways exist involving the enzymes FSP1, DHODH or GCH1 which generate lipid radical scavenging effector molecules. Together with GPX4, these pathways collectively contribute to the prevention of ferroptotic cell death by inhibiting the propagation of PL peroxidation. However, many other intracellular mechanisms including iron and selenium homeostasis, PUFA metabolism and regulation of non-lipid ROS are shaping cellular resistance or susceptibility towards ferroptosis, which have been reviewed in detail by others [203-205,222,234]. Importantly, the GXP4, FSP1, DHODH and GCH1 pathways all act to suppress ferroptosis in a cell-intrinsic way (Figure 9). By contrast, the pathway of ferroptosis suppression I discovered in my PhD project operates cell-extrinsic and is controlled by regulated amino acid metabolism.

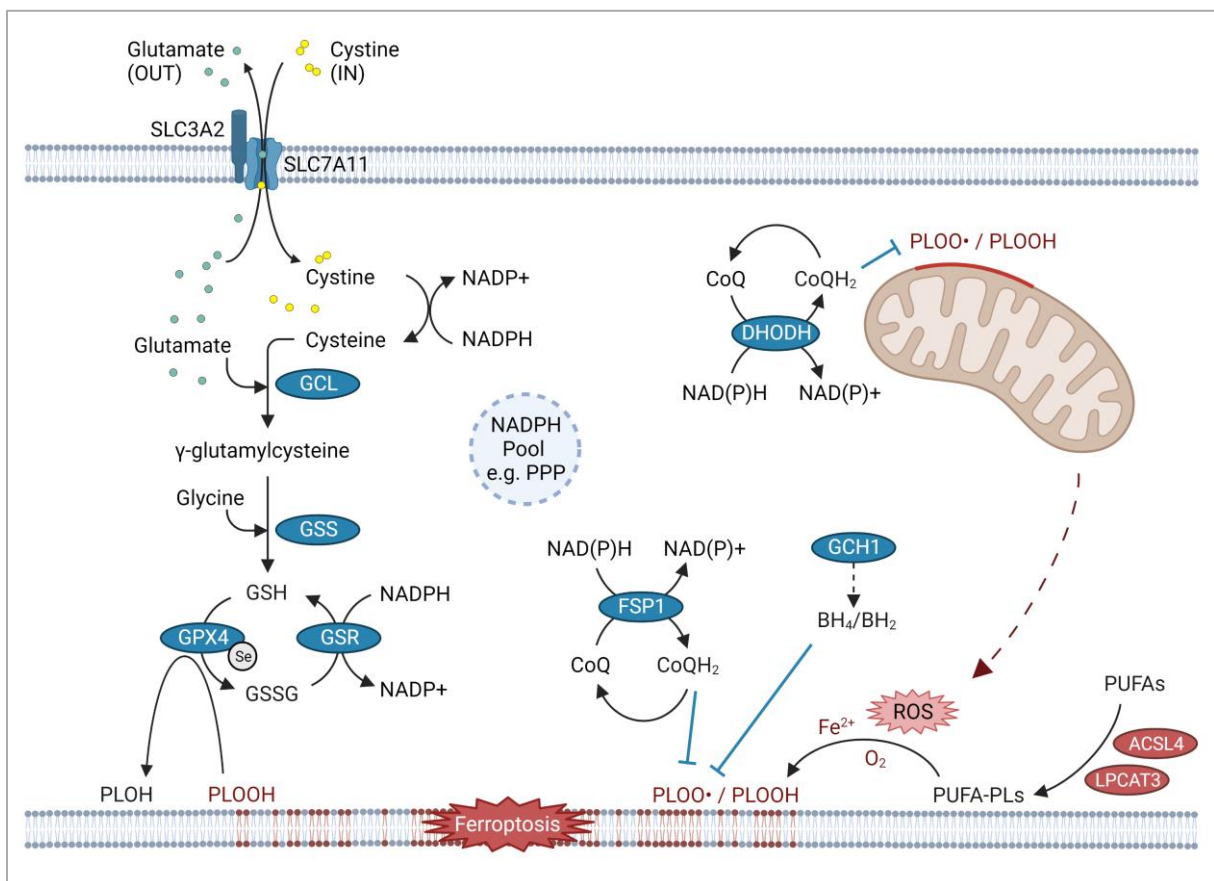


Figure 9 Overview of cell intrinsic ferroptosis-suppressive pathways modified from Jiang et al. [205]

Schematic overview of ferroptosis suppressive pathways required to detoxify PLOOHs and reactive radical intermediates resulting from the peroxidation of PUFAs in membrane PLs. The GPX4-GSH-cysteine axis (1.3.1.1) is depicted on the left side. GPX4-independent mechanisms (1.3.1.2) are shown on the right side.

1.3.1.3. The Keap1-Nrf2 pathway

The Keap1-Nrf2 axis is a key pathway in the transcriptional response to oxidative stress and is associated with the induction of a gene network protecting cells from oxidative damage [235]. Nrf2 is a basic leucine zipper (bZIP) transcription factor tightly controlled by its interactor

protein Keap1, which forms a homodimer to bind Nrf2 at two distinct binding sites, an ETGE and a DLG motif, located at the N-terminal region of Nrf2 [236,237]. Keap1 acts as an adaptor for the Cullin 3-based ubiquitin E3-ligase complex (Cul3) and promotes permanent Nrf2 ubiquitination and proteasomal degradation under steady-state conditions [238,239] (Figure 10). This leads to an extremely high turnover of Nrf2 (e.g. ~13 min half-life time in hepatoma cells [240]) and very low basal levels. However, Keap1 has a very high content of cysteine residues (27 residues) of which some, e.g. Cys151, Cys257, Cys273, Cys288 and Cys297, are known to act as 'sensors' for redox stress [239,241]. These residues can undergo several modifications including the oxidation to sulfenic acid, the formation of disulfide bonds or the covalent binding of electrophiles, such as different types of ROS [242]. Modifications of these free thiol groups result in conformational changes of Keap1 which prevent the ubiquitination and degradation of Nrf2. This is suggested to result from the destabilization of the Nrf2-Keap1 interaction at the DLG motif [243]. Although Nrf2 remains bound to Keap1 via the ETGE motif and is thereby retained in the cytoplasm, the lack of Nrf2 degradation leads to a saturation of Keap1 molecules. Thus, newly synthesized Nrf2 molecules cannot be captured by Keap1 and translocate into the nucleus (Figure 10) [242]. Somatic mutations in *KEAP1* that interfere with the regulation of Nrf2 and thus cause constitutive Nrf2 activation are frequently found in malignancies, especially in lung cancers [242,244,245]. In the nucleus, Nrf2 dimerizes with small Maf (sMaf) proteins [246] and activates transcription by binding to antioxidant response elements (AREs) [247]. A second, non-canonical pathway interfering with Keap1-mediated Nrf2 degradation is deficient autophagy, which provokes accumulation of autophagy associated protein p62 (also SQSTM1). Direct interactions between p62 and Keap1 interfere with the Keap1-dependent regulation of Nrf2 levels, promoting Nrf2 stabilization and activation of Nrf2-mediated transcription [248,249] (Figure 10). Many target genes of Nrf2-mediated transcription are involved in the maintenance of the cellular redox balance including those required for GSH production and regeneration, such as SLC7A11, both subunits of the GCL and the GSH recycling enzyme GSR [247]. Other transcripts regulated by Nrf2 encode proteins involved in cellular iron and heme homeostasis for example subunits of the free iron sequestration protein ferritin, or the heme-degrading enzyme heme oxygenase 1 [250]. FSP1 and another NAD(P)H-quinone oxidoreductase, NQO1, are also regulated by Nrf2 [251]. Thus, Nrf2 is a transcriptional regulator of many factors involved in the suppression of ferroptotic cell death and may therefore represent an important modulator of the cellular ferroptosis susceptibility. Activation of the p62-Keap1-Nrf2 pathway was first linked to ferroptosis resistance in hepatocellular carcinoma cells [252]. Since then, further studies supported the protective effect of Nrf2 in cells exposed to ferroptosis inducing agents, suggesting also that inhibition of Nrf2 can be used to sensitize cells to ferroptotic death [253-257]. Whether Nrf2 acts via the regulation of distinct target genes or a broad anti-oxidative gene expression

program is not completely understood and may depend on the cellular context. For instance, while in hepatocellular carcinoma cells Nrf2-mediated metallothionein-1G upregulation was suggested to cause ferroptosis resistance [257], in glioma cells SLC7A11 was required for Nrf2-dependent cell protection [254]. However, this does not exclude the involvement of further ferroptosis-suppressive factors downstream of the cellular cystine import which are also controlled by Nrf2 such as the maintenance of GSH homeostasis [247]. Relevant findings linking Nrf2-mediated ferroptosis suppression to cancer biology derived from CRISPR screens in 3D spheroid models, which indicate that Nrf2 promotes survival of tumor cells residing in the core of the spheroids by suppressing ferroptosis [258]. Taken together, while not directly interfering with lipid peroxidation itself, Nrf2 appears to be an important transcriptional regulator of many ferroptosis-suppressive genes and may thereby modulate the ferroptosis susceptibility of cells.

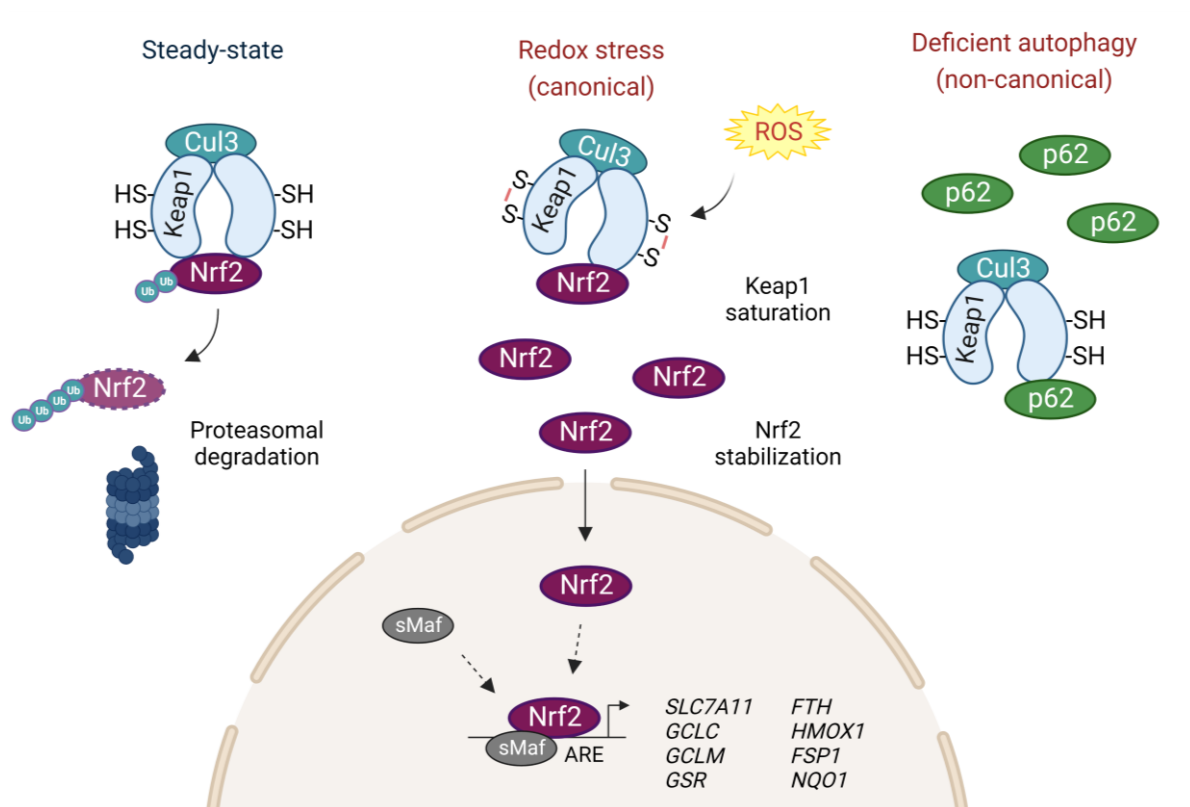


Figure 10 Scheme of the Keap1-Nrf2 pathway

1.3.2. Ferroptosis in cancer biology

1.3.2.1. Pro-ferroptotic effects of tumor suppressors

A major question in ferroptosis research concerns the link between ferroptosis and tumor formation and progression, which so far is not very well understood. Findings indicating that tumor suppressor genes increase cellular ferroptosis susceptibility hint to the possibility that ferroptosis has a physiologic function in tumor suppression. This was first described by Jiang

et al. [259] who discovered a non-canonical tumor suppressing function of p53 which negatively regulates cystine uptake by suppressing SLC7A11 expression and thereby sensitized tumor cells to ferroptosis. The study showed that an acetylation-defective p53 mutant (p53^{3KR}), which was deficient in canonical p53 functions including the induction of cell-cycle arrest, senescence and apoptosis retained tumor-suppressive activity *in vivo*. As the mutant retained its function to repress SLC7A11 and overexpression of SLC7A11 reversed the tumor suppressive effect, the authors concluded that the downregulation of the cystine transporter is a non-canonical tumor suppressing function of p53 [259]. This is further supported by the observation that an additional point mutation in the p53^{3KR} mutant that interfered with SLC7A11 downregulation completely abrogated p53-dependent tumor suppression [260]. Besides repression of SLC7A11, p53 may promote ferroptosis by other mechanisms involving for example the modulation of lipid and iron metabolism [261-263]. However, other studies also reported anti-ferroptotic effects mediated by p53 [264,265], suggesting the role of p53 in ferroptosis is complex and may depend on the cellular context. Nevertheless, further tumor suppressor genes were found to sensitize tumor cells to ferroptosis. Besides p53, the epigenetic regulator BRCA1-associated protein 1 (BAP1) represses SLC7A11 expression suggesting that ferroptosis may contribute to the tumor suppressive effect of the protein [266]. In addition, another tumor suppressive enzyme involved in epigenetic regulation [267], the lysine methyltransferase 2B (KMT2B, also known as MLL4) has recently been shown to promote expression of pro-ferroptotic lipoxygenases in the epidermis [268]. Finally, as described above, Keap1 is a tumor suppressor that represses the transcription of several anti-ferroptotic genes including e.g. SLC7A11 and FSP1 by mediating the degradation Nrf2 (see 1.3.1.3). Taken together, these studies hint at links between ferroptosis and tumor suppression. However, more research is required to completely understand to whether and to which extent ferroptosis is required to prevent the emergence of malignant cells.

1.3.2.2. Dependence of tumor cells on ferroptosis-suppressive pathways

Mounting evidence suggests malignant cells depend on the induction of ferroptosis-suppressive genes. High production of ROS is a general feature of many cancer cells and is accompanied by the upregulation of anti-oxidative gene expression, which may be required to cope with increasing oxidative stress [269,270]. In this regard, elevated Nrf2 has been detected in various types of cancers such as lung, breast, ovarian and endometrial carcinomas, which is associated with poor prognosis [242]. This can be a result of enhanced oncogene-driven Nrf2 transcription [271] or somatic mutations in Nrf2 or Keap1 preventing Nrf2 degradation and thereby leading to constitutive Nrf2 activity [242]. Increased relative Nrf2 activity may promote tumor progression via several mechanisms, one of which could be the suppression of ferroptosis since Nrf2 was found to prevent ferroptotic cell death inside 3D tumor spheroid

models *in vitro* [258]. Moreover, a recent study investigating Keap1-deficient lung adenocarcinoma reported Nrf2-mediated upregulation and dependence on the FSP1-CoQ pathway, which could be targeted to overcome radiation resistance *in vitro* and *in vivo* [272]. The upregulation of the cystine transporter SLC7A11 is a feature of many malignant cells and can for example be driven by Nrf2 or oncogenic K-Ras [217]. Dependence of tumor cells on SLC7A11-mediated cystine import was shown in pancreatic cancer, in which ablation of the transporter provoked ferroptosis in the cancer cells and inhibited tumor growth *in vivo* [273,274]. Therefore, while expression of ferroptosis protective genes may be advantageous for tumor cell growth and cancer progression, the cells also seem to be vulnerable to interference with ferroptosis-suppressive pathways. Targeting these pathways may present a promising approach for the development of novel cancer therapies [275]. This could be especially relevant for the treatment of tumor cells resistant to chemo- and/or radiotherapy: A study by Lei et al. showing that ionizing radiation can induce ferroptosis in cancer cells revealed that resistant cells were associated with the upregulation of ferroptosis-inhibiting gene expression and Keap1 deficiency. Interference with ferroptosis suppression by use of ferroptosis inducers sensitized tumor cells to irradiation *in vitro* and *in vivo* [276]. Furthermore, tumor cells displaying a high-mesenchymal cell state, which is associated with therapy resistance are highly dependent on the lipid peroxide detoxifying GPX4 [277] and also drug resistant 'persister-cells' were found to be highly susceptible to GPX4 inhibition [278]. Therefore, the dependence of neoplastic cells on the ferroptosis suppressing machinery appears to be a feature that could be exploited in cancer therapy.

1.3.2.3. Ferroptosis and immunosurveillance of cancer

Ferroptosis may also have implications for the immunosurveillance of cancer. In 2019, Wang et al. showed that IFN γ derived by CD8⁺ T cells activated by immunotherapy sensitized tumor cells to ferroptotic cell death and inhibition of ferroptosis decreased the efficacy of anti-PD-L1 therapy in a mouse model [279]. Mechanistically, IFN γ was found to be associated with decreased cysteine uptake by repression of the cystine transporter subunits SLC7A11 and SLC3A2 and thereby promoted lipid peroxidation in cancer cells [279-281]. In addition, CD8⁺ T cell-derived IFN γ provokes an increase of ACSL4 expression, which in combination with the PUFA arachidonic acid was potently inducing ferroptosis in tumor cells and diminished tumor growth *in vivo* [282]. Thus, ferroptosis may contribute to the cytotoxic effects involved in tumor immunosurveillance by CD8⁺ T cells. However, as IFN γ alone is not sufficient to induce ferroptosis in tumor cells [279,282], further factors such as the metabolite composition in the TME may have an important role in supporting or preventing CD8⁺ T cell-induced ferroptosis in the immune control of cancer as observed for arachidonic acid [282]. We could recently show that Trp metabolism by IDO1 can protect cancer cells from ferroptosis by inducing ferroptosis protective gene expression and the generation of the radical scavenging Kyn

metabolites 3HK and 3HAA [61]. Therefore, IDO1 expression in tumors, whether by myeloid or tumor cells, may be advantageous for tumor cells to prevent ferroptotic death and thereby support the pro-tumorigenic effects of the enzyme. In addition, Arg metabolism may modulate ferroptosis sensitivity of cancer cells as Arg depletion is associated with ferroptosis resistance [283]. Moreover, NO generated from Arg by iNOS in inflammatory macrophages is suggested to protect cells from ferroptosis by limiting PL peroxidation [284,285]. However, this potential link between immune cell-dependent amino acid metabolism and ferroptosis and its possible detrimental impact on the control of tumor progression will require further investigation.

An additional aspect that is relevant to better understand the role of ferroptosis in tumor immunosurveillance is the question whether ferroptosis is an immunogenic or tolerogenic type of cell death, which so far has been controversially discussed. Several groups reported the release or presentation of immunostimulatory damage-associated molecular patterns (DAMPs) by ferroptotic cells including ATP, HGMB1, oxidized phosphatidylethanolamine and calreticulin [286-289], suggesting that ferroptotic cells can elicit immune responses. In this regard, Efimova and colleagues reported that 'early-ferroptotic' but not 'late-ferroptotic' cells provoked DC maturation and facilitated T cell-mediated immune responses towards tumor cells [286]. However, opposing observations were published in a recent study from Wiernicki et al. who found that despite the release of DAMPs and pro-inflammatory cytokines, ferroptotic cells impaired the maturation of dendritic cells, dampened antigen cross-presentation and could not protect from tumor growth, in contrast to apoptotic or necroptotic cells [290]. Therefore, further research is required to understand whether and under which conditions ferroptosis can provoke immune responses or which mechanisms prevent immunogenicity of ferroptotic cells. This information will be valuable to understand if induction of ferroptosis, e.g. by therapeutic use of ferroptosis inhibitors, can boost or rather impede the immune responses towards cancerous tissue.

Taken together, although the mechanisms are not completely clear, mounting research suggests an involvement of ferroptosis in different aspects of cancer biology. While tumor suppressor genes may prevent tumor formation by sensitizing cells to ferroptosis, anti-oxidative, ferroptosis-suppressing pathways seem to be activated in malignant cells. This could be required to control the large amount of ROS production resulting from the high metabolic activity of cancer cells. In addition, it is possible that tumor immunosurveillance by CD8⁺ partly involves the induction of ferroptosis in tumor cells by increasing their sensitivity to ferroptotic death. Overall, dependence of tumor cells on ferroptosis-suppressive mechanisms appears to be a vulnerability of cancer cells that may be exploited to develop new anti-cancer therapies. However, this will require a deeper understanding of the mechanisms controlling ferroptosis and ferroptosis resistance in the context of cancer.

2. Rationale and aims of the thesis

The regulated expression of amino acid-metabolizing enzymes in immune cells has evolved as a strategy to control and limit immune responses. While enzymes such as Arg1 or IDO1 have been extensively studied for many years, our knowledge about the secreted LAAO IL4i1 is limited. IL4i1 is proposed to mediate several immunoregulatory effects (1.2.6.3) and mounting evidence suggests that expression of IL4i1 by tumor-associated myeloid cells has detrimental effects on survival in cancer (1.2.6.5). However, the mechanisms by which IL4i1 controls the biology of immune cells and tumor cells are not well understood. Therefore, an overall aim of my thesis was to characterize downstream effects mediated by the metabolic modulation of the cellular environment via the enzymatic activity of IL4i1, which preferentially catalyzes the depletion of aromatic amino acids while generating the respective α -keto acids, H_2O_2 and ammonia (Figure 6). Notably, IL4i1 belongs to a family of conserved LAAO enzymes, which are for example present in snake venoms. As snake venom LAAOs can mediate toxic effects via the generation of H_2O_2 [153-156], an initial hypothesis for my project was that mammalian IL4i1 may also have cytotoxic functions. Therefore, the 1st aim of my thesis was to **use a comparison of mammalian IL4i1 and a snake venom LAAO to draw conclusions about their enzymatic function and potential toxicity**. This included the generation and testing of recombinant IL4i1, a cobra (*Naja naja*) venom LAAO and enzymatically inactive versions of the enzymes.

Besides H_2O_2 , IL4i1 generates α -keto acids from its amino acid substrates. When starting my thesis, other studies had only superficially investigated effects mediated by the α -keto acid PP generated from Phe, which after all did not contribute to the examined immunoregulatory effects [17,172,184,186]. However, IL4i1 does not exclusively metabolize Phe, but also the other aromatic amino acids Tyr and Trp [17,146] leading to the generation of the α -keto acids 4HPP and I3P, respectively. Thus, the 2nd aim of my thesis was to **uncover cellular downstream effects of the aromatic α -keto acids generated by IL4i1**. Herein, I started with a broad characterization of effects mediated by PP, 4HPP and I3P on cellular transcription by mRNA-Seq, which subsequently directed my work towards the investigation of AhR activation and ferroptosis suppression by IL4i1-derived aromatic α -keto acids.

Finally, in order to study and mechanistically dissect the interplay between IL4i1 secreting immune cells and different cells in their microenvironment, we require more complex *in vitro* models containing cells endogenously expressing IL4i1. However, our current knowledge of IL4i1 expression and regulation in myeloid cells, especially on protein level, is restricted (also due to the lack of good commercial antibodies). Therefore, the 3rd aim of my thesis was **the characterization of IL4i1 expression and regulation in macrophages and DCs**, which seem to be important IL4i1-producing cell populations in the context of cancer

[55,171,173,175]. I used the differentiation of macrophages and DCs from murine bone marrow as a model approach to characterize IL4i1 expression in systems applicable for large scale experiments by providing a high yield of the cells of interest.

3. Materials and Methods

3.1. Overview of materials

3.1.1. Chemicals and reagents

Chemicals and reagents	Supplier	Identifier
(1S, 3R)-RSL3	Selleckchem	S8155
0.25 % trypsin-EDTA	Gibco	25200-056
2,2-Diphenyl-1-pikryl-hydrazyl (DPPH)	Sigma	D9132
4-hydroxyphenylpyruvic acid	Sigma	114286
Agarose	Thermo Fisher	BP160500
Amplex UltraRed	Thermo Fisher	A36006
AmpliTaq Gold™ DNA Polymerase with Buffer II and MgCl ₂	Applied Biosystems	N8080241
Ascorbic acid	Sigma	A5960
BbsI-HF restriction enzyme	NEB	R3539
BbvCI restriction enzyme	NEB	R0601
BenchMark™ Pre-stained Protein Ladder	Invitrogen	10748010
BglII restriction enzyme	NEB	R0144
Biotin	Sigma	B4501
Bovine Serum Albumine	Sigma	A2059
C11 BODIPY 581/591	Invitrogen	D3861
Catalase from bovine liver	Sigma	C1345
CellTox™ Green	Promega	G8731
Chloroform	Fisher Scientific	10293850
CpG ODN 1826	IDT	na
Criterion™ TGX Stain-Free™ Protein Gel, 18 well (4 - 15 %)	BioRad	5678084
Criterion™ TGX Stain-Free™ Protein Gel, 26 well (4 - 15 %)	BioRad	5678085
CSF-1 (human)	in-house produced	na
DAPI	Sigma	10236276001
DMEM	Gibco	41966-029
DMEM w/o phenol red	Gibco	21063029
DNA Gel Loading Dye 6x	NEB	B7025
DNA Ladder 1 kb	NEB	N3232
DNA Ladder 100 bp	NEB	N3231
dNTPs	Thermo Fisher	R0181
Doxycycline hydrochloride	Sigma	D3447
Dry milk	Roth	170-6404
Erastin	Selleckchem	S7242
Ethanol	Honeywell	15642470
Ferrostatin-1	Sigma	SML0583
Fetal bovine serum (FBS)	Biochrome	S0115
FLT3L (human)	in-house produced	na

FreeStyle™ 293 Expression Medium	Gibco	12338018
G418	Sigma	G8168
GelRed nucleic acid stain	Biotium	41003
GM-CSF (murine)	PeptoTech	315-03
Halt™ Protease and Phosphatase Inhibitor Cocktail	Thermo Fisher	78440
HindIII restriction enzyme	NEB	R0104
Horseradish peroxidase	Sigma	P8375
Hydrogenperoxide (3 %)	Sigma	88597
IFN γ (murine)	PeptoTech	315-05
IL10 (murine)	PeptoTech	210-10
IL4 (murine)	in-house produced	na
IL4i1 (human) recombinant protein	R&D systems	5684-AO-020
IL4i1 (mouse) recombinant protein	R&D systems	5576-AO-020
IL6 (murine)	PeptoTech	216-16
Indole-3-pyruvic acid	Sigma	I7017
Isopropanol	Honeywell	33539
Ketoconazole	Acros Organics	455470010
Kynurenic acid	Sigma	K3375
Lipofectamine™ 3000	Invitrogen	L3000015
Lipofectamine™ RNAiMax transfection reagent	Invitrogen	13778075
L-Kynurenine	Sigma	K8625
LPS (E.coli O111:B4)	Sigma	L4391
Methanol	Honeywell	15663710
NheI restriction enzyme	NEB	R3131
Nitrocellulose membrane Protran 0.2 μ m	Amersham	10600001
NotI restriction enzyme	NEB	R0189
Oligo d(T)16 (50 μ M) Primer	Invitrogen	N8080128
OptiMEM	Gibco	31985062
Paraformaldehyde (16 %)	Alfa Aesar	43368
PBS	Gibco	10010015
Penicillin-streptomycin	Lonza	09-757F
PNGaseF	NEB	P0704
poly(I:C)	Invivogen	tlrl-pic
Precision Plus Protein Dual Color Standard	BioRad	1610374
Proteinase K	Invitrogen	25530049
Proteinogenic L-amino acids, Cellpure	Roth	na
Puromycin	Thermo Fisher	A1113802
Random hexamer primers	Invitrogen	N8080127
RIPA buffer (10X)	abcam	ab156034
RPMI	Gibco	61870-010
Sbfl restriction enzyme	NEB	R3642
siRNA HO-1	Invitrogen	4390824 (S6673)
siRNA Scrambled	Invitrogen	4390843
Sodiumphenylpyruvate	Alfa Aesar	H56767
SsoAdvanced Universal SYBR Green Supermix	BioRad	1725274
Strep-TactinXT Superflow Beads	lba	2-4090-002
Strep-TactinXT Superflow Cartridge	lba	2-1239-001

SuperScript IV Reverse Transcriptase	Invitrogen	18090050
T4 DNA Ligase	NEB	M0202
T4 Polynucleotide Kinase	NEB	M0201S
TaqMan™ Fast Advanced Mastermix	Applied Biosystems	4444557
TaqMan™ GAPDH (mouse) primer/probe	Applied Biosystems	4352932E
TNF α (murine)	PeptoTech	315-01A
Toyopearl Sulfate-650F 5 ml column	Tosoh Bioscience	0045241
Triton X-100	Sigma	X100
TRIzol reagent	Invitrogen	15596026
UltraPure™ Nuclease free water	Invitrogen	10977035
Zinc (II) protoporphyrin IX	Sigma	691550
β -mercaptoethanol ($\geq 99\%$)	Sigma	M3148
β -mercaptoethanol for cell culture (50 mM)	Gibco	31350010

Table 2 Overview of relevant chemicals and reagents

3.1.2. Antibodies

Reactivity	Identifier	Supplier	dilution
AhR (mouse, human)	83200S	Cell Signaling Technologies	1:1000
Grb2 (mouse, human)	610112	BD	1:1000
HO-1 (human)	ADI-SPA-895	Enzo	1:1000
Ido1 (mouse)	68572	Cell Signaling Technologies	1:1000
IL4i1 (mouse)	na	non-commercial generated in rabbit (verified in <i>Il4i1</i> ^{-/-} BMDMs)	1:1000
NF- κ B1 p105/p50 (mouse)	12540	Cell Signaling Technologies	1:1000
NQO1 (human)	11451-AP1	ProteinTech	1:1000
Nrf2 (human)	12721	Cell Signaling Technologies	1:1000
Sesn2 (human)	10795-1-AP	ProteinTech	1:1000
SLC7A11 (human)	12691	Cell Signaling Technologies	1:1000
Stat6 (mouse)	5397	Cell Signaling Technologies	1:1000
Strep-Tag	2-1507-001	Iba	1:2000
Vinculin (mouse, human)	13901	Cell Signaling Technologies	1:1000

Table 3 Primary antibodies used for immunoblotting

Reactivity	Conjugation	Identifier	Supplier	dilution
mouse IgG	HRP	15-035-003	Jackson ImmunoResearch	1:10,000
rabbit IgG	HRP	11-035-003	Jackson ImmunoResearch	1:10,000

Table 4 Secondary antibodies used for immunoblotting

Reactivity	Clone	Fluorophore	Supplier	Identifier	Dilution
CCR7	4B12	PE	Biolegend	120105	1:300
CD103	2E7	APC	Biolegend	121418	1:300
CD11b	M1/70	APC	Biolegend	101212	1:300
CD11c	N418	FITC	Biolegend	117306	1:300
MHC-II I-A/I-E	M5/114.15.2	Pacific blue	Biolegend	107620	1:300

Table 5 Antibodies used for flow cytometry

3.1.3. Commercial Kits

Kit	Supplier	Identifier
LookOut® Mycoplasma PCR Detection Kit	Sigma	MP0035
Mix2Seq Kit	Eurofins	na
NEBNext Poly(A) mRNA Magnetic Isolation Module	NEB	E7490
NEBNext Ultra II Directional RNA Library Prep Kit for Illumina	NEB	E7760
NextSeq 500 High Output Kit v2.5	Illumina	200249
Pierce BCA Protein Assay Kit	Thermo Fisher	23225
Pierce SuperSignal West Pico Substrate	Thermo Fisher	34080
QIAGEN Plasmid Maxi Kit	Qiagen	12162
QIAprep Spin Miniprep Kit	Qiagen	27106
QIAquick Gel extraction Kit	Qiagen	28706
QIAquick PCR purification Kit	Qiagen	28106
RNeasy Mini Kit	Qiagen	74104
TOPO™ TA Cloning™ Kit	Invitrogen	K457540

Table 6 Commercial Kits

3.1.4. Plastics

Plastics	Supplier	Identifier
μ-Slide 8 Well Glass Bottom	ibidi	80827
Amicon Ultra 10 kDa filters	Millipore	UFC901008
Amicon Ultra 3 kDa filters	Millipore	UFC800324
Cell culture dish, 10 cm	Falcon	353003
Cell culture dish, 15 cm	Corning	430599
Cell culture plate, 12 well	Corning	3513
Cell culture plate, 12 well suspension	Greiner	665102
Cell culture plate, 48 well	Corning	3548
Cell culture plate, 6 well	Greiner	657160
Cell culture plate, 96 well	Corning	3596
Cell culture T25 flask	Greiner	690175
Cell culture T75 flask	Greiner	658175
Cell scrapers	Sarstedt	833.951
Cell strainer, 70 μm	Falcon	352350
FINE-JECT 26G needles	Henke Sass Wolf	4710004525
HENKE-JECT 5 ml syringe	Henke Sass Wolf	5050.X00V0
Microcentrifuge tubes	Eppendorf	30.120.086
Microplate 96 well, black	Greiner	655900
Nalgene Rapid-Flow 75 mm bottle top filter	Thermo Scientific	10300461
PCR SingleCap 8er-SoftStrips, 0.2 ml	Biozym	710970
Polystyrene round-bottom tube, 5ml	Falcon	352054
Satocon Slice 200	Sartorius	3081442902E--SW

Table 7 Plastics

3.1.5. Buffers

Buffer	Composition
Red blood cell lysis buffer (10X)	41.45 g NH ₄ Cl
	1 ml 0.5M EDTA
	5.45 g KHCO ₃
	H ₂ O to final 500 ml, pH 7.3
TBE (5X)	216 g Trizma base
	110 g Boric acid
	H ₂ O to final 4 L
Cell lysis buffer (for DNA extraction)	100 ml 1M Tris pH 8
	10 ml 0.5 M EDTA
	20 ml 10% (w/v) SDS
	40 ml 5 M NaCl
	H ₂ O to final 1 L
TE	5 ml 1M Tris pH 8
	1 ml 0.5 M EDTA
	H ₂ O to final 500 ml
LB medium	10 g Tryptone
	5 g Yeast extract
	10 g NaCl
	H ₂ O to final 1 L, autoclave
SDS loading buffer	7.5 ml Tris-HCl pH 6.8
	2.4 g SDS
	12 ml Glycerol
	0.012 g Bromophenol blue
Tris-Glycine buffer (10X)	151.43 g Trizma base
	713.17 g Glycine
	H ₂ O to final 5 L
SDS running buffer	500 ml 10X Tris-Glycine buffer
	50 ml 10% SDS
	H ₂ O to final 5 L
Transfer buffer	500 ml 10X Tris-Glycine buffer
	500 ml Methanol
	H ₂ O to final 5 L
Ponceau red solution	1 g Ponceau S
	50 ml acetic acid
	H ₂ O to final 1 L
Stripping buffer	31.25 ml 1M Tris-HCl pH 6.8
	100 ml 10% (w/v) SDS
	3.52 ml β-mercaptoethanol
	H ₂ O to final 500 ml
TBS (10X)	60.6 g Trizma base
	87.6 g NaCl
	H ₂ O to final 1 L, pH 7.6

TBS-T	100 ml 10X TBS
	1 ml Tween-20
	H ₂ O to final 1 L
Sodium phosphate buffer (50 mM)	4.1 g Na ₂ HPO ₄
	3.29 g NaH ₂ PO ₄
	H ₂ O to final 1 L, pH 7.0

Table 8 Buffers

3.2. DNA-based methods

3.2.1. Agarose gel electrophoresis and DNA purification from agarose gels

Agarose gel electrophoresis was performed to separate DNA fragments according to their size or validating the size of PCR fragments. Depending on the expected size of the fragments 0.8 % – 2 % agarose gels (in TBE buffer) were prepared. GelRed was used as DNA staining agent and added to the samples together with a 6X loading dye. To estimate fragment sizes a DNA ladder (100 bp or 1 kb) was loaded. Gels were run for 30 – 90 min at 120-180 V and imaged using the Bio-Rad ChemiDoc imaging system. DNA fragments were purified from agarose gels with the QIAquick Gel Extraction Kit according to the manufacturer's instructions.

3.2.2. Genomic DNA extraction from cells

For genomic DNA extraction, cells were suspended in cell lysis buffer supplemented with proteinase K (1.5 U per sample) and incubated for ~ 1 h at 55 °C to enable complete cell lysis. 100 % isopropanol was added for DNA precipitation and the DNA was pelleted by 10 min centrifugation at 12,000 x g. The DNA pellet was washed with 70 % ethanol and finally dissolved in nuclease free water.

3.2.3. Basic PCR protocol for amplification DNA fragments

A standard PCR protocol was used for the amplification of DNA fragments <1 kb (genotyping of mice and verification of knockout cell lines). A reaction mix using the AmpliTaqGold DNA Polymerase Kit (applied biosystems) was prepared with 10 – 100 ng of template DNA as shown in Table 9. PCRs were run on the C1000 Touch thermal cycler (Bio-Rad) with the setup displayed in Table 10. The correct size of the PCR fragments was verified by agarose gel electrophoresis. If required for further processing, PCR fragments were purified using the QIAquick PCR purification Kit according to the manufacturer's protocol.

component	Volume/ amount per sample
10x PCR buffer II	3.0 µl
MgCl ₂ Solution (25 mM)	3.0 µl
dNTPs (10 mM)	0.3 µl
Primers (each)	0.1 µl
AmpliTaqGold DNA Polymerase	0.1 µl

DNA	10 - 100 ng
H ₂ O	adjust to 30 µl total

Table 9 PCR reaction mix

step	temperature	time
1. initial activation	95 °C	10 min
2. denaturation	95 °C	30 s
3. annealing	59 °C	1 min
4. extension	72 °C	1 min
5. final extension	72 °C	5 min
cycles: 32x step 2 - 4		

Table 10 PCR cyclor setup

3.2.4. Plasmid amplification in competent cells

3.2.4.1. Heat shock transformation

For the amplification of plasmids, competent Mach1 *E.coli* cells were transformed using a standard heat shock protocol. Competent cells were thawed for 15 min on ice. Plasmid DNA or ligation reaction was added to the bacteria and the mixture was incubated for further 30 min on ice. Subsequently, a heat shock was performed for 45 sec at 42 °C followed by 2 min incubation on ice. 950 µl SOC medium was added and bacteria were grown for 1 h shaking at 37 °C. Finally, bacteria were plated on LB agar plates containing the appropriate antibiotic for selection of transformed clones, which were subsequently picked for expansion in LB medium containing antibiotics for selection.

3.2.4.2. Plasmid isolation

Plasmids were isolated from bacteria cultures using the QIAprep Miniprep (3 ml cultures) and QIAGEN Maxiprep (300 ml) kits following the manufacturer's protocol. For long term storage plasmid DNA was dissolved in TE buffer.

3.2.5. Molecular cloning

3.2.5.1. Generation of PiggyBac PB-T-PAF plasmids for recombinant expression of *N. naja* LAAO, murine and human IL4i1

In order to express and purify recombinant secreted L-amino acid oxidases (*N. n.* LAAO, human IL4i1, murine IL4i1), the respective sequences were cloned into PB-T-PAF vectors of the PiggyBac expression system [291]. This system is described in more detail in chapter 4.1, since the generation and investigation of the recombinant proteins was part of the first aim of this thesis. The inserts containing a secretion sequence, the cDNA of the secreted part of the protein and a Twin-Strep-Tag were flanked by a NheI and NotI restriction site and synthesized by Genewiz (Leipzig, Germany). PB-T-PAF plasmid and inserts were digested with NheI and

NotI restriction enzymes and the PB-T-PAF backbone fragment was purified from a 1% agarose gel. Vector backbone and inserts were ligated in a 1:3 molar ratio using the NEB T4 ligase according to the supplier's protocol. The ligation reaction was transformed into competent cells and the correct insertions were confirmed by Sanger sequencing (Mix2Seq, Eurofins) of the isolated plasmids. Fragments carrying point mutations that potentially disrupt the enzymatic activity of the proteins were cloned into the respective PB-T-PAF expression plasmids using restriction sites that were included into the regions of the mutation when designing the insert fragments for synthesis. For the R320A, K324A mutation in the *N. naja* LAAO BbvCI and BglII sites were used, for the K351A mutation in murine IL4i1 BbvCI and SbfI sites and for the K354A mutation in human IL4i1 BbvCI and HindIII sites were used as marked in the plasmid maps (Figure 11, Supplementary Figure 1, Supplementary Figure 2).

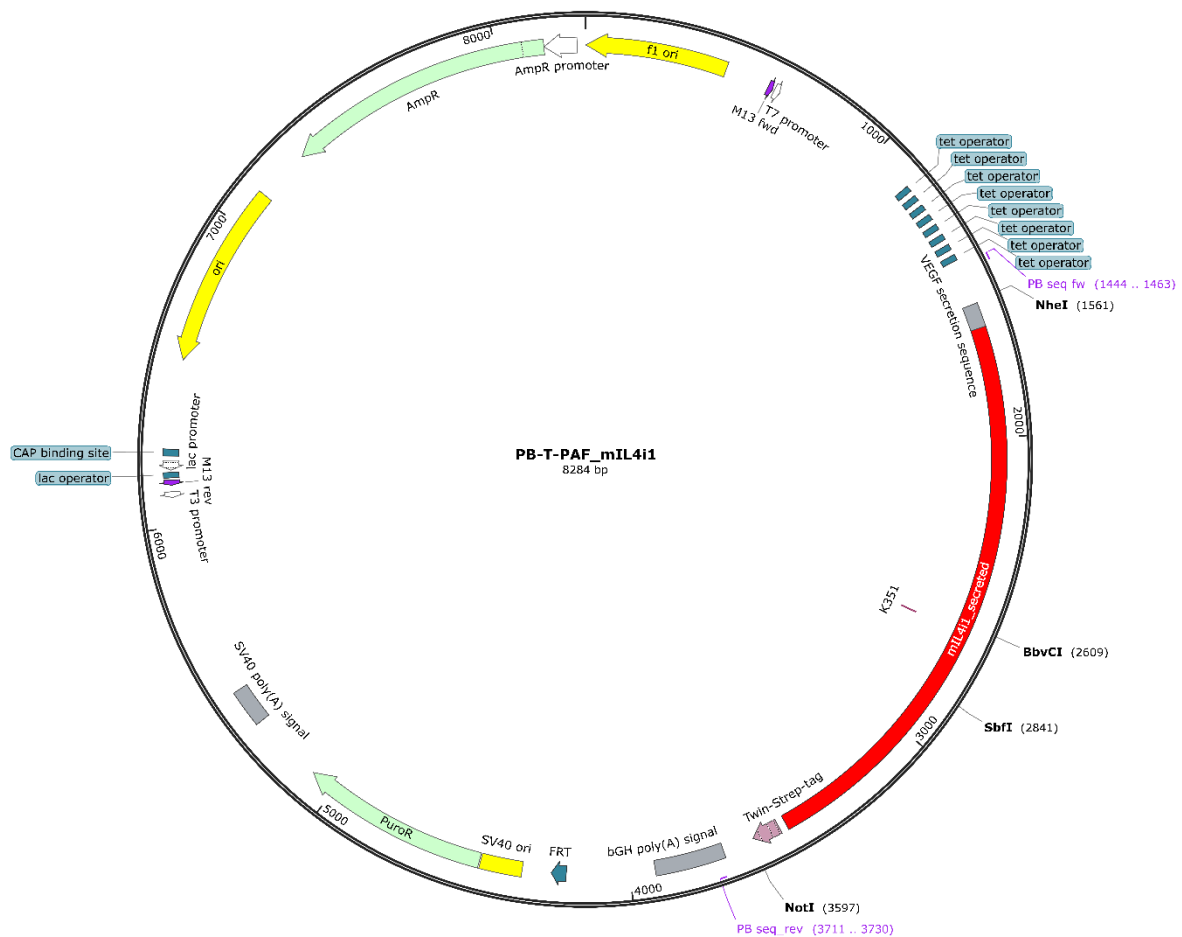


Figure 11 Plasmid map of PB-T-PAF_mIL4i1 encoding murine IL4i1

Plasmid map shows the PB-T-PAF vector of the PiggyBac system allowing doxycycline-inducible expression of murine IL4i1. NheI and NotI restriction sites were used for cloning. The human VEGF secretion sequence was added for optimal protein secretion in the human HEK293T expression cell line and a C-terminal Twin-Strep-Tag was added to enable efficient protein purification. BbvCI and SbfI sites were used to clone a fragment encoding the K351A mutation into the plasmid.

3.2.5.2. Generation of pX458 plasmids for AhR and Nrf2 knockout

To generate AhR and Nrf2-deficient cell lines, sequences encoding guideRNAs (gRNAs) targeting the respective genes were cloned into a plasmid from the Zhang lab [292] (pSpCas9(BB)-2A-GFP (pX458); #48138 Addgene) (Supplementary Figure 3), which additionally encodes a GFP-tagged Cas9. The used gRNA sequences were selected from the literature [293]. Oligonucleotides containing the gRNA sequence were ordered from IDT (Coralville, Iowa):

name	sequence (5' → 3')
AhR_fw	CACCGGGCAGCAGGCTAGCCAAA
AhR_rev	AAACTTTGGCTAGCCTGCTGCCCC
Nrf2_fw	CACCGGACAAGAACAACCTCCAAA
Nrf2_rev	AAACTTTGGAGTTGTTCTTGCTCC

Table 11 Oligonucleotides encoding AhR and Nrf2 targeting guideRNAs

Complementary oligonucleotides for cloning into PX458 plasmid. Gene targeting sequence is displayed in bold, the other bases represent overhangs.

Oligonucleotides were phosphorylated using a T4 polynucleotide kinase (NEB) according to the manufacturer's instructions and annealed through a decreasing temperature gradient from 95 °C to 25 °C in 5 °C steps. pX458 was linearized by BbsI digest and annealed oligonucleotides were inserted using the T4 DNA ligase (NEB) according to the manufacturer's protocol. The ligated construct was transformed into competent cells using heat shock transformation and 6 clones per ligation were picked for plasmid isolation. Correct insertion of the oligonucleotides was verified by Sanger sequencing (Mix2Seq, Eurofins) using a standard U6 primer (5'-ACTATCATATGCTTACCGTAA-3').

3.3. Mice

Animal experimentation described in this thesis was performed at the animal facility of the Max Planck-Institute of Biochemistry (MPIB) in accordance with the approval from the 'Regierung von Oberbayern'. The animal facility (Animal Welfare Officer, Dr. Eva Hesse) covers the housing and breeding of mice that is additionally approved by the European Union. C57BL/6 'wild type' (WT), *Tnfrsf1a*^{-/-} (purchased from the Jackson Laboratory, B6.129-*Tnfrsf1a*^{tm1Mak}/J; Bar Harbor, ME) and *Stat6*^{-/-} (purchased from the Jackson Laboratory, B6.129S2(C)-*Stat6*^{tm1Gru}/J; Bar Harbor, ME) mice were bred and maintained under specific pathogen free conditions. Genotyping was performed by PCR using specific primers for WT and knockout alleles (Table 12). Mice were euthanized by cervical dislocation following training by veterinary Dr. Corinna Mörth. Documentation was performed with the 'Max-Planck-Gesellschaft-PyRat system', which is used for reporting animal usage yearly to government entities. Bone marrow of *Nfkb1*^{-/-} mice (*Nfkb1*^{tm1Bal}) was frozen and transferred from St. Jude Children's Research Hospital, where mice were bred and sacrificed within the Animal Resource Center according

to the policies of the St. Jude Children's Research Hospital Institution Animal Care and Use Committee.

Gene	primers	sequence (5' → 3')
<i>Stat6</i>	Stat6 a mutant	AATCCATCTTGTTCAATG
	Stat6 b common	ACTCCGGAAAGCCTCATCTT
	Stat6 c WT	AAGTGGGTCCCCTTCACTCT
<i>Tnfrsf1a</i>	P55 q456 WT	TGTGAAAAGGGCACCTTTACGGC
	P55 q457 common	TGTGAAAAGGGCACCTTTACGGC
	P55 q45 mutant	ATTCGCAATGACAAGACGCTGG

Table 12 Genotyping primers

3.4. Cell culture

3.4.1. Cell lines and cultivation

HeLa, HEK293T, NIH/3T3, RS4;11 and THP-1 cell lines were purchased from the American Type Culture Collection (ATCC). HT1080 cells were kindly provided by Prof. Andreas Linkermann (University Hospital Dresden, Germany). All cell lines were tested to be free from Mycoplasma contamination by routine PCR screening using the LookOut® Mycoplasma PCR Detection Kit according to the manufacturer's protocol. HeLa, HEK293T, NIH/3T3 and HT1080 cells were cultivated in Dulbecco's modified Eagle's medium (DMEM) supplemented with 10 % fetal bovine serum (FBS) and 1 % penicillin-streptomycin in 10 cm dishes until reaching 80 - 90 % confluence. For subculturing, cells were washed with PBS and detached with 0.25 % trypsin. Cells were re-suspended in complete DMEM and the appropriate fraction was transferred to a fresh culture dish. RS4;11 and THP-1 suspension cells were grown in RPMI medium supplemented with 10 % FBS, 1 % penicillin-streptomycin and 50 µM β-mercaptoethanol in T25 or T75 flasks. Cells were passaged before reaching a density of 1 x 10⁶ cells/ml. The appropriate number of cells was taken from the culture, washed with PBS and centrifuged for 5 min at 350 x g. The cell pellet was re-suspended in an appropriate volume of culture medium and transferred into a new culture flask.

3.4.2. Primary cell cultures

3.4.2.1. Bone marrow-derived macrophages

For the generation of bone marrow derived macrophages (BMDMs), bone marrow was isolated from femur and tibia bones of WT or genetically modified C57BL/6 mice. Bone marrow was flushed through a 70 µM cell strainer into a conical 50 ml tube using PBS and a syringe with 26G needle. Cells were pelleted by 5 min centrifugation at 350 x g and erythrocytes were depleted by incubation with a hypotonic red blood cell (RBC) lysis buffer for 2 min. RBC buffer was neutralized by addition of PBS and cells were pelleted by 5 min centrifugation at 350 x g. After one additional washing step with PBS, cells derived from one mouse were re-suspended

in 45 ml DMEM with 10% FBS and 1% penicillin-streptomycin supplemented with 60 ng/ml human CSF-1. 15 ml were plated on one 15 cm dish and BMDMs were differentiated for 7-8 days, adding 3 ml of fresh medium containing 180 ng/ml CSF-1 on day 3, day 5 and day 7. After differentiation, the adherent BMDMs were detached from the dishes using a cell scraper and plated for experiments.

3.4.2.2. Bone marrow-derived dendritic cells

3.4.2.2.1. GM-CSF-differentiated dendritic cells

One type of bone marrow-derived dendritic cells (BMDCs) was differentiated using GM-CSF. Bone marrow was isolated and RBC lysis was performed as described above. 10 ml containing 1×10^6 cells/ml in RPMI medium with 10 % FBS, 1 % penicillin-streptomycin and 50 μ M β -mercaptoethanol supplemented with 20 ng/ml GM-CSF were plated in a 10 cm dish. On day 4 of differentiation, loosely adherent cells and cells in suspension were collected, centrifuged at 350 x g for 5 minutes re-plated at 1×10^6 cells/ml in fresh culture medium with 20 ng/ml GM-CSF. 5 ml of medium containing 20 ng/ml GM-CSF was added at day 6 and non-adherent cells were harvested on day 8 or 9 for experiments.

3.4.2.2.2. FLT3L-differentiated dendritic cells

For FLT3L differentiation of BMDCs, bone marrow cells were isolated as described above and plated at 1.5×10^6 cells/ml in 10 ml RPMI medium with 10 % FBS, 1 % penicillin-streptomycin and 50 μ M β -mercaptoethanol supplemented with 200 ng/ml FLT3L. On day 4, 5 ml of fresh medium containing 200 ng/ml FLT3L were added. BMDCs were harvested at day 8 or 9 of differentiation.

3.4.2.2.3. CD103 dendritic cells

The protocol for the differentiation of CD103 dendritic cells was adapted from Mayer et al. [294]. Bone marrow cells were isolated as described above and plated at 1×10^6 cells/ml in 10 ml RPMI medium with 10 % FBS, 1 % penicillin-streptomycin and 50 μ M β -mercaptoethanol supplemented with 200 ng/ml FLT3L and 10 ng/ml GM-CSF. On day 4, 5 ml of fresh medium containing 200 ng/ml FLT3L and 10 ng/ml GM-CSF were added. On day 8 of the differentiation, suspension cells and only slightly adherent cells were detached by pipetting and re-plated in a new 10 cm culture dish at 1×10^6 cells/ml in fresh RPMI supplemented with the same concentrations of the cytokines. At day 12, 5 ml of medium containing 100 ng/ml FLT3L and 5 ng GM-CSF were added to the culture. CD103 BMDCs were harvested after 15 days of differentiation.

3.4.2.3. Stimulation of macrophages and dendritic cells

After differentiation, BMDMs or BMDCs were plated for mRNA or protein analysis. 1×10^6 cells were plated in 1 ml per well of a 12-well plate. On the next day, cells were either harvested for

the analysis of baseline mRNA and protein levels or different cytokines/ toll-like receptor (TLR) agonists were added at the concentrations and for the time frames indicated with each experiment.

3.4.2.4. Infection of BMDMs with *Salmonella enterica* serovar Typhimurium

Salmonella infections were performed by Marcel Hahn from Prof. Ivan Dikic's group at the Goethe University Frankfurt. 1×10^6 BMDMs were plated in 1 ml per well of a 12-well plate. Some BMDMs were pre-treated with 10 ng/ml IL4 for 12 h before infection. Infections with *Salmonella enterica* serovar Typhimurium strain SL1344 (gift from David Holden, Imperial College London) were performed as previously described [295] with a multiplicity of infection (MOI) of 10. Following the medium change after infection, a fraction of the BMDMs was treated with 10 ng/ml IL4 over the course of the experiment. BMDMs were harvested for protein isolation 8 h after infection.

3.5. Manipulation of gene expression in cell lines

3.5.1. Transient transfection with Lipofectamine

For transient transfections cells were seeded at ~ 60% confluence per well of a 6-well or 12-well plate. The following amounts were used for transfections in 6-well plates and were halved for the transfection in 12-well plates. In a first tube, 125 μ l OptiMEM were mixed with 7.5 μ l of Lipofectamine3000 reagent and in a second tube 1.5 μ g of DNA were mixed with 125 μ l of OptiMEM and 3 μ l of P3000 reagent. Subsequently, the content of both tubes was mixed, vortexed and incubated for 10 min at room temperature (RT). After the incubation time 250 μ l of the transfection mix were added per well.

3.5.2. Generation of knockout cell lines using the CRISPR/Cas9 system

3.5.2.1. Generation of knockout clones

HeLa cells were transfected with the pX458_AhR or pX458_Nrf2 plasmids described above (3.2.5.2). After 48 h, cells were detached with trypsin and transfected cells were identified and sorted due to Cas9-GFP expression with the FACS Aria device. Single cells were sorted into each well of a 96-well plate and clones were expanded over time.

3.5.2.2. Verification of knockouts

Genomic DNA was purified as described before (3.2.2) in order to verify the knockouts. PCRs covering the targeted region of AhR or Nrf2 with the primer sequences shown below (Table 13) were performed to amplify the region with potential mutations for sequencing. Sequences of the PCR product were determined by Sanger sequencing (Mix2Seq, Eurofins) and aligned to the WT sequence using the SnapGene 6.0 software to exclude WT clones and validate clones carrying the same mutations on both alleles (Figure 12). In case of an incomplete sequencing result because of different sequences on both alleles, PCR products were TOPO

cloned using the TOPO™ TA Cloning™ Kit from Invitrogen according to the manufacturer's instructions. Plasmids isolated from clones obtained after TOPO cloning were sequenced and sequences aligned to the WT sequences, allowing to characterize clones with different mutations on both alleles and to exclude clones with an incomplete, heterozygous knockout. The clones generated as part of this thesis (Figure 12) have been included into a previous publication from the group [61].

name	sequence (5' → 3')
AhR_PCR_fw	AAAGCCAATCCCAGCTGAAG
AhR_PCR_rev	CCAGGAGTGTATGTTTTGGCT
Nrf2_PCR_fw	CCAATTCCCACCATCAACAG
Nrf2_PCR_rev	GGGAGTAGTTGGCAGATCCA

Table 13 Primer sequences for validation of AhR and Nrf2 knockouts

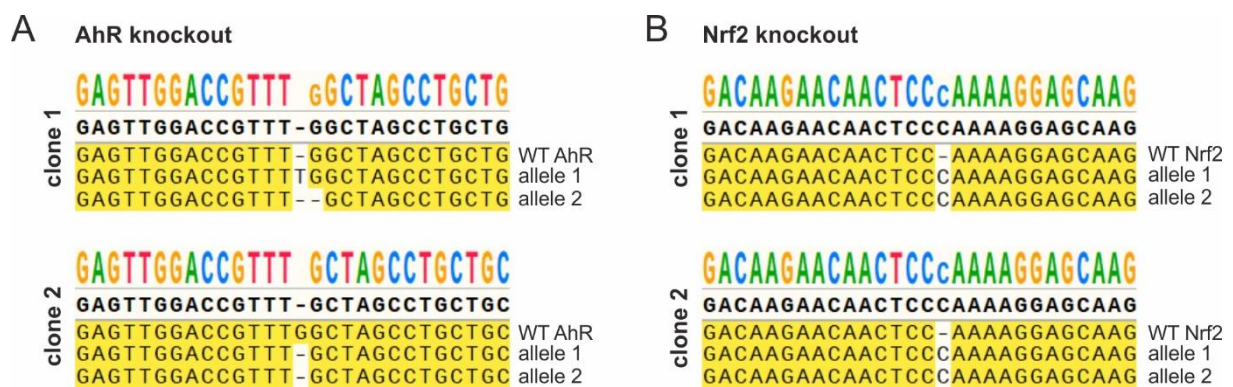


Figure 12 Validation of AhR and Nrf2 knockouts

Sequence alignments showing the genetic modifications in the genomic DNA of the knockout clones in the region targeted by the guide RNAs. Sequences were aligned to the WT reference sequences. (A) Sequencing result of AhR knockout clones used in this thesis. Clone 1 exhibits one allele with a one-base pair insertion and one allele with a one-base pair deletion. Clone 2 has a bi-allelic one-base pair deletion (B) Sequencing result of Nrf2 knockout clones used in this thesis. Both clones have a one-base pair insertion. All modifications display frameshift mutations.

3.5.3. siRNA-mediated knockdown

HO-1 was knocked down in HeLa cells using an siRNA-based approach. HeLa cells were plated at 2×10^5 cells/well in six well plates one day before transfection. The Lipofectamine RNAiMAX Transfection Reagent (Invitrogen) was used according to the manufacturer's instructions to transfect the cells with 50 nM of a scrambled siRNA (4390843, Invitrogen) control or an HO-1 siRNA (4390824, s6673, Invitrogen). 10 h after transfection the cells were re-plated for ferroptosis assays or stimulations for protein isolation, which were performed on the next day after the cells properly attached to the culture plates.

3.5.4. Generation of stable cell lines using the PiggyBac expression system

For the generation of recombinant proteins, stable cell lines using the PiggyBac transposon system, which is described in section 4.1.1. HEK293T cells were co-transfected with the PB-

T-PAF expression plasmids (3.2.5.1), PB-RN [291] (Supplementary Figure 4) and pCMV-hyPBase [296] (Supplementary Figure 5). 24 h after transfection, cells with stable integration of PB-T-PAF and PB-RN were selected by cultivation with 10 µg/ml puromycin and 500 µg/ml G418 for 21 days. After the selection, stable pools were grown in medium without antibiotics.

3.6. Protein-based methods

3.6.1. Generation and isolation of secreted recombinant proteins

Recombinant *N. naja* LAAO, murine and human IL4i1 were generated in collaboration with Dr. Sabine Suppmann and her team from the Protein Production Core Facility of the MPIB. Stable, inducible HEK293T pools generated with the PiggyBac system were grown at a density of 1×10^6 cells per ml in FreeStyle 293 Expression Medium. Protein expression was induced by 1 µg/ml doxycycline. 7 days after induction the supernatant containing the secreted proteins was harvested and filtered using a Nalgene Rapid-Flow 75 mm bottle top filter.

N. naja LAAO was purified from 2 l of supernatant, which was concentrated to 50 ml in 20 mM MES (pH 6.0) and 50 mM NaCl by diafiltration (Satocon Slice 200). The concentrate was loaded onto a Toyopearl Sulfate-650F 5 ml column (Tosoh Bioscience) for ion exchange chromatography with a linear gradient up to 20 mM MES (pH 6.0) and 2000 mM NaCl for elution. Fractions containing LAAO were further purified by incubation with Strep-TactinXT Superflow Beads for 1 h on a rotating wheel. After washing (PBS) the protein was eluted with 50 mM biotin in PBS.

For purification of human and murine IL4i1 the supernatant was loaded on a Strep-TactinXT Superflow cartridge using an ÄKTA pure chromatography system. After washing, the protein was eluted in two consecutive 30 min steps with 50 mM biotin in PBS. Protein purity was confirmed via sodium dodecyl sulfate polyacrylamide gel electrophoresis (SDS-PAGE).

3.6.2. Deglycosylation of recombinant proteins by PNGaseF digest

In order to test the glycosylation status of the purified proteins N-glycosylations were removed by PNGaseF digest. 1 µg of recombinant protein was digested with NEB PNGaseF following the manufacturer's protocol for denaturing reaction conditions. Samples without addition of PNGaseF were used as control to visualize the size shift via immunoblotting.

3.6.3. Cell lysis, protein extraction and determination of protein concentration

For the detection of proteins by immunoblotting, cells were usually plated in 12 well plates on the day before starting an experiment. Adherent cells were washed with cold PBS in the plate, which was placed on ice, prior to lysis with 60 – 100 µl of RIPA buffer supplemented with Halt™ Protease and Phosphatase Inhibitor Cocktail. Cells were scraped with the backside of a pipette tip and transferred to 1.5 ml tubes. THP-1 and BMDC suspension cells were collected by centrifugation at 350 x g at 4°C, washed with cold PBS and, after a further centrifugation, lysed

in RIPA buffer. Samples were vortexed and incubated for ~ 20 min on ice to ensure complete lysis. Subsequently, the lysates were cleared from debris by centrifugation at 14,000 x g for 10 min at 4°C. Supernatants were taken off and stored at -80°C until further usage.

Protein concentrations were determined with an Bicinchoninic acid (BCA) assay using the Pierce BCA Protein Assay Kit according to the instructions, measuring the absorbance with the Tecan Spark microplate reader. A standard curve generated from samples with known concentrations of bovine serum albumin (BSA) allowed the calculation of the protein concentration in the samples.

3.6.4. SDS-PAGE and Immunoblotting

Protein samples for immunoblotting (cell lysates or supernatants without any further protein concentration) were mixed with SDS loading buffer supplemented with 5 % β -mercaptoethanol and denatured for 5 min at 95 °C. Proteins were separated by SDS-PAGE using 4–15 % Criterion TGX Stain-Free protein gels in Criterion Vertical Electrophoresis Chambers (Bio-Rad) filled with Tris/glycine/SDS Running buffer. For the estimation of protein sizes a protein standard was loaded next to the samples (Precision Plus Protein Dual Color Standard or BenchMark™ Protein Ladder for the detection of Strep-tagged proteins). Electrophoresis was started at 90 V until samples had entered the gel and was subsequently set to 150 V. After separation, the proteins were blotted onto a 0.2 μ M nitrocellulose membrane (Amersham): A stack consisting of sponge pad – Whatman™ paper – gel – membrane – Whatman™ paper – sponge pad was put in a gel holder cassette and placed into a Bio-Rad Trans-Blot Cell filled with pre-cooled Transfer buffer and proteins were blotted for 2 h at 35 V. Successful blotting was confirmed by protein staining with Ponceau S solution and the membrane was cut into appropriate fragments for protein detection. Membranes were blocked for 1 h in 3 % milk in TBS-T, before incubation with the primary antibodies (Table 3) diluted in 3% milk in TBS-T over night (ON) at 4 °C. On the next day, membranes were washed three times in TBS-T and subsequently incubated with horse radish peroxidase (HRP)-coupled secondary antibody (Table 4) for 1 h at RT. After three washing steps in TBS-T and one final wash in ddH₂O membranes were developed using SuperSignal West Pico ECL Substrate and images were taken with the Bio-Rad ChemiDoc Imager. For re-probing with different primary antibodies, membranes were incubated shaking for 25 min at 65 °C in stripping buffer. After three washes in TBS-T membranes were again blocked and incubated with antibody as described above.

3.6.5. Mass spectrometry-based secretomics

For secretome analysis 2×10^6 BMDMs were plated per well of a 6-well plate in DMEM without phenol red supplemented with 10 % FBS and 1 % penicillin-streptomycin. On the next day, BMDMs were washed with FBS-free medium and treated in triplicates with IL4 (10 ng/ml), LPS (10 ng/ml) or IL4 + LPS (both 10 ng/ml) in FBS-free medium, which was also used for the

unstimulated control. Supernatant was collected 24 h after stimulation. Dead cells and debris were removed by a 5 min centrifugation step at 350 x g at 4 °C followed by a second centrifugation step for 5 min at 1000 x g. Cleared supernatants were frozen at -80 °C until further processing. Mass spectrometry (MS)-based secretome analysis was performed by Jonathan Swietlik from Prof. Matthias Mann's research group at the MPIB. Cell supernatants were concentrated to ~20 µl and washed with 50 mM Tris (pH 8) using Amicon Ultra 3-kDa cutoff filter units at 4 °C. Concentrated supernatants were supplemented with 10 mM Tris(2-carboxyethyl)phosphine and 40 mM 2-chloroacetamide, and heated in a thermoshaker for 10 min at 95 °C and 1000 rpm. Afterwards, samples were digested with 1 µg of trypsin/LysC for 16 h at 37 °C and 1000 rpm. Samples were acidified by adding 100 µl of isopropanol and 1 % trifluoroacetic acid, and desalted using in-house-produced styrenedivinylbenzene- reverse phase sulfonate (SDB-RPS) StageTips. Desalted peptide mixtures were reconstituted in buffer A (0.1 % formic acid) and analyzed with an EASY-nLC 1200 ultrahigh-pressure system (Thermo Fisher Scientific) coupled to an Orbitrap Exploris 480 instrument (Thermo Fisher Scientific). 300 ng peptides per sample were loaded on to a 50-cm in-house-produced column with 75-µm inner diameter, packed with C18 1.9-µm ReproSil beads (Dr. Maisch GmbH). Peptides were eluted with a nonlinear gradient starting at 5 % buffer B (80 % acetonitrile, 0.1 % formic acid) followed by a stepwise increase to 30 % in 95 min, 60 % in 5 min and a wash-out step for 20 min with an increase to 95 % buffer B and subsequent decrease to 5 % buffer B. Spectra were acquired with a data-independent acquisition (DIA) method using full scans with a range of 300 – 1650 m/z (AGC target = 3e6, maximum injection time = 60 ms, resolution = 120,000 at 200 m/z) followed by MS/MS scans in 32 windows (nce = 27 %, AGC target = 1e6, maximum injection time = 54 ms, resolution = 30,000 at 200 m/z). DIA MS raw files were processed by DIA-NN (version 1.8) with 'FASTA digest for library-free search', and 'deep learning-based spectra, RTs, and IMs prediction' enabled. Precursor false discovery rate (FDR) was set to 1 %, and default parameters were used with the following changes: The precursor range was restricted to 300 – 1650 m/z and the fragment ion range to 200 – 1650 m/z. The '--relaxed-prot-inf' option was enabled via the command line. Mass accuracies and scan windows were optimized for individual experiments as recommended by the developers. Match between runs (MBR) was enabled, neural network classifier was set to 'double-pass mode' and quantification strategy to 'robust LC (high accuracy)'. Spectra were matched against the mouse UniProt FASTA database (January 2022, 55,105 entries). The Perseus software (version 1.6.14.43) was used for further bioinformatic analysis. Data were log₂-transformed and filtered for protein groups detected in at least two of the three replicates in at least one of the experimental conditions. Missing values were imputed from a normal distribution with a downshift of 1.8 and a width of 0.3. Differences between the secretomes of stimulated BMDMs compared to unstimulated BMDMs were tested using a two-sided Student's t-test (250

randomizations, FDR threshold 0.05, $S_0=0.2$) and visualized by volcano plots. The 10 protein groups showing the highest increase of secretion upon IL4 + LPS stimulation were visualized in a heat map after generation of row z-scores and hierarchical clustering (Euclidean distance, average linkage).

3.7. Gene expression analysis

3.7.1. RNA isolation, cDNA generation and quantitative real-time PCR

To analyze gene expression changes by quantitative real-time PCR (qRT-PCR), cells were seeded in triplicates per condition in 12-well plates. For RNA extraction, cells were dissolved in 1 ml TRIzol reagent and transferred to a 1.5 ml tube. 200 μ l chloroform was added, the samples were mixed and subsequently centrifuged at 18,000 x g for 10 min at 4 °C to obtain phase separation. 400 μ l of the colorless liquid phase were added into a fresh tube containing 500 μ l of 100 % isopropanol. RNA was precipitated ON at -20 °C and pelleted by centrifugation at 18,000 x g for 10 min at 4 °C. RNA pellets were washed with 70 % ethanol and centrifuged again under the same conditions. Ethanol was carefully removed and the pellets were allowed to dry by leaving the tube caps open for ~5 min. Finally, 25 μ l of nuclease free water was added per tube and the samples were stored at -80°C. For cDNA generation by reverse transcription, RNA content was measured using a NanoPhotometer P330 (IMPLEN). 1 μ g of RNA was adjusted to a volume of 11 μ l with nuclease free water in a PCR tube and 1 μ l of a primer master mix (Table 14) was added per sample. Primer annealing was performed by 4 min incubation at 65 °C followed by 10 min incubation on ice. Subsequently, 8 μ l of the SuperScript IV (SSIV) reverse transcriptase master mix (Table 15) was added and the reaction was incubated for 2 h at 42 °C. After the reverse transcription the cDNA was diluted with 80 μ l nuclease free water.

component	volume per sample
oligo(dT) ₁₂₋₁₈ primer	0.4 μ l
random hexamer primer	0.06 μ l
nuclease free water	0.54 μ l

Table 14 Primer master mix for reverse transcription

component	volume per sample
5x SSIV first strand buffer	4 μ l
DTT	2 μ l
dNTPs (10 mM)	0.5 μ l
nuclease free water	1.25 μ l
SSIV reverse transcriptase	0.25 μ l

Table 15 Reverse transcriptase master mix

Quantification of gene expression changes was analyzed by qRT-PCR using specific primers for the respective transcripts (Table 16) with a SYBR Green-based reaction mix (Table 17). Mouse GAPDH housekeeper transcript was detected using a TaqMan-based primer/probe mix

(Table 18). qRT-PCR was run in a Bio-Rad CFX96 cycler programmed with the appropriate protocol (Table 19, Table 20). Ct values were determined using the regression mode for threshold determination in the Bio-Rad CFX Manager 3.1 Software. If not indicated otherwise, the relative gene expression was calculated by the $\Delta\Delta C_t$ method, normalizing the transcript level to the respective GAPDH housekeeper control and calculating the fold change to the mean of the untreated controls.

transcript	primer	sequence (5' → 3')
CYP1A1 (human)	hCYP1A1_fw	AGATCAACCATGACCAGAAGCTA
	hCYP1A1_rev	CGATAGCACCATCAGGGGTG
CYP1B1 (human)	hCYP1B1_fw	TCACCAGGTATCCTGATGTGC
	hCYP1B1_rev	GGTCACCCATACAAGGCAGA
GAPDH (human)	hGAPDH_fw	GTTTCGACAGTCAGCCGCATC
	hGAPDH_rev	GGAATTTGCCATGGGTGGA
IL4i1 (mouse)	mIL4i1_fw	GCGAATGCCAGCTCTCACAG
	mIL4i1_rev	TTCACATTATGCACCTCCGTCCAC

Table 16 Primers used for SYBR Green-based pRT-PCR

component	volume per sample
forward primer	0.2 μ l
reverse primer	0.2 μ l
SsoAdvanced SYBR Green Supermix	5 μ l
nuclease free water	2.6 μ l
cDNA	2 μ l

Table 17 SYBR Green qRT-PCR mix

component	volume per sample
GAPDH primer/probe	0.5 μ l
TaqMan™ Fast Advanced Mix	5 μ l
nuclease free water	0.5 μ l
cDNA	4 μ l

Table 18 TaqMan qRT-PCR mix for the detection of mouse GAPDH

step	temperature	time
1. initial activation	95 °C	30 s
2. denaturation	95 °C	10 s
3. annealing/extension	60 °C	30 s
cycles: 40x step 2 & 3		

Table 19 Cycler setup for SYBR Green-based qRT-PCR

step	temperature	time
1. initial activation	50 °C	2 min
	95 °C	2 min
2. denaturation	95 °C	3 s
3. annealing/extension	60 °C	30 s
cycles: 39x step 2 & 3		

Table 20 Cycler setup for TaqMan-based qRT-PCR

3.7.2. mRNA-Seq based transcriptomics

THP-1 cells were seeded at 0.3×10^6 cells/ml in 12-well plates and treated for 24 h in triplicates with 200 μ M PP, 4HPP or I3P dissolved in complete RPMI medium. Complete RPMI medium without addition of amino acid metabolites was used as control. HeLa cells were seeded at 0.1×10^6 cells/ml in 12-well plates and treated in triplicates for 24 h with complete DMEM containing 200 μ M I3P or complete DMEM pre-incubated for 72 h with 1 μ g/ml murine IL4i1 (WT or K351A mutant). Complete DMEM medium was used as control. RNA was purified using the QIAGEN RNeasy Mini kit according to the manufacturer's protocol.

mRNA sequencing and analysis was performed at the MPIB next generation sequencing (NGS) core facility by Dr. Rin Ho Kim and Dr. Assa Yeroslaviz. Sequencing libraries were prepared from 1 μ g of RNA from each sample using the NEBNext Ultra II Directional RNA Library Prep Kit for Illumina with a NEBNext Poly(A) mRNA Magnetic Isolation Module according to the supplier's protocol. Quality control from total RNA and final library were performed with the Qubit Flex Fluorometer (Q33327, Thermo Fisher Scientific) and the 2100 Bioanalyzer system (G2939BA, Agilent). Paired-end sequencing was performed on an Illumina NextSeq 500 device (2 x 43 bp reads). Samples were multiplexed and sequenced on one High Output Kit v2.5 to reduce batch effects. BCL raw data were converted to FASTQ format and bcl2fastq Conversion Software (Illumina) was used for de-multiplexing. BAM and bigwig files were generated by STAR alignment and file conversion scripts – bam2wig and wigToBigWig. After quality check with the FastQC (v.0.11.7) tool the files were mapped to the human genome (Genome build GRCh38 from Ensembl) using the star aligner (v. 2.7.3a) [297]. Mapped files were quantified on gene level based on the Ensembl annotations, using the featureCounts [298] tool from the SubRead package [299] (v. 1.4.6-p4). The DESeq2 package (R 3.6.0, DESeq version 1.26.0) [300] was used to normalize count data by the size factor to estimate the effective library size. After calculating the gene dispersion across all samples, the comparison of each two different conditions resulted in a list of differentially expressed genes for each comparison. A filtering step was used to remove genes with no reads in at least three samples.

For the generation of volcano plots (Figure 23) genes with an adjusted p-value <0.05 were considered to be differentially expressed. Gene ontology (GO) overrepresentation analysis (biological process) was performed using the web-based PANTHER tool with Fisher's exact

test and false discovery rate (FDR) calculation. GO term overrepresentation was analyzed for the most significantly I3P-upregulated genes (adjusted p-value cutoff at $p < 10^{-9}$) using all detected genes from the dataset as reference. Clustering analysis (Figure 34) was conducted with the Perseus software (version 1.6.14.0). Genes were filtered for protein-coding genes and the reads log₂ transformed. Multiple sample testing using ANOVA (FDR threshold: 0.0001) was performed and z-scores from significant genes were used for heat map generation by hierarchical clustering (Euclidean distance, average linkage).

3.8. Fluorimetric and optical methods

3.8.1. Fluorescence microscopy of fluorescence-tagged AhR

0.2 x10⁶ NIH/3T3 cells were plated per well of a 6-well plate and transfected with a plasmid encoding an mScarlet-tagged AhR protein (pcDNA3.1_hygro_AhR-mScarlet, Supplementary Figure 6) using lipofectamine (3.5.1). 24 h after transfection cells were detached by trypsin and 0.02 x10⁶ cells were seeded per well of an 8-chamber glass bottom slide in RPMI medium containing 10% FBS. On the next day, cells were incubated for 1 h with 1 mM kynurenine, I3P or control RPMI medium at 37 °C. After washing with PBS, cells were fixed with 4 % paraformaldehyde (PFA) for 15 min at RT. Cells were washed with PBS and permeabilized with 0.2 % Triton X-100 in PBS for 1 h at RT. Nuclei were stained with 0.1 µg/ml 4',6-Diamidino-2-phenylindol (DAPI) for 15 min at RT. After washing, cells were kept in PBS and imaged with a confocal microscope (Zeiss LSM 780) using a 40 x immersion objective and the Zeiss ZEN 2011 SP7 black software (Version 14.0.2.201). DAPI and AhR-mScarlet were imaged using the 405 nm and the 561 nm excitation lasers, respectively.

3.8.2. Cell death analysis by live cell imaging

Cell death was monitored using the IncuCyte S3 live cell imager. 0.015 x10⁶ - 0.02 x10⁶ cells were seeded per well of a 48-well plate. On the next day, CellTox green dye (1:4000 – 1:6000; stains nuclei of dead cells) was added and cell death was induced by the indicated concentrations of *N. naja* LAAO, Erastin or RSL3. Live cell imaging was started directly after cell death induction. If not indicated otherwise, a 10X objective was used to take 9 images/well (phase contrast and green channel) every 2 h. The IncuCyte 2019B and 2021C software were used to analyze the cell death by quantification of the green objects, which was displayed as CellTox⁺ cells per image. In experiments using WT Hela cells and AhR or Nrf2-deficient cells (Figure 33, Figure 32), the CellTox⁺ cell count was normalized to the cell confluence to adjust for slight differences in cell plating and growth.

3.8.3. Determination of I3P fluorescence spectrum

I3P was dissolved in ddH₂O to a final concentration of 2 mM. A CLARIOstar Plus microplate reader (BMG Labtech) was used to measure the I3P fluorescence in a black 96-well

microplate. The excitation spectrum was generated by measuring the fluorescence intensity for excitation wavelengths from 320 nm to 440 nm with a stepwidth of 1 nm at an emission wavelength of 470 nm (20 nm bandwidth). The emission spectrum was generated using an excitation wavelength of 395 nm (20 nm bandwidth) and detecting the emission at wavelengths from 430 nm to 600 nm with a stepwidth of 1 nm.

3.8.4. Flow cytometry

3.8.4.1. Staining, analysis and sorting of bone marrow-derived dendritic cells

After differentiation BMDCs were harvested, washed with cold PBS and re-suspended in PBS at $\sim 5\text{-}10 \times 10^6$ cells/ml. 10% normal mouse serum (NMS) was added for blocking 5 min prior to adding the antibodies. Fluorescent dye-conjugated antibodies were added (1:300 final dilution) (Table 5) and cells were incubated in the dark for 25 min at 4°C. Single stains and an unstained-control were prepared as controls. After staining, cells were washed in cold PBS and re-suspended in FACS buffer (PBS + 2 % FBS). Cells were filtered using 70 μm filters, transferred into 5 ml polystyrene tubes and kept on ice until analysis. For analysis of surface markers, a LSR Fortessa and for sorting a FACS Aria III device, both running with the BD DIVA software were used. If required, single stains were used for setting up compensations. For sorting, the populations of interest were gated (layouts in supplementary data) and sorted into culture medium supplemented with 20% FBS. Flow data were analyzed using the FlowJo software (Version 10.5.0).

3.8.4.2. Monitoring of I3P uptake

Different cell types were seeded in triplicates into 48-well plates (0.02×10^6 - 0.03×10^6). 24 h after plating, cells were treated with 200 μM I3P dissolved in the appropriate culture medium and incubated for the time indicated with the experiments. Adherent cells were detached by trypsin; suspension cells were directly taken from the dish. Cells were washed in PBS and re-suspended in FACS buffer. AmCyan fluorescence was acquired at the indicated time points on a LSR Fortessa with the BD DIVA software. Flow data were analyzed by FlowJo software (Version 10.5.0) and the AmCyan MFI (geometric mean) was determined.

3.8.4.3. Analysis of lipid peroxidation

Lipid peroxidation was analyzed using the C11-BODIPY 581/591 probe. 0.04×10^6 HeLa cells were plated per well of a 48 well plate. On the next day, cells were treated in triplicates with RSL3 or Erastin for 24 h in the absence or presence of 200 μM I3P. After 24 h supernatants were aspirated and medium containing 2 μM C11-BODIPY 581/591 probe was added. Cells were incubated for 30 min at 37 °C and subsequently detached from the plate using trypsin. After washing, cells were re-suspended in PBS + 2 % FBS and BODIPY fluorescence shift

indicating lipid peroxidation was determined by analyzing the fluorescence in the FITC channel on a LSRFortessa. Data analysis was performed using the FlowJo software (Version 10.5.0).

3.8.5. Quantification of L-amino acid oxidase activity

The specific activity of *N. naja* LAAO, murine IL4i1 and human IL4i1 towards the proteinogenic amino acids was measured by determination of H₂O₂ generation using Amplex UltraRed (AUR) (Figure 16A). 0.1 µg (final 1 µg/ml) of the recombinant enzymes were added to a mixture containing 1 U/ml HRP, 50 µM AUR, and 1 mM of the specific L-amino acid in 50 mM sodium phosphate buffer, pH 7.0 in a final volume of 100 µl per well of a black 96-well microplate. For the generation of a standard curve, an H₂O₂ titration (starting from 2000 pmol) was added to the mixture instead of the enzyme. H₂O₂ production was measured over 5 min at 37 °C using a CLARIOstar Plus microplate reader (BMG Labtech) at 530 nm excitation and 590 nm emission wavelength.

3.8.6. Free radical scavenging assay

The stable free radical 1,1-diphenyl-2-picrylhydrazyl (DPPH) was used to determine the radical scavenging activity of PP, 4HPP, and I3P. Ascorbic acid and the ferroptosis inhibitor Fer-1 were used as positive controls. A 200 µM DPPH solution in methanol was prepared, pipetted in quadruplicates into a 96-well plate and compounds (final 200 µM) were added. An equal volume of ddH₂O was used as negative control. After 10 min incubation, the absorbance was measured at 517 nm with a Tecan Spark microplate reader. The scavenging activity, leading to a decrease of DPPH absorbance, was calculated relative to H₂O.

3.8.7. Determination of GSH/GSSG ratio

For GSH/GSSG ratio determination 0.2 x10⁶ HeLa cells were plated per well of a 6-well plate. On the next day, cells were treated in quadruplicates with 200 µM I3P dissolved in culture medium or control medium without I3P for 24 h. Cells were detached with trypsin, GSH and GSSG levels determined as described by Rahman et al. [301] and the GSH/GSSG ratio was calculated relative to the untreated control.

3.9. Additional use of software

Further software that was used in this thesis comprised GraphPad Prism 9.3.1 for statistical analysis and SnapGene 6.0 for the generation of plasmid maps. AlphaFold [302] was used for protein structure prediction and structures were visualized using the PyMOL Molecular Graphics System (version 2.0 Schrödinger, LLC). CorelDraw2018 (version 20.1.0.708) was used for the generation of figures and conceptual graphics were generated with BioRender.com.

4. Results

The results of this thesis are structured in three main parts: The first section (4.1) is methodologic and focuses on the conceptualization, generation and testing of recombinant LAAOs. The second section (4.2) addresses the downstream cellular effects mediated by LAAOs. Herein, I mainly investigated the ability of IL4i1-mediated amino acid metabolism to generate an environment that protects cells from the oxidative cell death ferroptosis. Most of the results from the first two sections were published in 2021 [18]. The third part of the results (4.3) focuses on the expression and regulation of IL4i1 in BMDMs and BMDCs.

4.1. Generation and characterization of recombinant *Naja naja* LAAO and mammalian IL4i1 proteins

IL4i1 belongs to the family of LAAO enzymes which are conserved throughout the evolution and found in many different organisms. As LAAOs are a component of most snake venoms and the enzymatic reaction catalyzes the production of H₂O₂, an initial question of my PhD project was to investigate whether mediating toxicity is a general function of LAAOs including mammalian IL4i1. To address this, I first aimed to compare biochemistry and downstream cellular effects of murine and human IL4i1 with an LAAO from a snake venom. So far, 'high-quality' genomes from venomous snakes are limited as most published genomes were identified by short-read sequencing which results in highly fragmented assemblies [149]. Combining several genomic technologies and mass spectrometry our collaborators identified a reference genome and 'venom-ome' of the Indian cobra (*Naja naja*) [149] and provided the authentic sequence of the *Naja naja* (*N. naja*) LAAO (Figure 7), which I used in my experiments.

4.1.1. The PiggyBac expression system

The first step of my project was the generation of recombinant IL4i1 and *N. naja* LAAO. Two important considerations for the choice of the expression system were 1) the potential toxicity of the enzymes and 2) the fact that IL4i1 and snake LAAOs are secreted proteins that undergo post-translational modifications including glycosylation [17,146,303]. To avoid constitutive overexpression of the proteins and allow complex glycosylation, I used the inducible PiggyBac expression system [291,296] in mammalian HEK293T cells. The system requires the transfection of the cells with three plasmids (Figure 13): The first (pCMV-hyPBBase) encodes a PiggyBac transposase that recognizes the two constructs required for the inducible protein expression at their flanking terminal repeat (TR) sequences and stably integrates them into the cells' genome. The second plasmid (PB-RN) encodes a reverse tetracycline-controlled transactivator (rtTA) under the control of a CMV promoter, leading to constitutive expression of the rtTA. The third component of the expression system is the PB-T-PAF plasmid encoding the protein of interest under the control of a tetracycline response element (TRE) promoter.

Thus, upon treatment of the cells with a tetracycline derivative such as doxycycline (dox) the rtTA can bind to the TRE and induce the expression of the protein of interest.

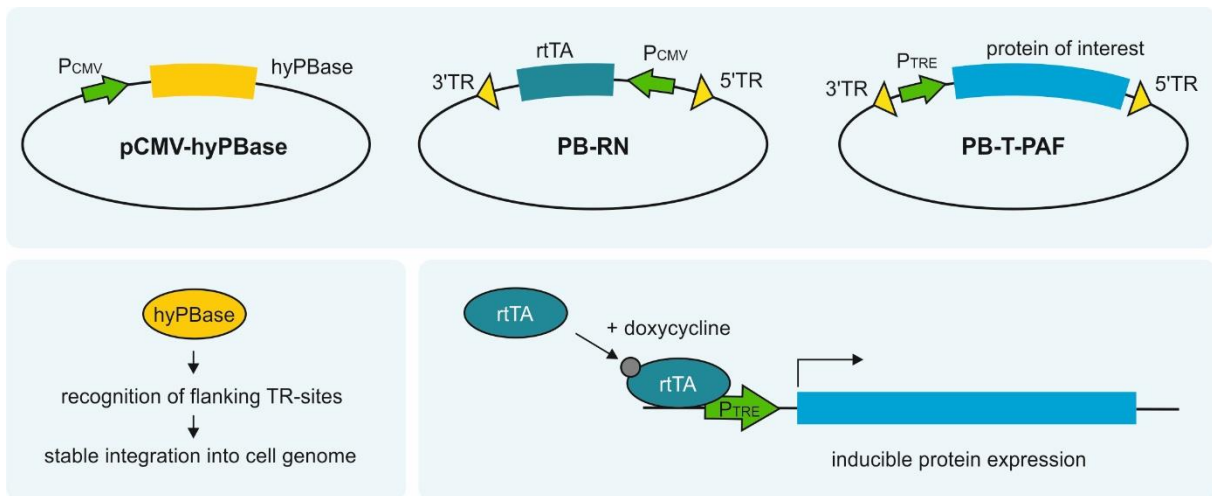


Figure 13 Schematic overview of PiggyBac transposon system

The PiggyBac transposon system used for stable protein expression consists of three plasmids. The first plasmid (pCMV-hyPBBase) encodes a PiggyBac transposase that recognizes and stably integrates the other two constructs (PB-RN and PB-T-PAF) at their terminal repeat (TR) sites. PB-RN encodes a reverse tetracycline-controlled transactivator (rtTA) which, upon addition of doxycycline, induces the expression of the protein of interest encoded on the PB-T-PAF construct.

4.1.2. Construct design

For the inducible expression of murine and human IL4i1 and the *N. naja* venom LAAO, I generated PB-T-PAF constructs for the PiggyBac system. To ensure efficient protein secretion from the human HEK293T cells, the endogenous secretion sequences of *N. naja* LAAO and murine IL4i1 were exchanged for the human VEGF leader sequence, while for human IL4i1 the endogenous leader sequence was retained (Figure 14A). A Twin-Strep-tag was added at the C-terminus to facilitate protein purification. Furthermore, I designed constructs to generate mutant versions of the enzymes lacking the enzymatic activity, which would allow to assign effects mediated by the recombinant proteins to their enzymatic activity as Aubatin et al. [184] speculated that IL4i1 may also act by receptor binding, independently of the enzymatic activity. Since there was no structural information on IL4i1 or *N. naja* LAAO, I took advantage of the strong conservation of the LAAOs and used the structure of the Malayan pit viper (*Calloselasma rhodostoma*) LAAO [145,304] to obtain information about amino acids relevant for the enzymatic activity (Figure 14B). To generate an inactive *N. naja* LAAO, I mutated two conserved amino acids most likely required for the catalytic activity of the enzyme, Arg322 and Lys324, which correspond to Arg322 and Lys326 in the catalytic domain of the pit viper LAAO (Figure 14C). Arg322 has been described to be a dynamic residue in the catalytic center of the pit viper LAAO and Lys326 is probably involved in the catalytic hydrogen transfer [145]. As the lysine residue is conserved in mammalian IL4i1, I chose to mutate this residue in the human

and murine enzyme. Comparable to the residue in the pit viper LAAO, this lysine is part of a β -strand facing the core of the IL4i1 enzyme as modelled by AlphaFold (Figure 14D). The codons in the constructs were exchanged to encode alanine residues resulting in the constructs for an Arg320Ala (R320A) and Lys324Ala (K320A) mutant *N. naja* LAAO, Lys351Ala (K351A) murine IL4i1 and Lys357Ala (K354A) human IL4i1 (Figure 14E).

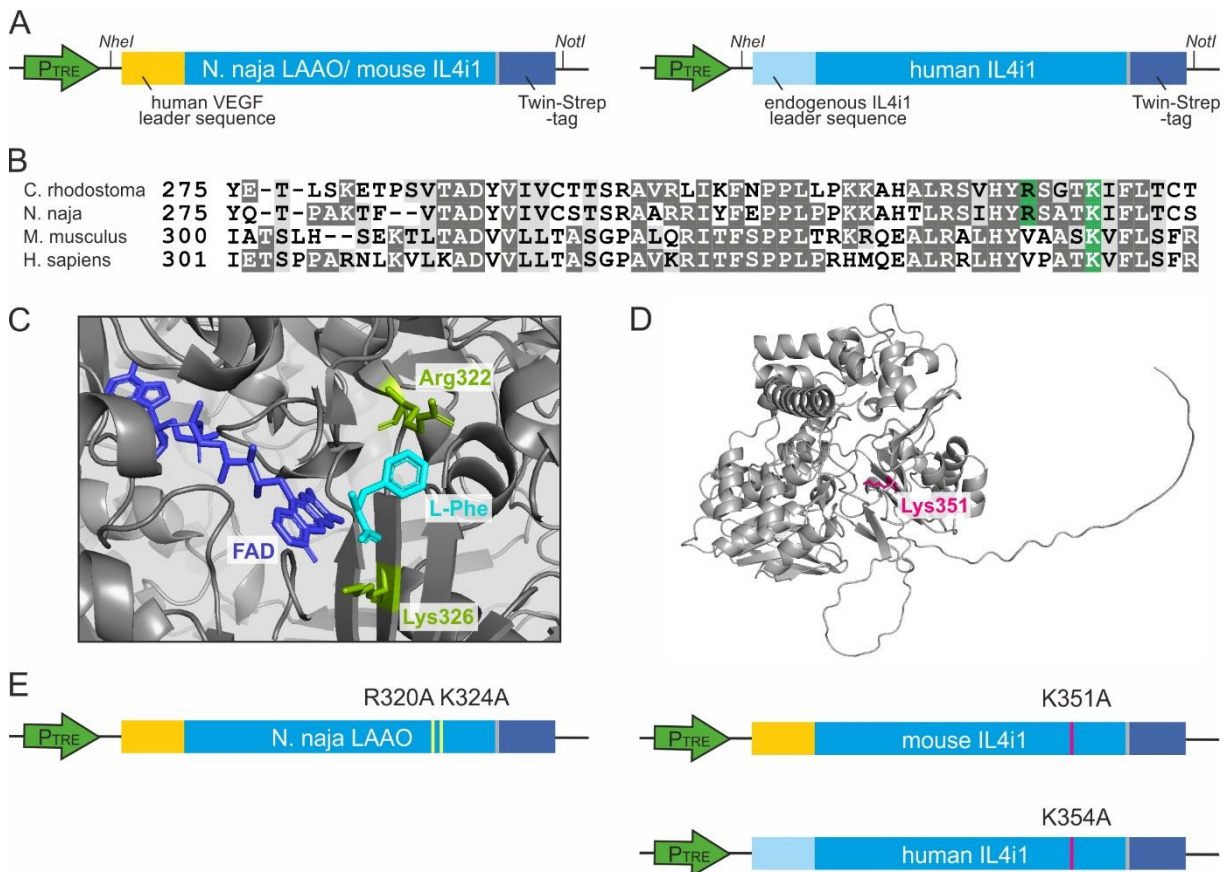


Figure 14 Design of constructs for recombinant *N. naja* LAAO, murine and human IL4i1 expression

(A) Scheme of PB-T-PAF constructs encoding the recombinant proteins which consist of a leader sequence, the secreted protein sequence and a Twin-Strep-tag. For *N. naja* LAAO and murine IL4i1 the human VEGF secretion sequence was used, while for human IL4i1 the endogenous secretion sequence was retained. (B) Amino acid sequence alignment of *C. rhodostoma* LAAO, *N. naja* LAAO, *M. musculus* and *H. sapiens* IL4i1 in the region of the generated mutations. Residues marked in green were used to generate mutant versions. (C) Active site of *C. rhodostoma* LAAO with L-Phe and co-factor FAD deposited by Moustafa et al. [145] on PDB (2IID). Side chains of Arg322 and Lys326 are depicted in green. (D) Structure of murine IL4i1 (UniProt O09046) as predicted by AlphaFold [302]. Lys351 side chain is displayed in pink. (E) Scheme of constructs for mutated LAAO and IL4i1 enzymes including the respective point mutations.

4.1.3. Generation of the recombinant proteins

After generation of stable HEK293T pools using the PiggyBac system (Figure 13), I confirmed the induction of the protein expression by dox as shown here for *N. naja* LAAO (Figure 15A,B). While the protein was not expressed in the absence of dox, LAAO expression was clearly detectable in cell lysates 24 h after induction with dox (Figure 15A). Secretion of *N. naja* LAAO

was visualized by immunoblotting of culture supernatants, in which the protein enriched over the time course of 7 days (Figure 15B). Similar observations were made regarding the induction and secretion of murine and human IL4i1 protein (data not shown). Therefore, proteins were purified from the supernatant at day 7 after dox induction in collaboration with the Protein Production Core Facility of the MPIB (Figure 15C). Purified *N. naja* LAAO, murine and human IL4i1 were visualized by immunoblotting and N-glycosylation of the recombinant proteins was confirmed by PNGaseF digest (Figure 15D). Decrease in the molecular weight suggested that the proteins had undergone the regular protein secretion pathway and were not released as immature, non-modified proteins.

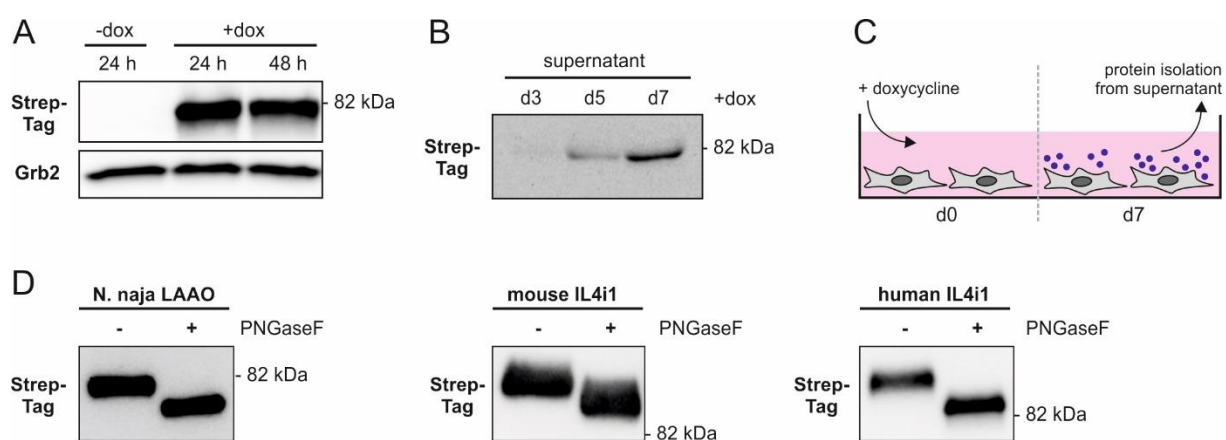


Figure 15 Expression of recombinant *N. naja* LAAO, murine IL4i1 and human IL4i1

(A) Detection of *N. naja* LAAO expression in lysates of the stable HEK293T pool after 24 h or 48 h treatment with 1 μ g/ml doxycycline via Western Blot using an antibody against the StrepTag. Grb2 was detected as loading control. (B) Enrichment of secreted *N. naja* LAAO protein in the culture supernatant at 3, 5 and 7 days after doxycycline treatment. (C) Scheme of expression strategy used to isolate the recombinant secreted proteins. (D) Immunoblotting of purified proteins. PNGaseF digest was performed to verify the glycosylation of the secreted proteins.

4.1.4. Enzymatic activity of the purified proteins

I next tested whether the purified proteins were enzymatically active. Phe is a substrate of murine and human IL4i1 [17,146] and various snake venom LAAOs [305,306]. Therefore, I determined the ability of the purified recombinant proteins to metabolize Phe. The conversion of Phe to PP is accompanied by the production H_2O_2 which can be quantified using the Amplex UltraRed (AUR) reagent (Figure 16A): In presence of H_2O_2 HRP converts AUR into the strongly fluorescent Amplex UltroxRed (AUoxR) in a 1:1 stoichiometric ratio, which was detected using a microplate reader. Addition of the recombinant *N. naja* LAAO to Phe-containing sodium phosphate buffer led to the generation of H_2O_2 , which was not detectable in absence of the enzyme (Figure 16B), suggesting that the recombinant protein was enzymatically active. I also observed H_2O_2 production by recombinant murine IL4i1 (mIL4i1) in presence of Phe. The enzymatic activity was comparable to a commercially available mIL4i1 protein (R&D systems)

(Figure 16C). However, our in-house recombinant human IL4i1 (hIL4i1) was enzymatically inactive as no H₂O₂ was detected (Figure 16D), whereas commercial hIL4i1 (R&D systems) was capable to metabolize Phe and produce H₂O₂, which suggested that there may be a problem in our construct design or the purification of the human protein.

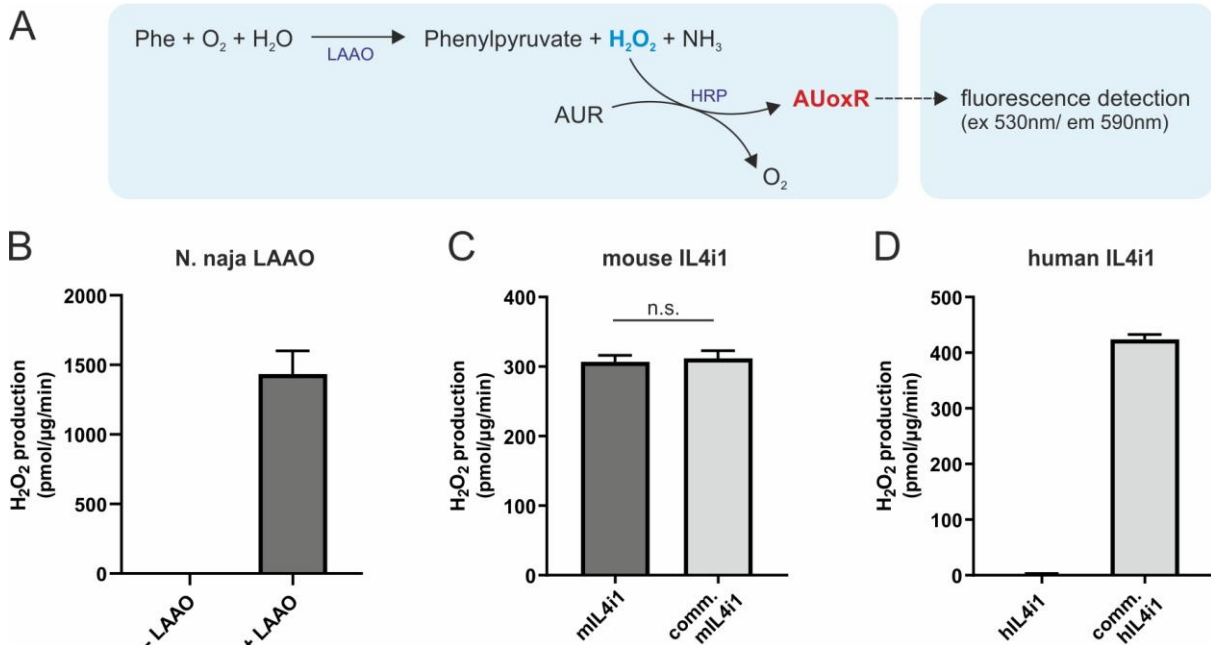


Figure 16 Enzymatic activity of the purified proteins

(A) Scheme of the Amplex UltraRed assay to detect L-amino acid oxidase activity towards Phe by fluorimetric quantification of H₂O₂ generation. (B) Measurement of LAAO activity towards 1 mM Phe in absence or presence of *N. naja* LAAO via H₂O₂ quantification. (C) Comparison of H₂O₂ production of the in-house produced mIL4i1 versus commercial (comm.) mIL4i1 from R&D systems in presence of 1 mM Phe. No significant difference ($p > 0.05$) in the enzymatic activity was detected using an unpaired t-test. (D) Comparison of H₂O₂ production of the in-house produced hIL4i1 versus commercial (comm.) hIL4i1 from R&D systems in presence of 1 mM Phe. No enzymatic activity could be detected in the in-house produced recombinant protein. (B)-(D) $n = 3$, error bars indicate standard deviation.

A plausible explanation for the apparent inactivity of the human protein was that a factor in the protein eluate may inhibit the enzymatic activity. To test this, I mixed the commercial, active hIL4i1 enzyme with the in-house produced inactive enzyme in different ratios. In case of the presence of a soluble inhibiting factor, I would have expected a non-linear decline of enzyme activity as soon as an inhibitor was present. However, the activity decreased linear to the amount of active enzyme input, suggesting that no soluble inhibitor of the active commercial hIL4i1 is present in our recombinant protein eluate (Figure 17A). Compared to mIL4i1, which has a very long C-terminal region, the hIL4i1 C-terminus is shorter (Figure 7). Therefore, I next reasoned that the C-terminal Strep-Tag may interfere with the activity of the human enzyme, for example by inhibiting protein folding. Thus, I generated an N-terminally Strep-tagged version of human IL4i1 (Figure 17B). After purification and verification of the glycosylation by PNGaseF digest (Figure 17C), I tested the enzymatic activity towards Phe. As observed before

for the C-terminally tagged version, the N-terminally tagged hIL4i1 did not show any L-amino acid oxidase activity as no production of H₂O₂ could be detected in the presence of Phe, while the commercial hIL4i1 enzyme potently generated H₂O₂ (Figure 17D). Therefore, all following experiments investigating hIL4i1 were performed with the commercial enzyme from R&D systems. Overall, it is possible that hIL4i1 is highly sensitive to unfold or aggregate during the expression or purification process and further experiments will be required to investigate why the in-house-produced hIL4i1 was enzymatically inactive, which will help to generate functional hIL4i1 for future research in my group.

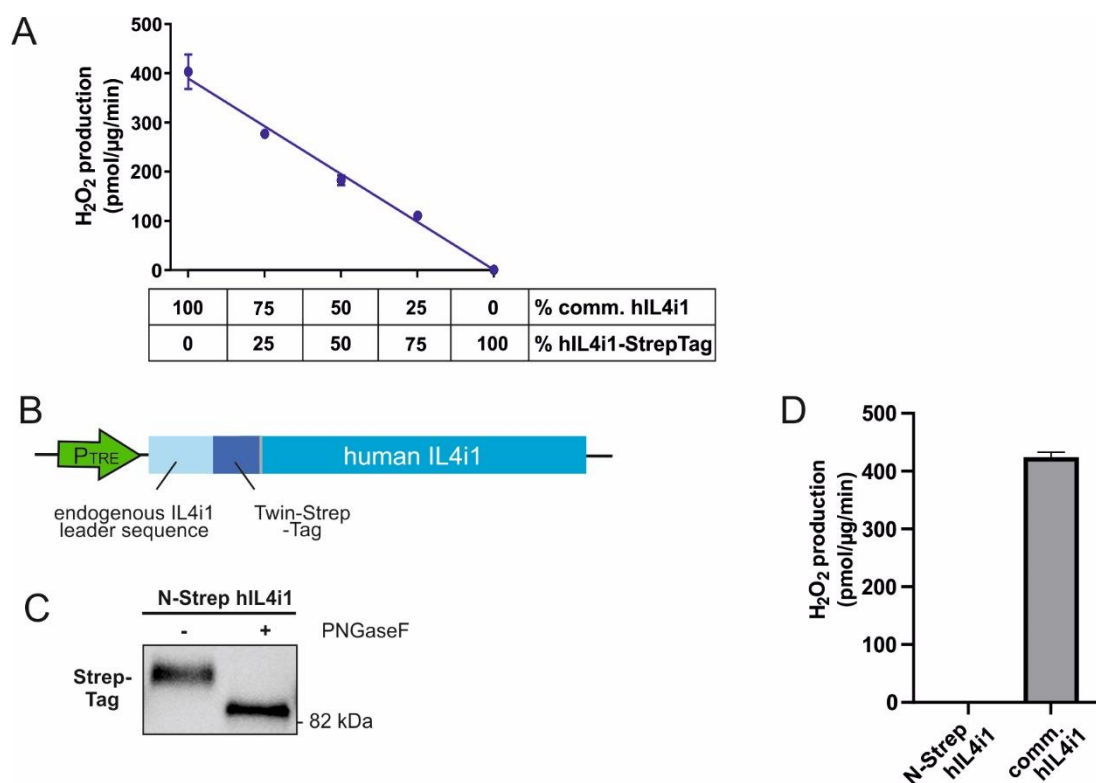


Figure 17 Activity of human IL4i1

(A) Measurement of LAAO activity towards 1 mM Phe of mixtures of in-house-produced and commercial hIL4i1. Activity increases linear with the increase of active commercial hIL4i1. $n=2$, error bars indicate standard deviation. (B) Scheme of PB-T-PAF construct encoding an N-terminally tagged hIL4i1 version. The sequence encoding the Twin-Strep tag follows the endogenous human IL4i1 leader sequence in order to maintain the tag after cleavage of the secretion sequence. (C) Immunoblotting of purified N-terminally tagged hIL4i1. Glycosylation of the secreted protein was confirmed by PNGaseF digest. (D) Comparison of H₂O₂ production of the N-terminally tagged hIL4i1 versus commercial (comm.) hIL4i1 from R&D systems in presence of 1 mM Phe. No enzymatic activity could be detected in the in-house produced recombinant protein; $n=3$, error bars indicate standard deviation.

4.1.5. Loss of enzymatic activity in mutant *N. naja* LAAO and murine IL4i1

To distinguish between effects that are caused by the enzymatic activity of the recombinant enzymes and effects that may be mediated by direct interactions with other proteins, I mutated residues in the active sites of the LAAOs to interfere with their catalytic activity (Figure 14C-E). Purified WT and mutant enzymes showed similar size and glycosylation pattern as determined by immunoblotting with and without previous PNGaseF digest (Figure 18A,B). Next, I tested whether the exchange of the amino acids in the catalytic sites of the enzymes indeed abrogated the enzymatic activity towards Phe. Both, R320A K324A *N. naja* LAAO and K351A mL4i1, completely lost their ability to metabolize Phe as no H₂O₂ production was detectable in the AUR assay (Figure 18C,D). Thus, the mutant enzyme versions in comparison to their enzymatically active counterparts are a key tool to investigate downstream effects of LAAOs on cells in their environment that are dependent on the catalytic activity.

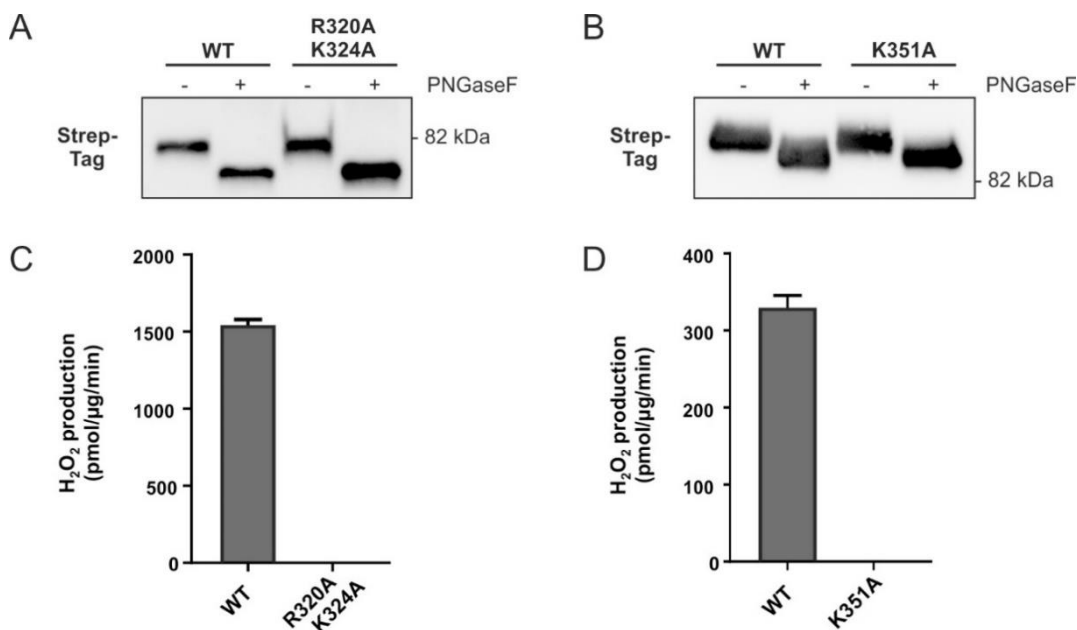


Figure 18 Catalytically inactive enzyme versions

(A) Immunoblotting of purified WT and R320A K324A mutant *N. naja* LAAO. Glycosylation of the secreted protein was confirmed by PNGaseF digest. (B) Immunoblotting of purified WT and K351A mutant mL4i1. Glycosylation of the secreted protein was confirmed by PNGaseF digest. (C) H₂O₂ production in presence of 1 mM Phe by WT and R320A K324A *N. naja* LAAO shows lacking enzymatic activity of the mutant protein. n=3 (D) H₂O₂ production in presence of 1 mM Phe by WT and K351A mL4i1 shows lacking enzymatic activity of the mutant protein. n=2; error bars indicate standard deviation.

4.1.6. Comparison of *N. naja* LAAO, human and murine IL4i1 enzyme activity towards the proteinogenic amino acids

Although *N. naja* venom LAAO and IL4i1 catalyze the oxidative deamination of amino acids, their activity and substrate specificity may differ. Indeed, while human and murine IL4i1 were shown to mainly metabolize aromatic amino acids, such as Phe, Tyr and Trp, snake venom LAAOs have been reported to additionally metabolize further hydrophobic amino acids [305-307]. Yet, no direct comparison (in the same assay) of IL4i1 orthologues and other LAAOs existed. Therefore, I tested the activity of *N. naja* LAAO, human and murine IL4i1 towards all proteinogenic amino acids (Figure 19). Both mammalian IL4i1 enzymes showed a preference towards Phe > Tyr > Trp > Met. Human IL4i1 displayed a higher activity than the murine orthologue as indicated by higher H₂O₂ production. However, the catalytic activity of both IL4i1 enzymes was lower than the activity of *N. naja* LAAO, which in addition to Phe, Tyr, Trp and Met showed a high preference to metabolize Leu. This agrees with previous observations made for other snake venom LAAOs, which also metabolized Leu alongside with further hydrophobic amino acids [305,306]. Notably, *N. naja* LAAO metabolized all 'main substrates' at high levels showing less preference between its substrates as compared to IL4i1. Therefore, compared to mammalian IL4i1, venom LAAOs may have a faster kinetic and a broader substrate range leading to rapid generation of H₂O₂.

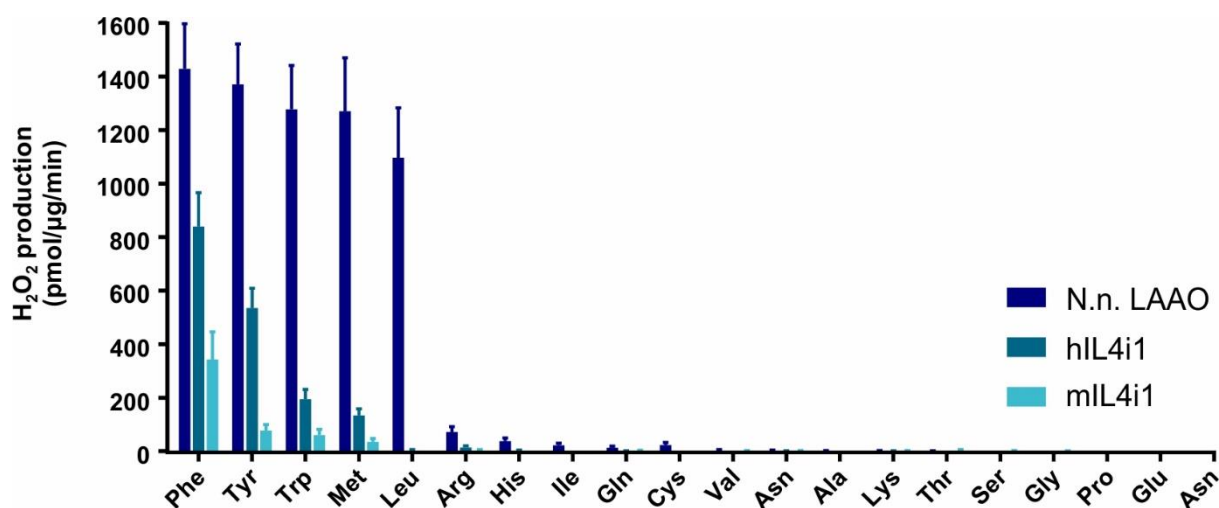


Figure 19 Comparison *N. naja* LAAO, human and murine IL4i1 enzymatic activity

Enzymatic activity of *N. naja* LAAO, human and murine IL4i1 was measured by quantification of H₂O₂ production towards 1 mM of the 20 proteinogenic L-amino acids respectively. n=3 replicates from independent experiments; error bars indicate standard deviation.

4.2. Downstream cellular effects of L-amino acid oxidases

Due to their enzymatic activity LAAOs can provoke changes in the metabolic environment by depleting amino acids and generating α -keto acids, H_2O_2 and ammonia, which may influence the biology of cells in their environment. Therefore, I next aimed to investigate downstream cellular effects that are mediated by LAAO activity to better understand the mechanistic basis underlying the immunoregulatory and pro-tumorigenic effects of mammalian IL4i1 [19,172,173,186,188].

4.2.1. Toxicity of LAAOs

The presence of LAAOs in snake venoms together with their ability to produce H_2O_2 , suggests that the enzymes can mediate cytotoxic effects. Indeed, LAAOs from several snake venoms have been found to induce death in different cell types [153-155], whereas cell death mediated by purified IL4i1 towards mammalian cells has not extensively been studied. Therefore, I next investigated the cytotoxic potential of *N. naja* LAAO, murine and human IL4i1.

4.2.1.1. *Naja naja* LAAO mediates cytotoxicity via generation of H_2O_2

To evaluate the toxicity of *N. naja* LAAO, I treated HeLa cells with the recombinant enzyme and followed cell fate by live cell imaging using the CellTox Green dye, which upon cell death enters the cells and leads to a green staining of the nuclei by binding to the DNA. Exposure of HeLa cells with 2.5 $\mu\text{g/ml}$ *N. naja* LAAO provoked cell death, which started after ~4-5 h with the formation of large membrane blebs and resulted in the death of all cells within 12-16 h (Figure 20A,B). The toxic effect of the enzyme was concentration dependent. While concentrations of 0.62 $\mu\text{g/ml}$ could kill a fraction of the cells, uniform cell death of all cultured cells was achieved at concentrations from 1.25 $\mu\text{g/ml}$ (Figure 20B). Importantly, the enzymatic LAAO activity was required for the induction of cell death, as the R320A K324A mutant LAAO lacking the enzymatic activity (Figure 18C) was not able to kill the cells (Figure 20), suggesting that the toxic effect is mediated by LAAO activity and not by direct effects of protein interaction such as receptor binding, which could activate downstream death signaling pathways.

Based on the findings that LAAO enzymatic activity was required to kill HeLa cells, I next asked whether the production H_2O_2 was responsible for the induction of cell death. In order to interfere with the accumulation of H_2O_2 , I added the H_2O_2 -neutralizing enzyme catalase while treating HeLa cells with a toxic dose of *N. naja* LAAO (Figure 21A). All tested doses of catalase resulted in a complete protection from *N. naja* LAAO-induced cell death, indicating that H_2O_2 is the mediator of *N. naja* LAAO toxicity according to previous studies investigating the toxicity of snake venom LAAOs [153-156]. These studies reported the emergence of apoptotic and necrotic cell death induced by the LAAOs. The morphology of cells killed by *N. naja* LAAO however, did not resemble apoptotic cells (Figure 20A), as typical features of apoptosis could not be observed [308]: The nuclei stained by CellTox Green did not show any fragmentation

and no formation of apoptotic bodies occurred, while the membrane blebs which formed within the first hours rather hinted to a loss of membrane integrity. Additionally, *N. naja* LAAO-induced cell death could not be blocked by the addition of the pan-caspase inhibitor Z-VAD-FMK (Figure 21B), which further suggests that *N. naja* LAAO induces a non-apoptotic, H₂O₂-dependent cell death.

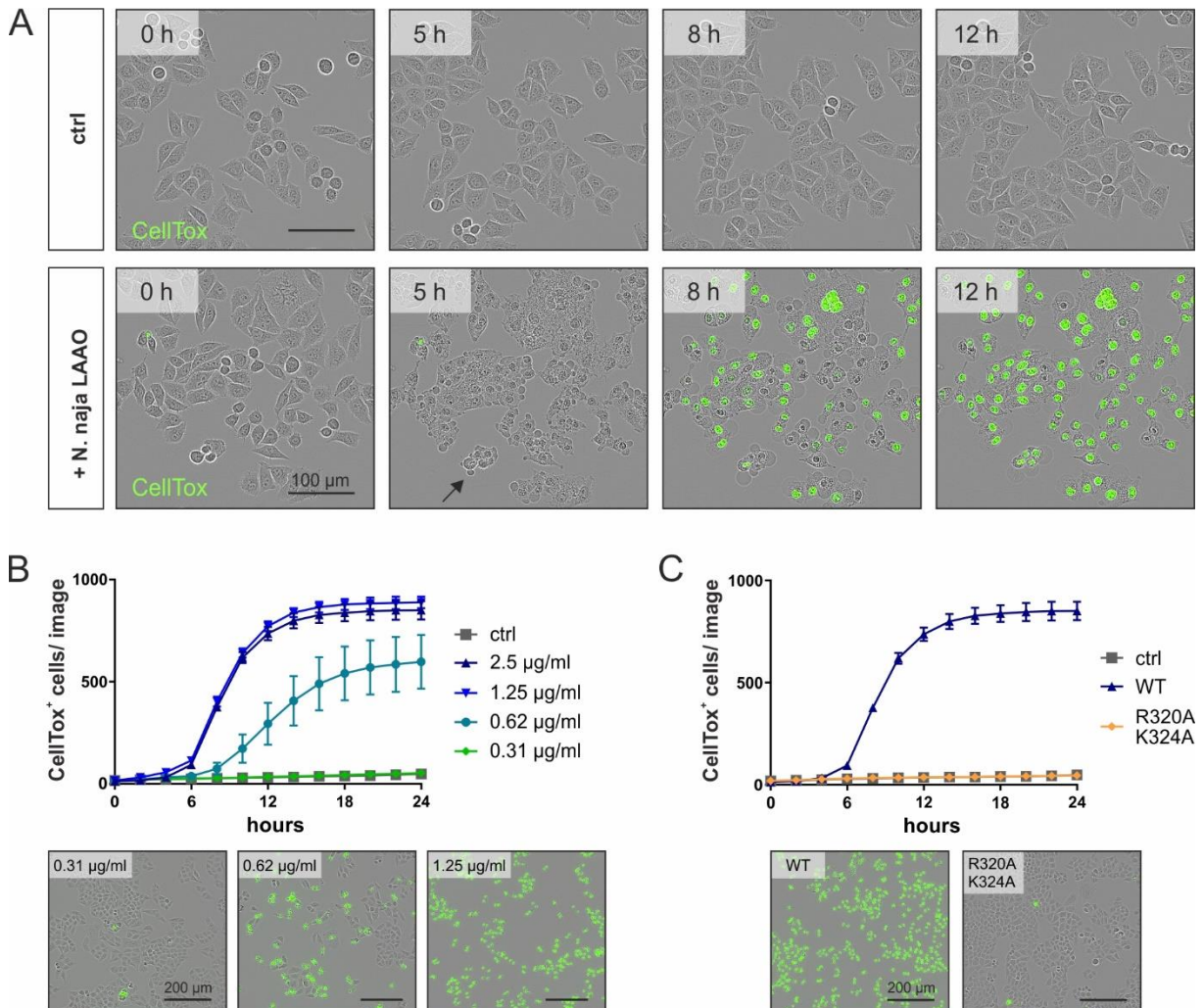


Figure 20 Cytotoxic effects of *N. naja* LAAO require enzymatic activity

(A) Microscopy images (20X) of HeLa cells in absence or presence of 2.5 µg/ml *N. naja* LAAO taken from the same field of view over time using the IncuCyte live imaging device. Membranes of HeLa cells treated with *N. naja* LAAO started to form blebs (example marked by arrow) after 5 h of treatment. CellTox green dye stains nuclei of dead cells. (B) Quantification of dead cells over time using the IncuCyte live imaging device and CellTox green dye. HeLa cells were treated with different concentrations of *N. naja* LAAO for 24 h. Cells treated with control medium (ctrl) not containing the LAAO were used as control. Representative image sections at 24 h are shown below. (C) Quantification of cell death over time using 2.5 µg/ml WT or R320A K324A mutant *N. naja* LAAO. Cells treated with control medium (ctrl) not containing the LAAO were used as control. Representative image sections at 24 h are shown below. (C,D) n=3 biological replicates; results are representative for three independent experiments; error bars indicate standard deviation.

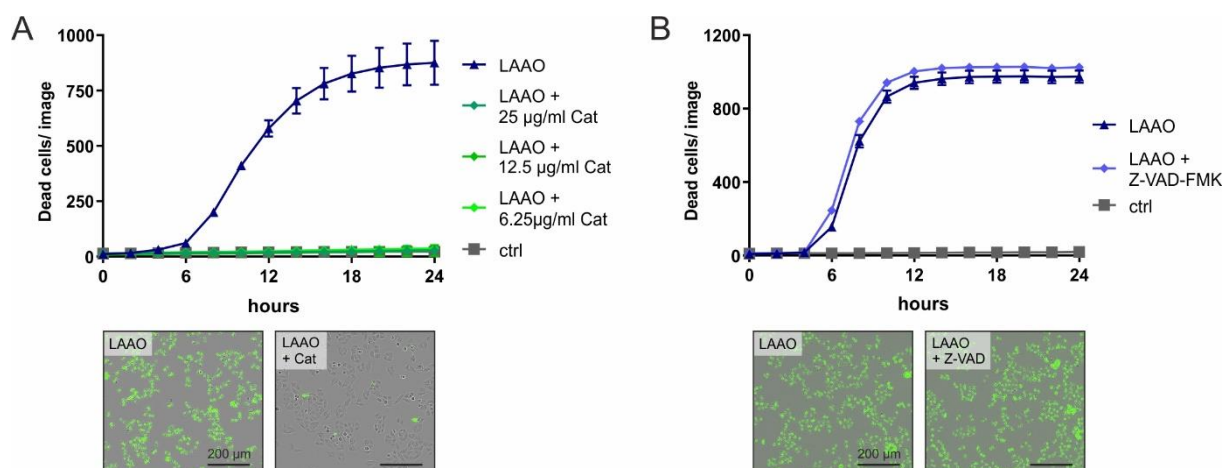


Figure 21 *N. naja* LAAO induced cell death is H₂O₂-dependent and non-apoptotic

(A) Quantification of dead cells over time using the IncuCyte live imaging device and CellTox green dye. HeLa cells were treated with 2.5 µg/ml *N. naja* LAAO for 24 h in absence or presence of the indicated concentrations of catalase (Cat). Cells treated with control medium (ctrl) not containing the LAAO were used as control. Representative image sections of cells treated with *N. naja* LAAO alone and *N. naja* LAAO + 12.5 µg/ml catalase at 24 h are shown below. (B) Quantification of cell death over 24 h using 2.5 µg/ml *N. naja* LAAO in absence or presence of 20 µM Z-VAD-FMK. Cells treated with control medium (ctrl) not containing the LAAO were used as control. Representative image sections at 24 h are shown below. (A,B) n=3 biological replicates; error bars indicate standard deviation.

4.2.1.2. Mammalian IL4i1 exhibits low cytotoxicity

The results using *N. naja* LAAO together with observations regarding the cytotoxicity of other LAAOs [153-156] indicated that LAAOs in general may have the potency to mediate H₂O₂-dependent cell death. Thus, I investigated whether the mammalian LAAO IL4i1 was able induce cell death. However, while *N. naja* LAAO potently killed HeLa cells, I could not observe cell death upon treatment with equal concentrations of murine or human IL4i1 (Figure 22A), even when further increasing the enzyme concentration to 5 µg/ml (not shown). Therefore, I next aimed to investigate the potential toxicity in a cell system that was particularly susceptible to LAAO toxicity. The acute lymphoblastic leukemia cell line RS4;11 already showed substantial cell death upon treatment with *N. naja* LAAO at concentrations of 80 ng/ml (Figure 22B). Consistent with my results in HeLa cells this was dependent on the enzymatic LAAO activity. Compared to *N. naja* LAAO, mammalian IL4i1 required much higher concentrations (~ 30 fold higher) in order to evoke toxic effects (Figure 22C). Concentrations higher than 2 µg/ml of mL4i1 were sufficient to kill the RS4;11 cells, which was not observed when exposing the cells to the K354A mutant (Figure 22D) that lacks the enzymatic activity (Figure 18D). Taken together, these observations show that in contrast to venom LAAO, the mammalian relatives have a much lower cytotoxic activity, which most likely depends on the slower enzymatic activity and the reduced amino acid substrates as shown before (Figure 19),

suggesting that within the evolution of LAAO enzymes, mammalian IL4i1 lost most of the cytotoxic potential.

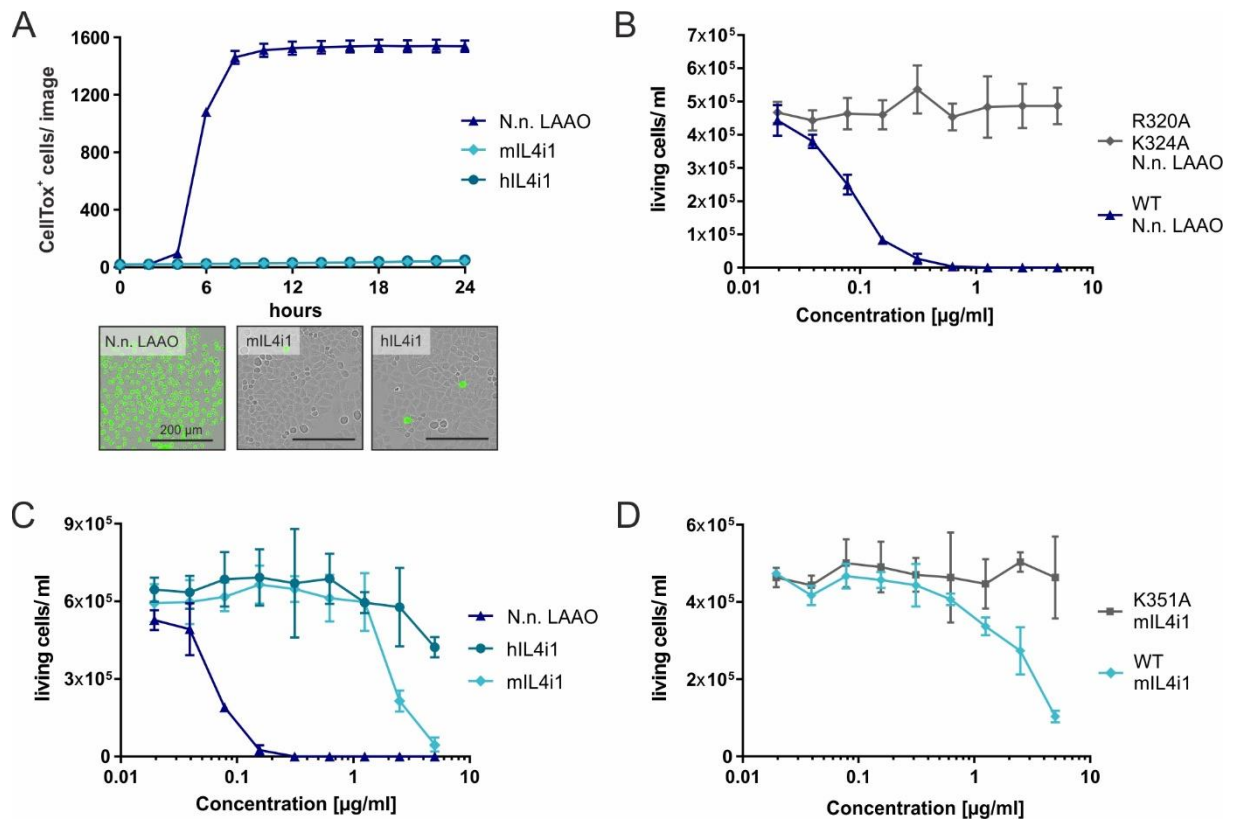


Figure 22 Mammalian IL4i1 is only toxic at high concentrations

(A) HeLa cells were treated with 2.5 µg/ml *N. naja* LAAO, mL4i1 or hIL4i1 for 24 h. Cell death was quantified over time using the Incucyte live imaging device and CellTox green dye. Representative image sections are shown below. (B) RS4;11 leukemia cells were treated with titrations of WT or R320 K324A mutant *N. naja* LAAO. The number of viable cells was determined after 72 h. (C) RS4;11 cells were treated with titrations of *N. naja* LAAO, mL4i1 or hIL4i1. The number of viable cells was determined after 72 h. (D) RS4;11 leukemia cells were treated with titrations of WT or K351A mutant mL4i1. The number of viable cells was determined after 72 h. (A,B,D) n=3 biological replicates (C) n=4 biological replicates; error bars indicate standard deviation.

4.2.2. Downstream effects of IL4i1-produced aromatic amino acid metabolites

Since mammalian IL4i1 enzymes exhibited a much lower cytotoxic activity than the relative *N. naja* venom LAAO, I hypothesized that instead of mediating toxicity, the amino acid metabolites generated by IL4i1 may have certain regulatory functions. IL4i1 exhibits the strongest substrate affinity to Phe, however it can also metabolize the other aromatic amino acids Tyr and Trp [17,19,146] (Figure 19) leading to the generation of the α -keto acids phenylpyruvate (PP), 4-hydroxyphenylpyruvate (4HPP) and indole-3-pyruvate (I3P), respectively (Figure 23A). However, by the beginning of this thesis project, the downstream cellular effects mediated by these α -keto acids were almost unknown. If studied at all, only PP was included into experiments, which however did not contribute to the examined immunoregulatory effects [17,172,184,186].

4.2.2.1. I3P induces stress-protective gene expression

Due to the limited knowledge about the effects mediated by the aromatic α -keto acids PP, 4HPP and I3P, I aimed to investigate whether the metabolites modulate gene expression on transcriptional level. I performed an RNAseq experiment in the human myeloid THP-1 cell line stimulated with PP, 4HPP or I3P, since myeloid cells may be the main producers of IL4i1 [55,171,173]. While PP caused only minor effects on the transcriptome, the Trp metabolite I3P provoked a highly significant induction of certain mRNAs encoding e.g. SLC7A11, NQO1, CYP1B1 and AKR1C family enzymes (Figure 23B). Although 4HPP had weaker effects, several of these mRNAs were also regulated by the Tyr metabolite. Analysis of the gene ontology (GO) of the transcripts most significantly upregulated by I3P revealed the overrepresentation of GO terms associated with processes such as amino acid metabolism and the responses to cellular stress including chemical stress (GO:0062197) and oxidative stress (GO:0006979) (Figure 23C). When analyzing the significant transcripts detected under the term 'response to oxidative stress' in I3P treated cells, I observed that also 4HPP regulated a part of these mRNAs, while PP had almost no effect on their expression (Figure 23C, right panel). In line with the response to oxidative stress also the terms 'reactive oxygen species metabolic process' (GO:0072593), 'cysteine biosynthetic process from serine' (GO:0006535) and 'glutathione metabolic process' (GO:0006749) were significantly enriched, suggesting that I3P induces a broad network of genes involved in the protection from oxidative stress e.g. by increasing cystine import by upregulating SLC7A11 and cysteine biosynthesis from serine. Cysteine is regarded as the rate-limiting substrate for the generation of glutathione (GSH), which is considered to be the major intracellular antioxidant [208,214]. Additionally, upregulated transcripts may be involved in the elimination of ROS-dependent cytotoxic metabolites such as the enzymes of the aldo-keto reductase 1C (AKR1C) family, which were found to metabolize toxic aldehydes derived from lipid peroxidation [309,310].

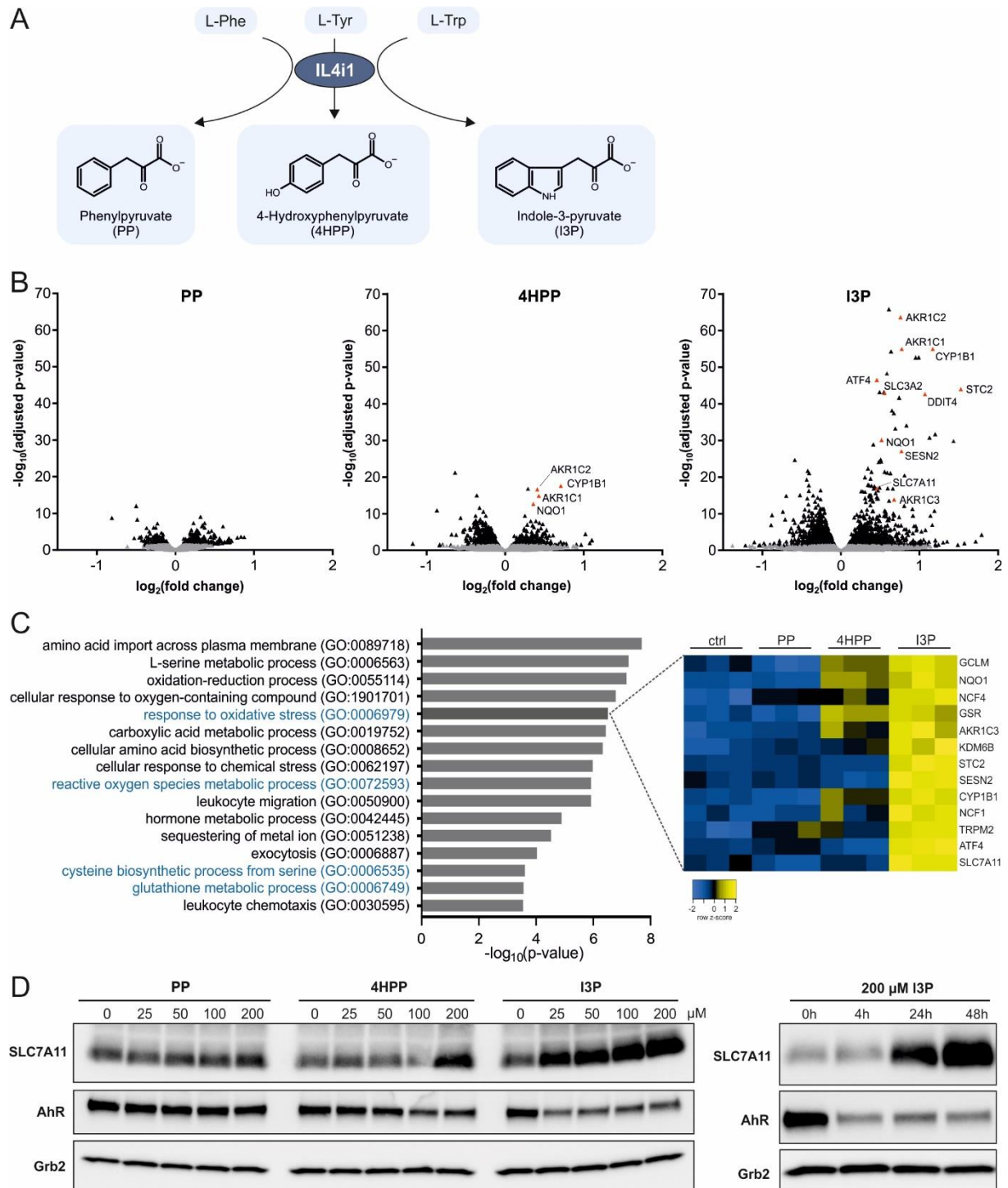


Figure 23 I3P induces stress-protective gene expression

(A) Overview of main amino acid metabolites generated by IL4i1 from the aromatic amino acids L-Phe, L-Tyr and L-Trp respectively. (B) Differentially expressed genes as determined by RNA-seq from THP-1 cells treated for 24 h with 200 μM PP, 4HPP or I3P compared to untreated cells. Genes marked in black/red have a p-value < 0.05 . (C) Selection of overrepresented GO terms from genes most significantly upregulated by I3P treatment (p-value cutoff $p < 10^{-9}$). Heat map of genes detected in the analysis under the term 'response to oxidative stress' (GO:0006979) is shown on the right. (D) Immunoblotting of SLC7A11 and AhR protein in lysates of THP-1 cells. Grb2 was used as loading control. Titrations of PP, 4HPP and I3P for 48 h are shown on the right. A time course of I3P treatment is shown on the left.

Notably, many of the induced genes are target genes of the anti-oxidative Nrf2 pathway and the AhR pathway, which also share common targets [311], suggesting that these pathway may be activated by I3P. Investigating the cysteine importer SLC7A11 on protein level, I could observe a dose-dependent increase induced by I3P, even at low concentrations of 25 μ M, while 4HPP only upregulated SLC7A11 at the highest tested concentration of 200 μ M (Figure 23D). The I3P-induced SLC7A11 upregulation was detectable 24 h after treatment and further increased at the 48 h time point, indicating that the presence of I3P may have a long-lasting effect on the cell state and does not only provoke a short-lived response. I also observed an I3P-dependent decrease in AhR levels, which considering the induction of AhR target genes such as CYP1B1, may reflect the activation of AhR signaling: Upon activation the receptor first translocates to the nucleus and subsequently gets degraded via the proteasome upon nuclear export [110]. A slight decrease in AhR protein levels could also be observed with high concentrations of 4HPP.

Overall, this set of experiments was a key clue indicating that the Trp and Tyr metabolites, I3P and 4HPP, generated by IL4i1 may participate in IL4i1-mediated downstream cellular effects and hinted towards a potential involvement of AhR signaling and the activation of pathways implicated in cellular protection from oxidative stress, which I further addressed in my thesis.

4.2.2.2. I3P uptake can be visualized by flow cytometry

Several Trp metabolites such as Kyn and KynA exhibit endogenous fluorescence at longer wavelengths as compared to Trp [312]. This property was previously used to monitor Kyn uptake into cells by flow cytometry [61,313]. Therefore, I investigated whether also I3P uptake could be visualized. First, measuring the excitation and emission spectra of I3P, I found that I3P has an excitation maximum at 360 – 370 nm and an emission maximum between 475 and 490 nm (Figure 24A). The excitation maximum for Trp in contrast, lies at 297 nm and the emission maximum at 350 nm [312], suggesting that the conversion of Trp to I3P indeed shifts the endogenous fluorescence of the metabolite towards wavelengths that lie within the detectable range of our flow cytometer. In agreement, flow cytometry revealed a clear shift in fluorescence of HeLa cell treated for 24 h with I3P in the AmCyan channel as compared to untreated cells (Figure 24B,C), suggesting that it was possible monitor I3P within the cells. To exclude that I3P may cause autofluorescence due to cell damage, I verified that the increase of fluorescence was reversible by subsequent removal of I3P (Figure 24D), which additionally suggested that an intracellular flux of I3P existed. Finally, I tested I3P uptake in several cell lines and could robustly detect the increase in AmCyan fluorescence (Figure 24E). Interestingly, the cell lines showed differences in the baseline fluorescence but also in the extent of fluorescence shift, suggesting that there may be different kinetics of I3P uptake or downstream I3P metabolism, which could be investigated in future projects.

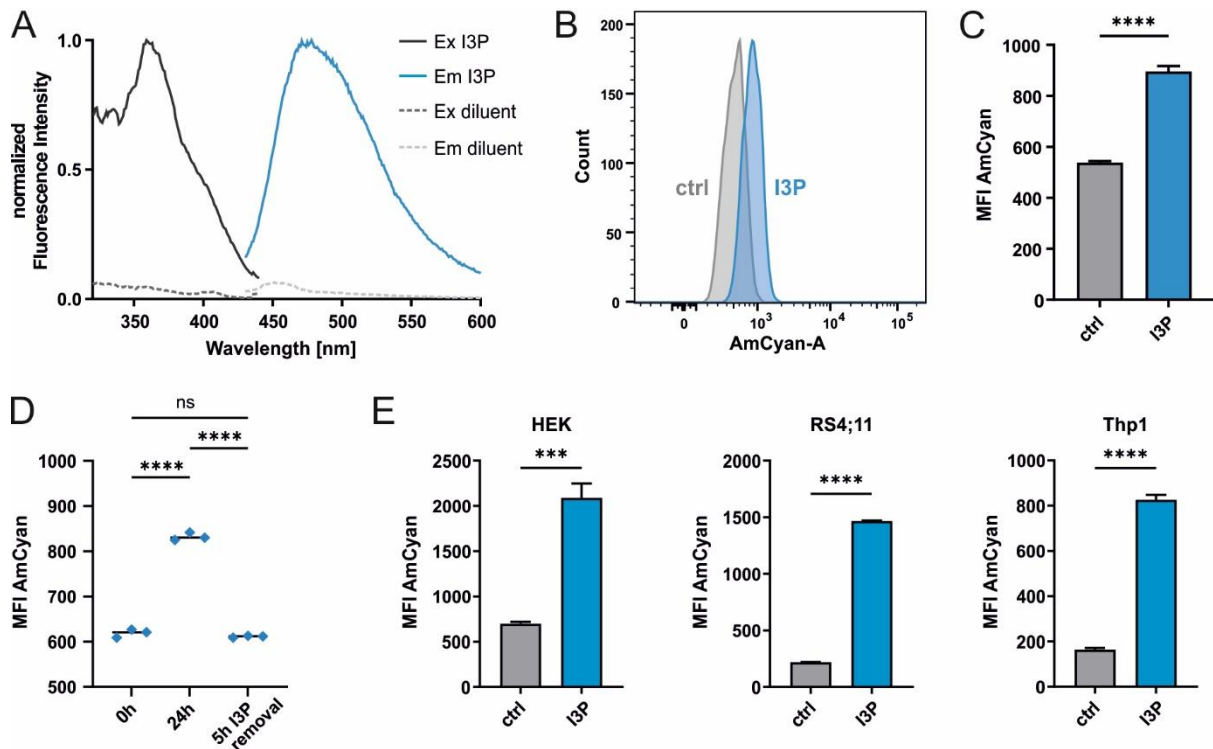


Figure 24 I3P uptake can be monitored by flow cytometry

(A) Fluorescence spectrum of I3P in aqueous solution. Solid gray line represents the excitation (Ex) spectrum and solid blue line the emission (Em) spectrum. Dotted lines represent the spectrum control of the diluent. (B) Shift of fluorescence in HeLa cells treated for 24 h with 200 μ M I3P is detectable by flow cytometry in the AmCyan channel (405 nm laser, 500-550 nm detection). (C) Quantification of AmCyan MFI in HeLa cells treated for 24 h with 200 μ M I3P or control medium. $n=3$; T-test was used for statistics: ****: $p<0.0001$. (D) Quantification of AmCyan MFI in HeLa cells that were left untreated, treated for 24 h with 200 μ M I3P and cells that were treated for 24 h with I3P followed by washing and 5 h incubation in medium without I3P. One-way ANOVA with Tukey's multiple comparisons test was used for statistics: ns: not significant; ****: $p<0.0001$ (E) Quantification of AmCyan MFI in different cell lines treated for 24 h with 200 μ M I3P or control medium. $n=3$; T-tests were used for statistics: ***: $p<0.001$; ****: $p<0.0001$. (C-E) all error bars indicate standard deviation.

4.2.2.3. I3P is an activator of AhR signaling

Based on the first hints indicating that I3P can activate AhR signaling (Figure 23), I aimed to further evaluate a role of I3P in the activation of the receptor. The AhR is a ligand-activated transcription factor associated with the sensing of environmental signals such as exogenous environmental toxins, but also endogenous stimuli in order to maintain cellular homeostasis [96]. Importantly, AhR signaling is involved in the regulation of immune responses (see 1.2.4.3) and the IDO/TDO-dependent Trp metabolite Kyn, as an endogenous AhR ligand, is involved in suppressing immune responses and promoting tumor progression [100,101]. Therefore, IL4i1-dependent generation of a further Trp metabolite that can act as AhR agonist may be an important clue to understand the role of IL4i1 in immunoregulation and cancer progression. In line with recent results from Sadik et al. [19], my experiments suggest that I3P indeed activates the AhR. I treated NIH/3T3 cells transiently transfected with an mScarlet-tagged AhR with I3P

or Kyn, which was used as positive control and visualized the localization of the fluorescently labeled protein by confocal microscopy (Figure 25A). Cells treated with Kyn and I3P showed increased nuclear localization of the tagged AhR protein as compared to untreated cells, suggesting that besides Kyn also I3P can activate AhR signaling. In addition, I analyzed the induction of two main AhR target genes CYP1A1 and CYP1B1 in HeLa cells by qPCR (Figure 25 B,C) and found a significant induction of both mRNAs upon stimulation with I3P. 4HPP was also able to increase CYP1A1 and CYP1B1 mRNA levels, but the effect was clearly weaker than the I3P-mediated effect, suggesting that 4HPP is a less potent AhR agonist. A final verification that the observed CYP enzyme induction is completely AhR-dependent is shown later in this thesis using AhR knockout clones (Figure 33D).

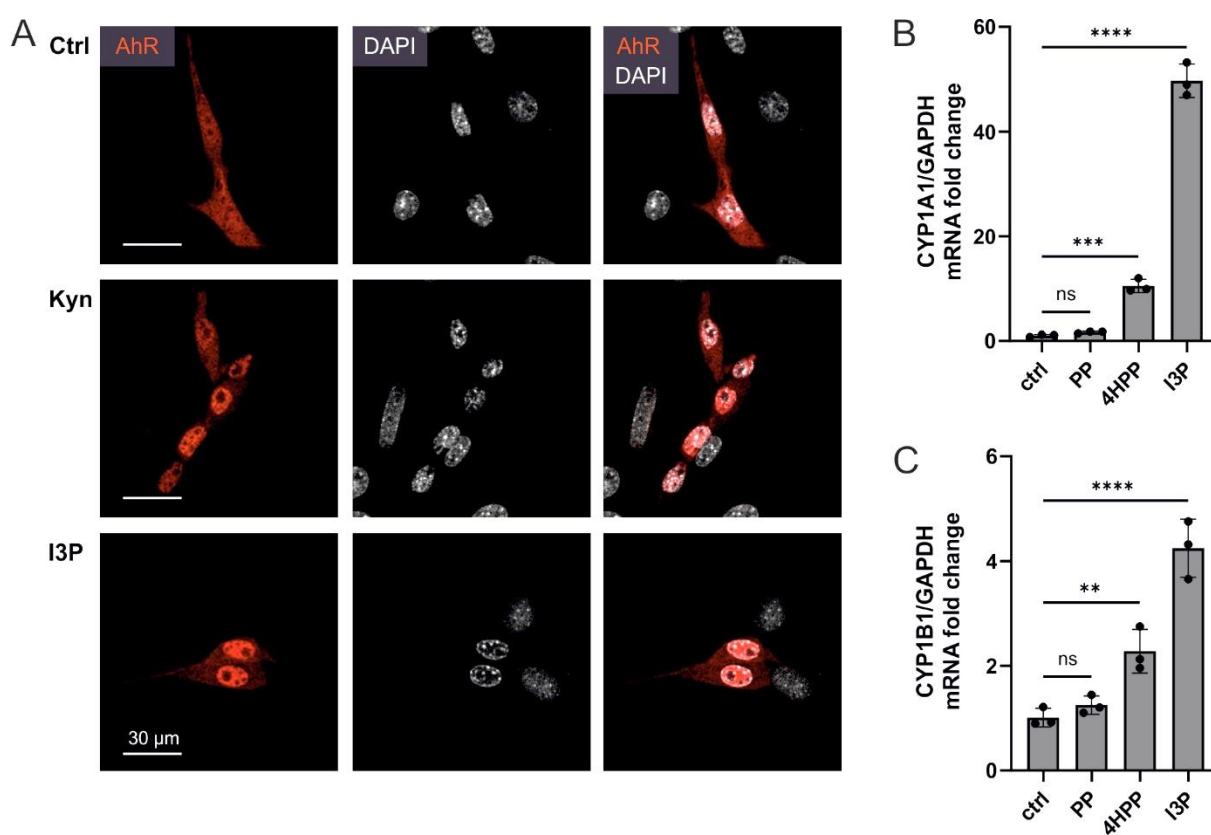


Figure 25 I3P activates the aryl hydrocarbon receptor

(A) Fluorescence microscopy of AhR nuclear translocation induced by 1 h treatment with 1 mM of Kyn and I3P in NIH/3T3 cells transiently transfected with mScarlet-tagged AhR. Nuclei were stained with DAPI. Unstimulated cells were used as control. Images are representative for two independent experiments. (B) and (C) Quantification of mRNA induction of the AhR target genes CYP1A1 and CYP1B1 by qRT-PCT upon 24 h stimulation of HeLa cells with 200 μ M of PP, 4HPP and I3P. The mRNA levels were normalized to GAPDH and the fold change compared to the unstimulated control (ctrl) was determined. n=3 biological replicates; error bars indicate standard deviation; One-way ANOVA with Dunnett's multiple comparisons test, comparing all treatments to the untreated control, was used for statistics: ns: not significant; **: p<0.01; ***: p<0.001; ****: p<0.0001.

4.2.3. Anti-ferroptotic effects of IL4i1 and its amino acid metabolites

I previously observed that the IL4i1 metabolites I3P and 4HPP induced oxidative stress-protective gene expression (Figure 23). Significantly upregulated transcripts were for example involved in cysteine production and import as well as GSH metabolism. Notably, cysteine is the rate-limiting substrate for the synthesis of GSH, which is one of the main intracellular antioxidants [208,214]. Therefore, I speculated that I3P and 4HPP may have an impact on the cellular redox balance. Availability of cysteine and GSH play a major role in cellular protection from ferroptosis, a form of oxidative cell death characterized by uncontrolled phospholipid peroxidation, resulting in cell membrane disruption [203-205,314] (1.3). Under steady-state conditions PLOOHs are permanently detoxified by GPX4, which requires GSH as substrate (1.3.1.1, Figure 26A). Therefore, cells depend on cysteine to generate sufficient amounts of GSH required for GPX4-mediated the detoxification of PLOOHs and thereby protection from ferroptotic cell death.

4.2.3.1. I3P is a potent and 4HPP a weak ferroptosis suppressor

The observations that I3P and 4HPP upregulated the expression of several genes involved in cysteine homeostasis and GSH production suggested that I3P and 4HPP may contribute to cellular protection from ferroptosis, which I addressed in collaboration with Dr. Alessandra Fiore a former Postdoc in my research group. Using live cell imaging, we first investigated whether I3P and 4HPP could interfere with ferroptotic cell death induced in HeLa cells by the ferroptosis inducers Erastin, blocking cystine uptake via SLC7A11, and the GPX4 inhibitor RSL3. We observed that I3P completely rescued both, Erastin- and RSL3-induced ferroptosis (Figure 26B,C). The effect was comparable to Ferrostatin-1 (Fer-1), a known and potent synthetic ferroptosis inhibitor [199]. In line with the protective effect, we found that I3P was able to completely revert Erastin- and RSL3-mediated lipid peroxidation as measured by flow cytometry using C11-bodipy 581/591, a lipid peroxidation sensor (Figure 26D,E). As expected, PP had no effect on ferroptosis while 4HPP which induced less of the stress-protective genes compared to I3P (Figure 23) displayed a weaker protective potential: Erastin-induced ferroptosis was partly inhibited, while RSL-induced ferroptosis could not be prevented by concurrent treatment with 4HPP (Figure 26B,C). However, when pre-treating the cells for 24 h with 200 μ M 4HPP a partial protection from RSL3-induced cell death occurred (Supplementary Figure 7).

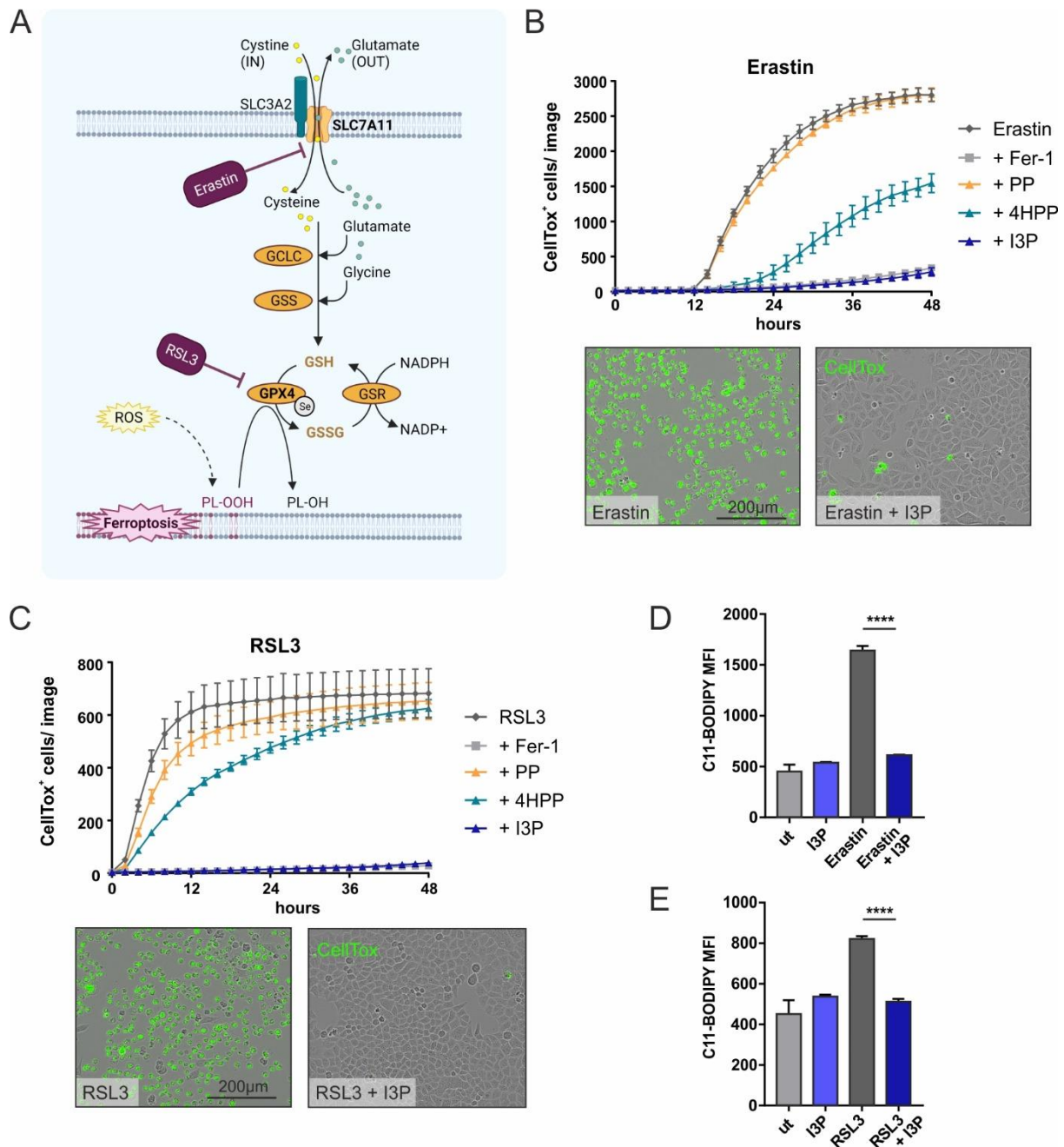


Figure 26 I3P and 4HPP can protect cells from ferroptosis

(A) Simplified scheme depicting components of ferroptotic cell death and the inhibitory GPX4-glutathione-cysteine axis. (B) Quantification of Erastin-induced ferroptosis over 48 h using the IncuCyte live imaging device and CellTox green dye. HeLa cells were concurrently treated with 10 μ M Erastin in absence or presence of 200 μ M PP, 4HPP, or I3P. Fer-1 (2 μ M) was used as a control for a known inhibitor of ferroptotic cell death. $n=3$ biological replicates; error bars indicate standard deviation. The results are representative for three independent experiments. Representative image sections showing I3P-mediated protection from ferroptosis at 48 h are shown next to the graph. (C) As described in (B), but using 1 μ M RSL3 to induce ferroptosis. (D) Determination of lipid peroxidation by flow cytometry using C11-Bodipy 581/591 sensor in HeLa cells after 24 h treatment with 10 μ M Erastin, 200 μ M I3P or combinations of both. $n=3$ biological replicates; One-way ANOVA with Tukey's multiple comparisons test was used for statistics: ****: $p<0.0001$; Error bars indicate standard deviation. (E) As described in (D), but using 1 μ M RSL3 for ferroptosis induction.

Next, to get a better idea about the effective range of the metabolites, we performed titration experiments and evaluated the anti-ferroptotic activity of I3P and 4HPP in HeLa cells. We observed that I3P protected potently from Erastin-induced ferroptosis at 200 μM and 100 μM , but had only minimal protective effects at concentrations of 50 μM and 25 μM (Figure 27A, left). However, when pre-incubating the cells for 24 h with I3P before ferroptosis induction also a concentration of 50 μM could efficiently prevent cell death (Supplementary Figure 7A). The partial inhibition of Erastin-mediated ferroptosis of 4HPP required concentrations of 100 μM or 200 μM (Figure 27A, right). When analyzing RSL3-induced ferroptosis, we found that cell death was almost completely blocked by I3P concentration going down to 50 μM and even 25 μM I3P partly prevented cell death (Figure 27B, left), while 4HPP had almost no effect in the simultaneous addition with RSL3 (Figure 27B, right). Finally, to exclude cell line specificity of the ferroptosis inhibition, we confirmed the protective effects of I3P in HT1080 cells, a human fibrosarcoma cell line frequently used in ferroptosis studies (Supplementary Figure 8) and our collaborators of Prof. Linkermann's group in Dresden additionally validated the anti-ferroptotic effect of I3P using a flow cytometry-based assay in HT1080 and murine NIH/3T3 cells upon treatment with further ferroptosis inducers [18].

Taken together, our data show that at concentrations of ~ 100 μM 4HPP conferred partial ferroptosis protection, while I3P potently blocked ferroptosis. I3P was already effective at concentrations of 50 μM , which lies in the range of physiological the serum Trp concentration (~ 70 μM) [315]. Importantly, we confirmed that Trp itself can neither interfere with Erastin- nor with RSL3-induced ferroptosis (Figure 27C,D), highlighting that IL4i1-catalyzed conversion of Trp into I3P is required to obtain the protective effect.

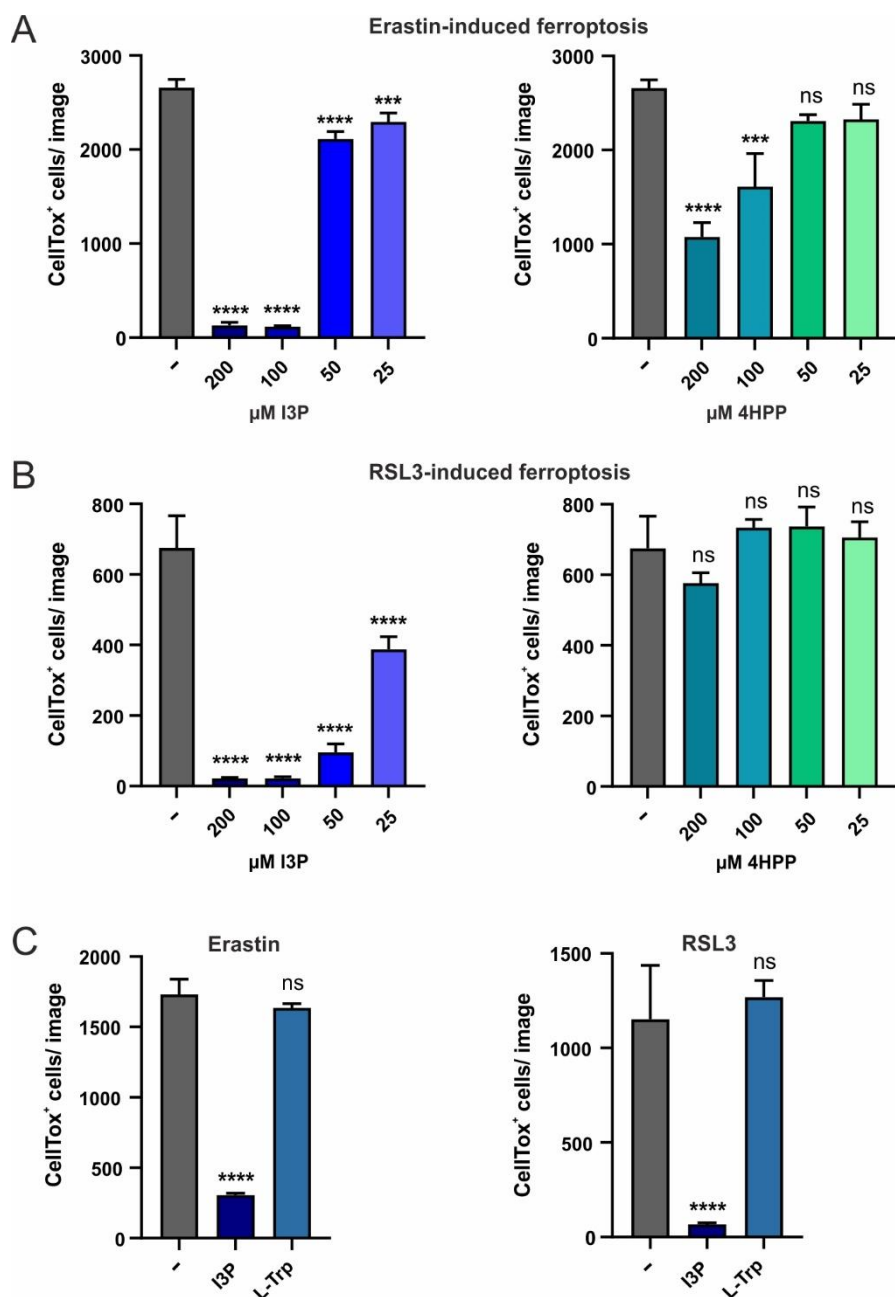


Figure 27 Anti-ferroptotic activity of I3P and 4HPP

Quantification of death cells 36 h after ferroptosis induction by Erastin or RSL3. The anti-ferroptotic activity of the indicated compounds was assessed in comparison to samples treated only with Erastin/RSL3 (-). (A) HeLa cells were concurrently treated with 10 μM Erastin and the indicated titrations of I3P and 4HPP. (B) HeLa cells were concurrently treated with 1 μM RSL3 and the indicated titrations of I3P and 4HPP. (C) HeLa cells were concurrently treated with 10 μM Erastin (left) or 1 μM RSL3 (right) and 200 μM of I3P or L-Trp. (A-C) n=3 biological replicates; error bars indicate standard deviation; One-way ANOVA with Dunnett's multiple comparisons test was used for statistics, comparing the effect of each metabolite to the Erastin/RSL3 alone (-) control: ns: not significant; ***: p<0.001; ****: p<0.0001.

4.2.3.2. Ferroptosis inhibition is mediated by free radical scavenging and anti-oxidative gene expression

We next aimed to investigate the mechanisms underlying the ferroptosis suppressive effects of the IL4i1-derived metabolites. As described above, I observed that I3P induced a network of genes involved in cellular protection from oxidative stress in THP-1 cells (Figure 23). An additional mechanism that has previously been reported to be involved in metabolite-dependent protection from ferroptosis is the trapping lipid radicals, which is required for ferroptosis suppression by CoQH₂ [227,228] and BH₄ [232] (1.3.1.2). As a study from the 1990s suggested that I3P can act as an antioxidant [316], we tested the ability of the IL4i1-generated aromatic α -keto acids to scavenge free radicals using the stable radical diphenyl-2-picrylhydrazyl (DPPH) (Figure 28). Ascorbic acid and the ferroptosis inhibitor Fer-1, which scavenges free radicals [199], were used as positive controls. Indeed, while PP did not show anti-oxidative properties (Figure 28A), 4HPP and I3P were able to scavenge the DPPH radical in a dose dependent way (Figure 28B,C). Notably, the I3P scavenging potential was comparable to the scavenging potential of Fer-1, whereas 4HPP showed a weaker radical scavenging activity. Overall, this suggests that not only anti-oxidative gene expression, but also free radical scavenging contributes to the anti-ferroptotic properties of the amino acid metabolites.

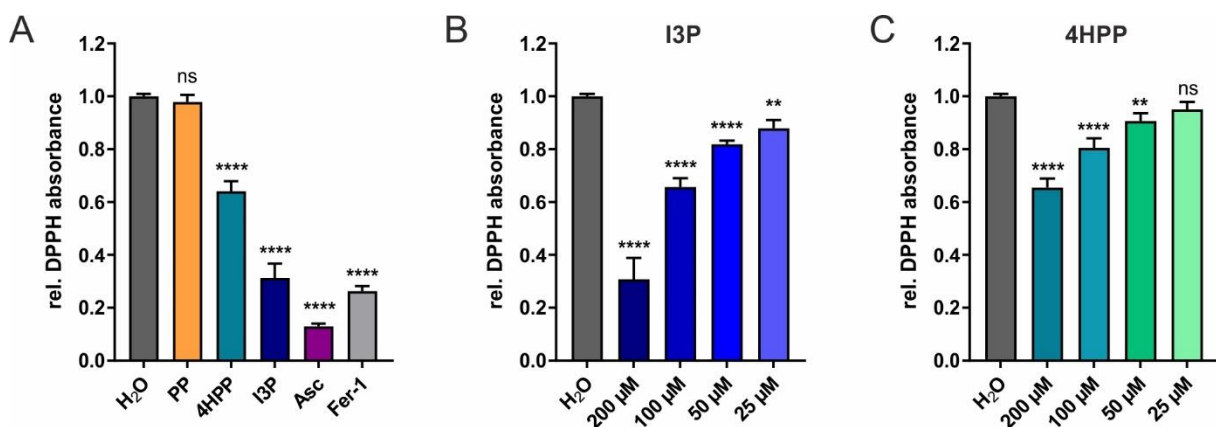


Figure 28 Free radical scavenging activity of I3P and 4HPP

(A) Radical scavenging properties of 200 μ M PP, 4HPP, I3P, ascorbic acid (Asc) and Fer-1 relative to H₂O as determined by the decrease in DPPH radical absorbance. (B) DPPH scavenging by the indicated concentrations of I3P was determined relative to H₂O. (C) DPPH scavenging by the indicated concentrations of 4HPP was determined relative to H₂O. (A-C) n=4; error bars indicate standard deviation; One-way ANOVA with Dunnett's multiple comparisons test was used for statistics, comparing the effect of each metabolite to the H₂O control: ns: not significant; **: p<0.01; ****: p<0.0001.

In order to assess the relative contribution of the two potential mechanisms involved in ferroptosis suppression, free radical scavenging and anti-oxidative gene expression, we focused on I3P, the more potent anti-ferroptotic metabolite generated by IL4i1. The following experiments are based on the hypothesis that in order to protect cells from ferroptosis by

radical scavenging I3P would need to be physically present (Figure 29). By contrast, ferroptosis suppression by initiation of a protected cell state via anti-oxidative gene expression would not require the presence of I3P at the moment of ferroptosis induction, suggesting that I3P would still confer protection from ferroptosis even when no longer present inside a cell after I3P removal.

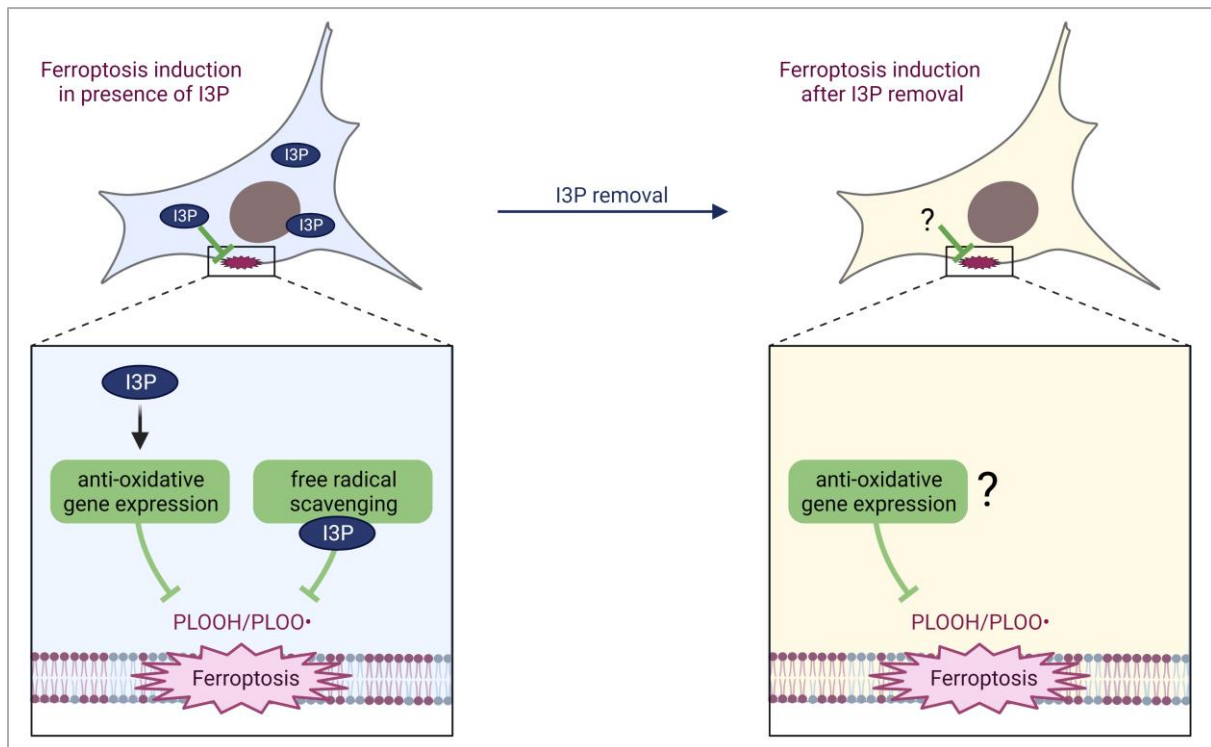


Figure 29 Conceptual model used for testing mechanisms of I3P-mediated ferroptosis protection

When ferroptosis is induced while I3P is present inside a cell, I3P could potentially confer cellular protection by a dual mechanism consisting of the induction of anti-oxidative gene expression and the scavenging of free radicals, which requires the direct presence of I3P. The expression of anti-oxidative genes would be retained for a certain time even when I3P was no longer present and could still protect cells from ferroptosis after I3P removal.

Thus, we took advantage of the endogenous I3P fluorescence and the observation that intracellular I3P fluorescence fades after removing I3P, suggesting that it is no longer present after a certain time (Figure 24). In order narrow down the exact timing of I3P decline within the cells, we washed out the metabolite after 24 h incubation and subsequently monitored I3P fluorescence over time by flow cytometry (Figure 30A,B). A strong decline in fluorescence was already observed within the first hour after I3P removal reaching the baseline fluorescence of untreated cells at ~4-5 h, suggesting the depletion of intracellular I3P. Therefore, we decided to induce ferroptosis 5 h after I3P removal to validate whether the metabolite was still protective under these conditions (Figure 30C,D). We observed that I3P retained the protective effect towards Erastin-induced ferroptosis, but lost its protective effect towards RSL3-induced ferroptosis. This result suggested that while I3P can act by a combination of ROS scavenging and upregulation of protective gene expression, the protection from RSL3-induced ferroptosis

required I3P radical scavenging, whereas for the protection from Erastin the induction of protective gene expression was sufficient.

We further studied which components may contribute to the protected cell state induced by changes in gene expression. A crucial metabolite that is required to prevent ferroptosis is GSH, as it is essential for GPX4-mediated PLOOH detoxification, resulting in the generation of oxidized GSH (GSSG) (Figure 26A). The limiting factor for GSH synthesis is cysteine, which is imported into the cell in form of cystine by SLC7A11. Furthermore, GSH can be recycled from GSSG in an NADPH-dependent manner by the glutathione-disulfide reductase (GSR) [222]. As shown before, RNAseq analysis of THP-1 cells treated with I3P showed significant enrichment of genes associated with 'glutathione metabolic process' (GO:0006749) including GSR and the modulatory subunit of GCL, the rate limiting enzyme for GSH synthesis. In addition, I3P induced genes involved in several modes of cysteine acquisition (uptake and generation) and enhanced SLC7A11 on protein level (Figure 23). Thus, we examined whether I3P changes the availability of GSH in the cells (Figure 30E). Indeed, we observed that I3P treatment of HeLa cells led to a significant increase in the GSH/GSSG ratio, suggesting that cells have more GSH for PLOOH decomposition. Moreover, confirming the experiments in THP-1 cells, I3P treatment increased SLC7A11 levels in HeLa cells under steady state conditions (ctrl) (Figure 30E). Erastin treatment itself also upregulated SLC7A11 [224] likely as a mechanism to compensate decreased cysteine levels. However, the induction was strongly enhanced in the presence of I3P and also the levels of heme oxygenase-1 (HO-1), another Nrf2 target gene, were markedly increased suggesting that I3P enhances the response to the oxidative stress induced by Erastin.

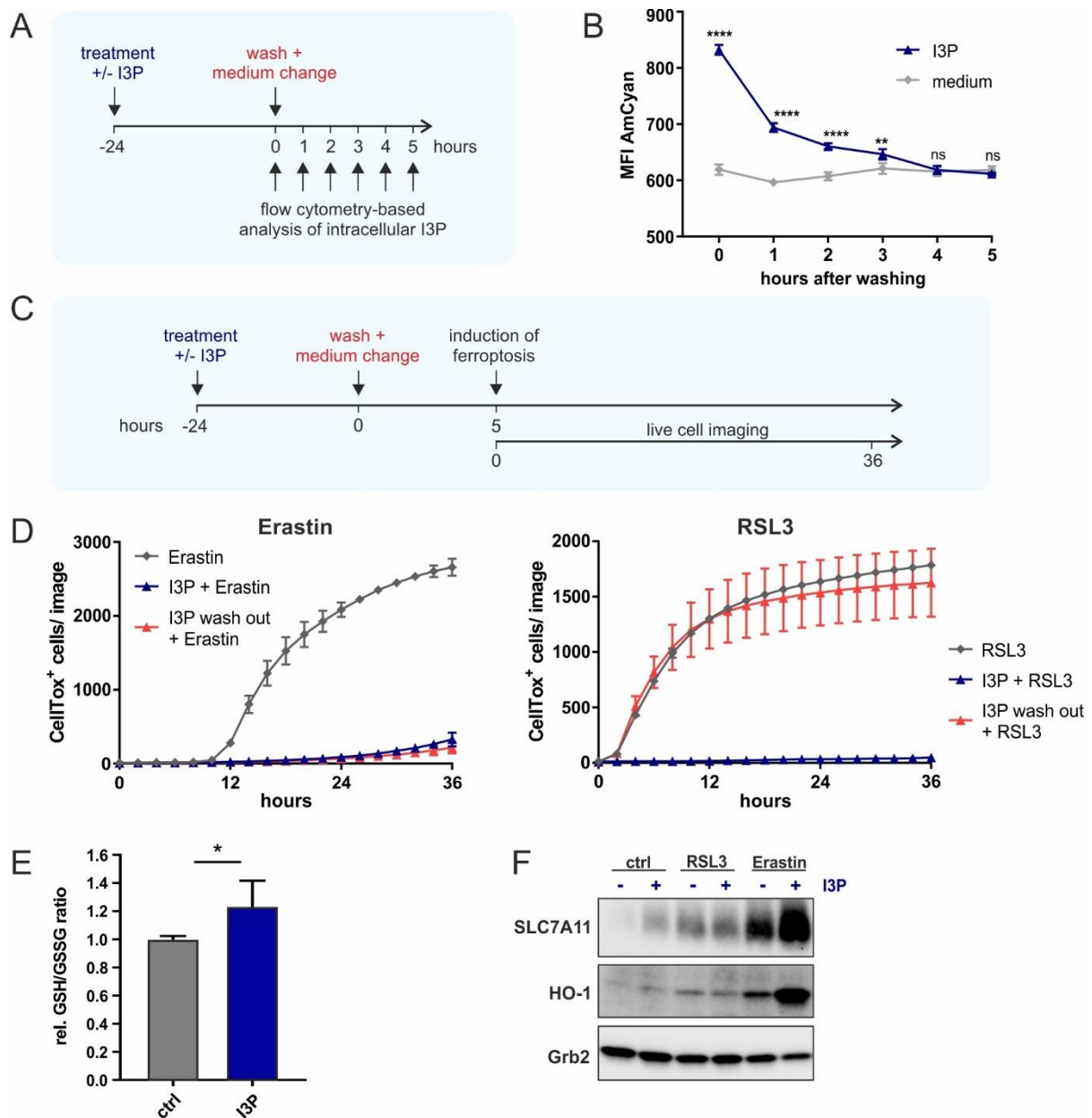


Figure 30 Distinct modes of anti-ferroptotic effects mediated by I3P

(A) Overview of experimental design to determine intracellular I3P. HeLa cells were pre-treated with medium without or with 200 μ M of I3P. After 24 h the cells were washed and medium without I3P was added. Remaining intracellular I3P was analyzed by flow cytometry as shown before (Figure 24) at the indicated time points. (B) Flow cytometry-based quantification of I3P fluorescence after wash-out as described in (A). $n=3$ biological replicates; 2-way ANOVA with Sidak's multiple comparisons test was used for statistics: ns: not significant; **: $p<0.01$; ****: $p<0.0001$ (C) Experimental design of ferroptosis induction after I3P wash-out to discriminate between direct and indirect effects of I3P on ferroptosis protection. HeLa cells were pre-treated with 200 μ M I3P for 24 h, followed by a wash-out step in parts of the samples. After 5 h ferroptosis was induced with 10 μ M Erastin or 1 μ M RSL3 and cell death was determined by live cell imaging. (D) Quantification of ferroptotic cell death in HeLa cells with or without wash-out of I3P before ferroptosis induction. $n=2$ biological replicates; the graphs are representative for three independent experiments. (E) GSH/GSSG ratio of HeLa cells determined after 24 h treatment with 200 μ M I3P. $n=4$ biological replicates; T-test was used for statistics: *: $p<0.05$ (F) Immunoblotting of SLC7A11 and HO-1 in protein lysates of HeLa cells concurrently treated for 24 h without or with 1 μ M RSL3 or 10 μ M Erastin and 200 μ M I3P.

4.2.3.2.2. HO-1 induction is not required for I3P-mediated ferroptosis protection

In mammals, two heme oxygenase isoenzymes exist, HO-1 and HO-2. While HO-2 is constitutively expressed, HO-1 is a highly inducible enzyme whose expression is for example controlled by oxidative stress via Nrf2 [317]. However, although HO-1 is induced by the anti-oxidative Nrf2 pathway, its role in redox stress and ferroptosis is controversial [318]. Whereas some studies report detrimental roles of HO-1 in the context of ferroptosis [319,320], other studies describe protective properties of HO-1 [252,256,321]. Both, pro- and anti-ferroptotic effects, may result from the HO-1 catalytic activity: HO-1-dependent heme degradation leads to the release of free iron, which may promote lipid peroxidation. On the other hand, the metabolites biliverdin and bilirubin generated from heme are known antioxidants [318,322].

As we observed a strong increase in HO-1 expression induced by I3P in the presence of Erastin (Figure 30F), we sought to investigate whether upregulation of HO-1 contributed to ferroptosis suppression mediated by I3P. First, we used the chemical HO-1 inhibitors Zinc protoporphyrin (ZnPP) and ketoconazole to block HO-1 activity [323]. We observed that the HO-1 inhibitors, while slightly delaying ferroptosis *per se*, strongly reduced the protective potential of I3P (Figure 31A,B). 48 h after ferroptosis induction, almost all cells treated with I3P died in the presence of the inhibitors, which would support the hypothesis that HO-1 upregulation in the presence of I3P was important for the protective effect. However, when genetically interfering with HO-1 expression using an siRNA-mediated knockdown, we could not observe any difference between cells with (siHO-1) or without (siScr) HO-1 knockdown (Figure 31C,D). I3P treatment retained its anti-ferroptotic effect even when HO-1 was no longer induced. Since the knockdown was very potent, our experiments indicate that HO-1 upregulation is not required to mediate the I3P-dependent ferroptosis suppression. Yet, our observations also suggest that the inhibitors may not be completely specific to HO-1 and may target other proteins such as HO-2 or further heme-dependent enzymes that could affect I3P-mediated cell protection, which requires further investigation.

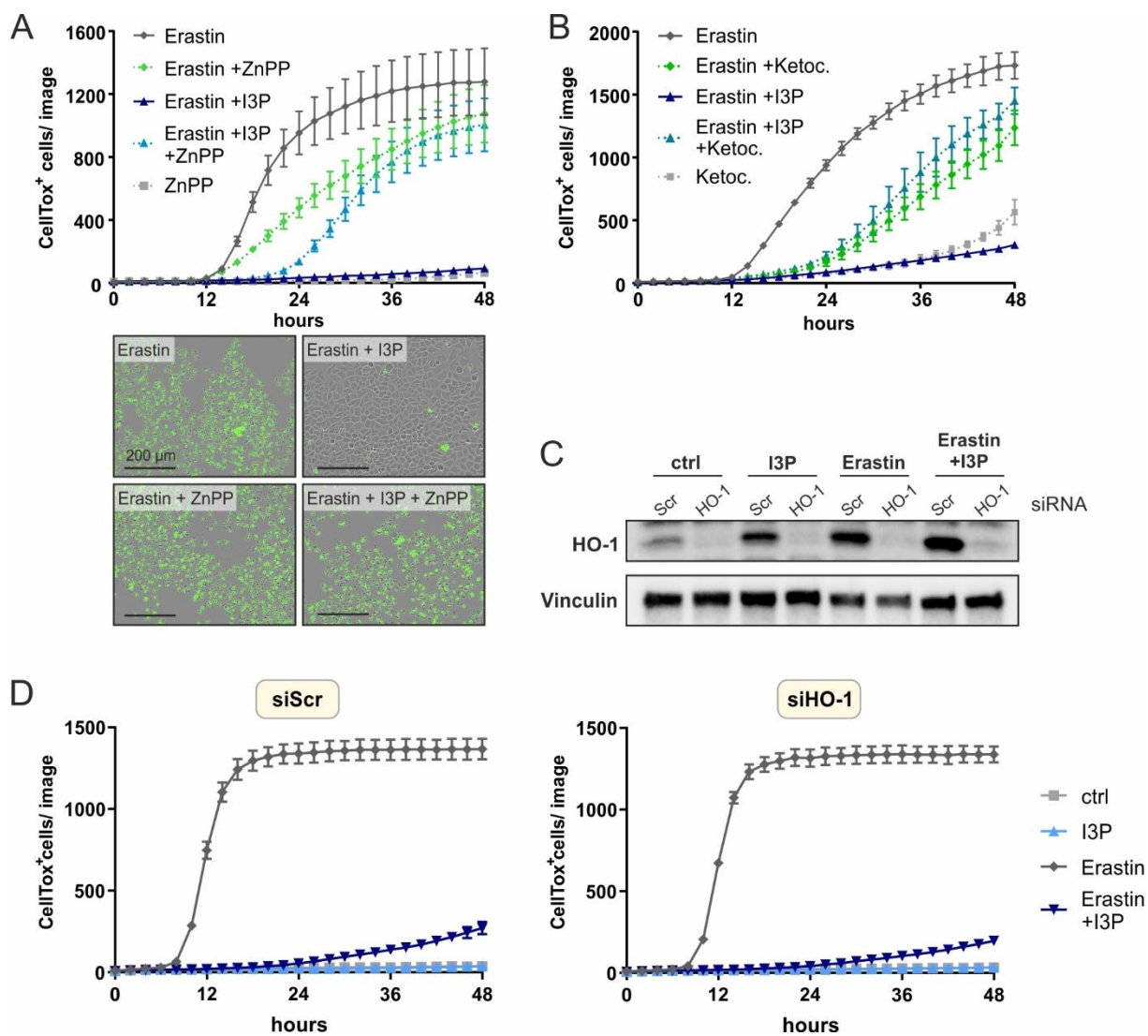


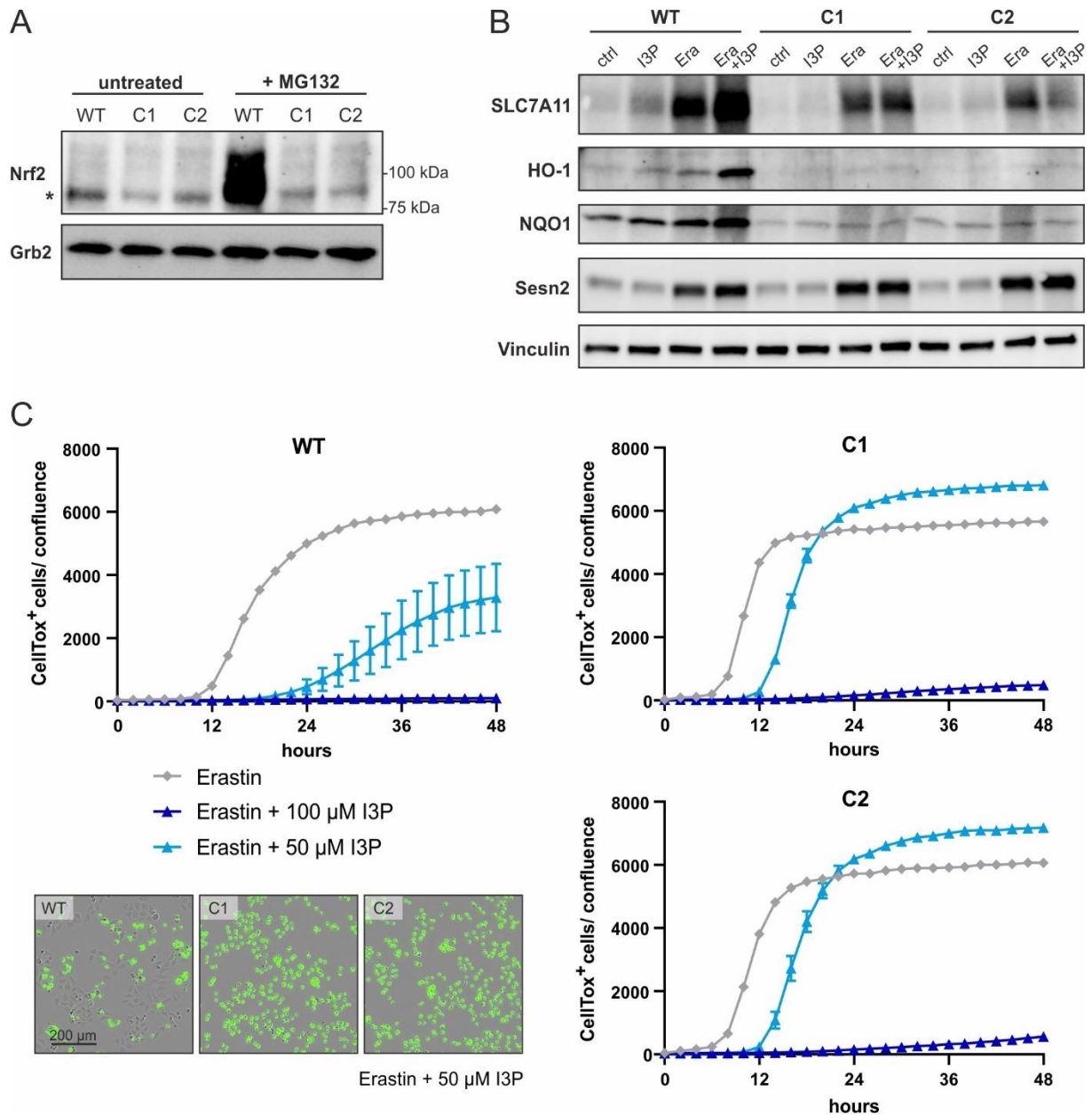
Figure 31 HO-1 induction is not required for I3P-mediated ferroptosis protection

(A) Analysis of I3P-mediated ferroptosis protection over 48 h in absence or presence of ZnPP. Ferroptosis in HeLa cells was induced by 10 μ M Erastin with concurrent treatment with 200 μ M I3P, 10 μ M of ZnPP or combinations of both. $n=2$ biological replicates; the graph is representative for three independent experiments. Representative image sections with CellTox staining are shown below the graph. (B) Same experimental setup as in (A) using 100 μ M ketoconazole (Ketoc.) instead of ZnPP. (C) Confirmation of HO-1 knockdown after transfections with 50 nM siRNA (siScr negative ctrl or siHO-1) by immunoblotting. 10 h after transfection cells were re-plated and treated for 15 h with 200 μ M I3P, 10 μ M Erastin, or a combination of both. Vinculin was used as loading control. (D) Quantification of ferroptotic cell death over 48 h in HeLa cells transfected with siScr (left) or siHO-1 (right). Ferroptosis was induced with 10 μ M Erastin in absence or presence of 200 μ M I3P. $n=3$ biological replicates; the graph is representative for three independent experiments. Error bars represent standard deviation.

4.2.3.2.1 Nrf2 contributes to I3P-mediated ferroptosis suppression

Since I3P induced several Nrf2 target genes in THP-1 cells (Figure 23) and enhanced the expression of SLC7A11 and HO-1, two known Nrf2 target genes, in the presence of Erastin (Figure 30F), I next investigated the role of Nrf2 in I3P-mediated ferroptosis suppression. Nrf2 is the key transcription factor that induces protective gene expression upon oxidative stress and is mainly regulated via the Keap1-Nrf2 axis [239,242] (1.3.1.3): Under steady state conditions Nrf2 is bound by Keap1, which is a substrate adaptor for the Cullin 3-based ubiquitin E3-ligase complex (Cul3) and facilitates Nrf2 ubiquitination. Thus, under steady state conditions Nrf2 is degraded by the proteasome. However, oxidative stress can promote modifications of cysteine residues in Keap1, which disrupts Nrf2 degradation and thereby enables Nrf2-dependent transcription (Figure 10). Nrf2 induces several genes involved in cysteine and GSH homeostasis [247] and was previously linked to ferroptosis suppression by several research groups [252-256]. Therefore, I aimed to investigate whether activation of Nrf2 was required for I3P-mediated ferroptosis suppression. Together with my Master's student Maria Hiller, I generated Nrf2-deficient HeLa clones using the CRISPR/Cas9 system. The knockouts in the two clones (C1 and C2) used in the further experiments were validated on genomic DNA and protein level (Figure 12, Figure 32A). I first tested whether Nrf2 knockout affected the upregulation of the Nrf2 target genes SLC7A11, HO-1 and NQO1 in HeLa cells that were treated for 24 h with I3P, Erastin or a combination of both compared to untreated cells. (Figure 32B). As expected, HO-1 and NQO1 upregulation upon I3P or Erastin treatment was almost completely abrogated in the Nrf2-deficient clones. SLC7A11 was still upregulated in all Erastin treated conditions, however not as strong as in WT cells. By contrast, the I3P-mediated increase of SLC7A11 levels was completely lost. Taken together, this suggests that I3P indeed mediates anti-oxidative gene expression via activation of Nrf2 signaling. The Erastin-induced, incomplete upregulation SLC7A11 on the other hand may result from amino acid starvation (cysteine starvation) activating the GCN2 stress kinase [61,274]. In accordance, I observed induction of Sestrin2 (Sesn2) which is regulated by GCN2 signaling [324] in all Erastin treated samples regardless of the Nrf2 expression.

To test if Nrf2 was required for the protective effect of I3P, I induced ferroptosis with Erastin in WT and Nrf2-deficient HeLa cells in absence or presence of different I3P concentrations (Figure 32C). A high I3P concentration (100 μ M) was still potent in protecting Nrf2-deficient clones from ferroptosis, which is likely mediated by the antioxidant properties of I3P (Figure 28). However, at a lower concentration (50 μ M), where radical scavenging decreases, I3P could only slightly delay but not prevent ferroptosis in the Nrf2-deficient clones, while in the WT cells only a part of the cells died from ferroptosis. Thus, Nrf2 activation clearly contributes to the inhibition of ferroptosis, which in combination with the radical scavenging effect results in the protective effect of I3P.



4.2.3.2.3. I3P-mediated ferroptosis suppression is independent of AhR activation

My previous results (Figure 25) and the research from Sadik et al. [19] and Zhang et al. [196] indicate that I3P is an activator of AhR signaling. Notably, there is evidence for an overlap of a fraction of AhR and Nrf2 target genes [311]. However, the role of AhR in ferroptosis remains controversial. While Kwon and colleagues [325] reported that AhR expression alongside with Nrf2 represents a predictive marker for Erastin resistance in pan-cancer cell lines, another study reported that AhR inhibition by CH223191 protected cells from ferroptosis [326]. To approach the question whether I3P-mediated AhR activation contributed to ferroptosis suppression, I first tested if kynurenic acid (KynA) shows anti-ferroptotic effects since KynA was found to be a downstream metabolite of I3P, that activates the AhR [19] (Figure 33A). However, when inducing ferroptosis in presence of KynA, all cells died exactly with the same kinetic as cells that were not treated with the metabolite (Figure 33B). This gave a first hint that AhR activation was probably not required or sufficient to mediate anti-ferroptotic effects in our setup. To further test this, I generated AhR-deficient HeLa cells together with my Master's student Maria Hiller. AhR deficiency of the two clones (C1, C2) used for the experiments was confirmed in the genomic DNA and on protein level (Figure 12, Figure 33C). Functionally, I verified the AhR deficiency by the loss of the CYP1A1 and CYP1B1 mRNA induction mediated by I3P (Figure 33B). Notably, the baseline expression of the mRNAs was lower in the knockout clones as compared to WT cells indicating that WT HeLa cells have baseline activation of AhR-dependent transcription under steady state conditions. Next, I tested if I3P-mediated AhR activation contributed to ferroptosis suppression (Figure 33C). However, AhR deficiency did not interfere with I3P-dependent cell protection. In contrary, the fraction of cells dying from ferroptosis in the presence of 50 μ M I3P was even slightly decreased, suggesting that loss of AhR may even be advantageous for the cells. Overall, the experiments indicate that I3P-mediated ferroptosis suppression is independent of the metabolite's capability to activate AhR signaling, which nevertheless appears to be an important mechanism for other IL4i1-dependent processes [19].

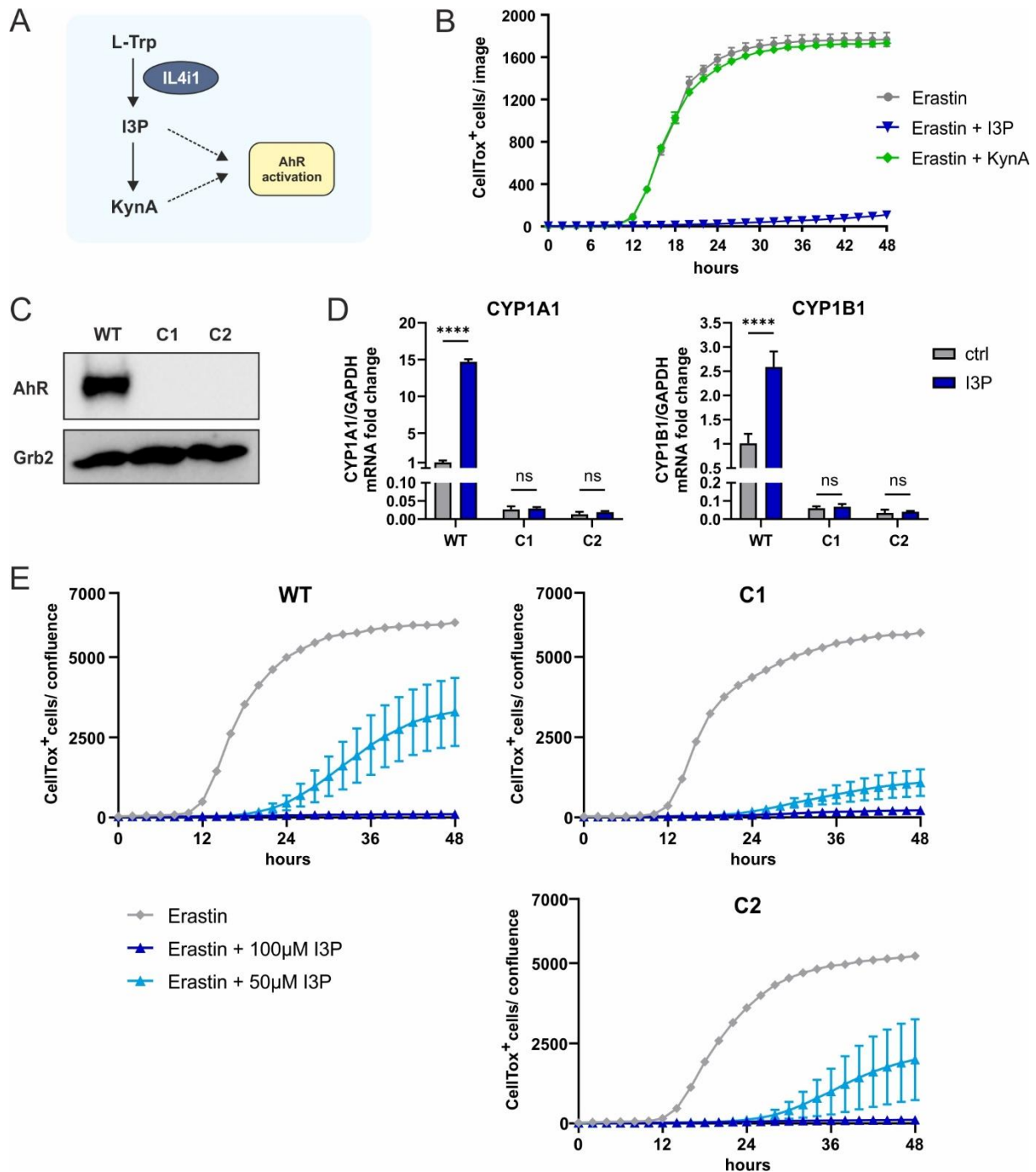


Figure 33 AhR is not required for I3P-mediated ferroptosis suppression

(A) Scheme of I3P and KynA as AhR activators. (B) Quantification of ferroptotic cell death induced by 10 μ M Erastin in HeLa cells with concurrent addition of 200 μ M I3P or KynA. (C) Immunoblot verifying AhR ko in two HeLa clones (C1, C2) on protein level. A lysate from WT HeLa cells was used as control. Grb2 was used as loading control. (D) Functional verification of the AhR ko using qRT-PCR analyzing the AhR target genes CYP1A1 (left) and CYP1B1 (right). RNA from WT HeLa cells and AhR ko clones was isolated after 24 h treatment with 200 μ M I3P or medium without I3P (ctrl). n=3 biological replicates; error bars indicate standard deviation; 2-way ANOVA with Sidak's multiple comparisons test was used for statistics: ns: not significant; ****: p<0.0001. (E) Quantification of ferroptotic cell death in WT or AhR-deficient HeLa cells induced by 2.5 μ M Erastin. 100 μ M or 50 μ M I3P were added simultaneously to ferroptosis induction. (B,E) n=3 biological replicates; error bars represent standard deviation.

4.2.3.3. IL4i1 generates a ferroptosis-suppressive milieu

In the previous experiments we could show that the metabolites I3P and 4HPP generated by IL4i1 from Trp and Tyr respectively, interfere with ferroptotic cell death. This implicates that IL4i1, when secreted to the extracellular space [17], could metabolize those amino acids to generate an anti-ferroptotic environment that promotes cell survival under redox stress. To test this, I first examined the effects of IL4i1 on gene expression in HeLa cells. Since I was interested in IL4i1-dependent changes of the cell environment, I added WT or enzymatically inactive K351A mutant mIL4i1 to complete DMEM culture medium. The medium was incubated for 72 h at 37 °C to allow the enzyme to metabolize amino acids and subsequently transferred to HeLa cells. Untreated control medium and medium supplemented with I3P were used as controls. After 24 h mRNA was isolated and the transcriptome was analyzed by RNAseq. Hierarchical clustering of significantly regulated transcripts clearly showed that untreated cells clustered together with cells treated with K351A IL4i1-conditioned medium, while I3P treated samples clustered with cells treated with WT IL4i1-conditioned medium (Figure 34A). This suggested that the enzymatic activity (and not direct protein interaction) was required for the IL4i1-dependent changes in the cells' transcriptome. Further, I3P seemed to contribute to the gene expression profile mediated by IL4i1, which may additionally be complemented by other factors such as 4HPP and the sub-lethal levels of H₂O₂. When analyzing the most significantly regulated transcripts I found that almost all I3P-dependent transcripts were also found to be regulated by IL4i1, which again showed a signature of Nrf2 and AhR signaling (Figure 34B).

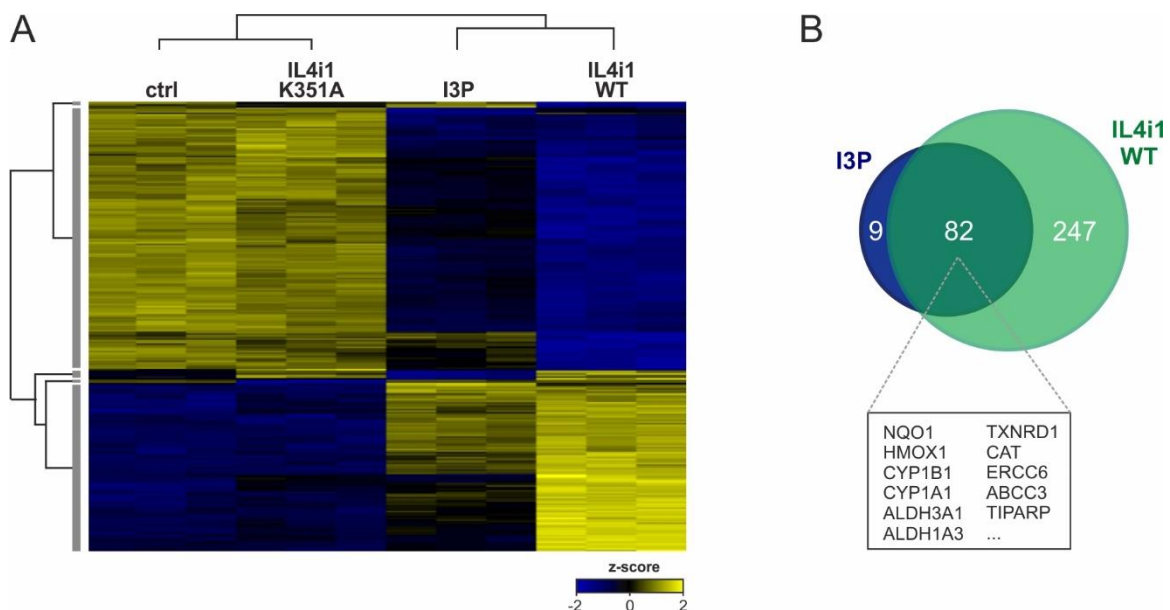


Figure 34 Effects of IL4i1 on gene expression in HeLa cells

(A) Hierarchical clustering of differentially expressed genes in HeLa cells determined by RNA-Seq. Cells were treated for 24 h with WT or K351A IL4i1-conditioned DMEM (containing 1 µg/ml IL4i1), 200 µM I3P or untreated control medium. n=3 biological replicates. (B) Overlap of most significantly upregulated genes (adjusted p-value <10⁻⁹) by I3P and WT IL4i1 conditioned medium compared to the untreated control.

Differential gene expression induced by IL4i1-conditioned DMEM displayed large overlap with the I3P-induced profile, suggesting that I3P was generated and acted on the cells. Therefore, I next investigated if IL4i1-conditioned medium provokes effects that we previously observed to be mediated by I3P (Figure 35A). First, I analyzed I3P fluorescence induced by WT or K351A IL4i1-conditioned medium in HeLa cells by flow cytometry (Figure 35B). As expected I did not observe changes in the AmCyan fluorescence in cells treated with the inactive IL4i1 mutant. However, cells treated with WT IL4i1-conditioned medium showed a dose-dependent fluorescence increase, suggesting that I3P was produced in a dose-dependent manner and imported into the cells. In line with this, I observed a dose-dependent increase in HO-1 and SLC7A11 expression on protein level induced by WT but not K351A-conditioned medium (Figure 35C,D). Finally, I tested if IL4i1 could protect cells from ferroptosis. DMEM conditioned with 1 $\mu\text{g/ml}$ WT or K351A IL4i1 was transferred to HeLa cells and ferroptosis induced with Erastin or RSL3 (Figure 35E,F). While the mutant enzyme could not prevent cell death, WT IL4i1 effectively interfered with Erastin and RSL3-induced ferroptosis. Titration of the enzyme, revealed that concentrations down to 125 ng/ml were sufficient to protect HeLa cells, only at 63 ng/ml IL4i1 could just delay but not prevent ferroptotic cell death (Figure 35G,H). As a last series of experiments, I removed IL4i1 from the conditioned medium by filtration to finally evaluate if IL4i1-mediated medium re-composition alone was sufficient to prevent ferroptosis (Figure 36A). Successful IL4i1 removal from the medium was confirmed by immunoblotting (Figure 36B). Even after depleting the enzyme from the medium, IL4i1-conditioned medium was capable of inducing SLC7A11 and HO-1 protein expression (Figure 36B) and protected cells from Erastin- and RSL3-induced ferroptosis.

Taken together, my results suggest that IL4i1 has the capability to generate ferroptosis-suppressive environment promoting cell survival under redox stress. This does not require direct protein-protein interactions but depends on the enzymatic LAAO activity and involves the generation of anti-ferroptotic metabolites.

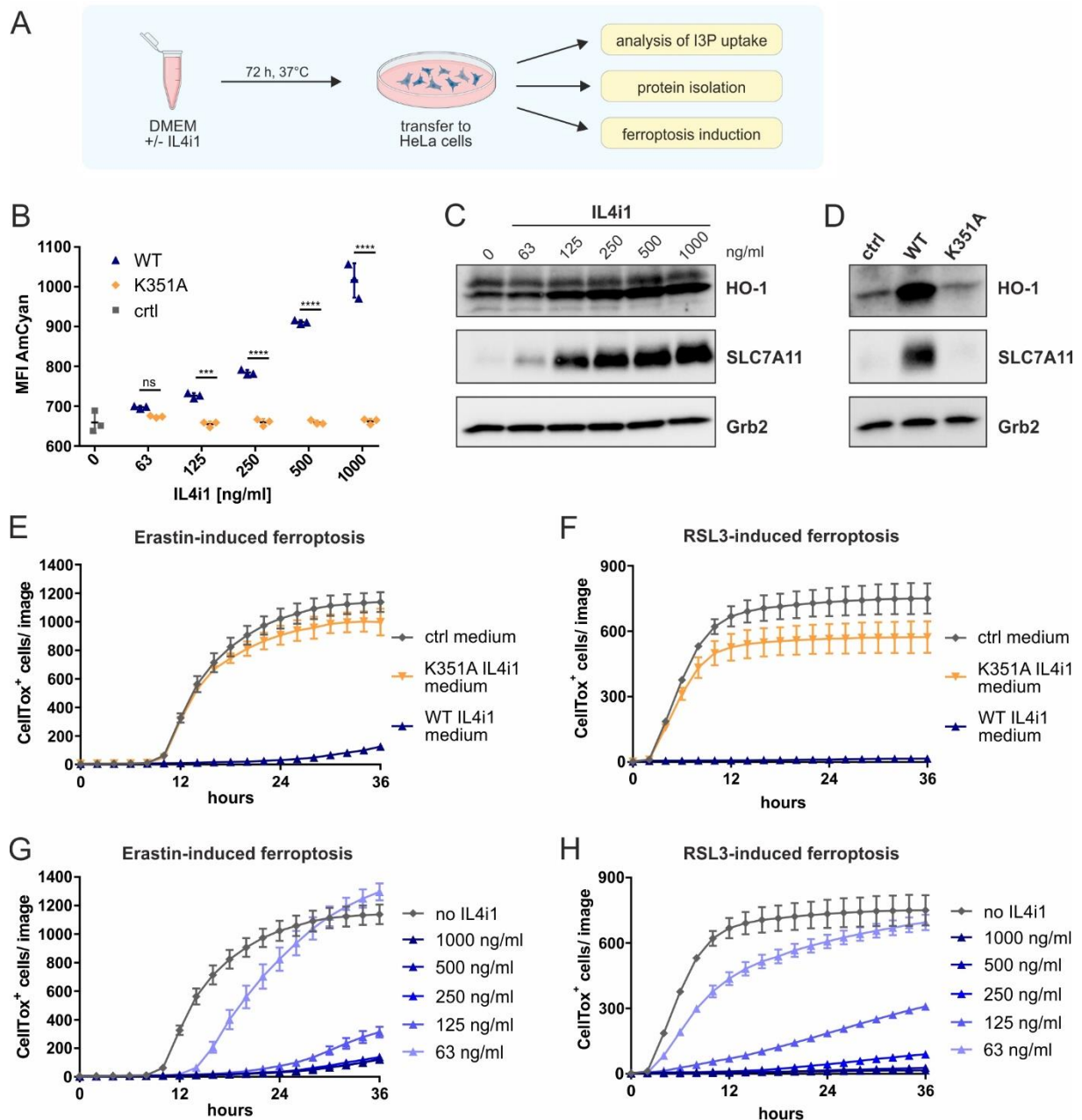


Figure 35 Anti-ferroptotic effects of IL4i1

(A) Scheme of experimental setups: Complete DMEM was conditioned with WT/ K351A mutant IL4i1 or left without IL4i1 for 72 h at 37°C. The conditioned medium was transferred to HeLa cells and different experiments were performed. (B) Analysis of I3P-uptake by flow cytometry 24 h after incubation of HeLa cells with medium conditioned with the indicated concentrations of IL4i1. n=3 biological replicates; 2-way ANOVA with Sidak's multiple comparisons test was used for statistics: ns: not significant; ***: $p < 0.001$; ****: $p < 0.0001$ (C) Immunoblotting of SLC7A11 and HO-1 in protein lysates of HeLa cells after 24 h incubation with WT IL4i1-conditioned medium. Grb2 was used as leading control. (D) As (C) comparing conditioned medium without IL4i1 or 1 $\mu\text{g/ml}$ WT or K351A mutant IL4i1. (E) Quantification of cell death via live cell imaging induced by 10 μM Erastin in HeLa cells incubated with 1 $\mu\text{g/ml}$ WT/ K351A mutant IL4i1-conditioned medium or medium without IL4i1 at the time of ferroptosis induction. (F) As in (E) using 1 μM RSL3 for ferroptosis induction. (G) As in (E) using titrations of WT IL4i1 for medium conditioning. (H) As in (G) using 1 μM RSL3 for ferroptosis induction. (E-F) n=2 biological replicates; Data are representative for three independent experiments. Error bars indicate standard deviation.

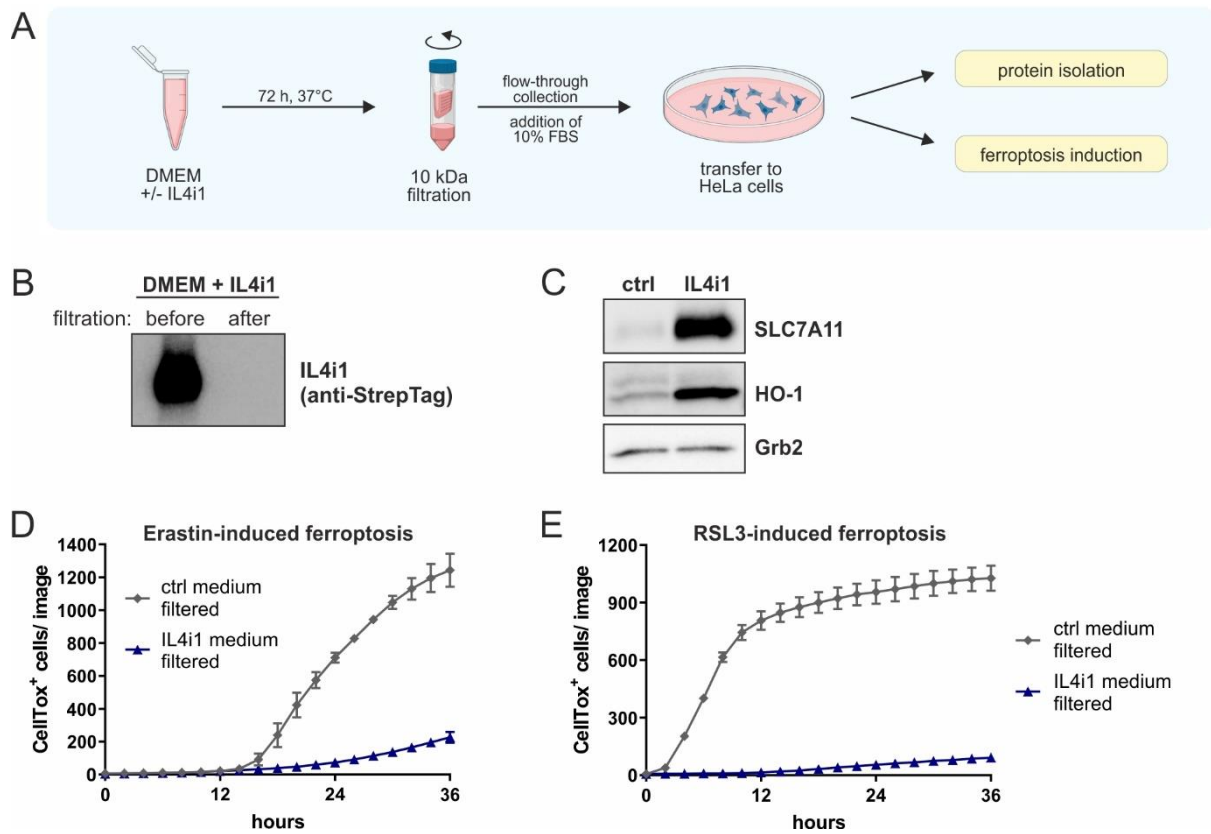


Figure 36 IL4i1-mediated changes in culture medium are sufficient to block ferroptosis

(A) Scheme of experimental setup: IL4i1 was removed from the conditioned DMEM using a 10 kDa cut-off filter before starting the experiments. After filtration FBS was re-added to the medium. (B) Verification of IL4i1 removal by immunoblotting of DMEM conditioned with 1 µg/ml WT IL4i1 before and after filtration. (C) Immunoblotting of SLC7A11 and HO-1 in HeLa cells treated for 24 h with filtrated media pre-conditioned without (ctrl) or with 1 µg/ml IL4i1. (D) Quantification of cell death via live cell imaging induced by 10 µM Erastin. HeLa cells were incubated with filtrated DMEM pre-conditioned without (ctrl) or with 1 µg/ml IL4i1 at the time of ferroptosis induction. n=3 biological replicates; error bars indicate standard deviation (E) as in (D) using 1 µM RSL3 for ferroptosis induction.

4.3. Expression and regulation of IL4i1 in bone marrow-derived myeloid cells

So far, I defined that IL4i1-mediated amino acid metabolism protected cells from ferroptosis. Considering the fact IL4i1 is associated with poor prognosis in cancer [19,172,173], it is possible that IL4i1 not only suppresses immune responses to tumors [19,188] but also mediates tumor cell resistance to redox stress, which could additionally result in tumor progression. However, in order to better understand and mechanistically dissect the interplay between IL4i1-secreting immune cells and different cells in the TME, more complex *in vitro* models are required. Therefore, in this part of my thesis I aimed to better characterize 'IL4i1-producer cells' and the factors driving IL4i1 expression. Herein, I focused on macrophages and DCs, which may represent the most important IL4i1-producing populations in the TME [19,55,171,173,175,179]. I used the differentiation of macrophages and DCs from murine bone marrow as a model approach to characterize IL4i1 regulation in systems that are applicable for large scale experiments by providing a high yield of the cells of interest.

4.3.1. Baseline expression of IL4i1 in BMDMs and BMDCs

To investigate the expression of IL4i1 in macrophages and dendritic cells *in vitro*, I differentiated BMDMs using CSF-1 and BMDCs using GM-CSF (GM-DCs), FLT3L (FL-DCs) or a combination of GM-CSF and FLT3L leading to the generation of CD103⁺ DCs (CD103 DCs) from bone marrow isolated from WT C57BL/6 mice (Figure 37A). After differentiation, I isolated mRNA and compared IL4i1 levels between the differentiations by qRT-PCR (Figure 37B). Interestingly, unstimulated BMDMs had the lowest baseline IL4i1 expression. Within the BMDCs, FL-DCs showed the lowest IL4i1 expression, while GM-DCs and CD103 DCs exhibited significantly higher baseline IL4i1 mRNA levels, with CD103 DCs having the highest IL4i1 expression. This was also reflected on protein level (Figure 37C). Whereas IL4i1 was not detectable in BMDMs and FL-DCs, the protein could be detected in both, lysates and supernatants of GM-DCs and CD103 DCs. In line with the mRNA levels, the expression and secretion was most prominent in the CD103 DCs. This indicates that IL4i1 is expressed and secreted from certain DC populations on a baseline level without additional stimulation. However, this does not exclude that IL4i1 may be inducible in the other cell types by certain stimuli.

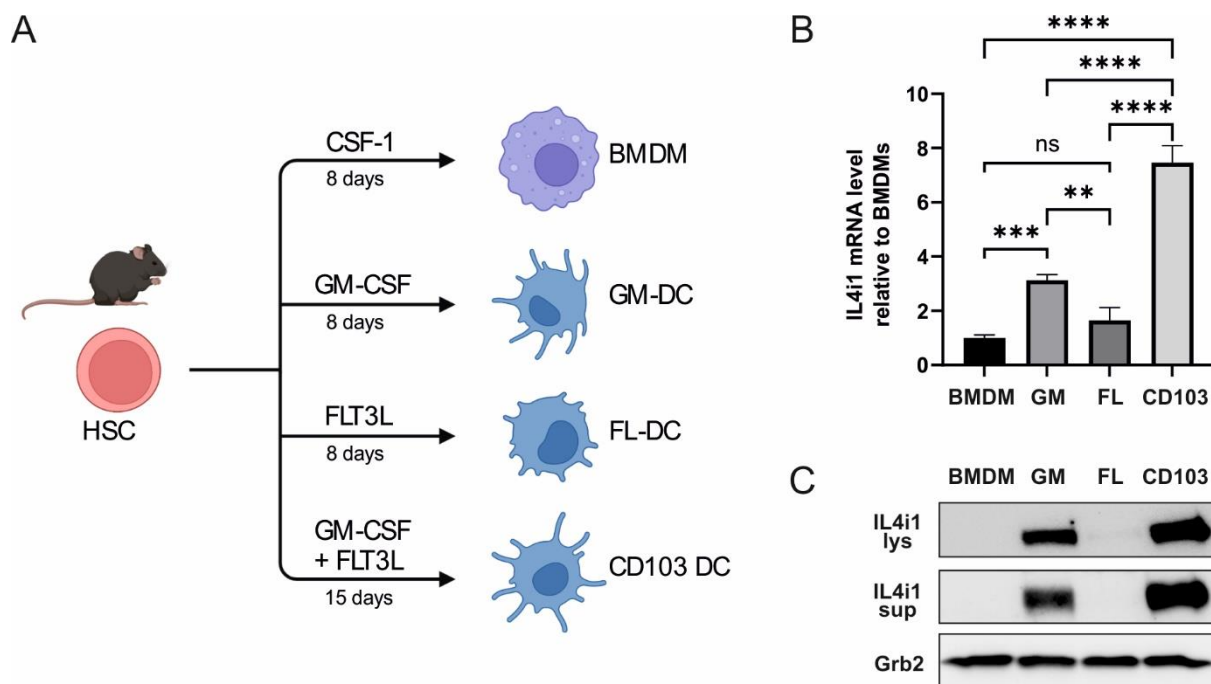


Figure 37 Baseline IL4i1 expression in bone marrow-derived macrophages and dendritic cells

(A) Overview of different differentiation methods used to generate macrophages and dendritic cells from murine bone marrow as described in 3.4.2 (B) Determination of baseline IL4i1 mRNA expression via qRT-PCR in unstimulated BMDMs, GM-DCs (GM), FL-DCs (FL) and CD103 DCs (CD103) relative to expression level in BMDMs. n=3 biological replicates; error bars indicate standard deviation; One-way ANOVA with Tukey's multiple comparisons test was used for statistics: ns: not significant; **: p<0.01; ***: p< 0.001; ****: p<0.0001 (C) Immunoblotting of baseline IL4i1 protein level in 10 µg protein lysate and the corresponding sample supernatant of unstimulated BMDMs, GM-DCs (GM), FL-DCs (FL) and CD103 DCs (CD103).

4.3.2. IL4i1 expression in GM-CSF differentiated dendritic cells

The differentiation of DCs from bone marrow using GM-CSF was first described by Inaba et al. [327], suggesting that during the differentiation next to CD11c⁺ non-adherent DCs, also an adherent CD11c⁻ macrophage population develops. I found previously that IL4i1 was expressed in the non-adherent cells, which I called GM-DCs (Figure 37C). However, there is evidence that also the CD11c⁺ cells consist of DC and macrophage populations [328]. Analyzing the non-adherent cells by flow cytometry, I detected a CD11c⁺ population with intermediate MHCII (MHCII^{int}) and high CD11b (CD11b^{hi}) expression representing the macrophage population, and a CD11c⁺ population with high MHCII (MHCII^{hi}) and intermediate CD11b (CD11b^{int}) expression, which represents the DCs as reported by Helft et al. [328] (Figure 38A). In accordance with this study, I also observed CCR7 expression in the MHCII^{hi}, CD11b^{int} DC population. Expression of the chemokine receptor CCR7 is associated with DC maturation and migration [329] and often correlates with IL4i1 expression in single cell datasets (Table 1). To further investigate the expression of IL4i1 in the CD11c⁺ subpopulations, I sorted the cells into the macrophage and DC populations (Supplementary Figure 9): When re-plating the cells the macrophages attached to the dish, while the DCs, clearly exhibiting dendritic

processes, remained non-adherent (Figure 38B). Notably, under unstimulated conditions IL4i1 expression was completely restricted to the DC population as determined by immunoblotting (Figure 38C), suggesting that IL4i1 expression as observed before in the non-adherent cells of the GM-CSF differentiation comes from the MHCII^{hi}, CD11b^{int} DC population.

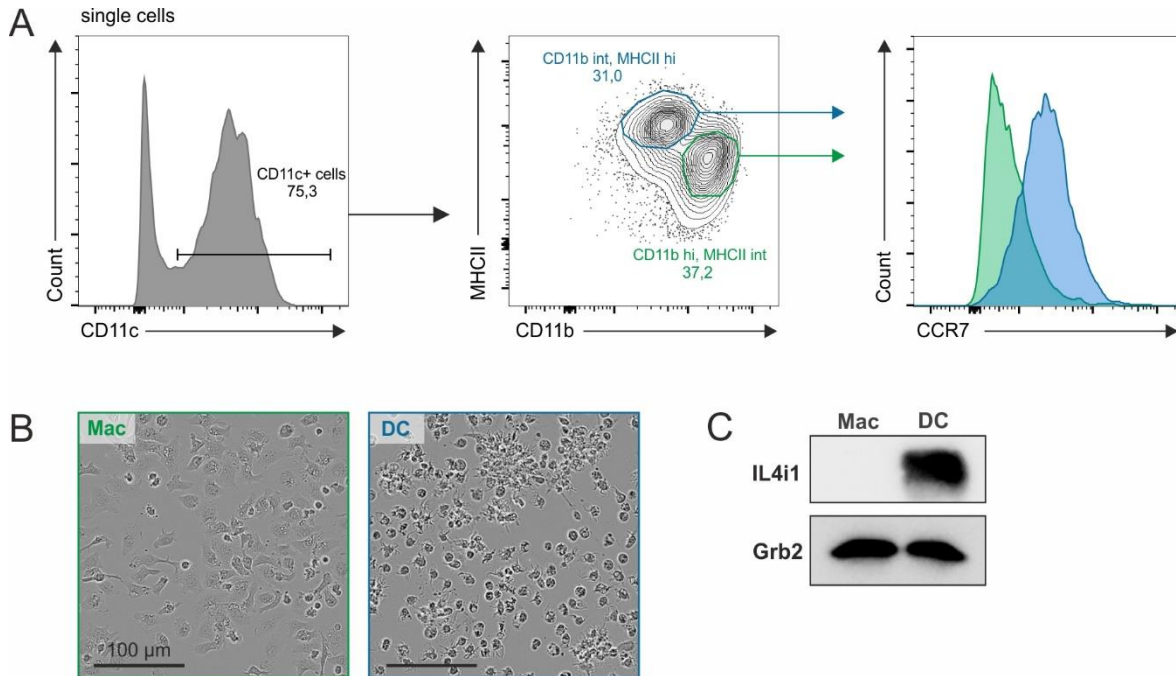


Figure 38 IL4i1 expression in GM-CSF differentiated culture

(A) Flow cytometry of BMDC culture differentiated with GM-CSF for 8 days. The CD11c⁺ cells consist of two main populations: A CD11b^{int}, MHCII^{hi} population which has been reported to represent the DCs and a CD11b^{hi}, MHCII^{int} population which represents a Macrophage (Mac) population [328]. In accordance, higher CCR7 expression was detected in the DC population. (B) Representative image sections (20X objective) of the CD11c⁺, CD11b^{hi}, MHCII^{int} Mac population and the CD11c⁺, CD11b^{int}, MHCII^{hi} DC population obtained by fluorescence activated cell sorting. (C) Immunoblot of sorted populations shows IL4i1 expression in the DC population under unstimulated conditions. Grb2 was used as loading control.

4.3.3. IL4i1 expression in bone marrow-derived CD103⁺ dendritic cells

Next, I analyzed IL4i1 expression in the CD103 DCs, generated by differentiation with GM-CSF and FLT3L adapted from Mayer et al. [294], which showed the highest IL4i1 expression within the tested differentiations. The CD11c⁺ CD103⁺ population comprised a MHCII^{int}, CCR7⁻ population and a MHCII^{hi}, CCR7⁺ population, which likely reflects mature CD103 DCs [294] (Figure 39A). To test if IL4i1 expression correlates with the CCR7⁺ mature CD103 DCs, I sorted the cells for CD103⁺ and CCR7⁻ or CCR7⁺ populations (Supplementary Figure 10) and analyzed IL4i1 expression by immunoblotting (Figure 39B). IL4i1 expression was completely restricted to the CCR7⁺ population. These cells also expressed high levels of IDO1, another Trp metabolizing enzyme, which is consistent with a recent publication by Gargaro et al. [53] showing high IDO1 expression in CCR7⁺ DCs. Since both enzymes, IL4i1 and IDO1 are capable to generate AhR ligands (Figure 25), I3P and Kyn respectively, I investigated the AhR

expression in the two populations. AhR was hardly detectable in the CCR7⁺ population contrast to the CCR7⁻ population. This may reflect an activation of AhR signaling in the CCR7⁺ population (Figure 23D) [110], which at this point is purely speculative and requires further investigation. Taken together, the experiments suggest that IL4i1 expression is associated with a mature CD103 DC phenotype that is CCR7⁺ and expresses IDO1.

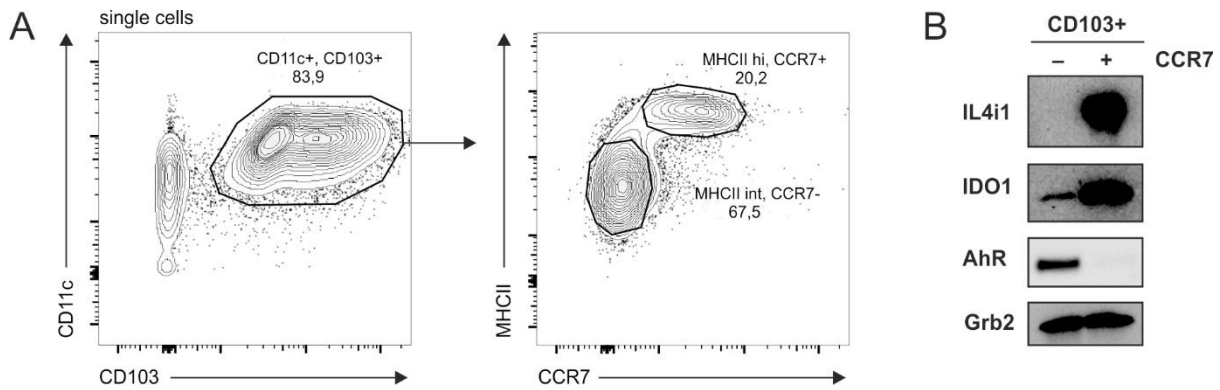


Figure 39 IL4i1 expression in CD103 DCs

(A) Flow cytometry of BMDCs differentiated with GM-CSF and FLT3L at day 14. Within the CD11c⁺, CD103⁺ cells a MHCII^{int}, CCR7⁻ population and a MHCII^{hi}, CCR7⁺ population is detectable. (B) Immunoblotting of IL4i1, IDO1 and AhR in CD103 DCs after sorting for CD103⁺, CCR7⁻ and CD103⁺, CCR7⁺ cells. Grb2 was used as loading control.

4.3.4. IL4i1 induction in bone marrow-derived macrophages

4.3.4.1. IL4i1 is highly inducible by the combination of IL4 and TNF

In BMDMs the expression of IL4i1 was not detectable on protein level under unstimulated conditions (Figure 37). Originally, IL4i1 has been found as IL4-inducible gene in B cells [161]. Moreover, the enzyme has been associated with the anti-inflammatory (IL4-induced) M2 macrophage phenotype [164], however the regulation seems to be complex, as both, IL4 and pro-inflammatory, M1-associated stimuli were found to induce IL4i1 expression and IL4i1 was present in Th1 but much less in Th2 granulomas [164,168]. Yet, is not known whether these stimuli may intersect to drive expression of IL4i1 when macrophages encounter and integrate multiple signals in a complex environment. Therefore, I stimulated macrophages with different cytokines in the combination with IL4. Additionally, I tested the combination of TNF and IFN γ which was reported to induce IL4i1 in mesenchymal stromal cells derived from head-neck cancer [330]. While single stimulations with cytokines had only minor effects on IL4i1 mRNA level (the greatest induction, about 15-fold, was observed with TNF), the combination of IL4 and TNF potently induced IL4i1 expression (Figure 40A). The increase was more than 200-fold, which to my knowledge is the highest fold of induction that has been shown for IL4i1 on mRNA level. Also on protein level, the BMDMs showing no IL4i1 expression under unstimulated conditions exhibited clear IL4i1 expression in cell lysates 8 h after IL4 + TNF stimulation (Figure 40B). Additionally, the protein was detectable in the supernatant, indicating

that it was also secreted. As the time-dependent resolution of IL4i1 expression and secretion has not been studied in detail before, I next investigated the dynamics of IL4 + TNF-mediated IL4i1 induction. IL4i1 mRNA induction occurred in a tightly regulated timeframe, peaking 6 h after stimulation (Figure 40C). 24 h after the stimulation the induction had strongly declined and the mRNA level almost reached the baseline level. Also on protein level the highest intracellular expression of IL4i1 was detectable at 6 h which continuously decreased until 24 h (Figure 40D). At the same time IL4i1 increased in the supernatant and was clearly detectable 10 h after stimulation, suggesting that upon stimulation IL4i1 is newly synthesized in BMDMs and secreted to the extracellular space.

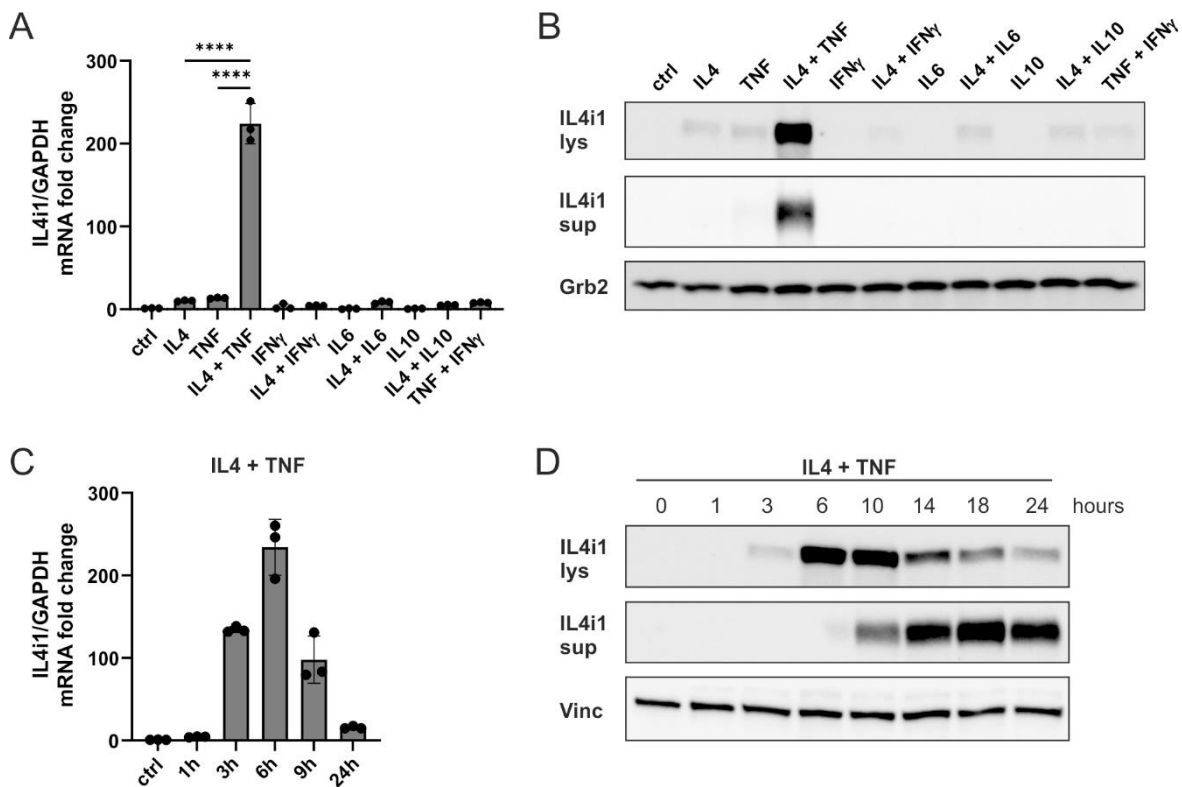


Figure 40 IL4i1 is highly inducible by the combination of IL4 and TNF

(A) Quantification of IL4i1 mRNA levels by qRT-PCT upon 6 h treatment of BMDMs with IL4 (10 ng/ml), TNF (10 ng/ml), IFN γ (2 ng/ml), IL6 (10 ng/ml), IL10 (10 ng/ml) or combinations of the cytokines. IL4i1 levels were normalized to GAPDH and the fold change compared to the unstimulated control (ctrl) was determined. n=3 biological replicates; error bars indicate standard deviation; One-way ANOVA with Tukey's multiple comparisons test was used for statistics: ****: p<0.0001 (B) Immunoblotting of BMDM cell lysates (lys) and their respective supernatants (sup) after 8 h treatment with the indicated cytokines (same concentrations as in (A)). Grb2 was used as loading control. (C) Time course of IL4i1 induction in BMDMs upon IL4 + TNF treatment (both 10 ng/ml) on mRNA level compared to the unstimulated ctrl. n=3 biological replicates; error bars indicate standard deviation. (D) Immunoblotting of a time course of IL4i1 induction in cell lysates and secretion to the respective supernatants in BMDMs stimulated for the indicated time with IL4 + TNF (both 10 ng/ml). Vinculin was used as loading control.

4.3.4.2. IL4 enhances the induction of IL4i1 by TLR ligands

Stimulation of toll-like receptors (TLRs) can induce IL4i1 expression [164,168]. Since IL4 in combination with the pro-inflammatory cytokine TNF strongly stimulated IL4i1 production in BMDMs, I next investigated whether IL4 would enhance the induction of the enzyme by TLR ligands. I tested three different TLR agonists: LPS (stimulating TLR4), GpG (stimulating TLR9) and polyI:C (stimulating TLR3) [2]. LPS, GpG and polyI:C were able to upregulate IL4i1 on mRNA level (Figure 41A). LPS treatment led to the strongest induction of IL4i1 mRNA (~35-fold change). However, in combination with IL4 the IL4i1 mRNA induction provoked by the TLR ligands was significantly enhanced. This was also reflected on protein level, where under the IL4 + TLR ligand stimulated conditions high IL4i1 levels were detectable inside the cells 8 h after stimulation and in the supernatants after 24 h (Figure 41B). Next, I tested the time frame of IL4i1 induction for the IL4 + LPS stimulation. As observed for IL4 + TNF treatment IL4 + LPS led to a timely restricted induction of IL4i1 on mRNA and protein level (Figure 41C,D). Comparable to the IL4 + TNF treatment, the highest IL4i1 mRNA and intracellular protein level was detected 6 h after IL4 + LPS stimulation. Subsequently, reflecting its secretion, IL4i1 accumulated in the supernatant, while intracellular IL4i1 constantly declined (Figure 41D). Overall, the dynamics of IL4i1 induction by IL4 + LPS seemed quite similar to the IL4 + TNF stimulation: IL4i1 was synthesized intracellularly with the levels peaking at 6 h and afterwards, within 24 h, almost completely secreted into the supernatant. In addition, to test if IL4i1 was also induced in BMDMs upon infection, I collaborated with Marcel Hahn from Prof. Ivan Dikic's group at the Goethe University Frankfurt. We were able to confirm that *Salmonella enterica* infection induced IL4i1 expression BMDMs, which was strongly enhanced by addition of IL4 directly after infection (Supplementary Figure 11).

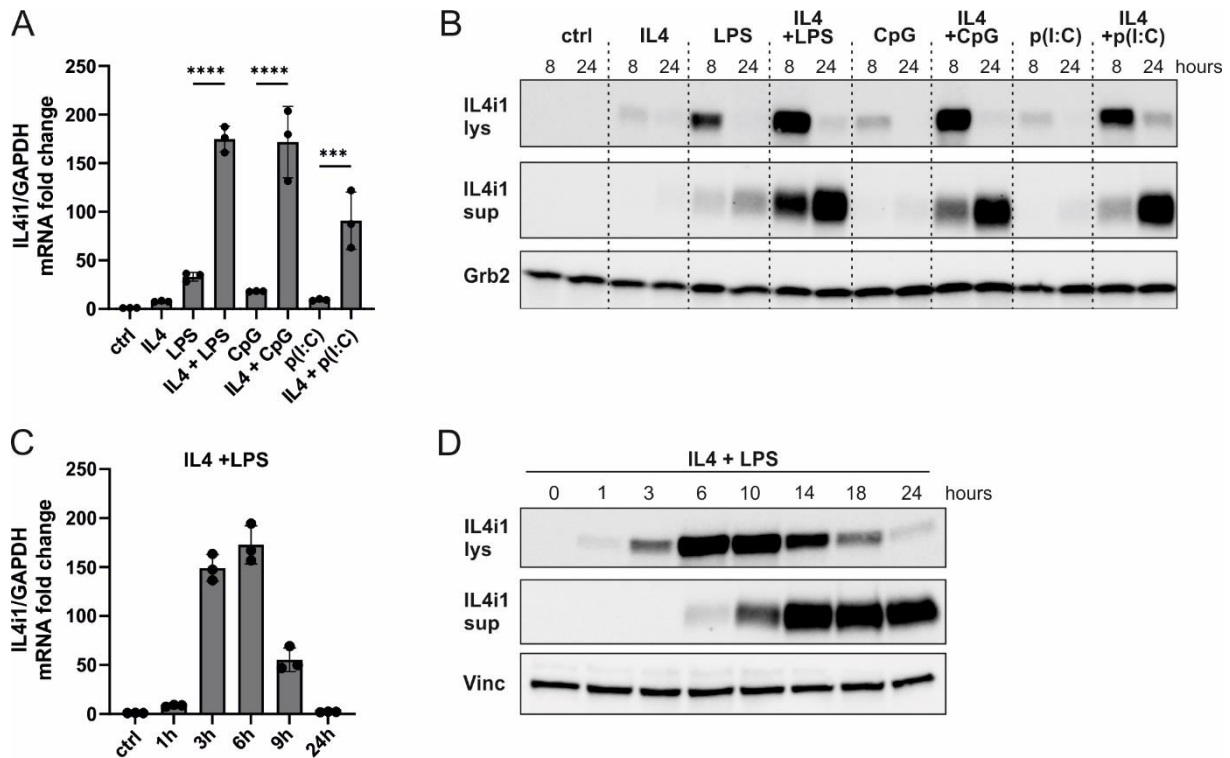


Figure 41 IL4 enhances the induction of IL4i1 by TLR ligands

(A) Quantification of IL4i1 mRNA levels by qRT-PCT upon 6 h treatments of BMDMs with IL4 (10 ng/ml), LPS (10 ng/ml), CpG (1 μ M), poly(I:C) (10 μ g/ml) or combinations of IL4 and the TLR agonists. IL4i1 levels were normalized to GAPDH and the fold change compared to the unstimulated control (ctrl) was determined. n=3 biological replicates; error bars indicate standard deviation; One-way ANOVA with Tukey's multiple comparisons test was used for statistics: ***: p<0.001; ****: p<0.0001 (B) Immunoblotting of BMDM cell lysates (lys) and their respective supernatants (sup) 8 h and 24 h after treatment with the indicated TLR agonists in presence or absence of IL4 (same concentrations as in (A)). Grb2 was used as loading control. (C) Time course of IL4i1 induction in BMDMs upon IL4 + LPS treatment (both 10 ng/ml) on mRNA level compared to the unstimulated ctrl. n=3 biological replicates; error bars indicate standard deviation. (D) Immunoblotting of a time course of IL4i1 induction in cell lysates and secretion to the respective supernatants in BMDMs stimulated for the indicated time with IL4 + LPS (both 10 ng/ml). Vinculin was used as loading control.

4.3.4.3. High increase of IL4i1 secretion can be detected by MS-based secretome analysis

As detailed above, I found that LPS alone, but especially combination with IL4 led to the generation and subsequent secretion of IL4i1. However, the extent of the induction compared to other secreted proteins was unclear. Thus, MS-based secretome analysis was performed in the supernatants of BMDMs in collaboration with Jonathan Swietlik from the Mann department at the MPIB. BMDMs were stimulated for 24 h with IL4, LPS, the combination of IL4 and LPS or left unstimulated and secreted proteins were analyzed by MS (Figure 42A). While IL4 treatment alone did not robustly induce protein secretion compared to unstimulated BMDMs (FDR cutoff 0.05), LPS and IL4 + LPS treatment provoked substantial protein secretion (Figure 42B). Along with several cytokines and chemokines such as TNF, IL6,

CXCL2 and CXCL10, a strong induction of IL4i1 was visible upon LPS treatment. Moreover, the secretome analysis confirmed an additional increase in secreted IL4i1 once BMDMs were additionally treated with IL4. While LPS stimulation induced a 500-fold increase in IL4i1 secretion, IL4 + LPS treatment provoked more than 2000-fold increased IL4i1 secretion as compared to the unstimulated control. The proteins showing the highest increase in secretion upon IL4 + LPS treatment (labeled in the volcano plots) were further analyzed by hierarchical clustering (Figure 42C). Notably, IL4i1 was the only protein showing higher secretion upon IL4 + LPS treatment as compared to LPS treatment, whereas the secretion of almost all other proteins decreased in presence of IL4. Taken together, the experiment revealed that the induction of IL4i1 secretion is very prominent, even when analyzed on a global level. In addition, the strong upregulation of IL4i1 upon IL4 + LPS treatment appears to be very specific for the enzyme.

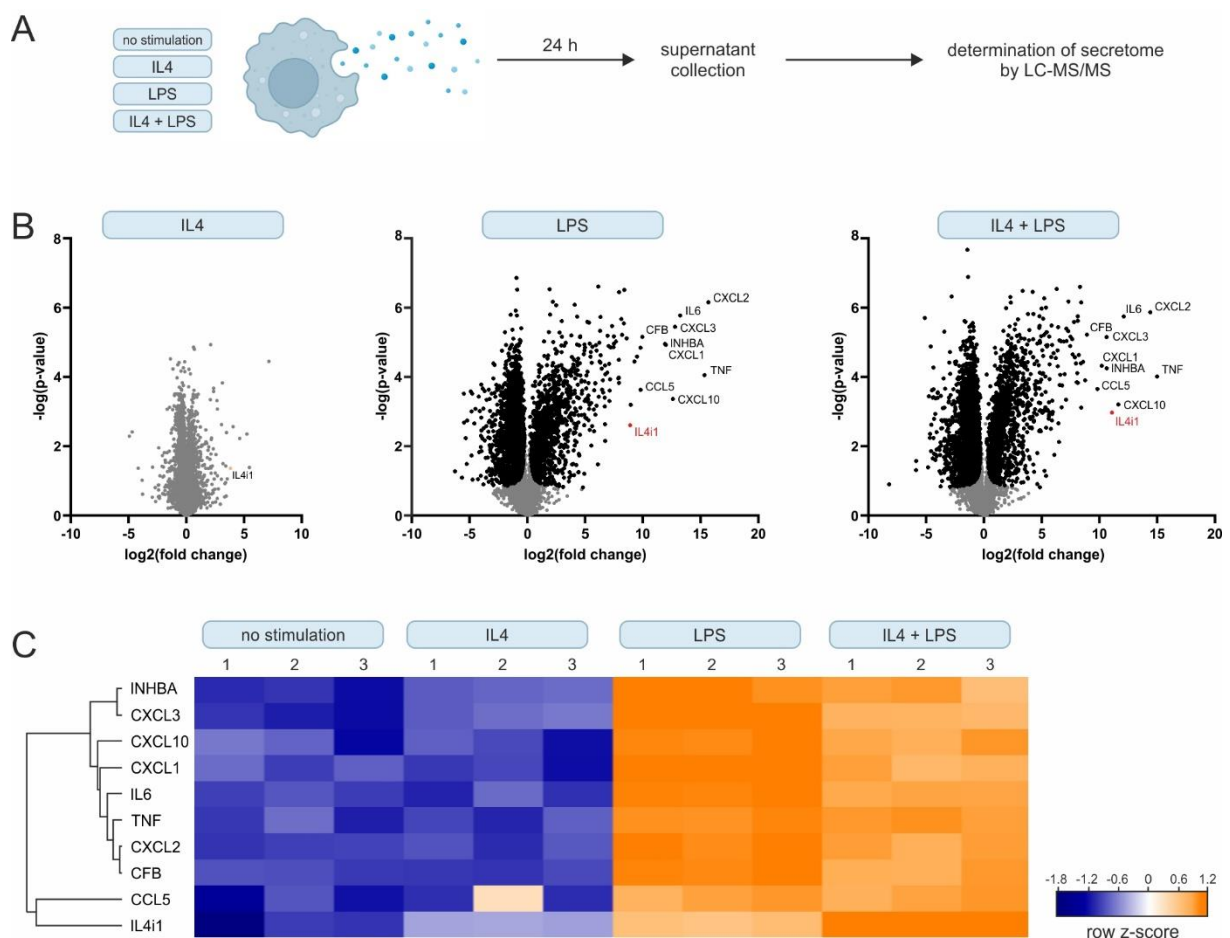


Figure 42 Secretome analysis of BMDMs treated with IL4 and LPS

(A) Overview of experimental setup: BMDMs were stimulated in triplicates with IL4 (10 ng/ml), LPS (10 ng/ml), IL4 + LPS (both 10 ng/ml) or with normal medium as unstimulated control. After 24 h the supernatant was collected and processed for analysis by LC-MS/MS (3.6.5). (B) Volcano plots showing the detected changes in the secretome after the indicated stimulations compared to the untreated control. Proteins marked in black/red have a FDR <0.05. The 10 proteins showing the highest increase in secretion upon IL4 + LPS treatment are labeled. (C) Hierarchical clustering and heat map of highly secreted proteins labelled in (B).

4.3.4.4. LPS-mediated IL4i1 induction does not depend on TNF signaling

It is well known that TNF is induced by TLR stimulation [2]. Accordingly, I detected a strong increase in TNF in the secretome analysis upon LPS stimulation (Figure 42B). Since TNF in combination with IL4 strongly upregulates IL4i1 (Figure 40), I investigated whether the LPS-dependent IL4i1 induction required TNF-signaling. This would suggest a model, where LPS would first lead to the release of TNF, which could activate TNF receptor (TNFR) signaling and subsequently together with the IL4-mediated effects induce IL4i1 (Figure 43A). To test this, I generated BMDMs from mice lacking the TNFR1 (encoded by *Tnfrsf1a*), which should interfere with the TNF-mediated effects in these cells as TNFR1 is supposed to be the main receptor for soluble TNF in BMDMs [331]. As expected, IL4i1 mRNA induction by TNF treatment was suppressed when using TNF alone and in combination with IL4 (Figure 43B). In contrast, loss of TNFR1 did not affect LPS-mediated IL4i1 induction. IL4i1 mRNA levels seemed even slightly, but not significantly, increased. On protein level, the effects mediated by TNF treatment were almost completely blocked in TNFR1-deficient BMDMs, whereas LPS potently upregulated intracellular production and secretion of IL4i1 in these cells (Figure 43C). The slight induction of IL4i1 in the IL4 + TNF treated TNFR1-deficient cells, which is still higher than in the IL4 treated BMDMs, may result from TNFR2 signaling. IL4i1 levels in the supernatant of TNFR1-deficient BMDMs induced by LPS and IL4 + LPS, seemed even increased when compared to WT BMDMs. Taken together, the results in BMDMs lacking TNFR1 suggest that TNF is not required for the LPS-mediated induction of IL4i1.

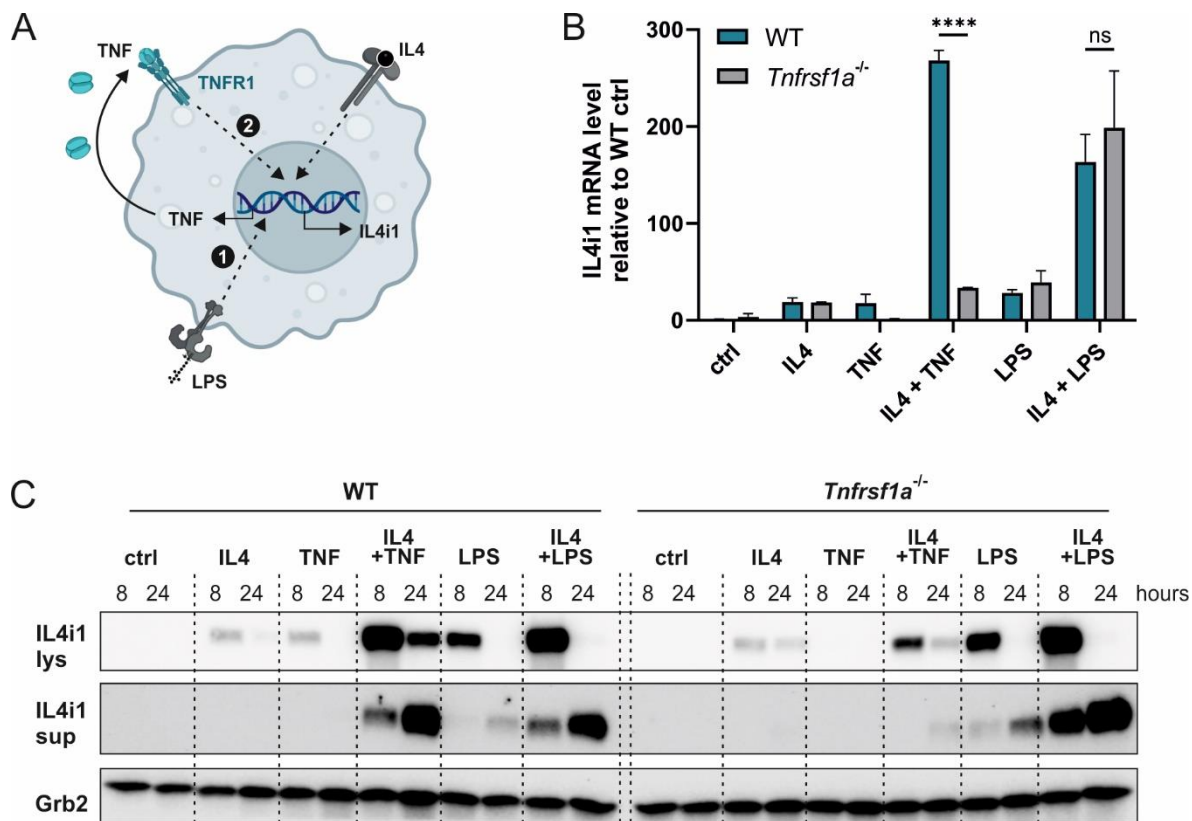


Figure 43 LPS-mediated IL4i1 induction does not depend on TNF signaling

(A) Model of a TNF-dependent IL4i1 induction mechanism mediated by LPS: In a first step (1) LPS mediates the expression and secretion of TNF, which in a second step (2), together with IL4, induces IL4i1 expression. (B) Quantification of IL4i1 mRNA levels by qRT-PCT upon 6 h stimulation of WT or *Tnfrsf1a*^{-/-} BMDMs with IL4 (10 ng/ml), TNF (10 ng/ml), LPS (10 ng/ml) and combinations of IL4 with TNF or LPS. IL4i1 levels were normalized to GAPDH and compared to the untreated WT control. n=3 biological replicates; error bars indicate standard deviation; 2-way ANOVA with Sidak's multiple comparisons test was used for statistics: ns: not significant; ****: p<0.0001 (C) Immunoblotting of WT or *Tnfrsf1a*^{-/-} BMDM lysates (lys) and their respective supernatants (sup) harvested 8 h and 24 h after the indicated stimulations (same concentrations as in (B)). Grb2 was used as loading control.

4.3.4.5. NF-κB is involved in TNF- and LPS-mediated IL4i1 induction

TNF was not required for LPS-mediated IL4i1 induction, suggesting that most likely both mediators induce IL4i1 expression by direct downstream signaling. Notably, both LPS and TNF are activators of the pro-inflammatory NF-κB signaling pathway, which has been linked to IL4i1 expression before [168,332]. The NF-κB protein family consists of two subfamilies, the 'NF-κB' and the 'Rel' subfamily. The two NF-κB proteins p50 (also NF-κB1) and p52 (also NF-κB1), derived from their p105 and p100 precursors respectively, have long C-terminal domains that control their activity: The C-terminus interacts with inhibitor of NF-κB (IκB) proteins to retain the NF-κB proteins in the cytosol [333]. Canonical NF-κB signaling pathway involves the ubiquitination and proteasomal degradation of IκB after its phosphorylation by IκB kinases upon receptor stimulation. Subsequently NF-κB can translocate to the nucleus and activate

transcription by forming heterodimers with cofactors such as the Rel proteins of the NF- κ B family [334].

Therefore, as a first way to test if NF- κ B is implicated in IL4i1 induction in my system, I used the proteasome inhibitor MG132, which prevents the degradation of I κ B and thus the activation of NF- κ B [335,336] (Figure 44A). Pre-treatment of BMDMs for 30 min with MG132 before inducing IL4i1 expression, clearly blocked the upregulation of IL4i1 on mRNA and on protein level (Figure 44B,C), suggesting that the proteasome and thus, possibly also NF- κ B signaling is involved in the induction of IL4i1 in the BMDMs. However, blocking the proteasome is a crude way to interfere with NF- κ B signaling, since the proteasome is required for a multitude of cellular processes. Therefore, I sought evidence for NF- κ B involvement using BMDMs from *Nfkb1*^{-/-} (encoding p105/p50) mice (Figure 44D), which should show reduced NF- κ B responses due to the interference with one part of the NF- κ B transcriptional machinery (p100/p52 and Rel proteins are still present). Indeed, I could observe a clear and significant decrease of IL4i1 induction on mRNA level upon IL4 + TNF, LPS and IL4 + LPS treatment (Figure 44E). In line with the results on transcriptional level, IL4i1 protein levels were clearly decreased (Figure 44F). However, the loss of p50 did not completely interfere with IL4i1 induction, indicating that other factors, such as p52 and the Rel proteins may be required, which will need further investigation. Nevertheless, the almost complete abrogation of IL4i1 upregulation upon proteasome inhibition alongside with the clear reduction by loss of NF- κ B1 suggests that NF- κ B signaling is involved the TNF- and LPS-mediated upregulation of IL4i1 in BMDMs.

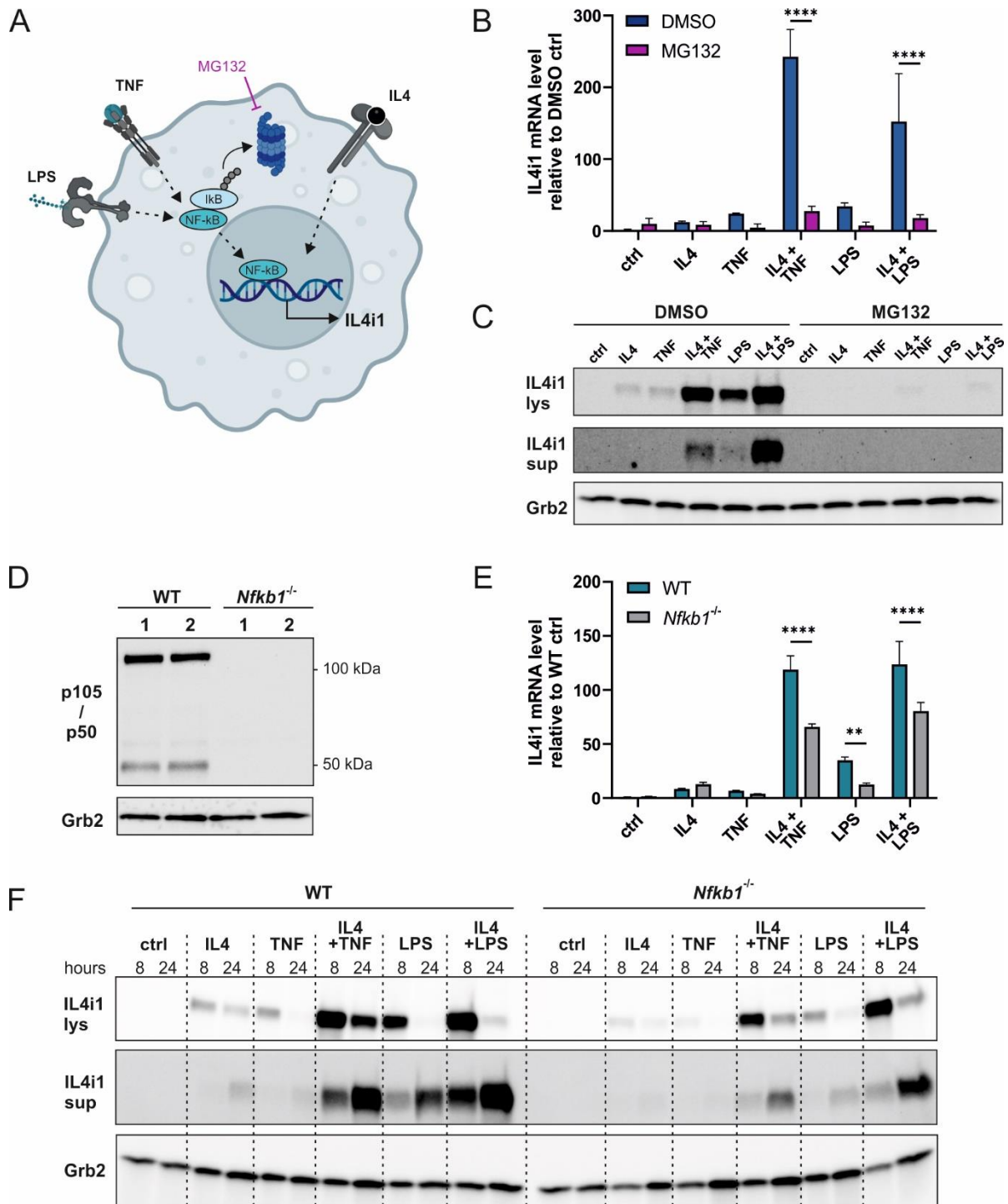


Figure 44 NF- κ B is involved in TNF- and LPS-mediated IL4i1 induction

(A) Scheme of hypothesized involvement of NF- κ B signaling in TNF- and LPS-mediated IL4i1 induction. (B) Quantification of IL4i1 mRNA levels in BMDMs pre-treated for 30 min with 2 μ M MG132 or the respective amount of DMSO. BMDMs were stimulated with IL4 (10 ng/ml), TNF (10 ng/ml), LPS (10 ng/ml) and combinations of IL4 with TNF or LPS. IL4i1 levels were normalized to GAPDH and compared to the DMSO control. (C) Immunoblotting of BMDM lysates (lys) and their respective supernatants (sup) after 30 min pre-treatment with DMSO or MG132 and subsequent 6 h stimulation with IL4, TNF, LPS or the indicated combinations (same concentrations as in (B)). Grb2 was used as loading control. (D) Validation of the loss of p105/p50 in BMDMs from *Nfkb1*^{-/-} mice by immunoblotting. (E) Quantification of IL4i1 mRNA levels by qRT-PCT upon 6 h stimulation of WT or *Nfkb1*^{-/-} BMDMs with IL4 (10 ng/ml), TNF (10 ng/ml), LPS (10 ng/ml) and combinations of IL4 with TNF or LPS. IL4i1 levels were

normalized to GAPDH and compared to the untreated WT control. (F) Immunoblotting of WT or *Nfkb1*^{-/-} BMDM lysates (lys) and their respective supernatants (sup) harvested 8 h and 24 h after the indicated stimulations (same concentrations as in (E)). Grb2 was used as loading control. (B,E) n=3 biological replicates; error bars indicate standard deviation; 2-way ANOVA with Sidak's multiple comparisons test was used for statistics: **: p<0.01; ****: p<0.0001.

4.3.4.6. IL4-mediated IL4i1 induction depends on STAT6

I observed the most effective IL4i1 induction when BMDMs were stimulated with IL4 in addition the pro-inflammatory factors TNF and LPS, which appear to induce IL4i1 expression via NF- κ B signaling (Figure 44). In order to further disentangle the mechanisms of IL4i1 induction in BMDMs, I next focused on the IL4-mediated aspect of IL4i1 regulation. Binding of IL4 to the IL4 receptor α (IL4R α) chain, leads to the recruitment of either the common γ -chain/IL2R γ (IL4R type I) or the IL13R α 1 chain (IL4R type II), which further activates the JAK/STAT signaling pathway [337,338]. Activated JAK family kinases phosphorylate the receptor complexes and lead in case of IL4 signaling predominantly to the recruitment of STAT6, which subsequently is phosphorylated and dimerizes. STAT6 dimers can translocate to the nucleus to activate transcription [339]. Therefore, I investigated whether STAT6 was required for IL4-dependent expression of IL4i1 (Figure 45A) and generated BMDMs from *Stat6*^{-/-} mice. Strikingly, the loss of STAT6 completely interfered with IL4i1 mRNA induction under all stimulation conditions comprising IL4 (Figure 45B): While IL4 alone could not induce any increase in IL4i1 mRNA expression in STAT6-deficient BMDMs, the levels of IL4 + TNF induction resembled the levels of TNF stimulation without addition of IL4. The same effect on IL4i1 mRNA induction could be observed for IL4 + LPS stimulation. This was also reflected on protein level, where all IL4-dependent effects were lost (Figure 45C) in the *Stat6*^{-/-} BMDMs, confirming the requirement of the transcription factor.

In summary, my results show that although not detectable on protein level under steady-state conditions, IL4i1 is highly inducible in BMDMs. Interestingly, I found the most prominent upregulation of the enzyme upon co-stimulation with IL4 and pro-inflammatory, NF- κ B activating stimuli such as TNF or LPS. Notably, the effects of the stimuli do not only add but appear to synergize suggesting there may be an intersection of the downstream STAT6 and NF- κ B signaling pathways to induce IL4i1. This is clearly reflected by the IL4 + TNF stimulation, which induced a ~200-fold IL4i1 increase on mRNA level, while IL4 and TNF alone only caused increases of ~11 and ~15-fold, respectively (Figure 40A). Understanding the exact mechanism however, requires further investigation. Nevertheless, the specific induction of an immunosuppressive enzyme by a combination of stimuli that are supposed to be pro- and anti-inflammatory may be an important clue to better understand the functions of IL4i1.

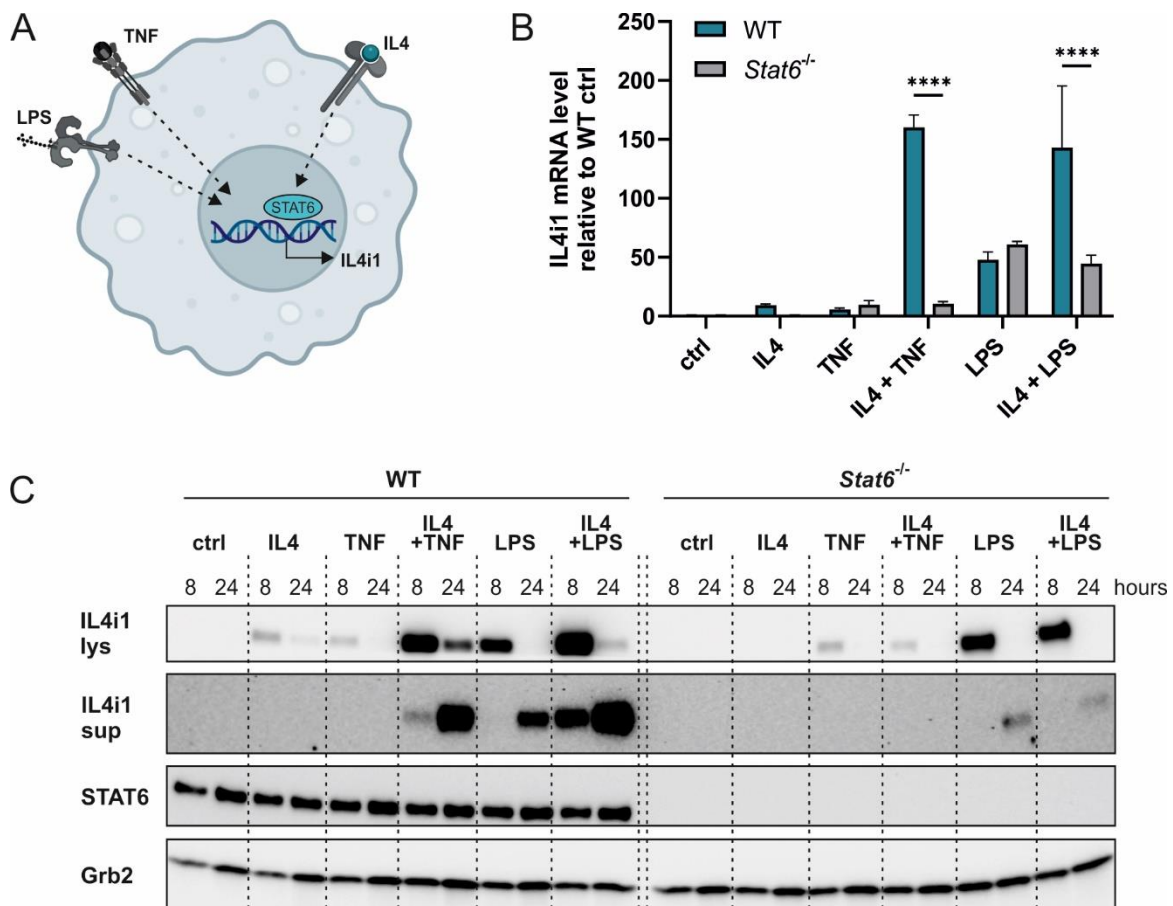


Figure 45 IL4-mediated IL4i1 induction depends on STAT6

(A) Hypothesized model of IL4-mediated IL4i1 induction via the transcription factor STAT6. (B) Quantification of IL4i1 mRNA levels by qRT-PCT upon 6 h stimulation of WT or Stat6^{-/-} BMDMs with IL4 (10 ng/ml), TNF (10 ng/ml), LPS (10 ng/ml) and combinations of IL4 with TNF or LPS. IL4i1 levels were normalized to GAPDH and compared to the untreated WT control. n=3 biological replicates; error bars indicate standard deviation; 2-way ANOVA with Sidak's multiple comparisons test was used for statistics. ****: p<0.0001 (C) Immunoblotting of WT or Stat6^{-/-} BMDM lysates (lys) and their respective supernatants (sup) harvested 8 h and 24 h after the indicated stimulations (same concentrations as in (B)). Grb2 was used as loading control.

4.3.5. IL4i1 induction in GM-DC and CD103 DC cultures

Since IL4i1 was highly inducible in BMDMs, I tested whether IL4i1 was inducible by the same stimuli in GM-DCs and CD103 DCs that already showed a baseline expression of IL4i1 (Figure 37). IL4i1 protein expression could be further upregulated by stimulations with IL4, TNF and LPS or combinations of IL4 with TNF or LPS (Figure 46). However, the effects were less clear than in the BMDMs. Nevertheless, cells differentiated with GM-CSF secreted more IL4i1 when stimulated for 24 h with IL4 or TNF and again, the combination of IL4 + TNF provoked the strongest increase of IL4i1 in the supernatants (Figure 46A). LPS and IL4 + LPS treatment also increased IL4i1 secretion, but the interpretation if IL4 could increase the effect of LPS remains difficult. For a better understanding, very sensitive and quantitative methods such as ELISAs would be required, which however are not available to this date (tested ELISAs were not specific; data not shown). In the CD103 DCs, treatments with TNF and LPS efficiently

induced IL4i1 expression and secretion (Figure 46B). Yet, in contrast to BMDMs and GM-DCs, higher levels of intracellular IL4i1 were detectable 24 h after stimulation, which may indicate a different dynamic of IL4i1 secretion in these DCs. IL4i1 induction was further enhanced by combining TNF or LPS with IL4, however the effect was less pronounced as observed in BMDMs, suggesting that IL4 may have a subsidiary role in regulating IL4i1 induction in the CD103 DCs while the inflammatory stimuli may be more important. This could be explained by the finding that IL4i1 expression was restricted to mature CCR7⁺ DCs (Figure 39B), which were found to largely increase upon stimulation with the TLR ligand CpG [294]. As the experiments were performed in the total cells obtained from the differentiations, it remains to be elucidated how distinct sub-populations contribute to the IL4i1 expression and secretion.

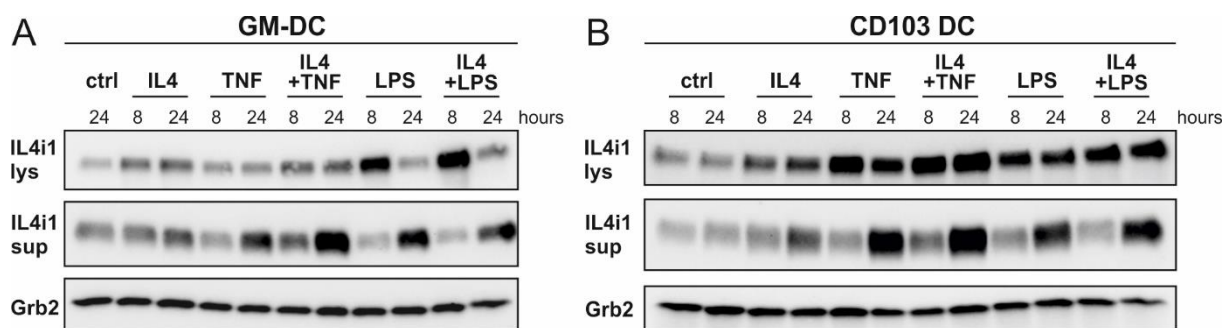


Figure 46 IL4i1 induction in GM-DC and CD103 DC cultures

(A) Immunoblotting of IL4i1 in lysates (lys) of GM-DCs (total cells, not sorted for 'DC' and 'macrophage' populations) and their respective supernatants (sup) 8 h and 24 h after treatment with IL4 (10 ng/ml), TNF (10 ng/ml), LPS (10 ng/ml) or combinations of IL4 and TNF/LPS used at the same concentrations. Grb2 was used as loading control. (B) Immunoblotting of IL4i1 as described in (A) using lysates and supernatants of CD103 DCs.

Overall, my results indicate that IL4i1 is expressed by different bone-marrow derived myeloid cells: While DCs differentiated with GM-CSF and GM-CSF + FLT3L (CD103 DCs) contain subpopulations expressing IL4i1 under unstimulated steady-state conditions, IL4i1 is highly inducible in BMDMs. IL4i1 expression in BMDMs is mediated by IL4 via STAT6 but also by NF- κ B activating factors including TNF, LPS and further TLR agonists. Importantly, the experiments suggest that that concurrent stimulation of both axes of IL4i1-inducing signals synergize to potently activate the synthesis and subsequent secretion of IL4i1. The identification of IL4i1-producing myeloid cells obtained from bone marrow will allow us to better investigate IL4i1-dependent effects in future *in vitro* co-culture assays between those myeloid cells, T cells and tumor cells to dissect the complex interplay of processes in the TME.

5. Discussion and perspectives

The secreted LAAO IL4i1 belongs to a group of amino acid-metabolizing enzymes that are inducible in immune cells and implicated in the regulation of immune responses [16]. However, in contrast to Arg1/2, iNOS or the IDO1/2 enzymes which have been subject of research for many years, our current understanding of the mechanisms by which IL4i1 controls downstream cellular effects is limited. Recent studies associated IL4i1 expression in cancer with tumor progression and poor survival [19,173,198,340]. In this regard, IL4i1 may act, 1) by the suppression of immune responses towards tumors [19,172,173,188] and 2) by directly affecting cancer cell biology, which has not been extensively studied before. Therefore, an overall goal of my thesis was to investigate underlying mechanisms by which IL4i1-mediated amino acid metabolism controls the biology of cells in its microenvironment. I focused on two main questions concerning 1) the potential toxicity of IL4i1-dependent amino acid metabolism, as IL4i1 is closely related to LAAOs occurring in snake venoms (Figure 7) and catalyzes a reaction that generates H₂O₂ [17,146], and 2) the role of the aromatic α -keto acids generated by IL4i1 from Phe, Tyr and Trp. Additionally, I investigated IL4i1 expression in bone-marrow derived myeloid cells, which will be useful for the generation of advanced *in vitro* co-culture models for the examination of IL4i1 biology.

5.1. Divergent functions of IL4i1 and snake venom LAAOs

LAAOs from snake venoms represent the most extensively studied group of LAAOs [148]. As several snake venom LAAOs were found to mediate cytotoxicity by H₂O₂ production [153-156], I hypothesized that, depending on the relative enzymatic activity, IL4i1 may mediate toxic effects. However, although studies have previously determined the enzymology of snake venom LAAOs [305-307] and mammalian IL4i1 [17,146], no side-by-side comparison of these closely related enzymes had been described. Generating a recombinant cobra (*N. naja*) venom LAAO and mammalian IL4i1, I was able to compare the enzymatic activity of the different enzymes towards the proteinogenic amino acids and determine their cytotoxicity. Overall, consistent with previous studies, murine and human IL4i1 showed the highest activity towards Phe followed by the other aromatic amino acids Tyr and Trp [17,19,146]. In addition, I also detected low activity towards methionine. *N. naja* LAAO potentially metabolized Phe, Tyr, Trp, Met and Leu, agreeing with studies of other snake venom LAAOs showing preference for aromatic and neutral amino acid substrates [305-307]. However, compared to the mammalian IL4i1 enzymes, *N. naja* LAAO metabolized its substrates faster, suggesting that the venom LAAO converts amino acids to rapidly generate increased H₂O₂ levels. This was also reflected when testing the cytotoxicity of the enzymes: *N. naja* LAAO induced cell death of HeLa cells in an H₂O₂-dependent fashion – inactivation of the enzymatic activity by point mutations or H₂O₂ decomposition by catalase interfered with the induction of cell death. By contrast, IL4i1 did not show toxicity in HeLa cells at any tested concentration (up to 5 μ g/ml) and only in a

highly susceptible leukemia cell line, IL4i1 mediated cell death, however at approximately 30-fold higher concentrations than *N. naja* LAAO. Overall, it seems that during the evolution of LAAOs, mammalian IL4i1 evolved to be a less potent member of the LAAO enzyme family. Therefore, I propose that mediating cytotoxicity is not a main function of IL4i1. In snake venoms on the other hand, LAAOs likely contribute to the poisonous effects in concert with other toxins such as the neurotoxic 3FTxs or phospholipases, which are considered to represent the most lethal venom components [150]. As the venoms evolved to maximize lethality to the snake's prey [341], the common presence of LAAOs in most snake venoms underlines their contribution to venom function. However, the amount of LAAOs in snake venoms can largely vary. While the protein may have a minor function in venoms where the LAAO makes up only 1 % of the total venom proteome in cobras (and most elapid snakes) [341], the cytotoxic effect of LAAOs may have a more pronounced function in the venom of viperid snakes such as the Malayan pit viper (*Calloselasma rhodostoma*) where the LAAO was found to make up 30 % of the total venom proteome [151].

Contradicting my initial supposition, instead of inducing cell death IL4i1 protected cells from the oxidative cell death ferroptosis by the generation of anti-oxidative amino acid metabolites which is discussed in detail in section 5.3. Importantly, ferroptosis suppression occurred at concentrations that did not have toxic effects, suggesting that instead of mediating cytotoxicity the protection of cells from oxidative cell death may be a relevant physiological function of IL4i1. However, a limitation so far is the lack of good commercially available detection reagents such as specific ELISAs to quantify IL4i1 levels in serum, tissues or the TME. We found that a commercially available ELISA that has been used before to quantify IL4i1 in mouse serum [19] is unspecific as it detected the same 'IL4i1' induction in stimulated BMDMs from WT and IL4i1-deficient mice (data not shown). Since IL4i1 expression is found in myeloid cells in the TME [55,171-173,175,179] we speculate that local IL4i1 levels, especially in low-perfused tissue environments, e.g. in solid tumors, can reach the ng/ml range in which IL4i1 protected cells from ferroptosis. Although it is more likely that IL4i1 occurs in a concentration that generates sub-lethal amounts of H₂O₂ and mediates cellular protection, I cannot exclude that under certain conditions IL4i1 could reach potentially toxic concentrations. Nevertheless, the fact that mammalian IL4i1 shows a much lower toxicity than the snake venom LAAO and even protects cells from oxidative cell death, suggests that the function of mammalian IL4i1 diverges from a role as a toxin.

5.2. Activation of AhR signaling by the aromatic α -keto acids I3P and 4HPP

One aim of my thesis was the characterization of the downstream effects mediated by IL4i1-generated α -keto acids. Since IL4i1 exhibits the highest substrate specificity towards Phe [17,146], studies investigating mechanistic basics of IL4i1-mediated immune cell regulation

initially only focused on the properties of the Phe metabolite PP [17,172,184,186]. However, none of these studies reported substantial impact of PP. Therefore, I decided to more broadly investigate downstream effects of aromatic amino acid metabolites generated by IL4i1. Transcriptome analysis of Thp1 cells exposed to PP but also the Tyr and Trp metabolites, 4HPP and I3P respectively, revealed that mainly 4HPP and I3P may contribute to IL4i1-mediated modulation of cell biology (Figure 23). My results suggest that especially I3P and to a lesser extent also 4HPP are able to activate AhR and Nrf2 signaling (the latter will be addressed in the next section). The link between IL4i1-mediated amino acid metabolism and AhR activation by I3P was independently reported by two other groups in 2020 [19,196]. However, Sadik et al. [19] did not detect AhR activation by 4HPP in glioblastoma cells, suggesting that it is possible that only high concentrations of 4HPP (200 μ M) can activate the receptor or cell-specific downstream metabolism is required to generate a weak AhR agonist from 4HPP. I3P generated from Trp appears to be the main AhR agonist generated by IL4i1. Considering the involvement of AhR in several aspects of immunoregulation (1.2.4.3) it is likely that AhR activation by I3P contributes to immunoregulatory effects mediated by IL4i1 including decreased CD8⁺ T cell responses [188] or increased differentiation of Tregs [186], effects that have previously been associated with AhR activation [100,115,117,118]. Thus, Trp can not only be metabolized via the IDO/TDO axis to form the AhR agonists Kyn and KynA [100-102], but also via IL4i1 generating I3P, which can act as endogenous AhR agonist. As IDO1 and IL4i1 are often found to be co-expressed in cancers/tumor-associated myeloid cells [55,179,342] and IDO1 has a higher affinity towards Trp than IL4i1, Castellano and colleagues [342] questioned the relevance of IL4i1-mediated Trp metabolism *in vivo*. However, since IDO1 is located inside cells and IL4i1 is a secreted protein [17] the enzymes may simultaneously drive the conversion of Trp into AhR agonists intracellularly and in the extracellular space. Moreover, as IL4i1 may act in parallel to IDO1, IL4i1 expression may be a relevant factor to consider regarding the use and efficacy of IDO1 inhibitors in the treatment of cancer, which have not been successful in phase III clinical trials [138,143]: It is possible that IL4i1-dependent Trp metabolism can compensate for the loss of IDO1 activity and thereby interfere with the efficacy of IDO1 inhibitors.

5.3. Ferroptosis suppression by IL4i1-mediated amino acid metabolism

Ferroptosis is a form of oxidative cell death driven by uncontrolled membrane lipid peroxidation (1.3). As lipid peroxidation can spread in an iron-dependent Fenton-like reaction [204] (Figure 8), cells evolved several mechanisms that allow the permanent detoxification of PLOOH and PLOO[•] under steady-state conditions to interfere with their spread and prevent ferroptotic death (described in detail in 1.3.1). The results of my project identify IL4i1 as a previously unknown factor protecting cells from ferroptosis [18]. Using a catalytically inactive IL4i1 mutant, I found that IL4i1 suppresses ferroptosis via its enzymatic activity and does not require a

previously speculated receptor binding [184]. In contrast to other ferroptosis suppressors such as GPX4 [202,223], FSP1 [227,228] or GCH1 [232], which confer cell-intrinsic protection, IL4i1 operates in a cell-extrinsic manner via the generation of a ferroptosis-suppressive environment by metabolizing amino acids. Thereby, IL4i1-expressing cells, such as tumor-associated myeloid cells [19,55,171-173,175,179], may promote ferroptosis resistance of cells in their environment, which will be further discussed in section 5.4.

As stated above, the enzymatic activity of IL4i1 is crucial for its protective effect. Mechanistically, the α -keto acids I3P and 4HPP generated by IL4i1 from Trp and Tyr respectively, but not PP derived from Phe can suppress ferroptotic cell death. Compared to I3P however, 4HPP is a weaker anti-ferroptotic metabolite: while 4HPP partly suppressed ferroptotic death at $\sim 100 \mu\text{M}$, I3P protected cells at $\sim 50 \mu\text{M}$. Since serum concentrations of Trp and Tyr are $\sim 70 \mu\text{M}$ and $\sim 90 \mu\text{M}$, respectively [315], protective concentrations of their catabolites seem to lie within the physiological range, especially as both protective metabolites can act simultaneously when IL4i1 metabolizes Trp and Tyr in the extracellular space. I3P levels that reach the ferroptosis-suppressive concentration have previously been detected *in vivo*: I3P, in this study derived from Trp metabolism by *Clostridium sporogenes* in the gut, was reported to reach serum concentrations of $80 \mu\text{M}$ in mice [343]. On a mechanistic level, I3P and 4HPP seem to suppress ferroptosis by two distinct mechanisms working in concert to confer cellular protection, which are 1) free radical scavenging and 2) the activation of anti-oxidative gene expression.

Several pathways protecting cells from ferroptosis involve the detoxification of PLOO• radicals. The ferroptosis-suppressive enzymes FSP1 and DHODH for example confer their protective effects by maintaining the generation of the lipid radical scavenging molecule CoQH₂ [227,228,230], while GCH1, a further enzyme mediating ferroptosis resistance, is the rate limiting enzyme for the *de novo* synthesis of the antioxidant BH₄ [232]. Thus, as I3P and slightly less efficiently 4HPP could scavenge the free radical DPPH, which has previously been used to study the antioxidant function of the synthetic ferroptosis inhibitor Fer-1 [199], the IL4i1-produced metabolites appear to mediate parts of their protective effect by radical scavenging. A study from the early 1990s, previously reporting that I3P can scavenge free radicals *in vitro* [344], invites to speculate that keto-enol tautomerism of the α -keto acids generated by IL4i1 may be of relevance for their anti-ferroptotic effect. Politi and colleagues described an increase in the I3P scavenging activity when the molecule was present in its enol form [344]. Notably, one of the first cytokines to be discovered, namely macrophage migration inhibitory factor (MIF) [345,346], was found to exhibit phenylpyruvate tautomerase activity showing activity towards 4HPP [347]. Additionally, it was speculated that I3P may be a substrate of MIF [348], which has never been experimentally validated. It is therefore possible that MIF has an impact on the balance between the keto and enol tautomers of the α -keto acids generated by IL4i1 which

could influence their radical scavenging activity and thereby their anti-ferroptotic potential. So far, this is purely speculative but the investigation whether MIF influences IL4i1-dependent ferroptosis suppression would represent an interesting follow-up.

Besides radical scavenging, I found that I3P and 4HPP activate the expression of several genes associated with oxidative stress protection including GCLM and GSR, genes involved in the generation and maintenance of GSH [221], which is essential for PLOOH detoxification via the GPX4, the main ferroptosis-suppressive protein in most cell types [202,223] (1.3.1.1). In addition, I3P and 4HPP induced expression of members of the AKR1C family, which can metabolize toxic aldehydes derived from lipid peroxidation [309,310] and have been suggested to confer partial resistance to ferroptosis [224]. As cysteine availability is rate-limiting for GSH synthesis [214], I3P-dependent upregulation of the cystine transporter SLC7A11, which is also the target of the ferroptosis inducer Erastin [224], may act in concert with the GSH-generating enzymes. I confirmed that I3P induced an elevated GSH/GSSG ratio, suggesting that I3P increases the availability of GSH, “fueling” GPX4 for PLOOH detoxification and protecting cells from ferroptotic death. Many of the transcripts and proteins regulated by I3P and also partially by 4HPP are target genes of Nrf2, a master transcription factor conferring protection from redox stress [235] and associated with ferroptosis resistance [252,254,257,258]. Genetically ablating Nrf2 in HeLa cells, I could show that I3P-mediated ferroptosis resistance partly depends on the activation of the Nrf2 pathway, especially at lower concentrations where the scavenging activity is not sufficient for complete protection of the cells. By contrast, I3P-dependent AhR activation as observed by us and others [19,196] is not required for ferroptosis suppression by I3P. Therefore, I3P-mediated activation of Nrf2 seems to display a further mechanism by which I3P mediates downstream effects and protects cells from ferroptosis. In addition, as IL4i1 protects cells from ferroptosis at concentrations which are not toxic, sub-lethal levels of H₂O₂ may additionally contribute to Nrf2 activation and cellular adaptation to oxidative stress as previously described [349-351].

A further factor that may additionally contribute to the ferroptosis-suppressive effect of IL4i1, which I did not study in detail so far, is the involvement of amino acid deprivation. Recent studies from us and others suggest that amino acid deprivation can confer cellular protection from ferroptosis ([61,283], unpublished data from Russier et al.). However, while we found partial ferroptosis inhibition upon complete Trp depletion in HeLa cells [61], Conlon et al. [283] did not observe any protective effect by depletion of the IL4i1 substrates Trp or Phe, but a protective effect of Tyr starvation in one of the tested cell lines. It therefore seems that ferroptosis protection by amino acid starvation is cell type-dependent. Notably, ferroptosis resistance upon amino acid-starvation may involve the induction of proliferative arrest ([283], Russier et al. unpublished data). As I did not observe decreased cell proliferation in presence of IL4i1 (data not shown), I propose that amino acid depletion does not play a major role in

IL4i1-dependent ferroptosis suppression. However, this does not exclude that an IL4i1-mediated decrease in Phe, Trp and Tyr levels could additionally contribute to the protective effects of the α -keto acids. Taken together, the work of my thesis therefore suggests that IL4i1 can act as a cell-extrinsic factor mediating ferroptosis resistance by enzymatically generating a ferroptosis-suppressive microenvironment, which mainly involves the generation of the potent anti-ferroptotic metabolite I3P from Trp and the weaker 4HPP from Tyr. The metabolites appear to act by a dual mechanism consisting of the scavenging of free radicals and the induction of a compendium of oxidative stress protective genes, which are, at least to a certain degree, regulated by Nrf2. Additionally, concurrent amino acid depletion and the generation of sub-lethal amounts of H₂O₂ may potentially act as accessory mechanisms involved in the ferroptosis-suppressive modulation of the extracellular environment by IL4i1.

5.4. Implications of IL4i1-mediated amino acid metabolism in the TME

Mounting evidence suggests that IL4i1 is a detrimental prognostic factor in cancer [19,173,198,340], where the protein may mainly derive from tumor-associated myeloid cells [55,171-173,175,179]. However, we are just at the beginning of understanding the mechanisms by which IL4i1 mediates its pro-tumorigenic effects. Our current model suggests that IL4i1 acts by modulating the composition of the TME, which involves two simultaneously occurring processes that can affect the biology of cells in the environment: IL4i1 mediates 1) the depletion of aromatic amino acids and 2) produces modulatory α -keto acids and H₂O₂ in the TME (Figure 47).

An important factor involved in IL4i1-associated tumor progression seems to be the interference with tumor immunosurveillance as IL4i1 was linked to decreased CD8⁺ T cell responses and increased tumor infiltration with regulatory immune cells in animal models and patients' samples [19,172,173,188]. Sensing of amino acid depletion via the kinase hubs GCN2 (activation) and mTORC1 (deactivation) is suggested to mediate immunoregulatory effects including reduced CD8⁺ T cell proliferation and modulation of CD4⁺ T cell differentiation towards regulatory T cells [72,73,85] (1.2.3). However, the role of GCN2 in the inhibition of T cell proliferation upon tryptophan depletion proposed by Munn and colleagues [72] is controversial as other studies observed proliferative arrest independent of GCN2 [85,86]. Future studies will be required to investigate if IL4i1-mediated amino acid metabolism activates GCN2 signaling and whether this is involved in the immunoregulatory activity of the enzyme. Cousin et al. [186] observed that IL4i1 provoked decreased mTOR signaling and proposed that this may contribute to IL4i1-dependent Treg differentiation observed *in vitro*. Moreover, since the activation of AhR signaling is also known to promote differentiation of regulatory T cells [100,117,118] I3P-mediated AhR activation may additionally support the increased emergence of regulatory T cells that is associated with IL4i1 expression in cancer [19,173].

Notably, in the context of IDO1-dependent T cell regulation, Fallarino et al. [73] reported a synergistic effect of Trp limitation and the generation of kynurenine metabolites, which could likewise occur upon IL4i1-mediated amino acid depletion and α -keto acid generation. Furthermore, an early study on IL4i1 by Boulland et al. [17] suggests that H₂O₂ production by IL4i1 has an immunoregulatory function by limiting the proliferative capacity of T cells. In summary, IL4i1 may therefore facilitate tumor immune escape by creating an immunosuppressive milieu which involves amino acid depletion, the activation of AhR signaling through I3P (and possibly 4HPP), and the generation of H₂O₂. So far, we do not know if IL4i1-dependent ferroptosis suppression may additionally contribute to immunosuppressive effects, which we aim to investigate in future experiments.

Besides suppression of cancer immunosurveillance, mounting evidence suggests that IL4i1-dependent modulation of the TME can directly affect cancer cell biology. A potentially important mechanism contributing to malignant progression of cancer cells is the I3P-dependent activation of AhR signaling, which enhanced glioblastoma cell migration as reported by Sadik et al. [19]. In line with this observation, a further study suggests that IL4i1 promotes ovarian cancer cell migration and increases the invasiveness of the tumor cells [198]. Additionally, the results of my PhD project, showing that the IL4i1 metabolites I3P and to some degree also 4HPP can act as free radical scavengers and activate Nrf2-dependent anti-oxidative gene expression, give clues about further mechanisms by which IL4i1 could promote tumor progression. Cancer cells are highly dependent on mechanisms controlling increased intracellular ROS levels accruing from their high bioenergetic activity [269,270]. Therefore, enrichment of I3P and 4HPP in the TME may support the survival and persistence of tumor cells by conferring resistance to redox stress and ferroptosis. The generation of a ferroptosis suppressive milieu could for example promote the emergence of tumor cells in an unfavorable mesenchymal cell state, which strongly depend on GPX4 [277] and show increased susceptibility to ferroptosis [277,352]. Accordingly, IL4i1 may help to protect cells undergoing epithelial-mesenchymal transition (EMT), a process considered to promote cancer invasiveness and metastatic activity [353]. Additionally, as ferroptosis may contribute to IFN γ -dependent cancer immune control by CD8⁺ T cells [279,282], IL4i1 could also indirectly contribute to cancer immune escape by suppressing ferroptosis and thereby promoting cancer cell resistance. IL4i1 expression in tumors may also have implications for cancer therapy as several studies suggest that induction of ferroptosis is at least partially involved in anti-tumor effects of conventional therapies including irradiation, chemotherapy and immune checkpoint inhibition [276,279,280,354,355]. By conferring ferroptosis-resistance, IL4i1 expression may increase the ratio of cells escaping the treatment and thereby interfere with therapy efficacy.

Taken together, the detrimental impact of IL4i1 in the context of cancer seems to involve an IL4i1-mediated modulation of the TME, which does not only promote immunosuppression, but

may also affect cancer cell biology to promote tumor progression. Although further research will be required to dissect the contribution and extent of the different pro-tumorigenic mechanisms supported by IL4i1, our current understanding of IL4i1-mediated biology suggests that the development of IL4i1 inhibitors could be useful in cancer therapy. IL4i1 inhibition may help to restore tumor immune control, interfere with cancer cell invasiveness and increase vulnerability to ferroptosis. Considering the observations that induction of ferroptosis partially contributes to the effect of several conventional cancer therapies, simultaneous targeting of IL4i1 could potentially be used to increase therapy efficacy.

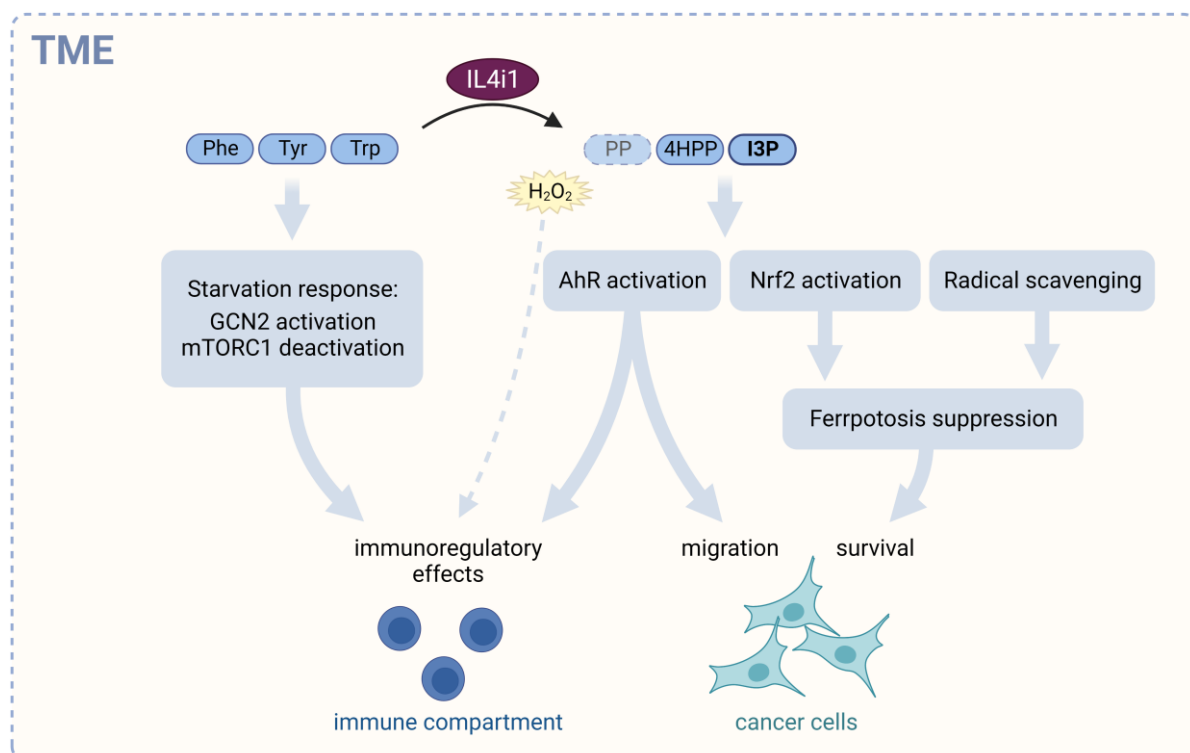


Figure 47 Model of IL4i1-dependent amino acid metabolism in the TME

In the TME IL4i1 acts via amino acid depletion and simultaneous product generation. Amino acid limitation suppresses tumor immune control by GCN2 activation and mTOR deactivation, which is associated with immunoregulatory effects such as reduced T cell activation and increased regulatory T cell differentiation. This may be complemented by the IL4i1-dependent generation of H₂O₂, which was suggested to limit T cell proliferation, and the α -keto acid(s) I3P (and 4HPP) activating immunoregulatory AhR signaling. Generation of AhR agonists could also promote cancer progression by enhancing tumor cell migration. Additionally, I3P and 4HPP activate anti-oxidative gene expression and scavenge free radicals which together confer protection from ferroptosis and may thereby promote the survival of tumor cells.

5.5. IL4i1 expression in bone-marrow derived myeloid cells

5.5.1. IL4i1 is expressed in distinct subsets of BMDCs

A current limitation of the research investigating IL4i1 biology, is that studies focusing on mechanistic effects of IL4i1, including my previously presented work, are mostly based on recombinant IL4i1 or IL4i1 overexpression [17,18,184,186]. Therefore, it would be important

to confirm and further investigate mechanistic concepts in the interplay between myeloid cells endogenously expressing IL4i1, tumor cells and/or T cells. As our knowledge on IL4i1 producing myeloid cells is still limited (especially on protein level), I investigated the expression of IL4i1 in bone-marrow derived macrophages and DCs as these cells are easy to obtain and applicable for large scale co-culture experiments by providing a high yield. In BMDCs, IL4i1 expression was detectable in cells obtained from differentiation with GM-CSF or a combination of GM-CSF and FLT3L, which leads to the differentiation of CD103⁺ DCs [294]. In line with a previous study [328], differentiation with GM-CSF alone resulted in a mixture of CD11c⁺ 'macrophages' and 'DCs'. However, IL4i1 expression was completely restricted to the 'DC' population and absent in the 'macrophage' population, which is consistent with the observation that BMDMs do not express IL4i1 under unstimulated conditions. DCs obtained from the GM-CSF culture are characterized by IRF4 and Sirp α expression [328] and therefore mostly likely resemble cDC2 cells, while the CD103 DCs appear to resemble a cDC1-subtype as they are Batf3 dependent and express Clec9a [294]. Therefore, IL4i1 expression does not seem to be restricted to one of the cDC1 or cDC2 subtypes, which agrees with transcriptomic studies of the myeloid compartment: Most information about IL4i1 expression in dendritic cells derives from studies using single cell RNAseq (Table 1), where IL4i1 was found to be expressed in migratory DCs [180,181], migratory cDC2s [182] or so-called mregDCs [175], which were suggested to represent a regulatory DC 'state' rather than a 'subtype' [176] as they can emerge from cDC1 or cDC2 cells [175]. mregDCs (also termed DC3 [178] or LAMP3⁺ DCs [179]) are conserved across solid human cancers [356] and limit anti-tumor immunity [175]. Therefore, mregDCs may represent an important source for IL4i1 in the TME. In general, IL4i1 expression in DCs correlates with CCR7 expression (Table 1), which is considered to be associated with DC maturation and migration [329]. Accordingly, I found that IL4i1 expression (detected by Western Blot) in CD103 DCs was completely restricted to a CCR7⁺ subpopulation that also showed high MHC-II expression. However, intracellular IL4i1 staining for flow cytometry would be required to determine if all cells of this population are IL4i1⁺ or if the expression is limited to a further subpopulation. However, due to the lack of good commercial IL4i1 antibodies, I could not yet address this question. A further observation was the co-expression of IDO1 in the IL4i1-expressing population, which has previously been found in single cell data sets of tumor-associated DCs and macrophages [55,179]. Additionally, IDO1 expression in CCR7⁺ cDC1 cells has recently been reported in a study from Gargaro et al. [53], which showed the propagation of IDO1 expression in dendritic cells mediated by Kyn-mediated AhR activation. On one hand, considering that besides Kyn, also I3P produced by IL4i1 can activate AhR signaling, it would be interesting to investigate if IL4i1-dependent AhR activation influences the expression of IDO1. On the other hand, Sadik et al. [19] proposed that also IL4i1 is regulated via AhR, which suggests that Kyn generation by IDO1 could likewise provoke an upregulation

of IL4i1. However, further investigation will be required to examine whether an AhR-dependent link between the expression of the enzymes exist. Nevertheless, independent of the regulation, co-expression of IL4i1 and IDO1 may promote simultaneous Trp metabolism within the cells and in the extracellular space, which seems to be important information when trying to therapeutically target one or the other enzyme as compensatory effects may occur (previously discussed in section 5.2).

5.5.2. Induction of IL4i1 in BMDMs

Whereas IL4i1 was not detectable on protein level in unstimulated BMDMs, the expression of the enzyme was highly inducible by specific signals I uncovered. Although IL4i1 was described to be expressed in IL4-driven M2-macrophages [164], IL4 alone had only a minor potential to induce IL4i1 in my experiments. In addition, TNF mediated a weak increase in IL4i1 expression and the most robust induction on RNA and protein level was visible when exposing the macrophages to TLR agonists such as LPS or CpG. This partly matches the findings of Marquet et al. [168] suggesting that in myeloid cells IL4i1 (indirectly measured via H₂O₂ generation) is mainly regulated by NF- κ B and STAT1 signaling. However, I could not detect any effect of IFN γ on IL4i1 expression. Notably, although IL4 alone only had minor effects on IL4i1 induction, the combination of IL4 with TNF or TLR agonists could induce more than 200-fold increases in the IL4i1 mRNA levels as compared to unstimulated BMDMs. So far, this seems to be the most potent stimulus inducing IL4i1 expression in macrophages [164,168]. It is important to point out that the combination of the stimuli did not only have an additive effect but clearly showed synergism, which I will discuss later in this section. MS-based analysis of the secretome revealed that the amount of secreted IL4i1 increased more than 2000-fold compared to the untreated control when BMDMs were concurrently stimulated with IL4 and LPS. My experiments also give insights into the dynamics of IL4i1 induction and secretion, which has not been studied in detail before. The mRNA and intracellular protein level of IL4i1 peak at ~6 h after induction. Subsequently, within 24 h the protein is almost completely secreted into the supernatant, which does not require another stimulus as e.g. IL1 β release [357]. Mechanistically, I found that the IL4-dependent part of the induction required signaling via STAT6, which is consistent with findings in B cells, where IL4 alone is potently inducing IL4i1 expression [168,169]. TNF and LPS on the other hand most likely mediate their effects via NF- κ B (Figure 48). *Nfkb1*^{-/-} BMDMs, which are partly deficient of NF- κ B signaling, exhibited significantly reduced TNF- and LPS-dependent IL4i1 induction and the proteasome inhibitor MG132, preventing NF- κ B activation by interfering with the degradation of I κ B [335,336], almost completely abrogated IL4i1 induction. This agrees with a previous observation by Marquet et al. [168] showing that LPS-mediated induction of IL4i1 (measured by enzymatic activity) could be reversed when cells expressed a dominant-negative I κ B mutant interfering with NF- κ B activation. In addition, it was suggested that RelA (p65) binds to the putative

regulatory region in *Il4i1* [332]. So far, we do not exactly understand how IL4 signaling via STAT6 and TNF- or LPS-activated NF-κB signaling intersect to synergistically enhance the induction of IL4i1 expression. Insights may come from a recent study by Czimmerer and colleagues [358], who reported that 24 h IL4-priming of BMDMs provoked STAT6-dependent epigenomic remodeling leading to enhanced NF-κB-p65 binding. Notably, the ChIP-seq data from this study suggests also enhanced p65 binding to the IL4i1 regulatory genomic region. However, our *Salmonella* infection experiment (Supplementary Figure 11) and further preliminary experiments (not shown) suggest that co-stimulation with IL4 is more effectively inducing IL4i1 expression than IL4-priming (12 - 24 h). Nevertheless, it is possible that STAT6-dependent epigenomic changes as reported after 24 h IL4-priming [358] can occur much earlier in the *Il4i1* regulatory region. Another possibility would be a direct interaction between STAT6 and NF-κB proteins, which has previously been speculated to synergistically activate gene expression [359].

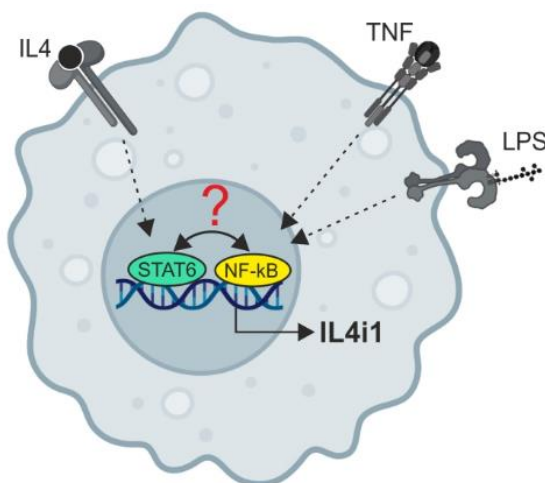


Figure 48 Model of synergistic IL4i1 induction by the combination of IL4 with TNF/LPS

IL4 and TNF/LPS can synergistically upregulate IL4i1 expression in BMDMs. IL4-dependent IL4i1 induction requires STAT6, while LPS and TNF signal via NF-κB. The exact mechanism by which STAT6 and NF-κB synergize to induce IL4i1 remains to be investigated.

5.6. Perspectives

The work of my PhD projects gives new insights into the mechanisms by which IL4i1-dependent changes in the extracellular milieu can affect the biology of cells in its environment. Instead of conferring toxic effects by H₂O₂ production, which was an initial hypothesis of my project, IL4i1 generates the anti-oxidative metabolites I3P and 4HPP (in combination with sub-lethal amounts of H₂O₂) and can mediate cellular resistance to ferroptosis. In addition, I observed that I3P can activate AhR signaling agreeing with two other studies published in 2020 [19,196]. Thus, besides amino acid depletion, especially the α-keto acid I3P generated from Trp appears to be an important mediator of IL4i1 downstream effects. However, although we start to better understand the basic mechanisms by which IL4i1-dependent amino acid metabolism can influence cells in its environment, most observations derive from systems where IL4i1 was overexpressed or recombinant protein was used. Therefore, we know very

little about the processes actually happening when cells endogenously expressing IL4i1 (e.g. myeloid cells) interact with other cells such as other immune cells or cancer cells. It is also possible that depending on the cellular context, IL4i1-mediated downstream effects such as AhR activation, oxidative stress protection or amino acid starvation responses may have different weighting. Therefore, we are aiming to set up advanced co-culture systems between myeloid 'IL4i1-producer' cells, T cells and tumor cells. In the work presented herein, I started to characterize the expression and regulation of IL4i1 in bone-marrow derived DCs and macrophages, which could be used as 'IL4i1-producer' cells in co-culture assays as the cultures allow to yield high amounts of the cells of interest. We are currently developing novel antibodies to enable intracellular IL4i1 staining for flow cytometry to further characterize IL4i1-expressing cell populations in our myeloid cell differentiations, but also to validate macrophage and DC populations expressing IL4i1 (on protein level) *in vivo*, which remain largely uncharacterized. As IL4i1 was suggested to be secreted into the immune synapse between antigen-presenting cells and T cells [184,185], co-cultures between 'IL4i1-producing' populations of myeloid cells (from WT or *Il4i1^{-/-}* mice) and ovalbumin-specific OT-I or OT-II T cells could help to specifically identify IL4i1-dependent effects on T cell biology in the context of antigen stimulation. In this regard, it would be interesting to investigate whether I3P-dependent anti-oxidative activity influences T cell fate and function, which we do not know at this point. Furthermore, 3D tumor spheroid models containing IL4i1-expressing myeloid cells may be useful to investigate IL4i1 biology in the context of cancer. While in 2D cultures IL4i1 gets diluted when secreted to the supernatant, 3D models could allow the local enrichment of the enzyme better mimicking processes in the TME, which may be useful to investigate IL4i1-dependent effects. A previous study from Takahashi and colleagues [258] showed that tumor cells in the center of 3D spheroids undergo ferroptosis. Introducing IL4i1-expressing myeloid cells into this system could help us to understand the role of IL4i1's anti-ferroptotic activity in the context of tumor growth and cancer cell survival. These 3D models could further display a useful platform to study the effect of potential IL4i1 inhibitors on tumor growth *in vitro*.

6. References

1. Beutler B: **Innate immunity: an overview.** *Mol Immunol* 2004, **40**:845-859.
2. Akira S, Takeda K: **Toll-like receptor signalling.** *Nat Rev Immunol* 2004, **4**:499-511.
3. Chaplin DD: **Overview of the immune response.** *J Allergy Clin Immunol* 2010, **125**:S3-23.
4. Ismail N, Olano JP, Feng HM, Walker DH: **Current status of immune mechanisms of killing of intracellular microorganisms.** *FEMS Microbiol Lett* 2002, **207**:111-120.
5. Labbe K, Saleh M: **Cell death in the host response to infection.** *Cell Death Differ* 2008, **15**:1339-1349.
6. Papp G, Boros P, Nakken B, Szodoray P, Zeher M: **Regulatory immune cells and functions in autoimmunity and transplantation immunology.** *Autoimmun Rev* 2017, **16**:435-444.
7. Nemazee D: **Mechanisms of central tolerance for B cells.** *Nat Rev Immunol* 2017, **17**:281-294.
8. Xing Y, Hogquist KA: **T-cell tolerance: central and peripheral.** *Cold Spring Harb Perspect Biol* 2012, **4**.
9. Iberg CA, Jones A, Hawiger D: **Dendritic Cells As Inducers of Peripheral Tolerance.** *Trends Immunol* 2017, **38**:793-804.
10. Mueller DL: **Mechanisms maintaining peripheral tolerance.** *Nat Immunol* 2010, **11**:21-27.
11. Fajgenbaum DC, June CH: **Cytokine Storm.** *N Engl J Med* 2020, **383**:2255-2273.
12. Vinay DS, Ryan EP, Pawelec G, Talib WH, Stagg J, Elkord E, Lichtor T, Decker WK, Whelan RL, Kumara H, et al.: **Immune evasion in cancer: Mechanistic basis and therapeutic strategies.** *Semin Cancer Biol* 2015, **35 Suppl**:S185-S198.
13. Buchbinder EI, Desai A: **CTLA-4 and PD-1 Pathways: Similarities, Differences, and Implications of Their Inhibition.** *Am J Clin Oncol* 2016, **39**:98-106.
14. Robert C: **A decade of immune-checkpoint inhibitors in cancer therapy.** *Nat Commun* 2020, **11**:3801.
15. Wartewig T, Ruland J: **PD-1 Tumor Suppressor Signaling in T Cell Lymphomas.** *Trends Immunol* 2019, **40**:403-414.
16. Murray PJ: **Amino acid auxotrophy as a system of immunological control nodes.** *Nat Immunol* 2016, **17**:132-139.
17. Boulland ML, Marquet J, Molinier-Frenkel V, Moller P, Guiter C, Lasoudris F, Copie-Bergman C, Baia M, Gaulard P, Leroy K, et al.: **Human IL4I1 is a secreted L-phenylalanine oxidase expressed by mature dendritic cells that inhibits T-lymphocyte proliferation.** *Blood* 2007, **110**:220-227.
18. Zeitler L, Fiore A, Meyer C, Russier M, Zanella G, Suppmann S, Gargaro M, Sidhu SS, Seshagiri S, Ohnmacht C, et al.: **Anti-ferroptotic mechanism of IL4i1-mediated amino acid metabolism.** *Elife* 2021, **10**.
19. Sadik A, Somarribas Patterson LF, Ozturk S, Mohapatra SR, Panitz V, Secker PF, Pfander P, Loth S, Salem H, Prentzell MT, et al.: **IL4I1 Is a Metabolic Immune Checkpoint that Activates the AHR and Promotes Tumor Progression.** *Cell* 2020, **182**:1252-1270 e1234.
20. Murray PJ: **Macrophage Polarization.** *Annu Rev Physiol* 2017, **79**:541-566.

21. Grohmann U, Bronte V: **Control of immune response by amino acid metabolism.** *Immunol Rev* 2010, **236**:243-264.
22. Bogdan C: **Nitric oxide and the immune response.** *Nat Immunol* 2001, **2**:907-916.
23. Bingisser RM, Tilbrook PA, Holt PG, Kees UR: **Macrophage-derived nitric oxide regulates T cell activation via reversible disruption of the Jak3/STAT5 signaling pathway.** *J Immunol* 1998, **160**:5729-5734.
24. Mazzone A, Bronte V, Visintin A, Spitzer JH, Apolloni E, Serafini P, Zanovello P, Segal DM: **Myeloid suppressor lines inhibit T cell responses by an NO-dependent mechanism.** *J Immunol* 2002, **168**:689-695.
25. Lu G, Zhang R, Geng S, Peng L, Jayaraman P, Chen C, Xu F, Yang J, Li Q, Zheng H, et al.: **Myeloid cell-derived inducible nitric oxide synthase suppresses M1 macrophage polarization.** *Nat Commun* 2015, **6**:6676.
26. Everts B, Amiel E, van der Windt GJ, Freitas TC, Chott R, Yarasheski KE, Pearce EL, Pearce EJ: **Commitment to glycolysis sustains survival of NO-producing inflammatory dendritic cells.** *Blood* 2012, **120**:1422-1431.
27. Dichtl S, Lindenthal L, Zeitler L, Behnke K, Schlosser D, Strobl B, Scheller J, El Kasmi KC, Murray PJ: **Lactate and IL6 define separable paths of inflammatory metabolic adaptation.** *Sci Adv* 2021, **7**.
28. Caputa G, Castoldi A, Pearce EJ: **Metabolic adaptations of tissue-resident immune cells.** *Nat Immunol* 2019, **20**:793-801.
29. El Kasmi KC, Qualls JE, Pesce JT, Smith AM, Thompson RW, Henao-Tamayo M, Basaraba RJ, Konig T, Schleicher U, Koo MS, et al.: **Toll-like receptor-induced arginase 1 in macrophages thwarts effective immunity against intracellular pathogens.** *Nat Immunol* 2008, **9**:1399-1406.
30. Qualls JE, Neale G, Smith AM, Koo MS, DeFreitas AA, Zhang H, Kaplan G, Watowich SS, Murray PJ: **Arginine usage in mycobacteria-infected macrophages depends on autocrine-paracrine cytokine signaling.** *Sci Signal* 2010, **3**:ra62.
31. Rath M, Muller I, Kropf P, Closs EI, Munder M: **Metabolism via Arginase or Nitric Oxide Synthase: Two Competing Arginine Pathways in Macrophages.** *Front Immunol* 2014, **5**:532.
32. Mills CD: **M1 and M2 Macrophages: Oracles of Health and Disease.** *Crit Rev Immunol* 2012, **32**:463-488.
33. Caldwell RW, Rodriguez PC, Toque HA, Narayanan SP, Caldwell RB: **Arginase: A Multifaceted Enzyme Important in Health and Disease.** *Physiol Rev* 2018, **98**:641-665.
34. Iyer RK, Yoo PK, Kern RM, Rozengurt N, Tsoa R, O'Brien WE, Yu H, Grody WW, Cederbaum SD: **Mouse model for human arginase deficiency.** *Mol Cell Biol* 2002, **22**:4491-4498.
35. Pesce JT, Ramalingam TR, Mentink-Kane MM, Wilson MS, El Kasmi KC, Smith AM, Thompson RW, Cheever AW, Murray PJ, Wynn TA: **Arginase-1-expressing macrophages suppress Th2 cytokine-driven inflammation and fibrosis.** *PLoS Pathog* 2009, **5**:e1000371.
36. Herbert DR, Orekov T, Roloson A, Ilies M, Perkins C, O'Brien W, Cederbaum S, Christianson DW, Zimmermann N, Rothenberg ME, et al.: **Arginase I suppresses IL-12/IL-23p40-driven intestinal inflammation during acute schistosomiasis.** *J Immunol* 2010, **184**:6438-6446.

37. Rodriguez PC, Quiceno DG, Ochoa AC: **L-arginine availability regulates T-lymphocyte cell-cycle progression.** *Blood* 2007, **109**:1568-1573.
38. Rodriguez PC, Zea AH, DeSalvo J, Culotta KS, Zabaleta J, Quiceno DG, Ochoa JB, Ochoa AC: **L-arginine consumption by macrophages modulates the expression of CD3 zeta chain in T lymphocytes.** *J Immunol* 2003, **171**:1232-1239.
39. Fletcher M, Ramirez ME, Sierra RA, Raber P, Thevenot P, Al-Khami AA, Sanchez-Pino D, Hernandez C, Wyczechowska DD, Ochoa AC, et al.: **I-Arginine depletion blunts antitumor T-cell responses by inducing myeloid-derived suppressor cells.** *Cancer Res* 2015, **75**:275-283.
40. Bronte V, Zanovello P: **Regulation of immune responses by L-arginine metabolism.** *Nat Rev Immunol* 2005, **5**:641-654.
41. Shi O, Morris SM, Jr., Zoghbi H, Porter CW, O'Brien WE: **Generation of a mouse model for arginase II deficiency by targeted disruption of the arginase II gene.** *Mol Cell Biol* 2001, **21**:811-813.
42. Dowling JK, Afzal R, Gearing LJ, Cervantes-Silva MP, Annett S, Davis GM, De Santi C, Assmann N, Dettmer K, Gough DJ, et al.: **Mitochondrial arginase-2 is essential for IL-10 metabolic reprogramming of inflammatory macrophages.** *Nat Commun* 2021, **12**:1460.
43. Dunand-Sauthier I, Irla M, Carnesecchi S, Seguin-Estevéz Q, Vejnar CE, Zdobnov EM, Santiago-Raber ML, Reith W: **Repression of arginase-2 expression in dendritic cells by microRNA-155 is critical for promoting T cell proliferation.** *J Immunol* 2014, **193**:1690-1700.
44. Eming SA, Murray PJ, Pearce EJ: **Metabolic orchestration of the wound healing response.** *Cell Metab* 2021, **33**:1726-1743.
45. Fiore A, Murray PJ: **Tryptophan and indole metabolism in immune regulation.** *Curr Opin Immunol* 2021, **70**:7-14.
46. Badawy AA: **Kynurenine Pathway of Tryptophan Metabolism: Regulatory and Functional Aspects.** *Int J Tryptophan Res* 2017, **10**:1178646917691938.
47. Ye Z, Yue L, Shi J, Shao M, Wu T: **Role of IDO and TDO in Cancers and Related Diseases and the Therapeutic Implications.** *J Cancer* 2019, **10**:2771-2782.
48. Yuasa HJ, Ball HJ, Ho YF, Austin CJ, Whittington CM, Belov K, Maghzal GJ, Jermini LS, Hunt NH: **Characterization and evolution of vertebrate indoleamine 2, 3-dioxygenases IDOs from monotremes and marsupials.** *Comp Biochem Physiol B Biochem Mol Biol* 2009, **153**:137-144.
49. Metz R, Duhadaway JB, Kamasani U, Laury-Kleintop L, Muller AJ, Prendergast GC: **Novel tryptophan catabolic enzyme IDO2 is the preferred biochemical target of the antitumor indoleamine 2,3-dioxygenase inhibitory compound D-1-methyl-tryptophan.** *Cancer Res* 2007, **67**:7082-7087.
50. Munn DH, Sharma MD, Hou D, Baban B, Lee JR, Antonia SJ, Messina JL, Chandler P, Koni PA, Mellor AL: **Expression of indoleamine 2,3-dioxygenase by plasmacytoid dendritic cells in tumor-draining lymph nodes.** *J Clin Invest* 2004, **114**:280-290.
51. Sharma MD, Baban B, Chandler P, Hou DY, Singh N, Yagita H, Azuma M, Blazar BR, Mellor AL, Munn DH: **Plasmacytoid dendritic cells from mouse tumor-draining lymph nodes directly activate mature Tregs via indoleamine 2,3-dioxygenase.** *J Clin Invest* 2007, **117**:2570-2582.
52. Fallarino F, Grohmann U, Vacca C, Bianchi R, Orabona C, Spreca A, Fioretti MC, Puccetti P: **T cell apoptosis by tryptophan catabolism.** *Cell Death Differ* 2002, **9**:1069-1077.

53. Gargaro M, Scalisi G, Manni G, Briseno CG, Bagadia P, Durai V, Theisen DJ, Kim S, Castelli M, Xu CA, et al.: **Indoleamine 2,3-dioxygenase 1 activation in mature cDC1 promotes tolerogenic education of inflammatory cDC2 via metabolic communication.** *Immunity* 2022, **55**:1032-1050 e1014.
54. Li A, Barsoumian HB, Schoenhals JE, Cushman TR, Caetano MS, Wang X, Valdecanas DR, Niknam S, Younes AI, Li G, et al.: **Indoleamine 2,3-dioxygenase 1 inhibition targets anti-PD1-resistant lung tumors by blocking myeloid-derived suppressor cells.** *Cancer Lett* 2018, **431**:54-63.
55. Mulder K, Patel AA, Kong WT, Piot C, Halitzki E, Dunsmore G, Khalilnezhad S, Irac SE, Dubuisson A, Chevrier M, et al.: **Cross-tissue single-cell landscape of human monocytes and macrophages in health and disease.** *Immunity* 2021, **54**:1883-1900 e1885.
56. Ball HJ, Sanchez-Perez A, Weiser S, Austin CJ, Astelbauer F, Miu J, McQuillan JA, Stocker R, Jermin LS, Hunt NH: **Characterization of an indoleamine 2,3-dioxygenase-like protein found in humans and mice.** *Gene* 2007, **396**:203-213.
57. Merlo LMF, DuHadaway JB, Montgomery JD, Peng WD, Murray PJ, Prendergast GC, Caton AJ, Muller AJ, Mandik-Nayak L: **Differential Roles of IDO1 and IDO2 in T and B Cell Inflammatory Immune Responses.** *Front Immunol* 2020, **11**:1861.
58. Prendergast GC, Metz R, Muller AJ, Merlo LM, Mandik-Nayak L: **IDO2 in Immunomodulation and Autoimmune Disease.** *Front Immunol* 2014, **5**:585.
59. Mondanelli G, Mandarano M, Belladonna ML, Suvieri C, Pelliccia C, Bellezza G, Sidoni A, Carvalho A, Grohmann U, Volpi C: **Current Challenges for IDO2 as Target in Cancer Immunotherapy.** *Front Immunol* 2021, **12**:679953.
60. Merlo LMF, Peng W, DuHadaway JB, Montgomery JD, Prendergast GC, Muller AJ, Mandik-Nayak L: **The Immunomodulatory Enzyme IDO2 Mediates Autoimmune Arthritis through a Nonenzymatic Mechanism.** *J Immunol* 2022, **208**:571-581.
61. Fiore A, Zeitler L, Russier M, Gross A, Hiller MK, Parker JL, Stier L, Kocher T, Newstead S, Murray PJ: **Kynurenine importation by SLC7A11 propagates anti-ferroptotic signaling.** *Mol Cell* 2022, **82**:920-932 e927.
62. Fallarino F, Grohmann U, Hwang KW, Orabona C, Vacca C, Bianchi R, Belladonna ML, Fioretti MC, Alegre ML, Puccetti P: **Modulation of tryptophan catabolism by regulatory T cells.** *Nat Immunol* 2003, **4**:1206-1212.
63. Mellor AL, Chandler P, Baban B, Hansen AM, Marshall B, Pihkala J, Waldmann H, Cobbold S, Adams E, Munn DH: **Specific subsets of murine dendritic cells acquire potent T cell regulatory functions following CTLA4-mediated induction of indoleamine 2,3 dioxygenase.** *Int Immunol* 2004, **16**:1391-1401.
64. Pfefferkorn ER: **Interferon gamma blocks the growth of Toxoplasma gondii in human fibroblasts by inducing the host cells to degrade tryptophan.** *Proc Natl Acad Sci U S A* 1984, **81**:908-912.
65. Pfefferkorn ER, Eckel M, Rebhun S: **Interferon-gamma suppresses the growth of Toxoplasma gondii in human fibroblasts through starvation for tryptophan.** *Mol Biochem Parasitol* 1986, **20**:215-224.
66. Byrne GI, Lehmann LK, Landry GJ: **Induction of tryptophan catabolism is the mechanism for gamma-interferon-mediated inhibition of intracellular Chlamydia psittaci replication in T24 cells.** *Infect Immun* 1986, **53**:347-351.
67. Munn DH, Zhou M, Attwood JT, Bondarev I, Conway SJ, Marshall B, Brown C, Mellor AL: **Prevention of allogeneic fetal rejection by tryptophan catabolism.** *Science* 1998, **281**:1191-1193.

68. Munn DH, Shafizadeh E, Attwood JT, Bondarev I, Pashine A, Mellor AL: **Inhibition of T cell proliferation by macrophage tryptophan catabolism.** *J Exp Med* 1999, **189**:1363-1372.
69. Gunther J, Dabritz J, Wirthgen E: **Limitations and Off-Target Effects of Tryptophan-Related IDO Inhibitors in Cancer Treatment.** *Front Immunol* 2019, **10**:1801.
70. Van de Velde LA, Gingras S, Pelletier S, Murray PJ: **Issues with the Specificity of Immunological Reagents for Murine IDO1.** *Cell Metab* 2016, **23**:389-390.
71. Mellor AL, Baban B, Chandler P, Marshall B, Jhaver K, Hansen A, Koni PA, Iwashima M, Munn DH: **Cutting edge: induced indoleamine 2,3 dioxygenase expression in dendritic cell subsets suppresses T cell clonal expansion.** *J Immunol* 2003, **171**:1652-1655.
72. Munn DH, Sharma MD, Baban B, Harding HP, Zhang Y, Ron D, Mellor AL: **GCN2 kinase in T cells mediates proliferative arrest and anergy induction in response to indoleamine 2,3-dioxygenase.** *Immunity* 2005, **22**:633-642.
73. Fallarino F, Grohmann U, You S, McGrath BC, Cavener DR, Vacca C, Orabona C, Bianchi R, Belladonna ML, Volpi C, et al.: **The combined effects of tryptophan starvation and tryptophan catabolites down-regulate T cell receptor zeta-chain and induce a regulatory phenotype in naive T cells.** *J Immunol* 2006, **176**:6752-6761.
74. Jitschin R, Braun M, Buttner M, Dettmer-Wilde K, Bricks J, Berger J, Eckart MJ, Krause SW, Oefner PJ, Le Blanc K, et al.: **CLL-cells induce IDOhi CD14+HLA-DRlo myeloid-derived suppressor cells that inhibit T-cell responses and promote TRegs.** *Blood* 2014, **124**:750-760.
75. Baban B, Chandler PR, Sharma MD, Pihkala J, Koni PA, Munn DH, Mellor AL: **IDO activates regulatory T cells and blocks their conversion into Th17-like T cells.** *J Immunol* 2009, **183**:2475-2483.
76. Sharma MD, Hou DY, Liu Y, Koni PA, Metz R, Chandler P, Mellor AL, He Y, Munn DH: **Indoleamine 2,3-dioxygenase controls conversion of Foxp3+ Tregs to TH17-like cells in tumor-draining lymph nodes.** *Blood* 2009, **113**:6102-6111.
77. Ravishankar B, Liu H, Shinde R, Chaudhary K, Xiao W, Bradley J, Koritzinsky M, Madaio MP, McGaha TL: **The amino acid sensor GCN2 inhibits inflammatory responses to apoptotic cells promoting tolerance and suppressing systemic autoimmunity.** *Proc Natl Acad Sci U S A* 2015, **112**:10774-10779.
78. Pallotta MT, Rossini S, Suvieri C, Coletti A, Orabona C, Macchiarulo A, Volpi C, Grohmann U: **Indoleamine 2,3-dioxygenase 1 (IDO1): an up-to-date overview of an eclectic immunoregulatory enzyme.** *FEBS J* 2021.
79. Harding HP, Zhang Y, Zeng H, Novoa I, Lu PD, Calfon M, Sadri N, Yun C, Popko B, Paules R, et al.: **An integrated stress response regulates amino acid metabolism and resistance to oxidative stress.** *Mol Cell* 2003, **11**:619-633.
80. Hara K, Yonezawa K, Weng QP, Kozlowski MT, Belham C, Avruch J: **Amino acid sufficiency and mTOR regulate p70 S6 kinase and eIF-4E BP1 through a common effector mechanism.** *J Biol Chem* 1998, **273**:14484-14494.
81. Wolfson RL, Chantranupong L, Saxton RA, Shen K, Scaria SM, Cantor JR, Sabatini DM: **Sestrin2 is a leucine sensor for the mTORC1 pathway.** *Science* 2016, **351**:43-48.
82. Chantranupong L, Scaria SM, Saxton RA, Gygi MP, Shen K, Wyant GA, Wang T, Harper JW, Gygi SP, Sabatini DM: **The CASTOR Proteins Are Arginine Sensors for the mTORC1 Pathway.** *Cell* 2016, **165**:153-164.

83. Dong J, Qiu H, Garcia-Barrio M, Anderson J, Hinnebusch AG: **Uncharged tRNA activates GCN2 by displacing the protein kinase moiety from a bipartite tRNA-binding domain.** *Mol Cell* 2000, **6**:269-279.
84. Costa-Mattioli M, Walter P: **The integrated stress response: From mechanism to disease.** *Science* 2020, **368**.
85. Cobbold SP, Adams E, Farquhar CA, Nolan KF, Howie D, Lui KO, Fairchild PJ, Mellor AL, Ron D, Waldmann H: **Infectious tolerance via the consumption of essential amino acids and mTOR signaling.** *Proc Natl Acad Sci U S A* 2009, **106**:12055-12060.
86. Van de Velde LA, Guo XJ, Barbaric L, Smith AM, Oguin TH, 3rd, Thomas PG, Murray PJ: **Stress Kinase GCN2 Controls the Proliferative Fitness and Trafficking of Cytotoxic T Cells Independent of Environmental Amino Acid Sensing.** *Cell Rep* 2016, **17**:2247-2258.
87. Halaby MJ, Hezaveh K, Lamorte S, Ciudad MT, Kloetgen A, MacLeod BL, Guo M, Chakravarthy A, Medina TDS, Ugel S, et al.: **GCN2 drives macrophage and MDSC function and immunosuppression in the tumor microenvironment.** *Sci Immunol* 2019, **4**.
88. Saxton RA, Sabatini DM: **mTOR Signaling in Growth, Metabolism, and Disease.** *Cell* 2017, **169**:361-371.
89. Kino T, Hatanaka H, Miyata S, Inamura N, Nishiyama M, Yajima T, Goto T, Okuhara M, Kohsaka M, Aoki H, et al.: **FK-506, a novel immunosuppressant isolated from a Streptomyces. II. Immunosuppressive effect of FK-506 in vitro.** *J Antibiot (Tokyo)* 1987, **40**:1256-1265.
90. Morice WG, Brunn GJ, Wiederrecht G, Siekierka JJ, Abraham RT: **Rapamycin-induced inhibition of p34cdc2 kinase activation is associated with G1/S-phase growth arrest in T lymphocytes.** *J Biol Chem* 1993, **268**:3734-3738.
91. Morice WG, Wiederrecht G, Brunn GJ, Siekierka JJ, Abraham RT: **Rapamycin inhibition of interleukin-2-dependent p33cdk2 and p34cdc2 kinase activation in T lymphocytes.** *J Biol Chem* 1993, **268**:22737-22745.
92. Powell JD, Lerner CG, Schwartz RH: **Inhibition of cell cycle progression by rapamycin induces T cell clonal anergy even in the presence of costimulation.** *J Immunol* 1999, **162**:2775-2784.
93. Yang K, Shrestha S, Zeng H, Karmaus PW, Neale G, Vogel P, Guertin DA, Lamb RF, Chi H: **T cell exit from quiescence and differentiation into Th2 cells depend on Raptor-mTORC1-mediated metabolic reprogramming.** *Immunity* 2013, **39**:1043-1056.
94. Delgoffe GM, Kole TP, Zheng Y, Zarek PE, Matthews KL, Xiao B, Worley PF, Kozma SC, Powell JD: **The mTOR kinase differentially regulates effector and regulatory T cell lineage commitment.** *Immunity* 2009, **30**:832-844.
95. Gutierrez-Vazquez C, Quintana FJ: **Regulation of the Immune Response by the Aryl Hydrocarbon Receptor.** *Immunity* 2018, **48**:19-33.
96. Rothhammer V, Quintana FJ: **The aryl hydrocarbon receptor: an environmental sensor integrating immune responses in health and disease.** *Nat Rev Immunol* 2019, **19**:184-197.
97. Poland A, Knutson JC: **2,3,7,8-tetrachlorodibenzo-p-dioxin and related halogenated aromatic hydrocarbons: examination of the mechanism of toxicity.** *Annu Rev Pharmacol Toxicol* 1982, **22**:517-554.

98. Bock KW: **From TCDD-mediated toxicity to searches of physiologic AHR functions.** *Biochem Pharmacol* 2018, **155**:419-424.
99. Hubbard TD, Murray IA, Perdew GH: **Indole and Tryptophan Metabolism: Endogenous and Dietary Routes to Ah Receptor Activation.** *Drug Metab Dispos* 2015, **43**:1522-1535.
100. Mezrich JD, Fechner JH, Zhang X, Johnson BP, Burlingham WJ, Bradfield CA: **An interaction between kynurenine and the aryl hydrocarbon receptor can generate regulatory T cells.** *J Immunol* 2010, **185**:3190-3198.
101. Opitz CA, Litzenburger UM, Sahn F, Ott M, Tritschler I, Trump S, Schumacher T, Jestaedt L, Schrenk D, Weller M, et al.: **An endogenous tumour-promoting ligand of the human aryl hydrocarbon receptor.** *Nature* 2011, **478**:197-203.
102. DiNatale BC, Murray IA, Schroeder JC, Flaveny CA, Lahoti TS, Laurenzana EM, Omiecinski CJ, Perdew GH: **Kynurenic acid is a potent endogenous aryl hydrocarbon receptor ligand that synergistically induces interleukin-6 in the presence of inflammatory signaling.** *Toxicol Sci* 2010, **115**:89-97.
103. Bessede A, Gargaro M, Pallotta MT, Matino D, Servillo G, Brunacci C, Bicciato S, Mazza EM, Macchiarulo A, Vacca C, et al.: **Aryl hydrocarbon receptor control of a disease tolerance defence pathway.** *Nature* 2014, **511**:184-190.
104. Perdew GH: **Association of the Ah receptor with the 90-kDa heat shock protein.** *J Biol Chem* 1988, **263**:13802-13805.
105. Nair SC, Toran EJ, Rimerman RA, Hjermstad S, Smithgall TE, Smith DF: **A pathway of multi-chaperone interactions common to diverse regulatory proteins: estrogen receptor, Fes tyrosine kinase, heat shock transcription factor Hsf1, and the aryl hydrocarbon receptor.** *Cell Stress Chaperones* 1996, **1**:237-250.
106. Meyer BK, Perdew GH: **Characterization of the AhR-hsp90-XAP2 core complex and the role of the immunophilin-related protein XAP2 in AhR stabilization.** *Biochemistry* 1999, **38**:8907-8917.
107. Enan E, Matsumura F: **Identification of c-Src as the integral component of the cytosolic Ah receptor complex, transducing the signal of 2,3,7,8-tetrachlorodibenzo-p-dioxin (TCDD) through the protein phosphorylation pathway.** *Biochem Pharmacol* 1996, **52**:1599-1612.
108. Lees MJ, Peet DJ, Whitelaw ML: **Defining the role for XAP2 in stabilization of the dioxin receptor.** *J Biol Chem* 2003, **278**:35878-35888.
109. Reyes H, Reisz-Porszasz S, Hankinson O: **Identification of the Ah receptor nuclear translocator protein (Arnt) as a component of the DNA binding form of the Ah receptor.** *Science* 1992, **256**:1193-1195.
110. Davarinos NA, Pollenz RS: **Aryl hydrocarbon receptor imported into the nucleus following ligand binding is rapidly degraded via the cytoplasmic proteasome following nuclear export.** *J Biol Chem* 1999, **274**:28708-28715.
111. Schmidt JV, Bradfield CA: **Ah receptor signaling pathways.** *Annu Rev Cell Dev Biol* 1996, **12**:55-89.
112. Mimura J, Ema M, Sogawa K, Fujii-Kuriyama Y: **Identification of a novel mechanism of regulation of Ah (dioxin) receptor function.** *Genes Dev* 1999, **13**:20-25.
113. Dong B, Cheng W, Li W, Zheng J, Wu D, Matsumura F, Vogel CF: **FRET analysis of protein tyrosine kinase c-Src activation mediated via aryl hydrocarbon receptor.** *Biochim Biophys Acta* 2011, **1810**:427-431.

114. Kerkvliet NI, Baecher-Steppan L: **Suppression of allograft immunity by 3,4,5,3',4',5'-hexachlorobiphenyl. I. Effects of exposure on tumor rejection and cytotoxic T cell activity in vivo.** *Immunopharmacology* 1988, **16**:1-12.
115. Kerkvliet NI, Baecher-Steppan L, Smith BB, Youngberg JA, Henderson MC, Buhler DR: **Role of the Ah locus in suppression of cytotoxic T lymphocyte activity by halogenated aromatic hydrocarbons (PCBs and TCDD): structure-activity relationships and effects in C57Bl/6 mice congenic at the Ah locus.** *Fundam Appl Toxicol* 1990, **14**:532-541.
116. Kerkvliet NI, Shepherd DM, Baecher-Steppan L: **T lymphocytes are direct, aryl hydrocarbon receptor (AhR)-dependent targets of 2,3,7,8-tetrachlorodibenzo-p-dioxin (TCDD): AhR expression in both CD4+ and CD8+ T cells is necessary for full suppression of a cytotoxic T lymphocyte response by TCDD.** *Toxicol Appl Pharmacol* 2002, **185**:146-152.
117. Funatake CJ, Marshall NB, Steppan LB, Mourich DV, Kerkvliet NI: **Cutting edge: activation of the aryl hydrocarbon receptor by 2,3,7,8-tetrachlorodibenzo-p-dioxin generates a population of CD4+ CD25+ cells with characteristics of regulatory T cells.** *J Immunol* 2005, **175**:4184-4188.
118. Quintana FJ, Basso AS, Iglesias AH, Korn T, Farez MF, Bettelli E, Caccamo M, Oukka M, Weiner HL: **Control of T(reg) and T(H)17 cell differentiation by the aryl hydrocarbon receptor.** *Nature* 2008, **453**:65-71.
119. Apetoh L, Quintana FJ, Pot C, Joller N, Xiao S, Kumar D, Burns EJ, Sherr DH, Weiner HL, Kuchroo VK: **The aryl hydrocarbon receptor interacts with c-Maf to promote the differentiation of type 1 regulatory T cells induced by IL-27.** *Nat Immunol* 2010, **11**:854-861.
120. Gandhi R, Kumar D, Burns EJ, Nadeau M, Dake B, Laroni A, Kozoriz D, Weiner HL, Quintana FJ: **Activation of the aryl hydrocarbon receptor induces human type 1 regulatory T cell-like and Foxp3(+) regulatory T cells.** *Nat Immunol* 2010, **11**:846-853.
121. Wu HY, Quintana FJ, da Cunha AP, Dake BT, Koeglsperger T, Starossom SC, Weiner HL: **In vivo induction of Tr1 cells via mucosal dendritic cells and AHR signaling.** *PLoS One* 2011, **6**:e23618.
122. Kimura A, Naka T, Nohara K, Fujii-Kuriyama Y, Kishimoto T: **Aryl hydrocarbon receptor regulates Stat1 activation and participates in the development of Th17 cells.** *Proc Natl Acad Sci U S A* 2008, **105**:9721-9726.
123. Veldhoen M, Hirota K, Christensen J, O'Garra A, Stockinger B: **Natural agonists for aryl hydrocarbon receptor in culture medium are essential for optimal differentiation of Th17 T cells.** *J Exp Med* 2009, **206**:43-49.
124. Gagliani N, Amezcua Vesely MC, Iseppon A, Brockmann L, Xu H, Palm NW, de Zoete MR, Licona-Limon P, Paiva RS, Ching T, et al.: **Th17 cells transdifferentiate into regulatory T cells during resolution of inflammation.** *Nature* 2015, **523**:221-225.
125. Hauben E, Gregori S, Draghici E, Migliavacca B, Olivieri S, Woisetschlager M, Roncarolo MG: **Activation of the aryl hydrocarbon receptor promotes allograft-specific tolerance through direct and dendritic cell-mediated effects on regulatory T cells.** *Blood* 2008, **112**:1214-1222.
126. Quintana FJ, Murugaiyan G, Farez MF, Mitsdoerffer M, Tukpah AM, Burns EJ, Weiner HL: **An endogenous aryl hydrocarbon receptor ligand acts on dendritic cells and T cells to suppress experimental autoimmune encephalomyelitis.** *Proc Natl Acad Sci U S A* 2010, **107**:20768-20773.

127. Goettel JA, Gandhi R, Kenison JE, Yeste A, Murugaiyan G, Sambanthamoorthy S, Griffith AE, Patel B, Shouval DS, Weiner HL, et al.: **AHR Activation Is Protective against Colitis Driven by T Cells in Humanized Mice.** *Cell Rep* 2016, **17**:1318-1329.
128. Kerkvliet NI, Steppan LB, Vorachek W, Oda S, Farrer D, Wong CP, Pham D, Mourich DV: **Activation of aryl hydrocarbon receptor by TCDD prevents diabetes in NOD mice and increases Foxp3+ T cells in pancreatic lymph nodes.** *Immunotherapy* 2009, **1**:539-547.
129. Nguyen NT, Kimura A, Nakahama T, Chinen I, Masuda K, Nohara K, Fujii-Kuriyama Y, Kishimoto T: **Aryl hydrocarbon receptor negatively regulates dendritic cell immunogenicity via a kynurenine-dependent mechanism.** *Proc Natl Acad Sci U S A* 2010, **107**:19961-19966.
130. Vogel CF, Goth SR, Dong B, Pessah IN, Matsumura F: **Aryl hydrocarbon receptor signaling mediates expression of indoleamine 2,3-dioxygenase.** *Biochem Biophys Res Commun* 2008, **375**:331-335.
131. Li Q, Harden JL, Anderson CD, Egilmez NK: **Tolerogenic Phenotype of IFN-gamma-Induced IDO+ Dendritic Cells Is Maintained via an Autocrine IDO-Kynurenine/AhR-IDO Loop.** *J Immunol* 2016, **197**:962-970.
132. Mor A, Tankiewicz-Kwedlo A, Krupa A, Pawlak D: **Role of Kynurenine Pathway in Oxidative Stress during Neurodegenerative Disorders.** *Cells* 2021, **10**.
133. Reyes Ocampo J, Lugo Huitron R, Gonzalez-Esquivel D, Ugalde-Muniz P, Jimenez-Anguiano A, Pineda B, Pedraza-Chaverri J, Rios C, Perez de la Cruz V: **Kynurenines with neuroactive and redox properties: relevance to aging and brain diseases.** *Oxid Med Cell Longev* 2014, **2014**:646909.
134. Gostner JM, Becker K, Fuchs D, Sucher R: **Redox regulation of the immune response.** *Redox Rep* 2013, **18**:88-94.
135. Hanahan D, Weinberg RA: **Hallmarks of cancer: the next generation.** *Cell* 2011, **144**:646-674.
136. Sullivan MR, Danai LV, Lewis CA, Chan SH, Gui DY, Kunchok T, Dennstedt EA, Vander Heiden MG, Muir A: **Quantification of microenvironmental metabolites in murine cancers reveals determinants of tumor nutrient availability.** *Elife* 2019, **8**.
137. Lemos H, Huang L, Prendergast GC, Mellor AL: **Immune control by amino acid catabolism during tumorigenesis and therapy.** *Nat Rev Cancer* 2019, **19**:162-175.
138. Platten M, Nollen EAA, Rohrig UF, Fallarino F, Opitz CA: **Tryptophan metabolism as a common therapeutic target in cancer, neurodegeneration and beyond.** *Nat Rev Drug Discov* 2019, **18**:379-401.
139. Tang D, Yue L, Yao R, Zhou L, Yang Y, Lu L, Gao W: **P53 prevent tumor invasion and metastasis by down-regulating IDO in lung cancer.** *Oncotarget* 2017, **8**:54548-54557.
140. D'Amato NC, Rogers TJ, Gordon MA, Greene LI, Cochrane DR, Spoelstra NS, Nemkov TG, D'Alessandro A, Hansen KC, Richer JK: **A TDO2-AhR signaling axis facilitates anoikis resistance and metastasis in triple-negative breast cancer.** *Cancer Res* 2015, **75**:4651-4664.
141. Sahn F, Oezen I, Opitz CA, Radlwimmer B, von Deimling A, Ahrendt T, Adams S, Bode HB, Guillemin GJ, Wick W, et al.: **The endogenous tryptophan metabolite and NAD+ precursor quinolinic acid confers resistance of gliomas to oxidative stress.** *Cancer Res* 2013, **73**:3225-3234.

142. Niu F, Yu Y, Li Z, Ren Y, Li Z, Ye Q, Liu P, Ji C, Qian L, Xiong Y: **Arginase: An emerging and promising therapeutic target for cancer treatment.** *Biomed Pharmacother* 2022, **149**:112840.
143. Van den Eynde BJ, Van Baren N, Baurain JF: **Is There a Clinical Future for IDO1 Inhibitors After the Failure of Epacadostat in Melanoma?** *Annual Review of Cancer Biology* 2020, **4**:241-256.
144. Castellano F, Molinier-Frenkel V: **An Overview of L-Amino Acid Oxidase Functions from Bacteria to Mammals: Focus on the Immunoregulatory Phenylalanine Oxidase IL4I1.** *Molecules* 2017, **22**.
145. Moustafa IM, Foster S, Lyubimov AY, Vrielink A: **Crystal structure of LAAO from Calloselasma rhodostoma with an L-phenylalanine substrate: insights into structure and mechanism.** *J Mol Biol* 2006, **364**:991-1002.
146. Mason JM, Naidu MD, Barcia M, Porti D, Chavan SS, Chu CC: **IL-4-induced gene-1 is a leukocyte L-amino acid oxidase with an unusual acidic pH preference and lysosomal localization.** *J Immunol* 2004, **173**:4561-4567.
147. Molinier-Frenkel V, Mestivier D, Castellano F: **Alterations of the immunosuppressive IL4I1 enzyme activity induced by naturally occurring SNP/mutations.** *Genes Immun* 2016, **17**:148-152.
148. Du XY, Clemetson KJ: **Snake venom L-amino acid oxidases.** *Toxicon* 2002, **40**:659-665.
149. Suryamohan K, Krishnankutty SP, Guillory J, Jevit M, Schroder MS, Wu M, Kuriakose B, Mathew OK, Perumal RC, Koludarov I, et al.: **The Indian cobra reference genome and transcriptome enables comprehensive identification of venom toxins.** *Nat Genet* 2020, **52**:106-117.
150. Oliveira AL, Viegas MF, da Silva SL, Soares AM, Ramos MJ, Fernandes PA: **The chemistry of snake venom and its medicinal potential.** *Nat Rev Chem* 2022, **6**:451-469.
151. Ponnudurai G, Chung MC, Tan NH: **Purification and properties of the L-amino acid oxidase from Malayan pit viper (Calloselasma rhodostoma) venom.** *Arch Biochem Biophys* 1994, **313**:373-378.
152. Izidoro LF, Sobrinho JC, Mendes MM, Costa TR, Grabner AN, Rodrigues VM, da Silva SL, Zanchi FB, Zuliani JP, Fernandes CF, et al.: **Snake venom L-amino acid oxidases: trends in pharmacology and biochemistry.** *Biomed Res Int* 2014, **2014**:196754.
153. Suhr SM, Kim DS: **Identification of the snake venom substance that induces apoptosis.** *Biochem Biophys Res Commun* 1996, **224**:134-139.
154. Ande SR, Kommoju PR, Draxl S, Murkovic M, Macheroux P, Ghisla S, Ferrando-May E: **Mechanisms of cell death induction by L-amino acid oxidase, a major component of ophidian venom.** *Apoptosis* 2006, **11**:1439-1451.
155. Burin SM, Berzoti-Coelho MG, Cominal JG, Ambrosio L, Torqueti MR, Sampaio SV, de Castro FA: **The L-amino acid oxidase from Calloselasma rhodostoma snake venom modulates apoptomiRs expression in Bcr-Abl-positive cell lines.** *Toxicon* 2016, **120**:9-14.
156. Costal-Oliveira F, Stransky S, Guerra-Duarte C, Naves de Souza DL, Vivas-Ruiz DE, Yarleque A, Sanchez EF, Chavez-Olortegui C, Braga VMM: **L-amino acid oxidase from Bothrops atrox snake venom triggers autophagy, apoptosis and necrosis in normal human keratinocytes.** *Sci Rep* 2019, **9**:781.

157. Puiffe ML, Lachaise I, Molinier-Frenkel V, Castellano F: **Antibacterial properties of the mammalian L-amino acid oxidase IL4I1**. *PLoS One* 2013, **8**:e54589.
158. Skarnes RC: **L-amino-acid oxidase, a bactericidal system**. *Nature* 1970, **225**:1072-1073.
159. Stiles BG, Sexton FW, Weinstein SA: **Antibacterial effects of different snake venoms: purification and characterization of antibacterial proteins from Pseudechis australis (Australian king brown or mulga snake) venom**. *Toxicon* 1991, **29**:1129-1141.
160. Stabeli RG, Marcussi S, Carlos GB, Pietro RC, Selistre-de-Araujo HS, Giglio JR, Oliveira EB, Soares AM: **Platelet aggregation and antibacterial effects of an L-amino acid oxidase purified from Bothrops alternatus snake venom**. *Bioorg Med Chem* 2004, **12**:2881-2886.
161. Chu CC, Paul WE: **Fig1, an interleukin 4-induced mouse B cell gene isolated by cDNA representational difference analysis**. *Proc Natl Acad Sci U S A* 1997, **94**:2507-2512.
162. Chavan SS, Tian W, Hsueh K, Jawaheer D, Gregersen PK, Chu CC: **Characterization of the human homolog of the IL-4 induced gene-1 (Fig1)**. *Biochim Biophys Acta* 2002, **1576**:70-80.
163. Meissner F, Scheltema RA, Mollenkopf HJ, Mann M: **Direct proteomic quantification of the secretome of activated immune cells**. *Science* 2013, **340**:475-478.
164. Yue Y, Huang W, Liang J, Guo J, Ji J, Yao Y, Zheng M, Cai Z, Lu L, Wang J: **IL4I1 Is a Novel Regulator of M2 Macrophage Polarization That Can Inhibit T Cell Activation via L-Tryptophan and Arginine Depletion and IL-10 Production**. *PLoS One* 2015, **10**:e0142979.
165. Wiemann S, Kolb-Kokocinski A, Poustka A: **Alternative pre-mRNA processing regulates cell-type specific expression of the IL4I1 and NUP62 genes**. *BMC Biol* 2005, **3**:16.
166. Bod L, Douguet L, Auffray C, Lengagne R, Bekkat F, Rondeau E, Molinier-Frenkel V, Castellano F, Richard Y, Prevost-Blondel A: **IL-4-Induced Gene 1: A Negative Immune Checkpoint Controlling B Cell Differentiation and Activation**. *J Immunol* 2018, **200**:1027-1038.
167. Molinier-Frenkel V, Prevost-Blondel A, Castellano F: **The IL4I1 Enzyme: A New Player in the Immunosuppressive Tumor Microenvironment**. *Cells* 2019, **8**.
168. Marquet J, Lasoudris F, Cousin C, Puiffe ML, Martin-Garcia N, Baud V, Chereau F, Farcet JP, Molinier-Frenkel V, Castellano F: **Dichotomy between factors inducing the immunosuppressive enzyme IL-4-induced gene 1 (IL4I1) in B lymphocytes and mononuclear phagocytes**. *Eur J Immunol* 2010, **40**:2557-2568.
169. Schroder AJ, Pavlidis P, Arimura A, Capece D, Rothman PB: **Cutting edge: STAT6 serves as a positive and negative regulator of gene expression in IL-4-stimulated B lymphocytes**. *J Immunol* 2002, **168**:996-1000.
170. Victora GD, Schwickert TA, Fooksman DR, Kamphorst AO, Meyer-Hermann M, Dustin ML, Nussenzweig MC: **Germinal center dynamics revealed by multiphoton microscopy with a photoactivatable fluorescent reporter**. *Cell* 2010, **143**:592-605.
171. Carbonnelle-Puscian A, Copie-Bergman C, Baia M, Martin-Garcia N, Allory Y, Haioun C, Cremades A, Abd-Alsamad I, Farcet JP, Gaulard P, et al.: **The novel immunosuppressive enzyme IL4I1 is expressed by neoplastic cells of several B-cell lymphomas and by tumor-associated macrophages**. *Leukemia* 2009, **23**:952-960.

172. Bod L, Lengagne R, Wrobel L, Ramspott JP, Kato M, Avril MF, Castellano F, Molinier-Frenkel V, Prevost-Blondel A: **IL4-induced gene 1 promotes tumor growth by shaping the immune microenvironment in melanoma.** *Oncoimmunology* 2017, **6**:e1278331.
173. Ramspott JP, Bekkat F, Bod L, Favier M, Terris B, Salomon A, Djerroudi L, Zaenker KS, Richard Y, Molinier-Frenkel V, et al.: **Emerging Role of IL-4-Induced Gene 1 as a Prognostic Biomarker Affecting the Local T-Cell Response in Human Cutaneous Melanoma.** *J Invest Dermatol* 2018, **138**:2625-2634.
174. Psachoulia K, Chamberlain KA, Heo D, Davis SE, Paskus JD, Nanescu SE, Dupree JL, Wynn TA, Huang JK: **IL4I1 augments CNS remyelination and axonal protection by modulating T cell driven inflammation.** *Brain* 2016, **139**:3121-3136.
175. Maier B, Leader AM, Chen ST, Tung N, Chang C, LeBerichel J, Chudnovskiy A, Maskey S, Walker L, Finnigan JP, et al.: **A conserved dendritic-cell regulatory program limits antitumour immunity.** *Nature* 2020, **580**:257-262.
176. Ginhoux F, Williams M, Merad M: **Expanding dendritic cell nomenclature in the single-cell era.** *Nat Rev Immunol* 2022, **22**:67-68.
177. Matusiak M, Hickey JW, Luca B, Lu G, Kidzinski L, Shu S, Colburg DRC, Phillips DJ, Brubaker SW, Charville GW, et al.: **A spatial map of human macrophage niches links tissue location with function.** *bioRxiv* 2022.
178. Zilionis R, Engblom C, Pfirschke C, Savova V, Zemmour D, Saatcioglu HD, Krishnan I, Maroni G, Meyerovitz CV, Kerwin CM, et al.: **Single-Cell Transcriptomics of Human and Mouse Lung Cancers Reveals Conserved Myeloid Populations across Individuals and Species.** *Immunity* 2019, **50**:1317-1334 e1310.
179. Liu Y, He S, Wang XL, Peng W, Chen QY, Chi DM, Chen JR, Han BW, Lin GW, Li YQ, et al.: **Tumour heterogeneity and intercellular networks of nasopharyngeal carcinoma at single cell resolution.** *Nat Commun* 2021, **12**:741.
180. Pombo Antunes AR, Scheyltjens I, Lodi F, Messiaen J, Antoranz A, Duerinck J, Kancheva D, Martens L, De Vlaminc K, Van Hove H, et al.: **Single-cell profiling of myeloid cells in glioblastoma across species and disease stage reveals macrophage competition and specialization.** *Nat Neurosci* 2021, **24**:595-610.
181. Van Hove H, Martens L, Scheyltjens I, De Vlaminc K, Pombo Antunes AR, De Prijck S, Vandamme N, De Schepper S, Van Isterdael G, Scott CL, et al.: **A single-cell atlas of mouse brain macrophages reveals unique transcriptional identities shaped by ontogeny and tissue environment.** *Nat Neurosci* 2019, **22**:1021-1035.
182. Bosteels C, Neyt K, Vanheerswynghe M, van Helden MJ, Sichien D, Debeuf N, De Prijck S, Bosteels V, Vandamme N, Martens L, et al.: **Inflammatory Type 2 cDCs Acquire Features of cDC1s and Macrophages to Orchestrate Immunity to Respiratory Virus Infection.** *Immunity* 2020, **52**:1039-1056 e1039.
183. Lukowski SW, Rodahl I, Kelly S, Yu M, Gotley J, Zhou C, Millard S, Andersen SB, Christ AN, Belz G, et al.: **Absence of Batf3 reveals a new dimension of cell state heterogeneity within conventional dendritic cells.** *iScience* 2021, **24**:102402.
184. Aubatin A, Sako N, Decrouy X, Donnadieu E, Molinier-Frenkel V, Castellano F: **IL4-induced gene 1 is secreted at the immune synapse and modulates TCR activation independently of its enzymatic activity.** *Eur J Immunol* 2018, **48**:106-119.
185. Bulitta B, Zuschmitter W, Bernal I, Bruder D, Klawonn F, von Bergen M, Garritsen HSP, Jansch L: **Proteomic definition of human mucosal-associated invariant T cells determines their unique molecular effector phenotype.** *Eur J Immunol* 2018, **48**:1336-1349.

186. Cousin C, Aubatin A, Le Gouvello S, Apetoh L, Castellano F, Molinier-Frenkel V: **The immunosuppressive enzyme IL411 promotes FoxP3(+) regulatory T lymphocyte differentiation.** *Eur J Immunol* 2015, **45**:1772-1782.
187. Puiffe ML, Dupont A, Sako N, Gatineau J, Cohen JL, Mestivier D, Lebon A, Prevost-Blondel A, Castellano F, Molinier-Frenkel V: **IL411 Accelerates the Expansion of Effector CD8(+) T Cells at the Expense of Memory Precursors by Increasing the Threshold of T-Cell Activation.** *Front Immunol* 2020, **11**:600012.
188. Lasoudris F, Cousin C, Prevost-Blondel A, Martin-Garcia N, Abd-Alsamad I, Ortonne N, Farcet JP, Castellano F, Molinier-Frenkel V: **IL411: an inhibitor of the CD8(+) antitumor T-cell response in vivo.** *Eur J Immunol* 2011, **41**:1629-1638.
189. Santarlaschi V, Maggi L, Capone M, Querci V, Beltrame L, Cavalieri D, D'Aiuto E, Cimaz R, Nebbioso A, Liotta F, et al.: **Rarity of human T helper 17 cells is due to retinoic acid orphan receptor-dependent mechanisms that limit their expansion.** *Immunity* 2012, **36**:201-214.
190. Santarlaschi V, Maggi L, Mazzoni A, Capone M, Querci V, Rossi MC, Beltrame L, Cavalieri D, De Palma R, Liotta F, et al.: **IL-4-induced gene 1 maintains high Tob1 expression that contributes to TCR unresponsiveness in human T helper 17 cells.** *Eur J Immunol* 2014, **44**:654-661.
191. Hinks TSC, Marchi E, Jabeen M, Olshansky M, Kurioka A, Pediongco TJ, Meehan BS, Kostenko L, Turner SJ, Corbett AJ, et al.: **Activation and In Vivo Evolution of the MAIT Cell Transcriptome in Mice and Humans Reveals Tissue Repair Functionality.** *Cell Rep* 2019, **28**:3249-3262 e3245.
192. Ye L, Pan J, Pasha MA, Shen X, D'Souza SS, Fung ITH, Wang Y, Guo B, Tang DD, Yang Q: **Mucosal-associated invariant T cells restrict allergic airway inflammation.** *J Allergy Clin Immunol* 2020, **145**:1469-1473 e1464.
193. Godfrey DI, Koay HF, McCluskey J, Gherardin NA: **The biology and functional importance of MAIT cells.** *Nat Immunol* 2019, **20**:1110-1128.
194. Nel I, Bertrand L, Toubal A, Lehuen A: **MAIT cells, guardians of skin and mucosa?** *Mucosal Immunol* 2021, **14**:803-814.
195. Scarlata CM, Celse C, Pignon P, Ayyoub M, Valmori D: **Differential expression of the immunosuppressive enzyme IL411 in human induced Aiolos+, but not natural Helios+, FOXP3+ Treg cells.** *Eur J Immunol* 2015, **45**:474-479.
196. Zhang X, Gan M, Li J, Li H, Su M, Tan D, Wang S, Jia M, Zhang L, Chen G: **Endogenous Indole Pyruvate Pathway for Tryptophan Metabolism Mediated by IL411.** *J Agric Food Chem* 2020, **68**:10678-10684.
197. Gatineau J, Nidercorne C, Dupont A, Puiffe ML, Cohen JL, Molinier-Frenkel V, Niedergang F, Castellano F: **IL411 binds to TMPRSS13 and competes with SARS-CoV-2 spike.** *Front Immunol* 2022, **13**:982839.
198. Zhao H, Teng Y, Hao W, Li J, Li Z, Chen Q, Yin C, Yue W: **Single-cell analysis revealed that IL411 promoted ovarian cancer progression.** *J Transl Med* 2021, **19**:454.
199. Dixon SJ, Lemberg KM, Lamprecht MR, Skouta R, Zaitsev EM, Gleason CE, Patel DN, Bauer AJ, Cantley AM, Yang WS, et al.: **Ferroptosis: an iron-dependent form of nonapoptotic cell death.** *Cell* 2012, **149**:1060-1072.
200. Eagle H, Piez KA, Oyama VI: **The biosynthesis of cystine in human cell cultures.** *J Biol Chem* 1961, **236**:1425-1428.
201. Tan S, Schubert D, Maher P: **Oxytosis: A novel form of programmed cell death.** *Curr Top Med Chem* 2001, **1**:497-506.

202. Seiler A, Schneider M, Forster H, Roth S, Wirth EK, Culmsee C, Plesnila N, Kremmer E, Radmark O, Wurst W, et al.: **Glutathione peroxidase 4 senses and translates oxidative stress into 12/15-lipoxygenase dependent- and AIF-mediated cell death.** *Cell Metab* 2008, **8**:237-248.
203. Stockwell BR: **Ferroptosis turns 10: Emerging mechanisms, physiological functions, and therapeutic applications.** *Cell* 2022, **185**:2401-2421.
204. Conrad M, Pratt DA: **The chemical basis of ferroptosis.** *Nat Chem Biol* 2019, **15**:1137-1147.
205. Jiang X, Stockwell BR, Conrad M: **Ferroptosis: mechanisms, biology and role in disease.** *Nat Rev Mol Cell Biol* 2021, **22**:266-282.
206. Dixon SJ, Winter GE, Musavi LS, Lee ED, Snijder B, Rebsamen M, Superti-Furga G, Stockwell BR: **Human Haploid Cell Genetics Reveals Roles for Lipid Metabolism Genes in Nonapoptotic Cell Death.** *ACS Chem Biol* 2015, **10**:1604-1609.
207. Doll S, Proneth B, Tyurina YY, Panzilius E, Kobayashi S, Ingold I, Irmeler M, Beckers J, Aichler M, Walch A, et al.: **ACSL4 dictates ferroptosis sensitivity by shaping cellular lipid composition.** *Nat Chem Biol* 2017, **13**:91-98.
208. Meister A: **Glutathione metabolism.** *Methods Enzymol* 1995, **251**:3-7.
209. Maiorino M, Conrad M, Ursini F: **GPx4, Lipid Peroxidation, and Cell Death: Discoveries, Rediscoveries, and Open Issues.** *Antioxid Redox Signal* 2018, **29**:61-74.
210. Ursini F, Maiorino M, Valente M, Ferri L, Gregolin C: **Purification from pig liver of a protein which protects liposomes and biomembranes from peroxidative degradation and exhibits glutathione peroxidase activity on phosphatidylcholine hydroperoxides.** *Biochim Biophys Acta* 1982, **710**:197-211.
211. Ingold I, Berndt C, Schmitt S, Doll S, Poschmann G, Buday K, Roveri A, Peng X, Porto Freitas F, Seibt T, et al.: **Selenium Utilization by GPX4 Is Required to Prevent Hydroperoxide-Induced Ferroptosis.** *Cell* 2018, **172**:409-422 e421.
212. Reich HJ, Hondal RJ: **Why Nature Chose Selenium.** *ACS Chem Biol* 2016, **11**:821-841.
213. Conrad M, Proneth B: **Selenium: Tracing Another Essential Element of Ferroptotic Cell Death.** *Cell Chem Biol* 2020, **27**:409-419.
214. Ishii T, Sugita Y, Bannai S: **Regulation of glutathione levels in mouse spleen lymphocytes by transport of cysteine.** *J Cell Physiol* 1987, **133**:330-336.
215. Liu N, Lin X, Huang C: **Activation of the reverse transsulfuration pathway through NRF2/CBS confers erastin-induced ferroptosis resistance.** *Br J Cancer* 2020, **122**:279-292.
216. Zhang HF, Klein Geltink RI, Parker SJ, Sorensen PH: **Transsulfuration, minor player or crucial for cysteine homeostasis in cancer.** *Trends Cell Biol* 2022, **32**:800-814.
217. Koppula P, Zhuang L, Gan B: **Cystine transporter SLC7A11/xCT in cancer: ferroptosis, nutrient dependency, and cancer therapy.** *Protein Cell* 2021, **12**:599-620.
218. Sato H, Tamba M, Ishii T, Bannai S: **Cloning and expression of a plasma membrane cystine/glutamate exchange transporter composed of two distinct proteins.** *J Biol Chem* 1999, **274**:11455-11458.
219. Liu X, Olszewski K, Zhang Y, Lim EW, Shi J, Zhang X, Zhang J, Lee H, Koppula P, Lei G, et al.: **Cystine transporter regulation of pentose phosphate pathway**

- dependency and disulfide stress exposes a targetable metabolic vulnerability in cancer.** *Nat Cell Biol* 2020, **22**:476-486.
220. Joly JH, Delfarah A, Phung PS, Parrish S, Graham NA: **A synthetic lethal drug combination mimics glucose deprivation-induced cancer cell death in the presence of glucose.** *J Biol Chem* 2020, **295**:1350-1365.
221. Lu SC: **Regulation of glutathione synthesis.** *Mol Aspects Med* 2009, **30**:42-59.
222. Tang D, Chen X, Kang R, Kroemer G: **Ferroptosis: molecular mechanisms and health implications.** *Cell Res* 2021, **31**:107-125.
223. Yang WS, SriRamaratnam R, Welsch ME, Shimada K, Skouta R, Viswanathan VS, Cheah JH, Clemons PA, Shamji AF, Clish CB, et al.: **Regulation of ferroptotic cancer cell death by GPX4.** *Cell* 2014, **156**:317-331.
224. Dixon SJ, Patel DN, Welsch M, Skouta R, Lee ED, Hayano M, Thomas AG, Gleason CE, Tatonetti NP, Slusher BS, et al.: **Pharmacological inhibition of cystine-glutamate exchange induces endoplasmic reticulum stress and ferroptosis.** *Elife* 2014, **3**:e02523.
225. Shimada K, Hayano M, Pagano NC, Stockwell BR: **Cell-Line Selectivity Improves the Predictive Power of Pharmacogenomic Analyses and Helps Identify NADPH as Biomarker for Ferroptosis Sensitivity.** *Cell Chem Biol* 2016, **23**:225-235.
226. Kandasamy P, Gyimesi G, Kanai Y, Hediger MA: **Amino acid transporters revisited: New views in health and disease.** *Trends Biochem Sci* 2018, **43**:752-789.
227. Bersuker K, Hendricks JM, Li Z, Magtanong L, Ford B, Tang PH, Roberts MA, Tong B, Maimone TJ, Zoncu R, et al.: **The CoQ oxidoreductase FSP1 acts parallel to GPX4 to inhibit ferroptosis.** *Nature* 2019, **575**:688-692.
228. Doll S, Freitas FP, Shah R, Aldrovandi M, da Silva MC, Ingold I, Goya Grocin A, Xavier da Silva TN, Panzilius E, Scheel CH, et al.: **FSP1 is a glutathione-independent ferroptosis suppressor.** *Nature* 2019, **575**:693-698.
229. Frei B, Kim MC, Ames BN: **Ubiquinol-10 is an effective lipid-soluble antioxidant at physiological concentrations.** *Proc Natl Acad Sci U S A* 1990, **87**:4879-4883.
230. Mao C, Liu X, Zhang Y, Lei G, Yan Y, Lee H, Koppula P, Wu S, Zhuang L, Fang B, et al.: **DHODH-mediated ferroptosis defence is a targetable vulnerability in cancer.** *Nature* 2021, **593**:586-590.
231. Werner ER, Blau N, Thony B: **Tetrahydrobiopterin: biochemistry and pathophysiology.** *Biochem J* 2011, **438**:397-414.
232. Kraft VAN, Bezjian CT, Pfeiffer S, Ringelstetter L, Muller C, Zandkarimi F, Merl-Pham J, Bao X, Anastasov N, Kossel J, et al.: **GTP Cyclohydrolase 1/Tetrahydrobiopterin Counteract Ferroptosis through Lipid Remodeling.** *ACS Cent Sci* 2020, **6**:41-53.
233. Soula M, Weber RA, Zilka O, Alwaseem H, La K, Yen F, Molina H, Garcia-Bermudez J, Pratt DA, Birsoy K: **Metabolic determinants of cancer cell sensitivity to canonical ferroptosis inducers.** *Nat Chem Biol* 2020, **16**:1351-1360.
234. Chen X, Yu C, Kang R, Tang D: **Iron Metabolism in Ferroptosis.** *Front Cell Dev Biol* 2020, **8**:590226.
235. Shaw P, Chattopadhyay A: **Nrf2-ARE signaling in cellular protection: Mechanism of action and the regulatory mechanisms.** *J Cell Physiol* 2020, **235**:3119-3130.
236. Tong KI, Katoh Y, Kusunoki H, Itoh K, Tanaka T, Yamamoto M: **Keap1 recruits Neh2 through binding to ETGE and DLG motifs: characterization of the two-site molecular recognition model.** *Mol Cell Biol* 2006, **26**:2887-2900.

237. Ogura T, Tong KI, Mio K, Maruyama Y, Kurokawa H, Sato C, Yamamoto M: **Keap1 is a forked-stem dimer structure with two large spheres enclosing the intervening, double glycine repeat, and C-terminal domains.** *Proc Natl Acad Sci U S A* 2010, **107**:2842-2847.
238. Cullinan SB, Gordan JD, Jin J, Harper JW, Diehl JA: **The Keap1-BTB protein is an adaptor that bridges Nrf2 to a Cul3-based E3 ligase: oxidative stress sensing by a Cul3-Keap1 ligase.** *Mol Cell Biol* 2004, **24**:8477-8486.
239. Zhang DD, Hannink M: **Distinct cysteine residues in Keap1 are required for Keap1-dependent ubiquitination of Nrf2 and for stabilization of Nrf2 by chemopreventive agents and oxidative stress.** *Mol Cell Biol* 2003, **23**:8137-8151.
240. Stewart D, Killeen E, Naquin R, Alam S, Alam J: **Degradation of transcription factor Nrf2 via the ubiquitin-proteasome pathway and stabilization by cadmium.** *J Biol Chem* 2003, **278**:2396-2402.
241. Dinkova-Kostova AT, Holtzclaw WD, Cole RN, Itoh K, Wakabayashi N, Katoh Y, Yamamoto M, Talalay P: **Direct evidence that sulfhydryl groups of Keap1 are the sensors regulating induction of phase 2 enzymes that protect against carcinogens and oxidants.** *Proc Natl Acad Sci U S A* 2002, **99**:11908-11913.
242. Jaramillo MC, Zhang DD: **The emerging role of the Nrf2-Keap1 signaling pathway in cancer.** *Genes Dev* 2013, **27**:2179-2191.
243. Baird L, Yamamoto M: **The Molecular Mechanisms Regulating the KEAP1-NRF2 Pathway.** *Mol Cell Biol* 2020, **40**.
244. Padmanabhan B, Tong KI, Ohta T, Nakamura Y, Scharlock M, Ohtsui M, Kang MI, Kobayashi A, Yokoyama S, Yamamoto M: **Structural basis for defects of Keap1 activity provoked by its point mutations in lung cancer.** *Mol Cell* 2006, **21**:689-700.
245. Singh A, Misra V, Thimmulappa RK, Lee H, Ames S, Hoque MO, Herman JG, Baylin SB, Sidransky D, Gabrielson E, et al.: **Dysfunctional KEAP1-NRF2 interaction in non-small-cell lung cancer.** *PLoS Med* 2006, **3**:e420.
246. Motohashi H, Katsuoka F, Engel JD, Yamamoto M: **Small Maf proteins serve as transcriptional cofactors for keratinocyte differentiation in the Keap1-Nrf2 regulatory pathway.** *Proc Natl Acad Sci U S A* 2004, **101**:6379-6384.
247. Tonelli C, Chio IIC, Tuveson DA: **Transcriptional Regulation by Nrf2.** *Antioxid Redox Signal* 2018, **29**:1727-1745.
248. Komatsu M, Kurokawa H, Waguri S, Taguchi K, Kobayashi A, Ichimura Y, Sou YS, Ueno I, Sakamoto A, Tong KI, et al.: **The selective autophagy substrate p62 activates the stress responsive transcription factor Nrf2 through inactivation of Keap1.** *Nat Cell Biol* 2010, **12**:213-223.
249. Lau A, Wang XJ, Zhao F, Villeneuve NF, Wu T, Jiang T, Sun Z, White E, Zhang DD: **A noncanonical mechanism of Nrf2 activation by autophagy deficiency: direct interaction between Keap1 and p62.** *Mol Cell Biol* 2010, **30**:3275-3285.
250. Kerins MJ, Ooi A: **The Roles of NRF2 in Modulating Cellular Iron Homeostasis.** *Antioxid Redox Signal* 2018, **29**:1756-1773.
251. Chorley BN, Campbell MR, Wang X, Karaca M, Sambandan D, Bangura F, Xue P, Pi J, Kleeberger SR, Bell DA: **Identification of novel NRF2-regulated genes by ChIP-Seq: influence on retinoid X receptor alpha.** *Nucleic Acids Res* 2012, **40**:7416-7429.
252. Sun X, Ou Z, Chen R, Niu X, Chen D, Kang R, Tang D: **Activation of the p62-Keap1-NRF2 pathway protects against ferroptosis in hepatocellular carcinoma cells.** *Hepatology* 2016, **63**:173-184.

253. Chen D, Tavana O, Chu B, Erber L, Chen Y, Baer R, Gu W: **NRF2 Is a Major Target of ARF in p53-Independent Tumor Suppression.** *Mol Cell* 2017, **68**:224-232 e224.
254. Fan Z, Wirth AK, Chen D, Wruck CJ, Rauh M, Buchfelder M, Savaskan N: **Nrf2-Keap1 pathway promotes cell proliferation and diminishes ferroptosis.** *Oncogenesis* 2017, **6**:e371.
255. Kuang F, Liu J, Xie Y, Tang D, Kang R: **MGST1 is a redox-sensitive repressor of ferroptosis in pancreatic cancer cells.** *Cell Chem Biol* 2021, **28**:765-775 e765.
256. Roh JL, Kim EH, Jang H, Shin D: **Nrf2 inhibition reverses the resistance of cisplatin-resistant head and neck cancer cells to artesunate-induced ferroptosis.** *Redox Biol* 2017, **11**:254-262.
257. Sun X, Niu X, Chen R, He W, Chen D, Kang R, Tang D: **Metallothionein-1G facilitates sorafenib resistance through inhibition of ferroptosis.** *Hepatology* 2016, **64**:488-500.
258. Takahashi N, Cho P, Selfors LM, Kuiken HJ, Kaul R, Fujiwara T, Harris IS, Zhang T, Gygi SP, Brugge JS: **3D Culture Models with CRISPR Screens Reveal Hyperactive NRF2 as a Prerequisite for Spheroid Formation via Regulation of Proliferation and Ferroptosis.** *Mol Cell* 2020, **80**:828-844 e826.
259. Jiang L, Kon N, Li T, Wang SJ, Su T, Hibshoosh H, Baer R, Gu W: **Ferroptosis as a p53-mediated activity during tumour suppression.** *Nature* 2015, **520**:57-62.
260. Wang SJ, Li D, Ou Y, Jiang L, Chen Y, Zhao Y, Gu W: **Acetylation Is Crucial for p53-Mediated Ferroptosis and Tumor Suppression.** *Cell Rep* 2016, **17**:366-373.
261. Ou Y, Wang SJ, Li D, Chu B, Gu W: **Activation of SAT1 engages polyamine metabolism with p53-mediated ferroptotic responses.** *Proc Natl Acad Sci U S A* 2016, **113**:E6806-E6812.
262. Zhang Y, Mohibi S, Vasilatis DM, Chen M, Zhang J, Chen X: **Ferredoxin reductase and p53 are necessary for lipid homeostasis and tumor suppression through the ABCA1-SREBP pathway.** *Oncogene* 2022, **41**:1718-1726.
263. Zhang Y, Qian Y, Zhang J, Yan W, Jung YS, Chen M, Huang E, Lloyd K, Duan Y, Wang J, et al.: **Ferredoxin reductase is critical for p53-dependent tumor suppression via iron regulatory protein 2.** *Genes Dev* 2017, **31**:1243-1256.
264. Tarangelo A, Magtanong L, Bieging-Rolett KT, Li Y, Ye J, Attardi LD, Dixon SJ: **p53 Suppresses Metabolic Stress-Induced Ferroptosis in Cancer Cells.** *Cell Rep* 2018, **22**:569-575.
265. Xie Y, Zhu S, Song X, Sun X, Fan Y, Liu J, Zhong M, Yuan H, Zhang L, Billiar TR, et al.: **The Tumor Suppressor p53 Limits Ferroptosis by Blocking DPP4 Activity.** *Cell Rep* 2017, **20**:1692-1704.
266. Zhang Y, Shi J, Liu X, Feng L, Gong Z, Koppula P, Sirohi K, Li X, Wei Y, Lee H, et al.: **BAP1 links metabolic regulation of ferroptosis to tumour suppression.** *Nat Cell Biol* 2018, **20**:1181-1192.
267. Ford DJ, Dingwall AK: **The cancer COMPASS: navigating the functions of MLL complexes in cancer.** *Cancer Genet* 2015, **208**:178-191.
268. Egolf S, Zou J, Anderson A, Simpson CL, Aubert Y, Prouty S, Ge K, Seykora JT, Capell BC: **MLL4 mediates differentiation and tumor suppression through ferroptosis.** *Sci Adv* 2021, **7**:eabj9141.
269. Reczek CR, Chandel NS: **The Two Faces of Reactive Oxygen Species in Cancer.** *Annual Review of Cancer Biology* 2017, **1**:79-98.

270. Sullivan LB, Chandel NS: **Mitochondrial reactive oxygen species and cancer.** *Cancer Metab* 2014, **2**:17.
271. DeNicola GM, Karreth FA, Humpton TJ, Gopinathan A, Wei C, Frese K, Mangal D, Yu KH, Yeo CJ, Calhoun ES, et al.: **Oncogene-induced Nrf2 transcription promotes ROS detoxification and tumorigenesis.** *Nature* 2011, **475**:106-109.
272. Koppula P, Lei G, Zhang Y, Yan Y, Mao C, Kondiparthi L, Shi J, Liu X, Horbath A, Das M, et al.: **A targetable CoQ-FSP1 axis drives ferroptosis- and radiation-resistance in KEAP1 inactive lung cancers.** *Nat Commun* 2022, **13**:2206.
273. Badgley MA, Kremer DM, Maurer HC, DelGiorno KE, Lee HJ, Purohit V, Sagalovskiy IR, Ma A, Kapilian J, Firl CEM, et al.: **Cysteine depletion induces pancreatic tumor ferroptosis in mice.** *Science* 2020, **368**:85-89.
274. Daher B, Parks SK, Durivault J, Cormerais Y, Baidarjad H, Tambutte E, Pouyssegur J, Vucetic M: **Genetic Ablation of the Cystine Transporter xCT in PDAC Cells Inhibits mTORC1, Growth, Survival, and Tumor Formation via Nutrient and Oxidative Stresses.** *Cancer Res* 2019, **79**:3877-3890.
275. Lei G, Zhuang L, Gan B: **Targeting ferroptosis as a vulnerability in cancer.** *Nat Rev Cancer* 2022, **22**:381-396.
276. Lei G, Zhang Y, Koppula P, Liu X, Zhang J, Lin SH, Ajani JA, Xiao Q, Liao Z, Wang H, et al.: **The role of ferroptosis in ionizing radiation-induced cell death and tumor suppression.** *Cell Res* 2020, **30**:146-162.
277. Viswanathan VS, Ryan MJ, Dhruv HD, Gill S, Eichhoff OM, Seashore-Ludlow B, Kaffenberger SD, Eaton JK, Shimada K, Aguirre AJ, et al.: **Dependency of a therapy-resistant state of cancer cells on a lipid peroxidase pathway.** *Nature* 2017, **547**:453-457.
278. Hangauer MJ, Viswanathan VS, Ryan MJ, Bole D, Eaton JK, Matov A, Galeas J, Dhruv HD, Berens ME, Schreiber SL, et al.: **Drug-tolerant persister cancer cells are vulnerable to GPX4 inhibition.** *Nature* 2017, **551**:247-250.
279. Wang W, Green M, Choi JE, Gijon M, Kennedy PD, Johnson JK, Liao P, Lang X, Kryczek I, Sell A, et al.: **CD8(+) T cells regulate tumour ferroptosis during cancer immunotherapy.** *Nature* 2019, **569**:270-274.
280. Lang X, Green MD, Wang W, Yu J, Choi JE, Jiang L, Liao P, Zhou J, Zhang Q, Dow A, et al.: **Radiotherapy and Immunotherapy Promote Tumoral Lipid Oxidation and Ferroptosis via Synergistic Repression of SLC7A11.** *Cancer Discov* 2019, **9**:1673-1685.
281. Wang W, Kryczek I, Dostal L, Lin H, Tan L, Zhao L, Lu F, Wei S, Maj T, Peng D, et al.: **Effector T Cells Abrogate Stroma-Mediated Chemoresistance in Ovarian Cancer.** *Cell* 2016, **165**:1092-1105.
282. Liao P, Wang W, Wang W, Kryczek I, Li X, Bian Y, Sell A, Wei S, Grove S, Johnson JK, et al.: **CD8(+) T cells and fatty acids orchestrate tumor ferroptosis and immunity via ACSL4.** *Cancer Cell* 2022, **40**:365-378 e366.
283. Conlon M, Poltorack CD, Forcina GC, Armenta DA, Mallais M, Perez MA, Wells A, Kahanu A, Magtanong L, Watts JL, et al.: **A compendium of kinetic modulatory profiles identifies ferroptosis regulators.** *Nat Chem Biol* 2021, **17**:665-674.
284. Homma T, Kobayashi S, Conrad M, Konno H, Yokoyama C, Fujii J: **Nitric oxide protects against ferroptosis by aborting the lipid peroxidation chain reaction.** *Nitric Oxide* 2021, **115**:34-43.

285. Kapralov AA, Yang Q, Dar HH, Tyurina YY, Anthony-muthu TS, Kim R, St Croix CM, Mikulska-Ruminska K, Liu B, Shrivastava IH, et al.: **Redox lipid reprogramming commands susceptibility of macrophages and microglia to ferroptotic death.** *Nat Chem Biol* 2020, **16**:278-290.
286. Efimova I, Catanzaro E, Van der Meeren L, Turubanova VD, Hammad H, Mishchenko TA, Vedunova MV, Fimognari C, Bachert C, Coppieters F, et al.: **Vaccination with early ferroptotic cancer cells induces efficient antitumor immunity.** *J Immunother Cancer* 2020, **8**.
287. Luo X, Gong HB, Gao HY, Wu YP, Sun WY, Li ZQ, Wang G, Liu B, Liang L, Kurihara H, et al.: **Oxygenated phosphatidylethanolamine navigates phagocytosis of ferroptotic cells by interacting with TLR2.** *Cell Death Differ* 2021, **28**:1971-1989.
288. Wen Q, Liu J, Kang R, Zhou B, Tang D: **The release and activity of HMGB1 in ferroptosis.** *Biochem Biophys Res Commun* 2019, **510**:278-283.
289. Yu B, Choi B, Li W, Kim DH: **Magnetic field boosted ferroptosis-like cell death and responsive MRI using hybrid vesicles for cancer immunotherapy.** *Nat Commun* 2020, **11**:3637.
290. Wiernicki B, Maschalidi S, Pinney J, Adjemian S, Vanden Berghe T, Ravichandran KS, Vandenabeele P: **Cancer cells dying from ferroptosis impede dendritic cell-mediated anti-tumor immunity.** *Nat Commun* 2022, **13**:3676.
291. Li Z, Michael IP, Zhou D, Nagy A, Rini JM: **Simple piggyBac transposon-based mammalian cell expression system for inducible protein production.** *Proc Natl Acad Sci U S A* 2013, **110**:5004-5009.
292. Ran FA, Hsu PD, Wright J, Agarwala V, Scott DA, Zhang F: **Genome engineering using the CRISPR-Cas9 system.** *Nat Protoc* 2013, **8**:2281-2308.
293. Michlits G, Jude J, Hinterndorfer M, de Almeida M, Vainorius G, Hubmann M, Neumann T, Schleiffer A, Burkard TR, Fellner M, et al.: **Multilayered VBC score predicts sgRNAs that efficiently generate loss-of-function alleles.** *Nat Methods* 2020, **17**:708-716.
294. Mayer CT, Ghorbani P, Nandan A, Dudek M, Arnold-Schrauf C, Hesse C, Berod L, Stuve P, Puttur F, Merad M, et al.: **Selective and efficient generation of functional Batf3-dependent CD103+ dendritic cells from mouse bone marrow.** *Blood* 2014, **124**:3081-3091.
295. Hahn M, Covarrubias-Pinto A, Herhaus L, Satpathy S, Klann K, Boyle KB, Munch C, Rajalingam K, Randow F, Choudhary C, et al.: **SIK2 orchestrates actin-dependent host response upon Salmonella infection.** *Proc Natl Acad Sci U S A* 2021, **118**.
296. Yusa K, Zhou L, Li MA, Bradley A, Craig NL: **A hyperactive piggyBac transposase for mammalian applications.** *Proc Natl Acad Sci U S A* 2011, **108**:1531-1536.
297. Dobin A, Davis CA, Schlesinger F, Drenkow J, Zaleski C, Jha S, Batut P, Chaisson M, Gingeras TR: **STAR: ultrafast universal RNA-seq aligner.** *Bioinformatics* 2013, **29**:15-21.
298. Liao Y, Smyth GK, Shi W: **featureCounts: an efficient general purpose program for assigning sequence reads to genomic features.** *Bioinformatics* 2014, **30**:923-930.
299. Liao Y, Smyth GK, Shi W: **The Subread aligner: fast, accurate and scalable read mapping by seed-and-vote.** *Nucleic Acids Res* 2013, **41**:e108.
300. Anders S, Huber W: **Differential expression analysis for sequence count data.** *Genome Biol* 2010, **11**:R106.

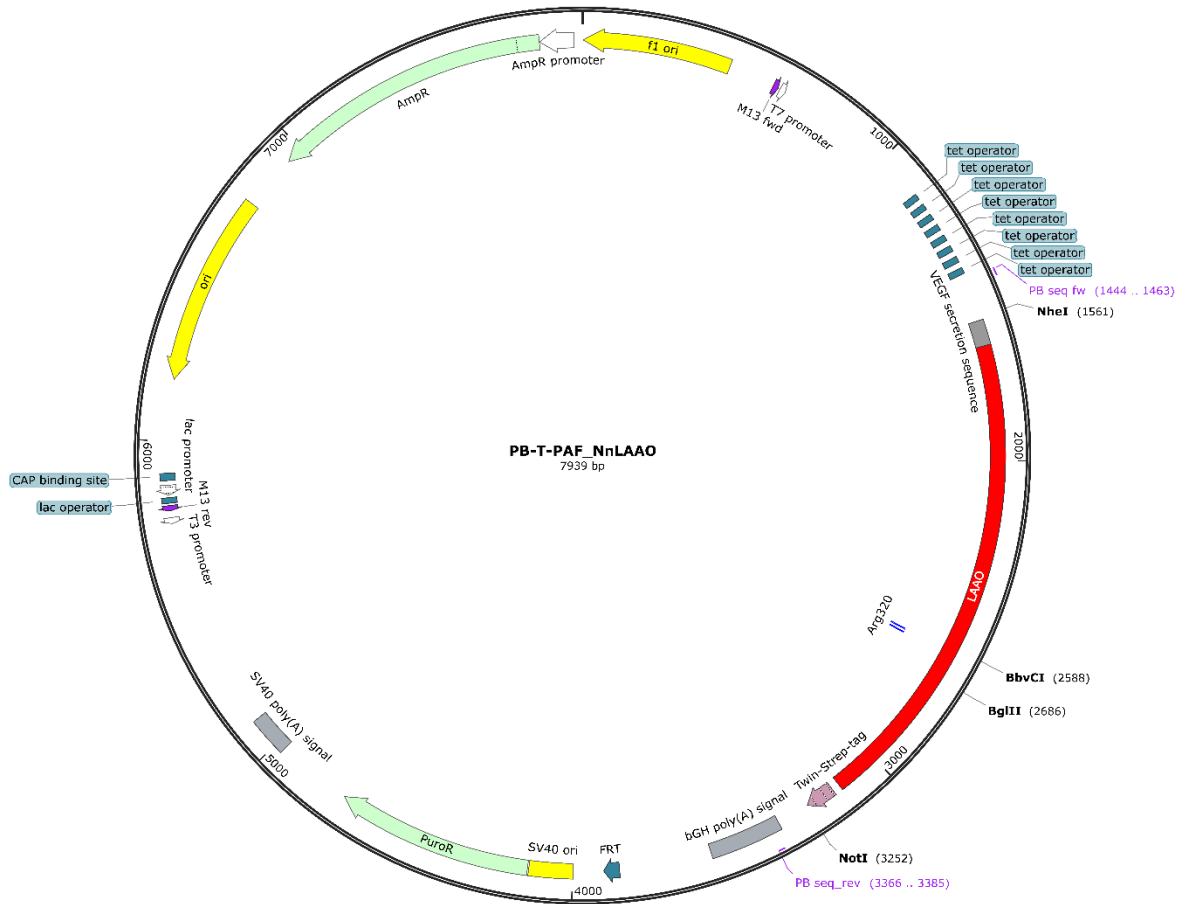
301. Rahman I, Kode A, Biswas SK: **Assay for quantitative determination of glutathione and glutathione disulfide levels using enzymatic recycling method.** *Nat Protoc* 2006, **1**:3159-3165.
302. Jumper J, Evans R, Pritzel A, Green T, Figurnov M, Ronneberger O, Tunyasuvunakool K, Bates R, Zidek A, Potapenko A, et al.: **Highly accurate protein structure prediction with AlphaFold.** *Nature* 2021, **596**:583-589.
303. Geyer A, Fitzpatrick TB, Pawelek PD, Kitzing K, Vrieling A, Ghisla S, Macheroux P: **Structure and characterization of the glycan moiety of L-amino-acid oxidase from the Malayan pit viper Calloselasma rhodostoma.** *Eur J Biochem* 2001, **268**:4044-4053.
304. Pawelek PD, Cheah J, Coulombe R, Macheroux P, Ghisla S, Vrieling A: **The structure of L-amino acid oxidase reveals the substrate trajectory into an enantiomerically conserved active site.** *EMBO J* 2000, **19**:4204-4215.
305. Izidoro LF, Ribeiro MC, Souza GR, Sant'Ana CD, Hamaguchi A, Homsí-Brandeburgo MI, Goulart LR, Belebóni RO, Nomizo A, Sampaio SV, et al.: **Biochemical and functional characterization of an L-amino acid oxidase isolated from Bothrops pirajai snake venom.** *Bioorg Med Chem* 2006, **14**:7034-7043.
306. Rodrigues RS, da Silva JF, Boldrini Franca J, Fonseca FP, Otaviano AR, Henrique Silva F, Hamaguchi A, Magro AJ, Braz AS, dos Santos JI, et al.: **Structural and functional properties of Bp-LAAO, a new L-amino acid oxidase isolated from Bothrops pauloensis snake venom.** *Biochimie* 2009, **91**:490-501.
307. Bregge-Silva C, Nonato MC, de Albuquerque S, Ho PL, Junqueira de Azevedo IL, Vasconcelos Diniz MR, Lomonte B, Rucavado A, Diaz C, Gutierrez JM, et al.: **Isolation and biochemical, functional and structural characterization of a novel L-amino acid oxidase from Lachesis muta snake venom.** *Toxicon* 2012, **60**:1263-1276.
308. Fink SL, Cookson BT: **Apoptosis, pyroptosis, and necrosis: mechanistic description of dead and dying eukaryotic cells.** *Infect Immun* 2005, **73**:1907-1916.
309. MacLeod AK, McMahon M, Plummer SM, Higgins LG, Penning TM, Igarashi K, Hayes JD: **Characterization of the cancer chemopreventive NRF2-dependent gene battery in human keratinocytes: demonstration that the KEAP1-NRF2 pathway, and not the BACH1-NRF2 pathway, controls cytoprotection against electrophiles as well as redox-cycling compounds.** *Carcinogenesis* 2009, **30**:1571-1580.
310. Matsunaga T, Yamaguchi A, Morikawa Y, Kezuka C, Takazawa H, Endo S, El-Kabbani O, Tajima K, Ikari A, Hara A: **Induction of aldo-keto reductases (AKR1C1 and AKR1C3) abolishes the efficacy of daunorubicin chemotherapy for leukemic U937 cells.** *Anticancer Drugs* 2014, **25**:868-877.
311. Zgheib E, Limonciel A, Jiang X, Wilmes A, Wink S, van de Water B, Kopp-Schneider A, Bois FY, Jennings P: **Investigation of Nrf2, AhR and ATF4 Activation in Toxicogenomic Databases.** *Front Genet* 2018, **9**:429.
312. Lesniak WG, Jyoti A, Mishra MK, Louissaint N, Romero R, Chugani DC, Kannan S, Kannan RM: **Concurrent quantification of tryptophan and its major metabolites.** *Anal Biochem* 2013, **443**:222-231.
313. Sinclair LV, Neyens D, Ramsay G, Taylor PM, Cantrell DA: **Single cell analysis of kynurenine and System L amino acid transport in T cells.** *Nat Commun* 2018, **9**:1981.
314. Tang D, Kroemer G: **Ferroptosis.** *Curr Biol* 2020, **30**:R1292-R1297.

315. Geisler S, Mayersbach P, Becker B, Schennach H, Fuchs D, Gostner JM: **Serum tryptophan, kynurenine, phenylalanine, tyrosine and neopterin concentrations in 100 healthy blood donors.** *Pteridines* 2015, **26**:31-36.
316. Politi V, D'Alessio S, Di Stazio G, De Luca G: **Antioxidant properties of indole-3-pyruvic acid.** *Adv Exp Med Biol* 1996, **398**:291-298.
317. Ayer A, Zarjou A, Agarwal A, Stocker R: **Heme Oxygenases in Cardiovascular Health and Disease.** *Physiol Rev* 2016, **96**:1449-1508.
318. Chiang SK, Chen SE, Chang LC: **A Dual Role of Heme Oxygenase-1 in Cancer Cells.** *Int J Mol Sci* 2018, **20**.
319. Fang X, Wang H, Han D, Xie E, Yang X, Wei J, Gu S, Gao F, Zhu N, Yin X, et al.: **Ferroptosis as a target for protection against cardiomyopathy.** *Proc Natl Acad Sci U S A* 2019, **116**:2672-2680.
320. Kwon MY, Park E, Lee SJ, Chung SW: **Heme oxygenase-1 accelerates erastin-induced ferroptotic cell death.** *Oncotarget* 2015, **6**:24393-24403.
321. Adedoyin O, Boddu R, Traylor A, Lever JM, Bolisetty S, George JF, Agarwal A: **Heme oxygenase-1 mitigates ferroptosis in renal proximal tubule cells.** *Am J Physiol Renal Physiol* 2018, **314**:F702-F714.
322. Stocker R: **Antioxidant activities of bile pigments.** *Antioxid Redox Signal* 2004, **6**:841-849.
323. Yang PS, Hsu YC, Lee JJ, Chen MJ, Huang SY, Cheng SP: **Heme Oxygenase-1 Inhibitors Induce Cell Cycle Arrest and Suppress Tumor Growth in Thyroid Cancer Cells.** *Int J Mol Sci* 2018, **19**.
324. Ye J, Palm W, Peng M, King B, Lindsten T, Li MO, Koumenis C, Thompson CB: **GCN2 sustains mTORC1 suppression upon amino acid deprivation by inducing Sestrin2.** *Genes Dev* 2015, **29**:2331-2336.
325. Kwon OS, Kwon EJ, Kong HJ, Choi JY, Kim YJ, Lee EW, Kim W, Lee H, Cha HJ: **Systematic identification of a nuclear receptor-enriched predictive signature for erastin-induced ferroptosis.** *Redox Biol* 2020, **37**:101719.
326. Eleftheriadis T, Pissas G, Filippidis G, Liakopoulos V, Stefanidis I: **Reoxygenation induces reactive oxygen species production and ferroptosis in renal tubular epithelial cells by activating aryl hydrocarbon receptor.** *Mol Med Rep* 2021, **23**.
327. Inaba K, Inaba M, Romani N, Aya H, Deguchi M, Ikehara S, Muramatsu S, Steinman RM: **Generation of large numbers of dendritic cells from mouse bone marrow cultures supplemented with granulocyte/macrophage colony-stimulating factor.** *J Exp Med* 1992, **176**:1693-1702.
328. Helft J, Bottcher J, Chakravarty P, Zelenay S, Huotari J, Schraml BU, Goubau D, Reis e Sousa C: **GM-CSF Mouse Bone Marrow Cultures Comprise a Heterogeneous Population of CD11c(+)MHCII(+) Macrophages and Dendritic Cells.** *Immunity* 2015, **42**:1197-1211.
329. Brandum EP, Jorgensen AS, Rosenkilde MM, Hjortø GM: **Dendritic Cells and CCR7 Expression: An Important Factor for Autoimmune Diseases, Chronic Inflammation, and Cancer.** *Int J Mol Sci* 2021, **22**.
330. Mazzoni A, Capone M, Ramazzotti M, Vanni A, Locatello LG, Gallo O, De Palma R, Cosmi L, Liotta F, Annunziato F, et al.: **IL411 Is Expressed by Head-Neck Cancer-Derived Mesenchymal Stromal Cells and Contributes to Suppress T Cell Proliferation.** *J Clin Med* 2021, **10**.

331. Etemadi N, Holien JK, Chau D, Dewson G, Murphy JM, Alexander WS, Parker MW, Silke J, Nachbur U: **Lymphotoxin alpha induces apoptosis, necroptosis and inflammatory signals with the same potency as tumour necrosis factor.** *FEBS J* 2013, **280**:5283-5297.
332. Szoltysek K, Janus P, Zajac G, Stokowy T, Walaszczyk A, Widlak W, Wojtas B, Gielniewski B, Cockell S, Perkins ND, et al.: **RRAD, IL4I1, CDKN1A, and SERPINE1 genes are potentially co-regulated by NF-kappaB and p53 transcription factors in cells exposed to high doses of ionizing radiation.** *BMC Genomics* 2018, **19**:813.
333. Gilmore TD: **Introduction to NF-kappaB: players, pathways, perspectives.** *Oncogene* 2006, **25**:6680-6684.
334. Napetschnig J, Wu H: **Molecular basis of NF-kappaB signaling.** *Annu Rev Biophys* 2013, **42**:443-468.
335. Scherer DC, Brockman JA, Chen Z, Maniatis T, Ballard DW: **Signal-induced degradation of I kappa B alpha requires site-specific ubiquitination.** *Proc Natl Acad Sci U S A* 1995, **92**:11259-11263.
336. Traenckner EB, Wilk S, Baeuerle PA: **A proteasome inhibitor prevents activation of NF-kappa B and stabilizes a newly phosphorylated form of I kappa B-alpha that is still bound to NF-kappa B.** *EMBO J* 1994, **13**:5433-5441.
337. Luzina IG, Keegan AD, Heller NM, Rook GA, Shea-Donohue T, Atamas SP: **Regulation of inflammation by interleukin-4: a review of "alternatives".** *J Leukoc Biol* 2012, **92**:753-764.
338. Wynn TA: **Type 2 cytokines: mechanisms and therapeutic strategies.** *Nat Rev Immunol* 2015, **15**:271-282.
339. Goenka S, Kaplan MH: **Transcriptional regulation by STAT6.** *Immunol Res* 2011, **50**:87-96.
340. Rao D, Yu C, Wang T, Sheng J, Lv E, Liang H, Huang W, Dong H: **Pan-cancer analysis combined with experimental validation revealed IL4I1 as an immunological and prognostic biomarker.** *Int Immunopharmacol* 2022, **111**:109091.
341. Tasoulis T, Isbister GK: **A Review and Database of Snake Venom Proteomes.** *Toxins (Basel)* 2017, **9**.
342. Castellano F, Prevost-Blondel A, Cohen JL, Molinier-Frenkel V: **What role for AHR activation in IL4I1-mediated immunosuppression ?** *Oncoimmunology* 2021, **10**:1924500.
343. Dodd D, Spitzer MH, Van Treuren W, Merrill BD, Hryckowian AJ, Higginbottom SK, Le A, Cowan TM, Nolan GP, Fischbach MA, et al.: **A gut bacterial pathway metabolizes aromatic amino acids into nine circulating metabolites.** *Nature* 2017, **551**:648-652.
344. Politi V, Lavaggi MV, Di Stazio G, Margonelli A: **Indole-3-pyruvic acid as a direct precursor of kynurenic acid.** *Adv Exp Med Biol* 1991, **294**:515-518.
345. Bloom BR, Bennett B: **Mechanism of a reaction in vitro associated with delayed-type hypersensitivity.** *Science* 1966, **153**:80-82.
346. David JR: **Delayed hypersensitivity in vitro: its mediation by cell-free substances formed by lymphoid cell-antigen interaction.** *Proc Natl Acad Sci U S A* 1966, **56**:72-77.
347. Rosengren E, Aman P, Thelin S, Hansson C, Ahlfors S, Bjork P, Jacobsson L, Rorsman H: **The macrophage migration inhibitory factor MIF is a phenylpyruvate tautomerase.** *FEBS Lett* 1997, **417**:85-88.

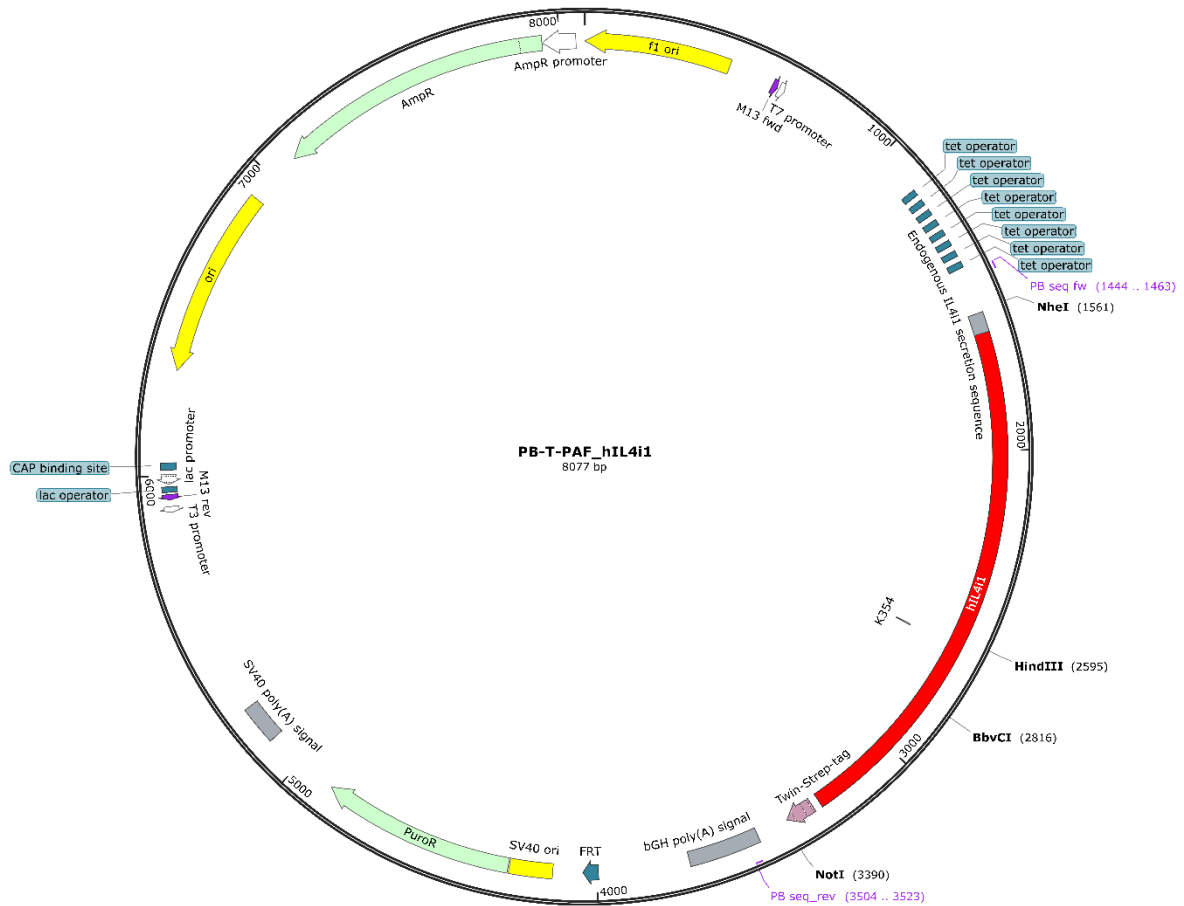
348. Bartolini B, Corniello C, Sella A, Somma F, Politi V: **The enol tautomer of indole-3-pyruvic acid as a biological switch in stress responses.** *Adv Exp Med Biol* 2003, **527**:601-608.
349. Garrido-Pascual P, Alonso-Varona A, Castro B, Buron M, Palomares T: **H₂O₂-preconditioned human adipose-derived stem cells (HC016) increase their resistance to oxidative stress by overexpressing Nrf2 and bioenergetic adaptation.** *Stem Cell Res Ther* 2020, **11**:335.
350. Luna-Lopez A, Triana-Martinez F, Lopez-Diazguerrero NE, Ventura-Gallegos JL, Gutierrez-Ruiz MC, Damian-Matsumura P, Zentella A, Gomez-Quiroz LE, Konigsberg M: **Bcl-2 sustains hormetic response by inducing Nrf-2 nuclear translocation in L929 mouse fibroblasts.** *Free Radic Biol Med* 2010, **49**:1192-1204.
351. Mesquita A, Weinberger M, Silva A, Sampaio-Marques B, Almeida B, Leao C, Costa V, Rodrigues F, Burhans WC, Ludovico P: **Caloric restriction or catalase inactivation extends yeast chronological lifespan by inducing H₂O₂ and superoxide dismutase activity.** *Proc Natl Acad Sci U S A* 2010, **107**:15123-15128.
352. Lee J, You JH, Kim MS, Roh JL: **Epigenetic reprogramming of epithelial-mesenchymal transition promotes ferroptosis of head and neck cancer.** *Redox Biol* 2020, **37**:101697.
353. Ribatti D, Tamma R, Annese T: **Epithelial-Mesenchymal Transition in Cancer: A Historical Overview.** *Transl Oncol* 2020, **13**:100773.
354. Guo J, Xu B, Han Q, Zhou H, Xia Y, Gong C, Dai X, Li Z, Wu G: **Ferroptosis: A Novel Anti-tumor Action for Cisplatin.** *Cancer Res Treat* 2018, **50**:445-460.
355. Ye LF, Chaudhary KR, Zandkarimi F, Harken AD, Kinslow CJ, Upadhyayula PS, Dovas A, Higgins DM, Tan H, Zhang Y, et al.: **Radiation-Induced Lipid Peroxidation Triggers Ferroptosis and Synergizes with Ferroptosis Inducers.** *ACS Chem Biol* 2020, **15**:469-484.
356. Gerhard GM, Bill R, Messemaker M, Klein AM, Pittet MJ: **Tumor-infiltrating dendritic cell states are conserved across solid human cancers.** *J Exp Med* 2021, **218**.
357. Lopez-Castejon G, Brough D: **Understanding the mechanism of IL-1beta secretion.** *Cytokine Growth Factor Rev* 2011, **22**:189-195.
358. Czimmerer Z, Halasz L, Daniel B, Varga Z, Bene K, Domokos A, Hoeksema M, Shen Z, Berger WK, Cseh T, et al.: **The epigenetic state of IL-4-polarized macrophages enables inflammatory cistromic expansion and extended synergistic response to TLR ligands.** *Immunity* 2022.
359. Shen CH, Stavnezer J: **Interaction of stat6 and NF-kappaB: direct association and synergistic activation of interleukin-4-induced transcription.** *Mol Cell Biol* 1998, **18**:3395-3404.

7. Supplement



Supplementary Figure 1 Plasmid map of PB-T-PAF_NnLAAO encoding Naja naja LAAO

Plasmid map shows the PB-T-PAF vector of the PiggyBac system allowing doxycycline-inducible expression of Naja naja LAAO. NheI and NotI restriction sites were used for cloning. The human VEGF secretion sequence was added for optimal protein secretion in the human HEK293T expression cell line and a C-terminal Twin-Strep-Tag was added to enable efficient protein purification. BbvCI and BglII sites were used to clone a fragment encoding the R320A, K324A mutations into the plasmid.

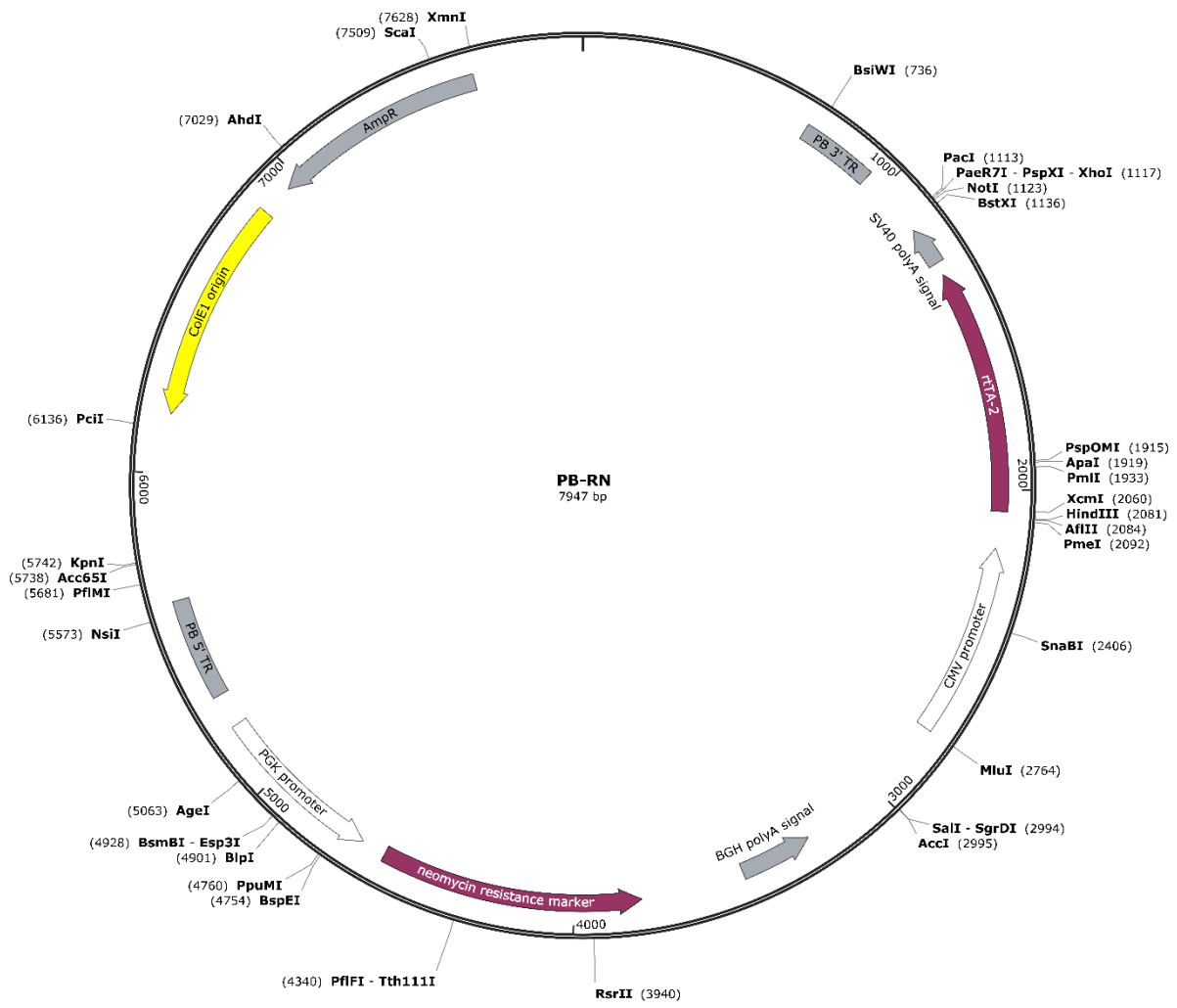


Supplementary Figure 2 Plasmid map of PB-T-PAF_hIL4i1 encoding human IL4i1

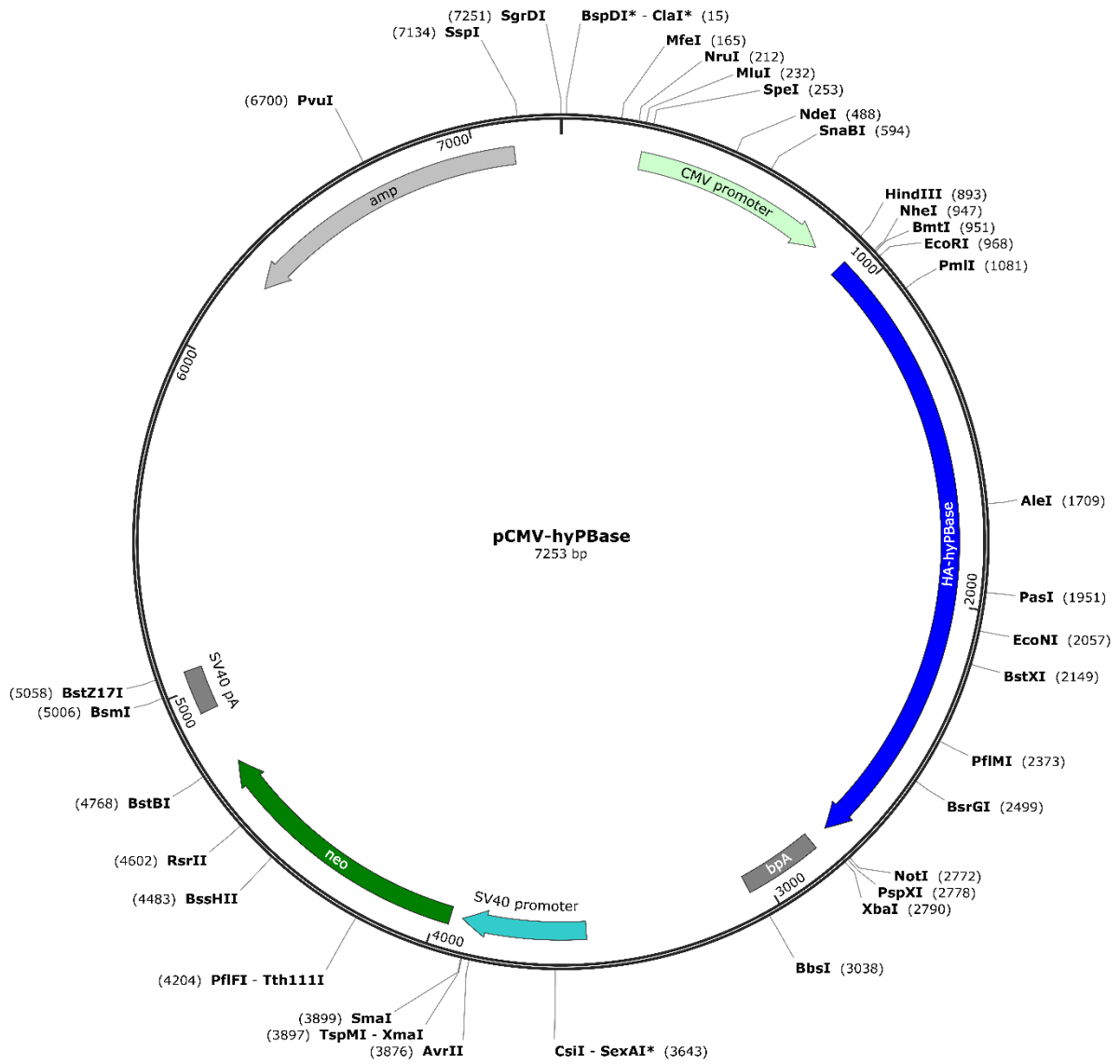
Plasmid map shows the PB-T-PAF vector of the PiggyBac system allowing doxycycline-inducible expression of human IL4i1. NheI and NotI restriction sites were used for cloning. A C-terminal Twin-Strep-Tag was added to enable efficient protein purification. BbvCI and SbfI sites were used to clone a fragment encoding the K354A mutation into the plasmid.



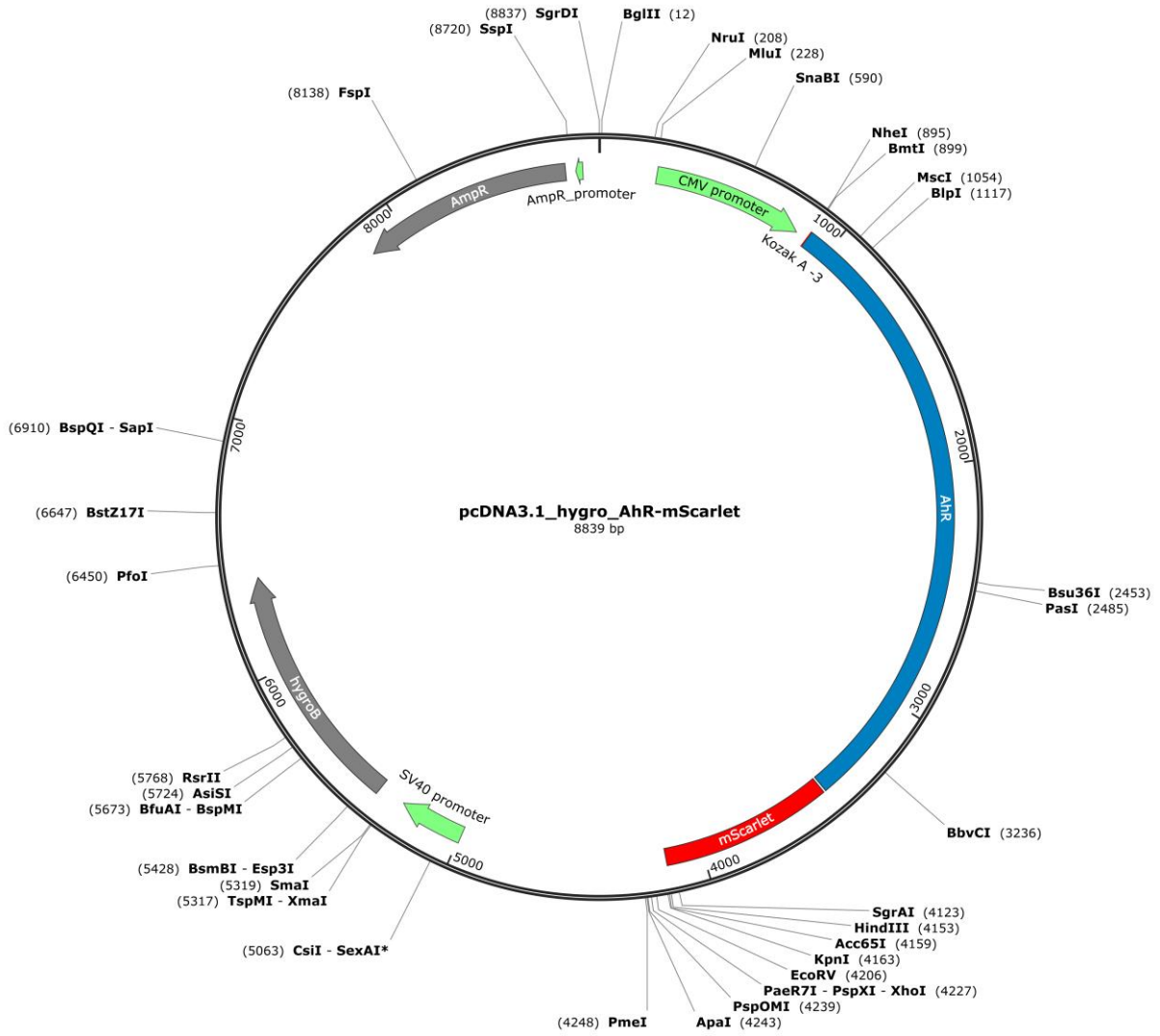
Supplementary Figure 3 Plasmid map of pSpCas9(BB)-2A-GFP (PX458)



Supplementary Figure 4 Plasmid map of PB-RN

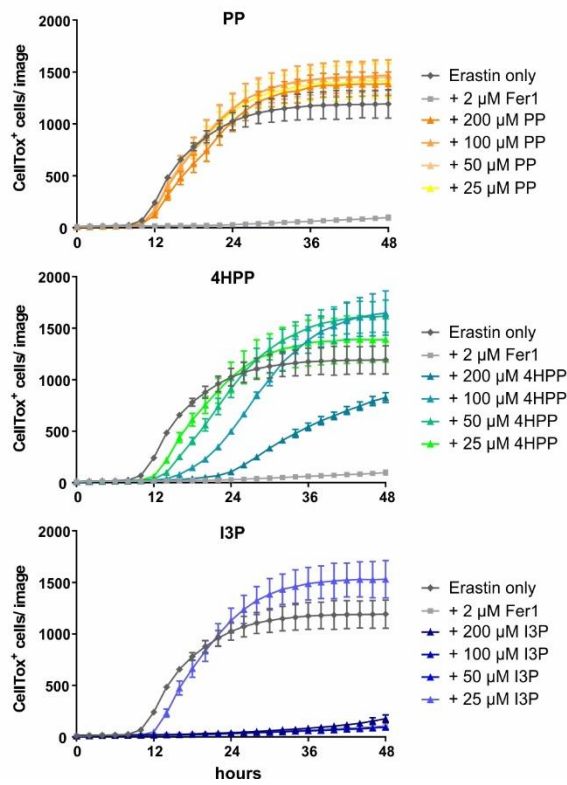


Supplementary Figure 5 Plasmid map of pCMV-hyPBase

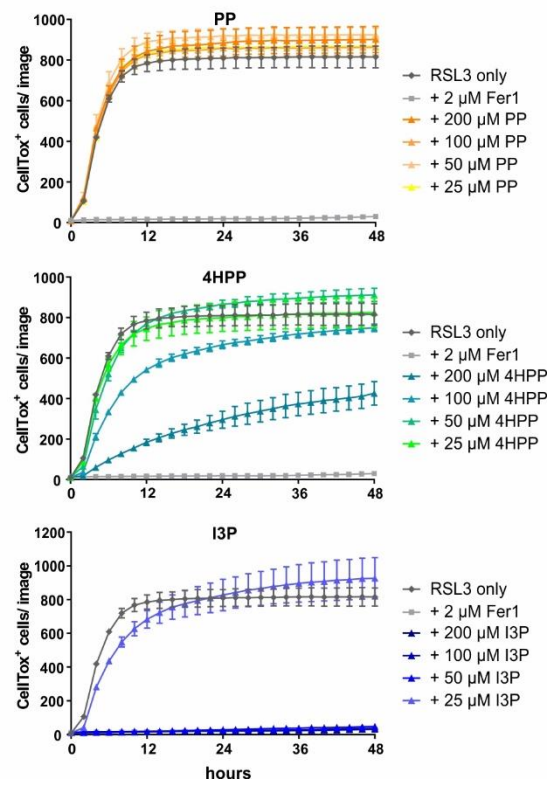


Supplementary Figure 6 Plasmid map of pcDNA3.1_hygro_AhR-mScarlet

A 24h pre-treatment before Erastin

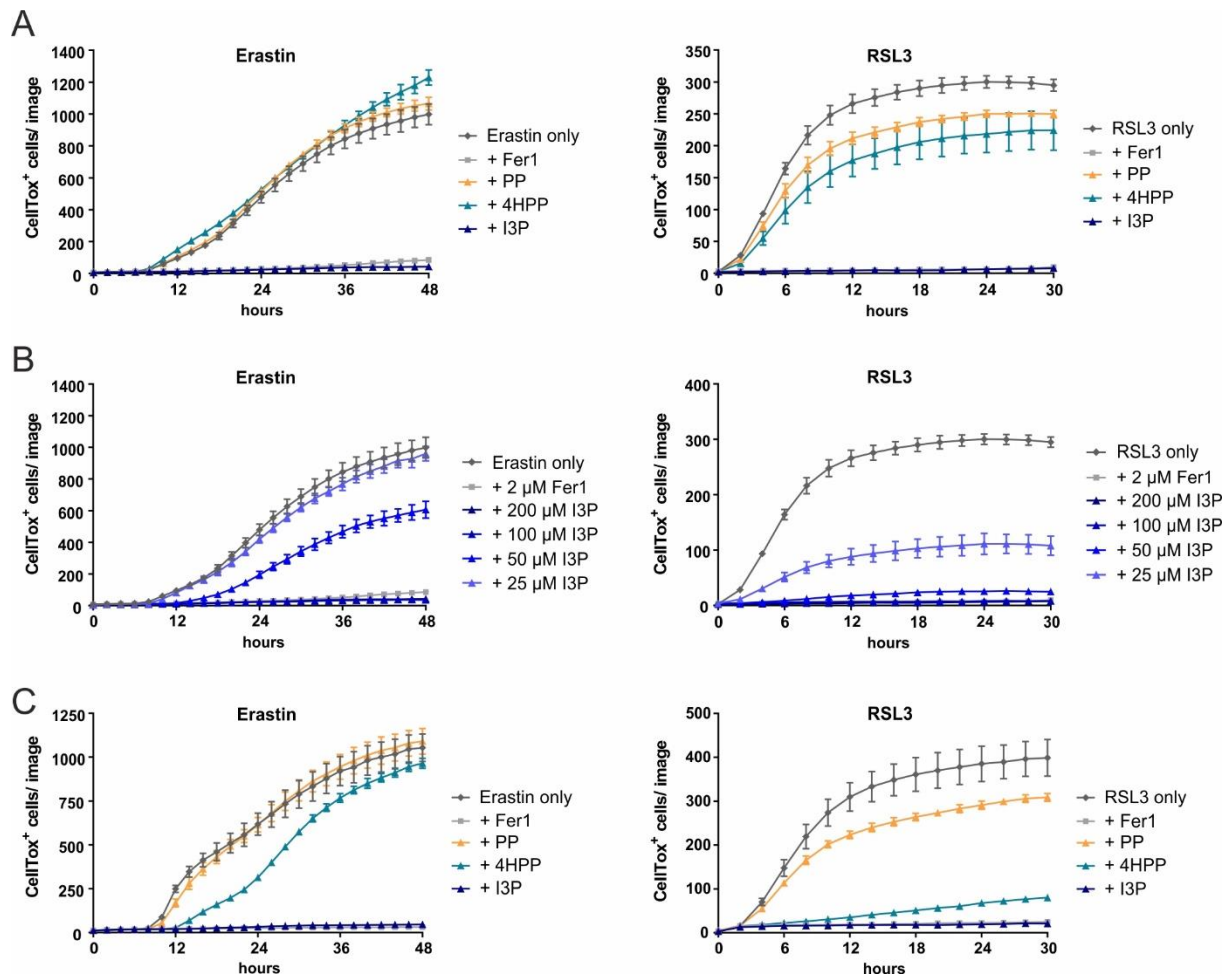


B 24h pre-treatment before RSL3



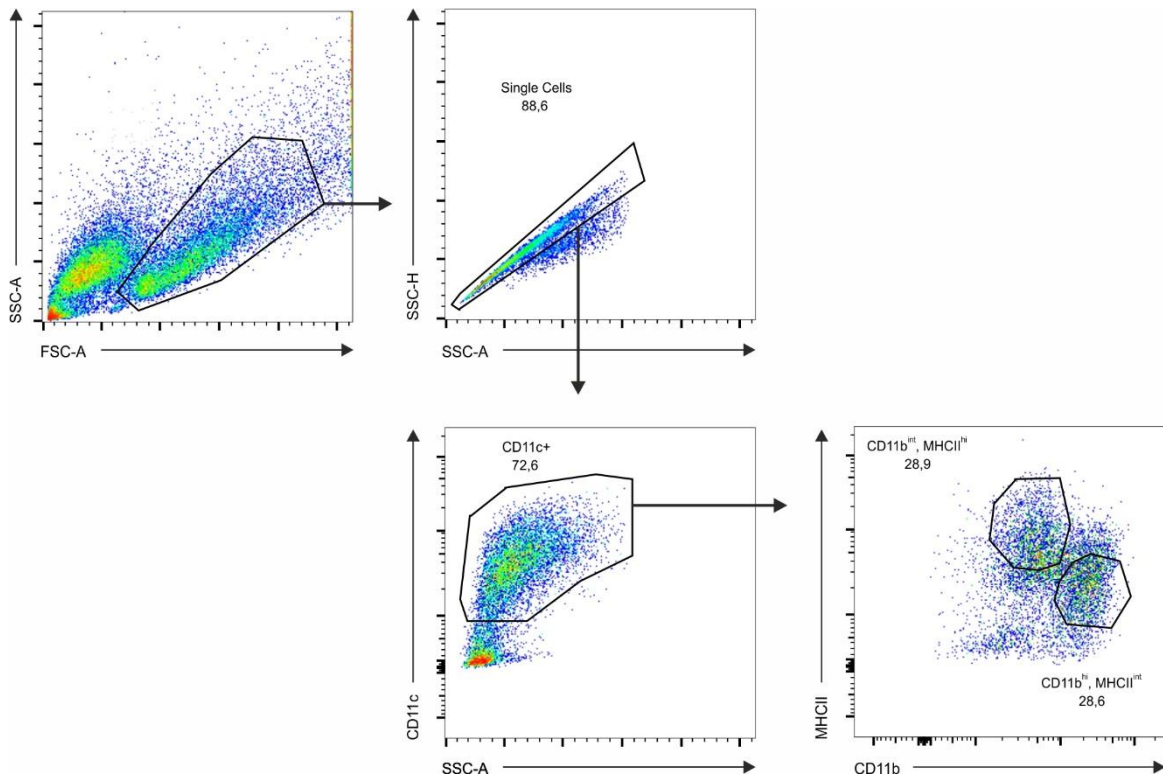
Supplementary Figure 7 Ferroptosis inhibition after pre-treatment with PP, 4HPP and I3P

(A) Quantification of Erastin-induced ferroptosis over 48 h using the IncuCyte live imaging device and CellTox green dye. HeLa cells were pre-treated with the indicated concentrations of PP, 4HPP and I3P. After 24 h 10 μM Erastin were added to induce ferroptosis and monitoring of cell death was started. Fer-1 was added concurrently with Erastin as a control for ferroptosis inhibition. (B) As described in (A) but using 1 μM RSL3 for ferroptosis induction. (A,B) n=3 biological replicates; error bars indicate standard deviation.



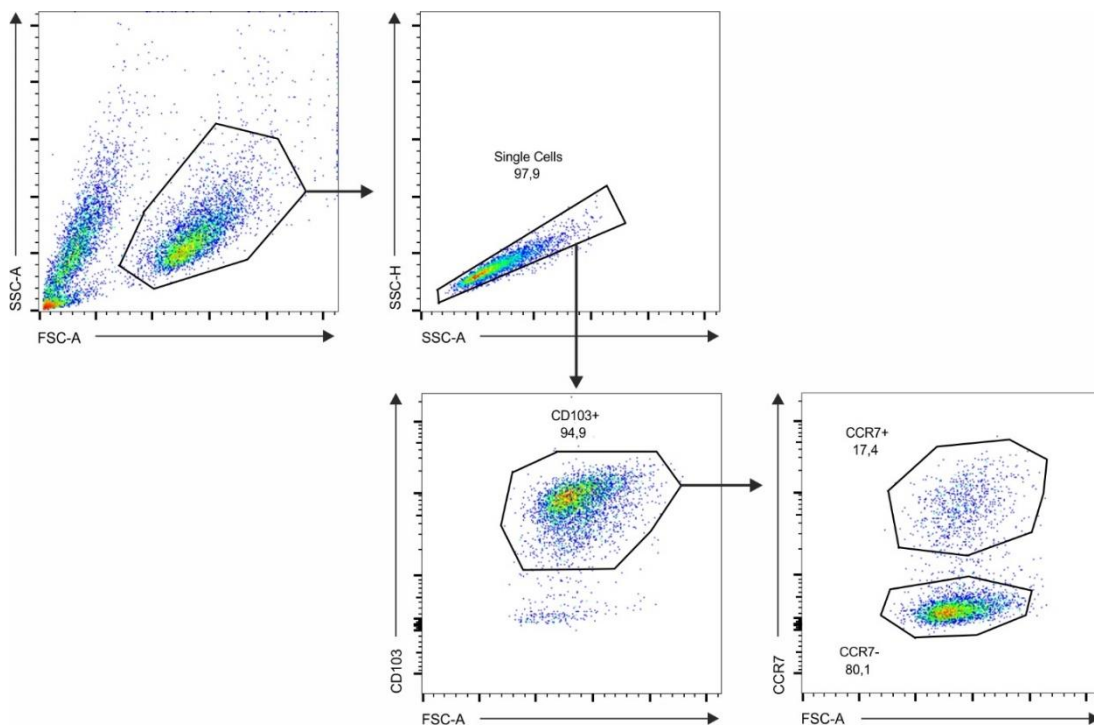
Supplementary Figure 8 Ferroptosis inhibition by I3P in HT1080 cells

(A) Quantification of ferroptotic cell death over 48 h using the IncuCyte live imaging device and CellTox green dye. HT1080 cells were concurrently treated with 5 μ M Erastin (left) or 1 μ M RSL3 (right) and 200 μ M of PP, 4HPP or I3P. Fer-1 was used as a control for ferroptosis inhibition. (B) As in (A) but using titrations of I3P to block ferroptosis. (C) Quantification of ferroptosis induced after 24 h pre-treatment with 200 μ M of the indicated metabolites. After 24 h 5 μ M Erastin (left) or 1 μ M RSL3 (right) were added to induce ferroptosis. Fer-1 was added concurrently to the ferroptosis inducer as a control for ferroptosis inhibition. (A-C) n=3 biological replicates; error bars indicate standard deviation.



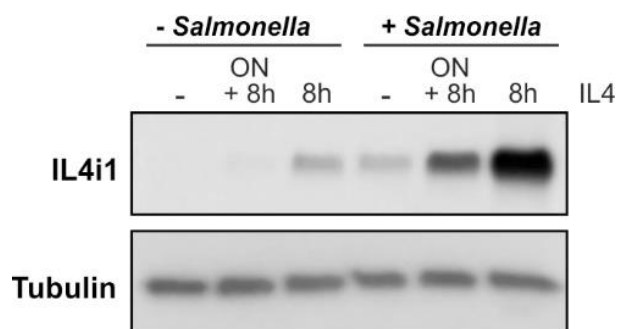
Supplementary Figure 9 Sorting strategy for CD11c⁺ DCs and macrophages in the GM-DC culture

Cells from the differentiation with GM-CSF were sorted on day 8. After gating on single cells, cells were gated for CD11c expression and subsequently for CD11b^{int} and MHCII^{hi} and CD11b^{hi} and MHCII^{int} cells.



Supplementary Figure 10 Sorting strategy for CD103⁺, CCR7⁺ or CCR7⁻ CD103 DCs

Cells from the CD103 DC differentiation were sorted on day 15. After gating on single cells, cells were gated for CD103 expression and subsequently for CCR7⁺ and CCR7⁻ cells.



Supplementary Figure 11 IL4 enhances IL4i1 induction by *Salmonella* infection

Immunoblot of BMDMs infected with *Salmonella enterica* serovar Typhimurium. 12 h before infection some BMDMs were primed with 10 ng/ml IL4 (ON). BMDMs were infected with *Salmonella* (MOI of 10) or left uninfected and some of the samples were additionally treated with 10 ng/ml IL4 directly after the infection. BMDMs were lysed for protein isolation 8 h post infection.

8. Acknowledgements

First and foremost, I would like to thank my supervisor Peter Murray for his support and guidance throughout the course of my PhD project. Your expertise and passion for science have been a constant inspiration and motivation for me. You were always approachable and open to discuss exciting findings as well as the obstacles I encountered during my project. Thank you for being always supportive, but also for giving me a lot of freedom in my research, which I appreciate a lot. I am truly grateful for being a part of your team.

Moreover, I would like to thank the members of my thesis advisory committee, Matthias Feige, Manajit Hayer-Hartl and Thomas Brocker for fruitful discussions and scientific input helping to shape my PhD project.

I am grateful for the valuable help from internal and external collaborators who provided their experimental and conceptual expertise. Many thanks to Jonathan Swietlik, Marcel Hahn, Claudia Meyer, Ivan Dikic and Andreas Linkermann for their work and scientific input. Moreover, I want to thank Sachdev Sidhu for providing the *Naja naja* LAAO sequence. I am thankful for the support from the MPIB core facilities, especially from Sabine Suppmann and her team from the 'Protein production' facility, Rinho Kim and Assa Yeroslaviz from the NGS facility and Markus Oster from the Imaging facility.

Furthermore, I want to thank my wonderful colleagues in the Murray lab without whom my PhD time would not have been half as nice and who made the daily work in the lab enjoyable even when experiments failed. Special thanks go to Alessandra who supported me a lot during my project. It was great teaming up with you to discover the connections between tryptophan metabolism and ferroptosis resistance. I also want to thank Marion who was constantly available to discuss my project and very helpful with her scientific experience. Thanks to both of you (and our pasta lunches) it was even ok to spend weekends in the lab. Annette, I am glad you are my "constant" in the lab and a great and supportive colleague. Many thanks to Steffi and Laura, who helped me out with any questions about macrophage biology and Johanna for being my cell culture companion. I would like to thank Alex and Nina for their technical support and a lot of work in the background concerning the lab organization. Many thanks also to Maria and Lisa who were/are wonderful and talented Master's students in the lab to whom I could hand over some parts of my projects. I am grateful for having amazing new colleagues in the "Murray lab 2.0". Moni, Charlotte, Teng Teng, Pat and Nuria, thank you so much for your support in the final phase of my PhD and your company in my writing breaks. Thanks also to Shuhan and Sophia for bringing some new scientific input from different research areas into our lab and to Klara for all kinds of administrative support.

A big thank you goes to the IMPRS-LS coordination office for organizing so many great events for the IMPRS-LS graduate school.

Finally, I would to thank my friends and family who have been accompanying me through all ups and downs of my PhD journey. I am incredibly grateful for the support and encouragement I experienced from my parents, my brother and my beloved grandparents. Coming to the end, I would like to thank Fynn for always being there for me. I hope you know how important you've been in all of this and how grateful I am to have you in my life.